

SECTION 4. PHOTOCHEMICAL DATA

Table of Contents

SECTION 4. PHOTOCHEMICAL DATA.....	4-1
4.1 Format and Error Estimates.....	4-3
4.2 Halocarbon Absorption Cross Sections and Quantum Yields.....	4-3
4.3 References.....	4-102

Tables

Table 4-1. Photochemical Reactions.....	4-4
Table 4-2. Combined Uncertainties for Cross Sections and Quantum Yields.....	4-6
Table 4-3. Absorption Cross Sections of O ₂ Between 205 and 240 nm.....	4-7
Table 4-4. Absorption Cross Sections of O ₃ at 273 K.....	4-8
Table 4-5. Parameters for the Calculation of O(¹ D) Quantum Yields.....	4-9
Table 4-6. Absorption Cross Sections of HO ₂	4-10
Table 4-7. Absorption Cross Sections of H ₂ O Vapor.....	4-11
Table 4-8. Absorption Cross Sections of H ₂ O ₂ Vapor.....	4-11
Table 4-9. Mathematical Expression for Absorption Cross Sections of H ₂ O ₂ as a Function of Temperature.....	4-12
Table 4-10. Absorption Cross Sections of NO ₂	4-13
Table 4-11. Quantum Yields for NO ₂ Photolysis.....	4-14
Table 4-12. Absorption Cross Sections of NO ₃ at 298 K.....	4-16
Table 4-13. Mathematical Expression for Absorption Cross Sections of N ₂ O as a Function of Temperature*.....	4-16
Table 4-14. Absorption Cross Sections of N ₂ O at 298 K.....	4-17
Table 4-15. Absorption Cross Sections of N ₂ O ₅	4-18
Table 4-16. Absorption Cross Sections of HONO.....	4-19
Table 4-17. Absorption Cross Sections and Temperature Coefficients of HNO ₃ Vapor.....	4-20
Table 4-18. Absorption Cross Sections of HO ₂ NO ₂ Vapor.....	4-20
Table 4-19. Absorption Cross Sections and Quantum Yields for Photolysis of CH ₂ O.....	4-21
Table 4-20. Absorption Cross Sections of CH ₃ O ₂ , C ₂ H ₅ O ₂ , and CH ₃ C(O)O ₂	4-22
Table 4-21. Absorption Cross Sections of CH ₃ OOH.....	4-23
Table 4-22. Absorption Cross Sections of PAN.....	4-25
Table 4-23. Absorption Cross Sections of FNO.....	4-26
Table 4-24. Absorption Cross Sections of CCl ₂ O, CCIFO, and CF ₂ O at 298 K.....	4-27
Table 4-25. Absorption Cross Sections of Cl ₂	4-28
Table 4-26. Absorption Cross Sections of ClOO.....	4-29
Table 4-27. Absorption Cross Sections of OCIO at the Band Peaks.....	4-30
Table 4-28. Absorption Cross Sections of Cl ₂ O.....	4-32
Table 4-29. Absorption Cross Sections of ClOOCl at 200–250 K.....	4-33
Table 4-30. Absorption Cross Sections of Cl ₂ O ₃	4-34
Table 4-31. Absorption Cross Sections of Cl ₂ O ₄	4-34
Table 4-32. Absorption Cross Sections of Cl ₂ O ₆	4-34
Table 4-33. Absorption Cross Sections of HCl Vapor.....	4-35
Table 4-34. Absorption Cross Sections of HOCl.....	4-36
Table 4-35. Absorption Cross Sections of ClNO.....	4-37
Table 4-36. Absorption Cross Sections of ClNO ₂	4-37
Table 4-37. Absorption Cross Sections of ClONO at 231 K.....	4-38
Table 4-38. Absorption Cross Sections of ClONO ₂	4-39
Table 4-39. Absorption Cross Sections of CCl ₄ at 295–298 K.....	4-41
Table 4-40. Absorption Cross Sections of CH ₃ OCl.....	4-42
Table 4-41. Absorption Cross Sections of CHCl ₃ at 295–298 K.....	4-43
Table 4-42. Absorption Cross Sections of CH ₂ Cl ₂ at 295–298 K.....	4-44
Table 4-43. Absorption Cross Sections of CH ₃ Cl at 295–298 K.....	4-46
Table 4-44. Absorption Cross Sections of CH ₃ CCl ₃ at 295–298 K.....	4-47
Table 4-45. Absorption Cross Sections of CH ₃ CH ₂ Cl at 298 K.....	4-47
Table 4-46. Absorption Cross Sections of CH ₃ CHClCH ₃ at 295 K.....	4-48
Table 4-47. Absorption Cross Sections of CFCl ₃ at 295–298 K.....	4-49
Table 4-48. Absorption Cross Sections of CF ₂ Cl ₂ at 295–298 K.....	4-50

Table 4-49. Absorption Cross Sections of CF ₃ Cl at 295 K.....	4-51
Table 4-50. Absorption Cross Sections of CF ₂ ClCFCl ₂ at 295–298 K.....	4-52
Table 4-51. Absorption Cross Sections of CF ₂ ClCF ₂ Cl at 295 K.....	4-53
Table 4-52. Absorption Cross Sections of CF ₃ CF ₂ Cl at 295–298 K.....	4-53
Table 4-53. Absorption Cross Sections of CHFCl ₂ at 295–298 K.....	4-54
Table 4-54. Absorption Cross Sections of CHF ₂ Cl at 295–298 K.....	4-55
Table 4-55. Absorption Cross Sections of CH ₂ FCl at 298 K.....	4-55
Table 4-56. Absorption Cross Sections of CF ₃ CHCl ₂ at 295 K.....	4-56
Table 4-57. Absorption Cross Sections of CF ₃ CHFCl at 295 K.....	4-57
Table 4-58. Absorption Cross Sections of CF ₃ CH ₂ Cl at 298 K.....	4-58
Table 4-59. Absorption Cross Sections of CH ₃ CFCl ₂ at 295–298 K.....	4-59
Table 4-60. Absorption Cross Sections of CH ₃ CF ₂ Cl at 295–298 K.....	4-60
Table 4-61. Absorption Cross Sections of CF ₃ CF ₂ CHCl ₂ and CF ₂ ClCF ₂ CFCl at 298 K.....	4-61
Table 4-62. Absorption Cross Sections at the Peak of Various Bands in the A ← X Spectrum of BrO.....	4-62
Table 4-63. Absorption Cross Sections of BrO.....	4-62
Table 4-64. Absorption Cross Sections of HOBr.....	4-65
Table 4-65. Absorption Cross Sections of BrONO ₂ at 298 K.....	4-66
Table 4-66. Absorption Cross Sections of BrCl at 298 K.....	4-67
Table 4-67. Absorption Cross Sections of CH ₃ Br at 295–296 K.....	4-69
Table 4-68. Absorption Cross Sections of CH ₂ Br ₂ at 295–298 K.....	4-70
Table 4-69. Absorption Cross Sections of CHBr ₃ at 295–296 K.....	4-71
Table 4-70. Absorption Cross Sections of CH ₂ BrCH ₂ Br at 295 K.....	4-72
Table 4-71. Absorption Cross Sections of C ₂ H ₅ Br at 295 K.....	4-72
Table 4-72. Absorption Cross Sections of CH ₂ ClBr at 295 K.....	4-73
Table 4-73. Absorption Cross Sections of CHClBr ₂ at 296 K.....	4-74
Table 4-74. Absorption Cross Sections of CHCl ₂ Br at 298 K.....	4-75
Table 4-75. Absorption Cross Sections of CCl ₃ Br at 298 K.....	4-75
Table 4-76. Absorption Cross Sections of CHF ₂ Br at 298 K.....	4-76
Table 4-77. Absorption Cross Sections of CF ₂ Br ₂ at 295–296 K.....	4-78
Table 4-78. Absorption Cross Sections of CF ₂ ClBr at 295–298 K.....	4-80
Table 4-79. Absorption Cross Sections of CF ₃ Br at 295–298 K.....	4-82
Table 4-80. Absorption Cross Sections of CF ₃ CH ₂ Br at 295 K.....	4-82
Table 4-81. Absorption Cross Sections of CF ₃ CHClBr at 295–298 K.....	4-84
Table 4-82. Absorption Cross Sections of CF ₃ CHBr at 295 K.....	4-84
Table 4-83. Absorption Cross Sections of CF ₂ BrCF ₂ Br at 296 K.....	4-86
Table 4-84. Absorption Cross Sections of CF ₃ CF ₂ Br at 298 K.....	4-87
Table 4-85. Absorption Cross Sections of CH ₃ I at 296–298 K and Temperature Coefficients.....	4-88
Table 4-86. Absorption Cross Sections of CH ₂ I ₂ at 298 K.....	4-89
Table 4-87. Absorption Cross Sections of C ₂ H ₅ I at 298 K and Temperature Coefficients.....	4-90
Table 4-88. Absorption Cross Sections of CH ₃ CHI ₂ at 298 K.....	4-91
Table 4-89. Absorption Cross Sections of C ₃ H ₇ I at 298 K and Temperature Coefficients.....	4-92
Table 4-90. Absorption Cross Sections of (CH ₃) ₃ CI at 298 K.....	4-93
Table 4-91. Absorption Cross Sections of CF ₃ I at 295–300 K.....	4-95
Table 4-92. Absorption Cross Sections of CF ₂ I ₂ at 294 K.....	4-96
Table 4-93. Absorption Cross Sections of C ₂ F ₅ I at 323 K.....	4-96
Table 4-94. Absorption Cross Sections of 1-C ₃ F ₇ I at 295–298 K.....	4-97
Table 4-95. Absorption Cross Sections of CH ₂ ICl at 298 K and Temperature Coefficients.....	4-98
Table 4-96. Absorption Cross Sections of CH ₂ BrI at 298 K and Temperature Coefficients.....	4-99
Table 4-97. Absorption Cross Sections of OCS.....	4-100
Table 4-98. Absorption Cross Sections of NaCl Vapor at 300 K.....	4-101

Figures

Figure 4-1. Absorption Spectrum of NO ₃	4-15
Figure 4-2. Absorption Spectrum of ClO.....	4-29
Figure 4-3. Absorption Spectrum of OCIO.....	4-31
Figure 4-4. Absorption Spectrum of BrO.....	4-63

4.1 Format and Error Estimates

In Table 4-1 we present a list of photochemical reactions considered to be of stratospheric interest. The absorption cross sections of O₂ and O₃ largely determine the extent of penetration of solar radiation into the stratosphere and troposphere. Some comments and references to these cross sections are presented in the text, but only a sample of the data is listed here. (See, for example, WMO Report No. 11 [1]; WMO Report No. 16 [434]) The photodissociation of NO in the O₂ Schumann-Runge band spectral range is another important process requiring special treatment and is not discussed in this evaluation (see, for example, Frederick and Hudson [123]; Allen and Frederick [8]; WMO Report No. 11 [1], and Minschwaner and Siskind [259]).

For some other species having highly structured spectra, such as CS₂ and SO₂, some comments are given in the text, but the photochemical data are not presented. The species CH₂O, NO₂, NO₃, ClO, BrO, and OClO also have complicated spectra, but in view of their importance for atmospheric chemistry a sample of the data is presented in the evaluation; for more detailed information on their high-resolution spectra and temperature dependence, the reader is referred to the original literature.

Table 4-2 gives recommended reliability factors for some of the more important photochemical reactions. These factors represent the combined uncertainty in cross sections and quantum yields, taking into consideration the atmospherically important wavelength regions, and they refer to the total dissociation rate regardless of product identity. The exception is O(¹D) production from photolysis of O₃: the reliability factor applies to the quantum yield at the indicated wavelengths.

The error estimates are not rigorous numbers resulting from a detailed error propagation analysis of statistical manipulations of the different sets of literature values; they merely represent a consensus among the panel members as to the reliability of the data for atmospheric photodissociation calculations, taking into account the difficulty of the measurements, the agreement among the results reported by various groups, etc.

The absorption cross sections are defined by the following expression of Beer's Law:

$$I = I_0 \exp(-\sigma n l),$$

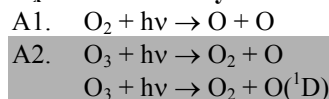
where I₀ and I are the incident and transmitted light intensity, respectively; σ is the absorption cross section in cm² molecule⁻¹; n is the concentration in molecule cm⁻³; and l is the pathlength in cm. The cross sections are room temperature values at the specific wavelengths listed in the table, and the expected photodissociation quantum yields are unity, unless otherwise stated.

4.2 Halocarbon Absorption Cross Sections and Quantum Yields

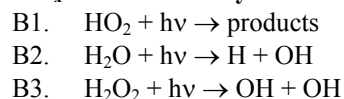
The primary process in the photodissociation of chlorinated hydrocarbons is well established: absorption of ultraviolet radiation in the lowest frequency band is interpreted as an n-σ* transition involving excitation to a repulsive electronic state (antibonding in C-Cl), which dissociates by breaking the carbon-chlorine bond (Majer and Simons [228]). As expected, the chlorofluoromethanes, which are a particular type of chlorinated hydrocarbons, behave in this fashion (Sandorfy [361]). Hence, the quantum yield for photodissociation is expected to be unity for these compounds. There are several studies that show specifically that this is the case for CF₂Cl₂, CFCl₃, and CCl₄. These studies, which have been reviewed in CODATA [82], also indicate that at shorter wavelengths, two halogen atoms can be released simultaneously in the primary process.

Table 4-1. Photochemical Reactions

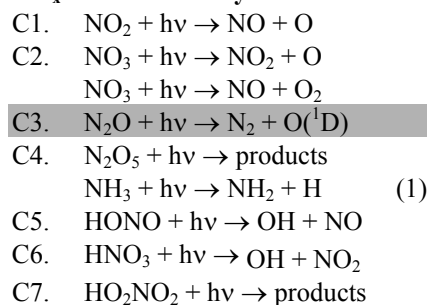
O_x Photochemistry



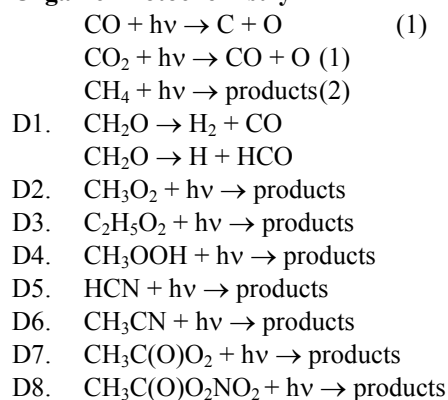
HO_x Photochemistry



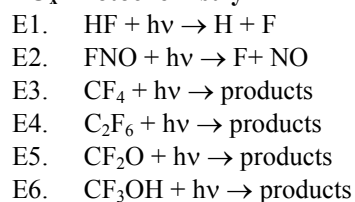
NO_x Photochemistry



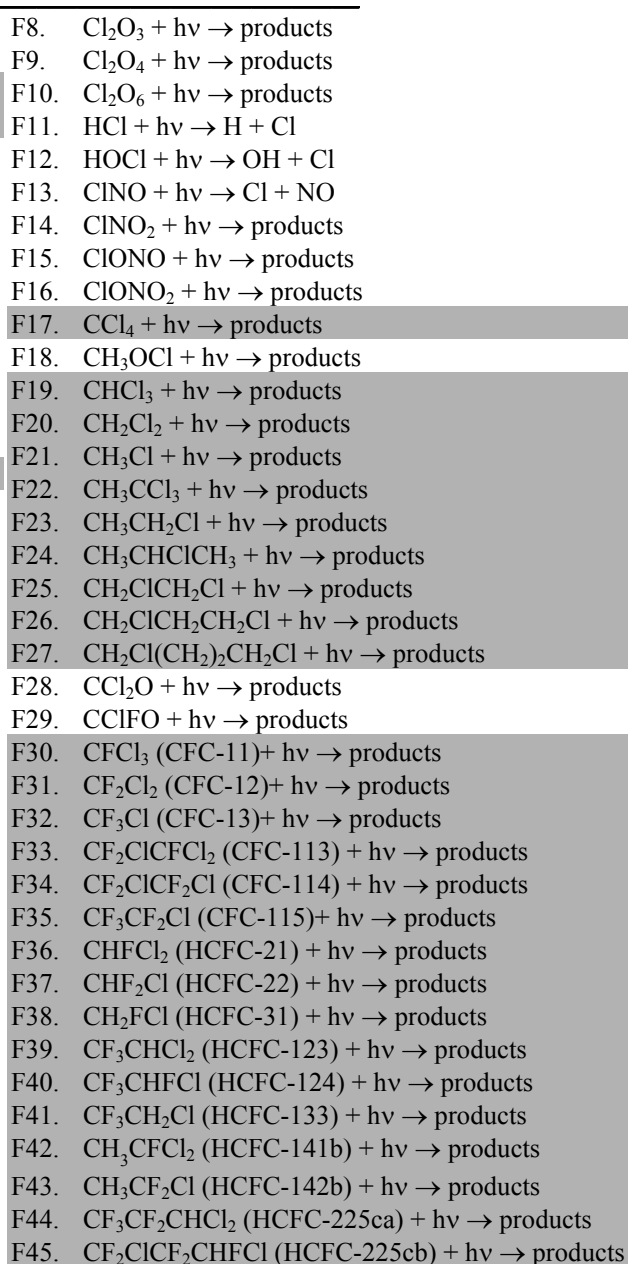
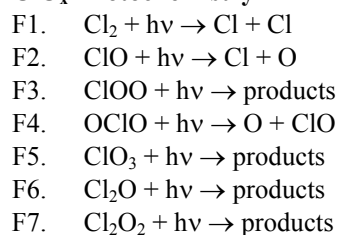
Organic Photochemistry



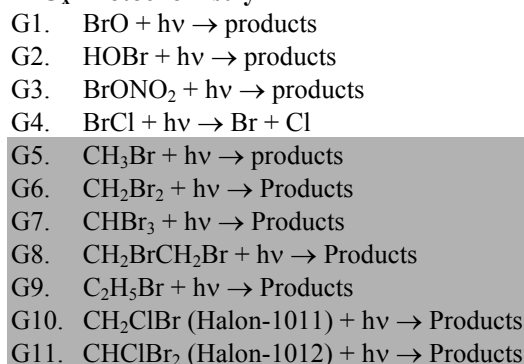
FO_x Photochemistry



ClO_x Photochemistry



BrO_x Photochemistry



G12. CHCl_2Br (Halon-1021) + $h\nu \rightarrow$ Products
 G13. CCl_3Br (Halon-1031) + $h\nu \rightarrow$ Products
 G14. CHF_2Br (Halon-1201) + $h\nu \rightarrow$ Products
 G15. CF_2Br_2 (Halon-1202) + $h\nu \rightarrow$ Products
 G16. CF_2ClBr (Halon-1211) + $h\nu \rightarrow$ Products
 G17. CF_3Br (Halon-1301) + $h\nu \rightarrow$ Products
 G18. $\text{CF}_3\text{CH}_2\text{Br}$ (Halon-2301) + $h\nu \rightarrow$ Products
 G19. CF_3CHClBr (Halon-2311) + $h\nu \rightarrow$ Products
 G20. CF_3CHFBr (Halon-2401) + $h\nu \rightarrow$ Products
 G21. $\text{CF}_2\text{BrCF}_2\text{Br}$ (Halon-2402) + $h\nu \rightarrow$ Products
 G22. $\text{CF}_3\text{CF}_2\text{Br}$ (Halon-2501) + $h\nu \rightarrow$ Products

IO_x Photochemistry

H1. $\text{CH}_3\text{I} + h\nu \rightarrow \text{CH}_3 + \text{I}({}^2\text{P}_{3/2})$
 H2. $\text{CH}_3\text{I} + h\nu \rightarrow \text{CH}_3 + \text{I}^*({}^2\text{P}_{1/2})$
 H3. $\text{CH}_2\text{I}_2 + h\nu \rightarrow \text{CH}_2\text{I} + \text{I}({}^2\text{P}_{3/2})$
 H4. $\text{CH}_2\text{I}_2 + h\nu \rightarrow \text{CH}_2\text{I} + \text{I}^*({}^2\text{P}_{1/2})$
 H5. $\text{C}_2\text{H}_5\text{I} + h\nu \rightarrow \text{C}_2\text{H}_5 + \text{I}({}^2\text{P}_{3/2})$
 H6. $\text{C}_2\text{H}_5\text{I} + h\nu \rightarrow \text{C}_2\text{H}_5 + \text{I}^*({}^2\text{P}_{1/2})$
 H7. $\text{CH}_3\text{CHI}_2 + h\nu \rightarrow$ Products
 H8. $\text{CH}_3\text{CH}_2\text{CH}_2\text{I} + h\nu \rightarrow$ Products
 H9. $\text{CH}_3\text{CHICH}_3 + h\nu \rightarrow$ Products
 H10. $\text{C}_4\text{H}_9\text{I} + h\nu \rightarrow \text{C}_4\text{H}_9 + \text{I}({}^2\text{P}_{3/2})$
 H11. $\text{C}_4\text{H}_9\text{I} + h\nu \rightarrow \text{C}_4\text{H}_9 + \text{I}^*({}^2\text{P}_{1/2})$
 H12. $(\text{CH}_3)_2\text{CHCH}_2\text{I} + h\nu \rightarrow (\text{CH}_3)_2\text{CCH}_2 + \text{I}({}^2\text{P}_{3/2})$
 H13. $(\text{CH}_3)_2\text{CHCH}_2\text{I} + h\nu \rightarrow (\text{CH}_3)_2\text{CCH}_2 + \text{I}^*({}^2\text{P}_{1/2})$
 H14. $\text{CH}_3)_3\text{CI} + \rightarrow (\text{CH}_3)_3\text{C} + \text{I}({}^2\text{P}_{3/2})$
 H15. $(\text{CH}_3)_3\text{CI} + \rightarrow (\text{CH}_3)_3\text{C} + \text{I}^*({}^2\text{P}_{1/2})$
 H16. $\text{C}_5\text{H}_{11}\text{I} + h\nu \rightarrow \text{C}_5\text{H}_{11} + \text{I}({}^2\text{P}_{3/2})$
 H17. $\text{C}_5\text{H}_{11}\text{I} + h\nu \rightarrow \text{C}_5\text{H}_{11} + \text{I}^*({}^2\text{P}_{1/2})$

H18. $\text{CF}_3\text{I} + h\nu \rightarrow \text{CF}_3 + \text{I}({}^2\text{P}_{3/2})$
 H19. $\text{CF}_3\text{I} + h\nu \rightarrow \text{CF}_3 + \text{I}^*({}^2\text{P}_{1/2})$
 H20. $\text{CF}_2\text{I}_2 + h\nu \rightarrow \text{CF}_2\text{I} + \text{I}({}^2\text{P}_{3/2})$
 H21. $\text{CF}_2\text{I}_2 + h\nu \rightarrow \text{CF}_2\text{I} + \text{I}^*({}^2\text{P}_{1/2})$
 H22. $\text{CF}_2\text{I}_2 + h\nu \rightarrow \text{CF}_2 + \text{I}({}^2\text{P}_{3/2}) + \text{I}({}^2\text{P}_{3/2})$
 H23. $\text{CF}_2\text{I}_2 + h\nu \rightarrow \text{CF}_2 + \text{I}({}^2\text{P}_{3/2}) + \text{I}^*({}^2\text{P}_{1/2})$
 H24. $\text{C}_2\text{F}_5\text{I} + h\nu \rightarrow \text{C}_2\text{F}_5 + \text{I}({}^2\text{P}_{3/2})$
 H25. $\text{C}_2\text{F}_5\text{I} + h\nu \rightarrow \text{C}_2\text{F}_5 + \text{I}^*({}^2\text{P}_{1/2})$
 H26. $\text{C}_3\text{F}_7\text{I} + h\nu \rightarrow \text{C}_3\text{F}_7 + \text{I}({}^2\text{P}_{3/2})$
 H27. $\text{C}_3\text{F}_7\text{I} + h\nu \rightarrow \text{C}_3\text{F}_7 + \text{I}^*({}^2\text{P}_{1/2})$
 H28. $\text{C}_4\text{F}_9\text{I} + h\nu \rightarrow \text{C}_4\text{F}_9 + \text{I}({}^2\text{P}_{3/2})$
 H29. $\text{C}_4\text{F}_9\text{I} + h\nu \rightarrow \text{C}_4\text{F}_9 + \text{I}^*({}^2\text{P}_{1/2})$
 H30. $\text{C}_6\text{F}_{13}\text{I} + h\nu \rightarrow \text{C}_6\text{F}_{13} + \text{I}({}^2\text{P}_{3/2})$
 H31. $\text{C}_6\text{F}_{13}\text{I} + h\nu \rightarrow \text{C}_6\text{F}_{13} + \text{I}^*({}^2\text{P}_{1/2})$
 H32. $\text{CH}_2\text{ICl} + h\nu \rightarrow \text{CH}_2\text{Cl} + \text{I}$
 H33. $\text{CH}_2\text{BrI} + h\nu \rightarrow \text{CH}_2\text{I} + \text{Br}$
 H34. $\text{CH}_2\text{BrI} + h\nu \rightarrow \text{CH}_2\text{Br} + \text{I}$
 H35. $\text{CF}_2\text{BrCF}_2\text{I} + h\nu \rightarrow \text{CF}_2\text{BrCF}_2 + \text{I}$
 H36. $\text{CF}_2\text{BrCF}_2\text{I} + h\nu \rightarrow \text{CF}_2\text{ICF}_2 + \text{Br}$

SO_x Photochemistry

I1. $\text{SO}_2 + h\nu \rightarrow \text{SO} + \text{O}$
 $\text{H}_2\text{S} + h\nu \rightarrow \text{HS} + \text{H}$ (1)
 I2. $\text{CS}_2 + h\nu \rightarrow \text{CS} + \text{S}$
 I3. $\text{OCS} + h\nu \rightarrow \text{CO} + \text{S}$
 I4. $\text{SF}_6 + h\nu \rightarrow$ products

Metal Photochemistry

J.1 $\text{NaOH} + h\nu \rightarrow \text{Na} + \text{OH}$
 J.2 $\text{NaCl} + h\nu \rightarrow \text{Na} + \text{Cl}$

- (1) Hudson and Kieffer [170].
- (2) Turco [405].
- (3) Shaded areas indicate changes or additions since JPL 97-4/JPL 00-3.

Table 4-2. Combined Uncertainties for Cross Sections and Quantum Yields

Species	Uncertainty	Notes
O ₂ (Schumann-Runge bands)	1.2	
O ₂ (Continua)	1.2	
O ₃ (Cross Sections Only)	1.1	
O ₃ → O(¹ D), λ > 310 nm	1.3	
O ₃ → O(¹ D), 290 < λ < 310 nm	1.2	
H ₂ O ₂	1.3	
NO ₂	1.2	
NO ₃	1.5	
N ₂ O	1.2	
N ₂ O ₅	2.0	
HNO ₃	1.3	
HO ₂ NO ₂	2.0	
CH ₂ O	1.4	
CH ₃ OOH	1.5	
CH ₃ C(O)O ₂ NO ₂	1.3	λ < 300 nm
CH ₃ C(O)O ₂ NO ₂	2.0	λ ≥ 300 nm
HCl	1.1	
HOCl	1.4	
ClOOCl	1.5	λ < 300 nm
ClOOCl	3.0	λ ≥ 300 nm
Cl ₂ O ₃	1.5	λ < 300 nm
Cl ₂ O ₃	3.0	λ ≥ 300 nm
ClONO ₂	1.3	
CCl ₄	1.1	
CCl ₃ F	1.1	
CCl ₂ F ₂	1.1	
CH ₃ Cl	1.1	
CF ₂ O	2.0	
CF ₃ Br	1.3	
CF ₂ ClBr	2.0	
CF ₂ Br ₂	2.0	
C ₂ F ₄ Br ₂	2.0	
HOBr	2.0	λ < 350 nm
HOBr	10	λ ≥ 350 nm
BrONO ₂	1.4	

- A1. $O_2 + h\nu \rightarrow O + O$. The photodissociation of molecular oxygen in the stratosphere is due primarily to absorption of solar radiation in the 200–220 nm wavelength region, i.e., within the Herzberg continuum. The 185–200-nm region—the O_2 Schumann-Runge band spectral range—is also very important, since solar radiation penetrates efficiently into the stratosphere at those wavelengths.

Frederick and Mentall [124] Herman and Mentall [158] and Anderson and Hall [14,15] estimated O_2 absorption cross sections from balloon measurements of solar irradiance in the stratosphere. These authors find the cross sections in the 200–210 nm range to be ~35% smaller than the smallest of the older laboratory results, which are those of Shardanand and Prasad Rao [373]. The more recent laboratory studies (Johnston et al. [190]; Cheung et al. [73,74], Jenouvrier et al. [183]) confirm the lower values obtained from solar irradiance measurements. The recommended absorption cross section values between 205 and 240 nm are listed in Table 4-3; they are taken from Yoshino et al. [438] and are based on the latter set of laboratory measurements. Amoruso et al. [11] have also carried out cross section measurements in this wavelength range (the Herzberg continuum); their values are ~15% lower than those reported by Yoshino et al.

Table 4-3. Absorption Cross Sections of O_2 Between 205 and 240 nm

λ (nm)	$10^{24} \sigma$ (cm ²)	λ (nm)	$10^{24} \sigma$ (cm ²)
205	7.35	223	3.89
206	7.13	224	3.67
207	7.05	225	3.45
208	6.86	226	3.21
209	6.68	227	2.98
210	6.51	228	2.77
211	6.24	229	2.63
212	6.05	230	2.43
213	5.89	231	2.25
214	5.72	232	2.10
215	5.59	233	1.94
216	5.35	234	1.78
217	5.13	235	1.63
218	4.88	236	1.48
219	4.64	237	1.34
220	4.46	238	1.22
221	4.26	239	1.10
222	4.09	240	1.01

The studies of the penetration of solar radiation in the atmosphere in the Schumann-Runge wavelength region were based originally on laboratory measurements of cross sections that were affected by instrumental parameters due to insufficient spectral resolution. Yoshino et al. [446] reported high resolution O_2 cross section measurements at 300 K, between 179 and 202 nm, obtaining the first set of results, which is independent of the instrument width. Additional studies at other temperatures, wavelengths, and isotopic compositions have been carried out by Yoshino et al. [439,442–445], Lewis et al. [214,215], Cheung et al. [72], and Chiu et al. [75]. More recently, Yoshino et al. [440] reported cross sections of the Schumann-Runge bands in the window region between the rotational lines for wavelengths between 180 and 195 nm; these measurements supersede their earlier ones. Minschwaner et al. [258] have fit temperature-dependent O_2 cross sections between 175 and 204 nm with polynomial expressions, providing accurate means of determining the Schumann-Runge band cross sections with a model that incorporates the most recent laboratory data. Coquart et al. [86] have reported Herzberg continuum absorption cross sections in the wavelength region 196–205 nm of the Schumann-Runge bands.

For parameterizations of the O_2 absorption in the Schumann-Runge bands used in atmospheric modeling calculations, see, e.g., the review in WMO Report No. 16 [434]. More recent work by Murtagh [285], Nicolet and Kennes, [294] and Minschwaner et al. [258] incorporates results of the later laboratory measurements into efficient schemes for computing broad-band transmission and photolysis rates. Transmission values obtained by Murtagh [285] agree well with the WMO [434] recommendations, although the high-resolution calculations of Minschwaner and Salawitch differ with the WMO values by as much as 10–20% at some wavelengths.

In view of the quality of the high-resolution laboratory measurements, the primary source of uncertainty in modeling O₂ photolysis in the Schumann-Runge bands (other than the issue of absolute solar irradiance) has shifted to the choice of broadband parameterization.

- A2. O₃ + hv → O + O₂. The O₃ absorption cross sections and their temperature dependence have been measured by several groups. An earlier review is presented in WMO Report No. 16 [434]; this reference should be consulted to obtain data for atmospheric modeling calculations. Table 4-4 lists merely a sample of the data taken from this review, namely the 273 K cross section values averaged over the wavelength intervals commonly employed in modeling calculations, except for the wavelength range 185 to 225 nm, where the present recommendation incorporates the averaged values from the work of Molina and Molina [270]; the older values were based on the work of Inn and Tanaka [179]. More recently, Daumont et al. [101] and Brion et al. [43] reported ozone absorption cross section measurements between 195 and 345 nm, in the temperature range 200–300 K; and Yoshino et al. [441] measured the cross sections in the 185 to 254 nm wavelength range at 195, 228, and 295 K; the results of these studies yield values in very good agreement with those reported by Molina and Molina [270]. Cacciani et al. [63] reported measurements of the ozone cross sections in the wavelength range from 339 to 355 nm, in reasonable agreement with the present recommendation; the same group has measured also the cross sections in the 590–610 nm region, at 230 K and at 299 K (Amoruso et al. [9]). The temperature effect on the cross sections is negligible for wavelengths shorter than ~260 nm. Recent work by Mauersberger et al. [245,246] yields a value of $1137 \times 10^{-20} \text{ cm}^2$ for the cross section at 253.7 nm, the mercury line wavelength; it is about 1% smaller than the commonly accepted value of $1147 \times 10^{-20} \text{ cm}^2$ reported by Hearn [156]; about 2% smaller than the value obtained by DeMore and Raper [106] and Molina and Molina [270], $1157 \times 10^{-20} \text{ cm}^2$; and 0.5% larger than the value obtained by Daumont et al. [101]. The reason for the small discrepancy, which appears to be beyond experimental precision, is unclear.

Malicet et al. [229] report cross section measurements in the 195–345 nm range, at temperatures between 218 and 295 K, with a spectral bandwidth of 0.01–0.02 nm.; the results are in good agreement with the recommended values. Their data are presented in graphical form, and are also available in electronic format.

Table 4-4. Absorption Cross Sections of O₃ at 273 K

λ (nm)	$10^{20} \sigma$ (cm ²) average	λ (nm)	$10^{20} \sigma$ (cm ²) average
175.439–176.991	81.1	238.095–240.964	797
176.991–178.571	79.9	240.964–243.902	900
178.571–180.180	78.6	243.902–246.914	1000
180.180–181.818	76.3	246.914–250.000	1080
181.818–183.486	72.9	250.000–253.165	1130
183.486–185.185	68.8	253.165–256.410	1150
185.185–186.916	62.2	256.410–259.740	1120
186.916–188.679	57.6	259.740–263.158	1060
188.679–190.476	52.6	263.158–266.667	965
190.476–192.308	47.6	266.667–270.270	834
192.308–194.175	42.8	270.270–273.973	692
194.175–196.078	38.3	273.973–277.778	542
196.078–198.020	34.7	277.778–281.690	402
198.020–200.000	32.3	281.690–285.714	277
200.000–202.020	31.4	285.714–289.855	179
202.020–204.082	32.6	289.855–294.118	109
204.082–206.186	36.4	294.118–298.507	62.4
206.186–208.333	43.4	298.507–303.030	34.3
208.333–210.526	54.2	303.030–307.692	18.5
210.526–212.766	69.9	307.692–312.5	9.80
212.766–215.054	92.1	312.5–317.5	5.01
215.054–217.391	119	317.5–322.5	2.49
217.391–219.780	155	322.5–327.5	1.20
219.780–222.222	199	327.5–332.5	0.617
222.222–224.719	256	332.5–337.5	0.274
224.719–227.273	323	337.5–342.5	0.117

λ (nm)	$10^{20} \sigma$ (cm ²) average	λ (nm)	$10^{20} \sigma$ (cm ²) average
227.273–229.885	400	342.5–347.5	0.0588
229.885–232.558	483	347.5–352.5	0.0266
232.558–235.294	579	352.5–357.5	0.0109
235.294–238.095	686	357.5–362.5	0.00549

The recommendation for the O(¹D) quantum yield from ozone photolysis as a function of wavelength and temperature is given by the expression,

$$\Phi(\lambda, T) = \left(\frac{q_1}{q_1 + q_2} \right) \times A_1 \times \exp \left\{ - \left(\frac{X_1 - \lambda}{\omega_1} \right)^4 \right\} + \left(\frac{q_2}{q_1 + q_2} \right) \times A_2 \times \left(\frac{T}{300} \right)^2 \times \exp \left\{ - \left(\frac{X_2 - \lambda}{\omega_2} \right)^2 \right\} + A_3 \times \left(\frac{T}{300} \right)^{1.5} \times \exp \left\{ - \left(\frac{X_3 - \lambda}{\omega_3} \right)^2 \right\} + c$$

where $q_i = \exp \left(- \frac{v_i}{RT} \right)$ and X_{1-3} , A_{1-3} , ω_{1-3} , v_{1-2} and c are best-fit parameters given in Table 4-5, λ is in nm, T is in K, and $R = 0.695$ (cm⁻¹/K). The parameter c is assumed to be temperature and wavelength independent. **This expression is valid only for the wavelength range 306–328 nm and temperature range 200–320 K.**

Table 4-5. Parameters for the Calculation of O(¹D) Quantum Yields

Parameter	i = 1	i = 2	i = 3
X_i (nm)	304.225	314.957	310.737
ω_i (nm)	5.576	6.601	2.187
A_i	0.8036	8.9061	0.1192
v_i (cm ⁻¹)	0	825.518	–
c	0.0765	–	–

At room temperature (298 K) the uncertainties of the quantum yield values calculated with the above expression are estimated to be $\pm 10\%$ (1σ) for $\Phi(\lambda, 298 \text{ K}) \geq 0.4$, while the uncertainties are estimated to be ± 0.04 for $\Phi(\lambda, 298 \text{ K}) < 0.4$. At temperatures other than room temperature, the uncertainties are estimated to be $\pm 15\%$ for $\Phi(\lambda, T) \geq 0.4$ and ± 0.06 for $\Phi(\lambda, T) < 0.4$.

In the wavelength range 329–340 nm we recommend the value of $\Phi(\text{O}^1\text{D}) = 0.08 \pm 0.04$, independent of temperature. For $\lambda > 340$ nm, the quantum yield may be non-zero but no recommendation is made. For $\lambda < 306$ nm, the recommended quantum yield is 0.90, independent of temperature.

The recommendation for the temperature and wavelength dependences of the quantum yield for O(¹D) production, $\Phi(\text{O}^1\text{D})$, is taken from the review of Matsumi et al. [244]. Matsumi et al. derived the recommended values using the following procedure: The measured O(¹D) quantum yields at 298 K between 306 and 328 nm from eight studies (Talukdar et al. [398], Takahashi et al. [392], Ball et al. [19], Armerding et al. [16], Bauer et al. [28], Brock and Watson [44], Trolier and Wiesenfeld [403] and Smith et al. [383], were normalized using $\Phi(\text{O}^1\text{D}) = 0.79$ at 308 nm. This value was derived from the studies listed in Table 1 of Matsumi et al. [244]. The resulting renormalized data were averaged. The wavelength dependence quantum yield data at various temperatures reported by Talukdar et al. [396,398], Takahashi et al. [392], Hancock and Hofzumahaus [149] (this includes all the data from the Oxford group), Bauer et al. [28] and Smith et al. [383] were normalized to the value at 308 nm given above. These normalized data were used to obtain the best-fit parameters for eqn. 4-1 for the wavelength range 306–328 nm and temperature range 200–320 K. Because of the large number of studies upon which the 298 K evaluation is based, the averaged 298 K data were given a larger weight in the fitting procedure than the data at other temperatures.

The major differences between this recommendation and that of JPL 00-3 [358] are: (1) inclusion of more recent data from Smith et al., Hancock and Hofzumahaus, and Bauer et al., (2) selective deletion of data from

the previous data from some of the groups, especially the use of data from Bauer et al. [28] which superseded the data of Silvente et al. [375] from the same group, (3) correcting for small differences in the absorption cross sections of ozone used by various groups, and (4) the normalization of all data to the selected value at 308 nm.

- B1. $\text{HO}_2 + h\nu \rightarrow \text{OH} + \text{H}$. The absorption cross sections of the hydroperoxyl radical, HO_2 , in the 190–260 nm region have been measured at room temperature by Paukert and Johnston [311], Hochanadel et al. [161], Cox and Burrows [89], McAdam et al. [250], Kurylo et al. [206], Moortgat et al. [280], Dagaut and Kurylo [99], Lightfoot and Jemi-Alade [218], who measured the cross sections up to 777 K, Crowley et al. [97], Maricq and Szente [238], Roehl et al. [342] and Sander et al. [359] at 227.5 nm. The absorption cross sections have been evaluated in earlier reviews by Lightfoot et al. [217] and Wallington et al. [426] who noted significant discrepancies in both the shapes of the spectra and the absolute magnitudes of the cross section values, particularly around 200 nm. The published ultraviolet absorption spectra have recently been reevaluated by Tyndall et al. [408]. Herein, the spectra were fitted to an analytical equation suggested by Maric et al. [237]:

$$\sigma = \frac{\sigma_{\text{med}}}{\nu(1-b)} \exp^{-a \left[\ln \left(\frac{\nu-b}{\nu_{\text{med}}-b} \right) \right]^2}$$

where $\sigma_{\text{med}} = 1.84 \times 10^{-18} \text{ cm}^2 \text{ molecule}^{-1}$, $a = 4.91$, $b = 30612 \text{ cm}^{-1}$ and $\nu_{\text{med}} = 50260 \text{ cm}^{-1}$. Absolute cross sections were based on relative measurements of absorption cross sections of HO_2 , CH_3O_2 and $\text{C}_2\text{H}_5\text{O}_2$ at 240 nm taken under identical conditions, combined with independent calibrations by Crowley et al. [97]. Table 4-6 lists the recommended cross sections, which are taken from the review by Tyndall et al. [408].

Lee [212] has detected $\text{O}(^1\text{D})$ as a primary photodissociation product at 193 and at 248 nm, with a quantum yield that is about 15 times larger at the longer wavelength. The absolute quantum yield for $\text{O}(^1\text{D})$ production has not been reported yet.

Photolysis of HO_2 in the stratosphere and troposphere is slow and can be neglected, but the UV absorption cross sections are important in laboratory studies of reaction kinetics.

Table 4-6. Absorption Cross Sections of HO_2

λ (nm)	$10^{20} \sigma$ (cm^2)
190	368
195	402
200	423
205	427
210	415
215	385
220	341
225	288
230	230
235	173
240	122
245	79.7
250	48.0
255	26.3
260	12.9

- B2. $\text{H}_2\text{O} + h\nu \rightarrow \text{H} + \text{OH}$. Water vapor has a continuum absorption spectrum at wavelengths longer than 145 nm, with a maximum around 165 nm, the cross sections falling off rapidly toward longer wavelengths; the photodissociation threshold occurs at 246 nm. Below 69 nm the spectrum is also a continuum, and between 69 and 145 nm it consists of diffuse bands. In the atmosphere water vapor is photodissociated mainly by the solar Lyman alpha line (121.6 nm).

The absorption cross sections and the photochemistry of water vapor have been reviewed, for example, by Hudson [168,169], by Hudson and Kiefer [170], by Calvert and Pitts [65], and by Okabe [300].

The recommended absorption cross sections are taken from the review by Hudson and Kiefer [170] and are listed in Table 4-7 between 175 and 190 nm. At these wavelengths the quantum yield for production of H and

OH is unity. At shorter wavelengths H₂ and O are also formed as primary products. Stief et al. [388] report a quantum yield of 0.11 for this process between 105 and 145 nm.

Table 4-7. Absorption Cross Sections of H₂O Vapor

$\lambda(\text{nm})$	$10^{20}\sigma(\text{cm}^2)$
175.5	262.8
177.5	185.4
180.0	78.1
182.5	23.0
185.0	5.5
186.0	3.1
187.5	1.6
189.3	0.7

- B3. H₂O₂ + hν → OH + OH. The recommended 298 K absorption cross section values, listed in Table 4-8, are the mean of the data of Lin et al. [221], Molina and Molina [267], Nicovich and Wine [295], and Vaghjiani and Ravishankara [414]. Molina and Molina [267] supersedes the earlier results of Molina et al. [273]. Nicovich and Wine measured the cross sections at $\lambda \pm 230$ relative to the values at 202.6, $\sigma = 4.32 \times 10^{-19} \text{ cm}^2$, and at 228.8 nm, $\sigma = 1.86 \times 10^{-19} \text{ cm}^2$. The values are within 2% of the recommended value.

Table 4-8. Absorption Cross Sections of H₂O₂ Vapor

$\lambda(\text{nm})$	$10^{20}\sigma(\text{cm}^2)$		$\lambda(\text{nm})$	$10^{20}\sigma(\text{cm}^2)$	
	298 K	355 K		298 K	355 K
190	67.2		270	3.3	3.5
195	56.4		275	2.6	2.8
200	47.5		280	2.0	2.2
205	40.8		285	1.5	1.6
210	35.7		290	1.2	1.3
215	30.7		295	0.90	1.0
220	25.8		300	0.68	0.79
225	21.7		305	0.51	0.58
230	18.2	18.4	310	0.39	0.46
235	15.0	15.2	315	0.29	0.36
240	12.4	12.6	320	0.22	0.27
245	10.2	10.8	325	0.16	0.21
250	8.3	8.5	330	0.13	0.17
255	6.7	6.9	335	0.10	0.13
260	5.3	5.5	340	0.07	0.10
265	4.2	4.4	345	0.05	0.06
			350	0.04	0.05

Nicovich and Wine have measured the temperature dependence of these cross sections. They expressed the measured cross sections as the sum of two components: σ_1 , due to absorption from H₂O₂, which has the O–O stretch excited; and σ_0 , due to absorption by ground state molecules. For atmospheric calculations the expression given in Table 4-9 may be used. The photodissociation quantum yield is believed to be unity. At and above 248 nm, the major photodissociation process is that leading to OH, i.e., the quantum yield for OH production is 2 (Vaghjiani and Ravishankara [415] and Vaghjiani et al. [416]). At 193 nm this quantum yield decreases to about 1.5 (Vaghjiani et al. [416]; Schiffman et al. [364]), and the quantum yield for O-atom production increases to about 0.16 (Vaghjiani et al. [416]).

Table 4-9. Mathematical Expression for Absorption Cross Sections of H₂O₂ as a Function of Temperature

$$10^{21} \sigma(\lambda, T) = \chi \sum_{n=0}^7 A_n \lambda^n + (1 - \chi) \sum_{n=0}^4 B_n \lambda^n$$

Where T: temperature K; λ : nm; $\chi = (1 + \exp(-1265/T))^{-1}$

$A_0 = 6.4761 \times 10^4$	$B_0 = 6.8123 \times 10^3$
$A_1 = -9.2170972 \times 10^2$	$B_1 = -5.1351 \times 10^1$
$A_2 = 4.535649$	$B_2 = 1.1522 \times 10^{-1}$
$A_3 = -4.4589016 \times 10^{-3}$	$B_3 = -3.0493 \times 10^{-5}$
$A_4 = -4.035101 \times 10^{-5}$	$B_4 = -1.0924 \times 10^{-7}$
$A_5 = 1.6878206 \times 10^{-7}$	
$A_6 = -2.652014 \times 10^{-10}$	
$A_7 = 1.5534675 \times 10^{-13}$	

Range 260–350 nm; 200–400 K

- C1. $\text{NO}_2 + h\nu \rightarrow \text{NO} + \text{O}$. Earlier recommendations for the absorption cross sections of nitrogen dioxide were taken from the work of Bass et al. [26]. More recent measurements have been reported by Schneider et al. [367], at 298 K, for the wavelength range from 200 to 700 nm, and by Davidson et al. [103], from 270 to 420 nm, in the 232–397 K temperature range. At room temperature the agreement between these three sets of measurements is good (within 5% between 305 and 345 nm and within 10% at the longer wavelengths). The agreement is poor below room temperature, as well as at the shorter wavelengths. A possible cause for the discrepancies is the presence of N₂O₄. The corrections needed to account for the presence of this species are largest around 200 nm, where it absorbs strongly. The corrections are also large at the lowest temperatures, because a significant fraction of the NO₂ forms N₂O₄. On the other hand, there is no error apparent in the corrections carried out by Bass et al., so that the reason for the discrepancy is not clear. Measurements of the absorption cross sections in the visible (440 to 460 nm), between 273 and 404 K, have been reported by Amoroso et al. [10], and Corcoran et al. [87] carried out high-resolution measurements at a few selected wavelength ranges between 470 and 616 nm, at 295, 573, and 673 K. Additional high-resolution studies of the cross sections, mainly aimed at improving the accuracy of atmospheric measurements, have been reported by Harwood and Jones [152], Coquart et al. [85], Mérienne et al. [257], Frost et al. [125], and Harder et al. [150].

Table 4-10 lists the recommended absorption cross sections, averaged over the wavelength intervals used for atmospheric photodissociation calculations. For the wavelength range from 200 to 274 nm the values are taken from Schneider et al. [367]; in this range the temperature effect is negligible. For the 274-to-420-nm region the temperature-dependent values are taken from Davidson et al. [103].

Table 4-10. Absorption Cross Sections of NO₂

λ (nm)	$10^{20} \sigma$, average at 25°C (cm ² molecule ⁻¹)	λ (nm)	$10^{20} \sigma$, average at 0°C (cm ² molecule ⁻¹)	$10^{22} a^*$ (cm ² molecule ⁻¹ degree ⁻¹)
202.02–204.08	41.45	273.97–277.78	5.03	0.075
204.08–206.19	44.78	277.78–281.69	5.88	0.082
206.19–208.33	44.54	281.69–285.71	7.00	-0.053
208.33–210.53	46.41	285.71–289.85	8.15	-0.043
210.53–212.77	48.66	289.85–294.12	9.72	-0.031
212.77–215.06	48.18	294.12–298.51	11.54	-0.162
215.06–217.39	50.22	298.51–303.03	13.44	-0.284
217.39–219.78	44.41	303.03–307.69	15.89	-0.357
219.78–222.22	47.13	307.69–312.50	18.67	-0.536
222.22–224.72	37.72	312.5–317.5	21.53	-0.686
224.72–227.27	39.29	317.5–322.5	24.77	-0.786
227.27–229.89	27.40	322.5–327.5	28.07	-1.105
229.89–232.56	27.78	327.5–332.5	31.33	-1.355
232.56–235.29	16.89	332.5–337.5	34.25	-1.277
235.29–238.09	16.18	337.5–342.5	37.98	-1.612
238.09–240.96	8.812	342.5–347.5	40.65	-1.890
240.96–243.90	7.472	347.5–352.5	43.13	-1.219
243.90–246.91	3.909	352.5–357.5	47.17	-1.921
246.91–250.00	2.753	357.5–362.5	48.33	-1.095
250.00–253.17	2.007	362.5–367.5	51.66	-1.322
253.17–256.41	1.973	367.5–372.5	53.15	-1.102
256.41–259.74	2.111	372.5–377.5	55.08	-0.806
259.74–263.16	2.357	377.5–382.5	56.44	-0.867
263.16–266.67	2.698	382.5–387.5	57.57	-0.945
266.67–270.27	3.247	387.5–392.5	59.27	-0.923
270.27–273.97	3.785	392.5–397.5	58.45	-0.738
		397.5–402.5	60.21	-0.599
		402.5–407.5	57.81	-0.545
		407.5–412.5	59.99	-1.129
		412.5–417.5	56.51	0.001
		417.5–422.5	58.12	-1.208

* The quantity **a** is the temperature coefficient of σ as defined in the equation:

$$\sigma(t) = \sigma(0^\circ \text{C.}) + aT,$$

where T is in degrees Celsius.

The earlier recommendation for quantum yields was based on the work of Harker et al. [151] and of Davenport [102] for the atmospherically important 375–470 nm region. The work by Gardner et al. [129] yields values that are in much better agreement with the values reported earlier by Jones and Bayes [193]. The recommended quantum yield values, listed in Table 4-11, are in agreement with the recommendation of Gardner et al. [129]; they are based on a smooth fit to the data of Gardner et al. [129] for the wavelength range from 334 to 404 nm; Harker et al. [151] for 397–420 nm (corrected for cross sections); Davenport [102] for 400–420 nm; and Jones and Bayes [193] for 297–412 nm. Direct measurements of the solar photodissociation rate of NO₂ in the troposphere by Parrish et al. [310] and by Shetter et al. [374] agree better with theoretical estimates based on this recommendation than with the earlier one.

Table 4-11. Quantum Yields for NO₂ Photolysis

λ , nm	Φ	λ , nm	Φ
<285	1.000	393	0.953
290	0.999	394	0.950
295	0.998	395	0.942
300	0.997	396	0.922
305	0.996	397	0.870
310	0.995	398	0.820
315	0.994	399	0.760
320	0.993	400	0.695
325	0.992	401	0.635
330	0.991	402	0.560
335	0.990	403	0.485
340	0.989	404	0.425
345	0.988	405	0.350
350	0.987	406	0.290
355	0.986	407	0.225
360	0.984	408	0.185
365	0.983	409	0.153
370	0.981	410	0.130
375	0.979	411	0.110
380	0.975	412	0.094
381	0.974	413	0.083
382	0.973	414	0.070
383	0.972	415	0.059
384	0.971	416	0.048
385	0.969	417	0.039
386	0.967	418	0.030
387	0.966	419	0.023
388	0.964	420	0.018
389	0.962	421	0.012
390	0.960	422	0.008
391	0.959	423	0.004
392	0.957	424	0.000

C2. $\text{NO}_3 + h\nu \rightarrow \text{NO} + \text{O}_2$ (Φ_1)

$\text{NO}_3 + h\nu \rightarrow \text{NO}_2 + \text{O}$ (Φ_2). The absorption cross sections of the nitrate free radical, NO₃, have been studied by (1) Johnston and Graham [188], (2) Graham and Johnston [144], (3) Mitchell et al. [262], (4) Marinelli et al. [242], (5) Ravishankara and Wine [330], (6) Cox et al. [88], (7) Burrows et al. [60], (8) Ravishankara and Mauldin [327], (9) Sander [356], (10) Cantrell et al. [69], (11) Canosa-Mas et al. [67], and (12) Yokelson et al. [437]. The 1st and 4th studies required calculation of the NO₃ concentration by modeling a complex kinetic system. The other studies are more direct, and the results in terms of integrated absorption coefficients are in good agreement. The recommended value at 298 K and 662 nm, $(2.00 \pm 0.25) \times 10^{-17}$ cm², is the average of the results of studies (4), (5), and (7) through (11). The values in the wavelength range 600–670 nm, shown in Figure 4-1 and listed in Table 4-12, were calculated using the spectra measured in studies (8), (9), and (11), and with the 662 nm value normalized to the above average. The spectra obtained in other studies are consulted for a more extended wavelength range. The temperature dependence of the 662 nm band has been studied by Ravishankara and Mauldin, Sander, Cantrell et al., and Yokelson et al. Except for Cantrell et al., these studies all showed that the cross section at 662 nm increases with decreasing temperature. The reason for this discrepancy is not clear.

The quantum yields Φ_1 and Φ_2 have been measured by Graham and Johnston [144], and under higher resolution by Magnotta and Johnston [227], who report the product of the cross section times the quantum yield in the 400-to-630-nm range. The total quantum yield value, $\Phi_1 + \Phi_2$, computed from the results of this latter study

and the cross sections of Graham and Johnston [144], is above unity for $\lambda < 610$ nm, which is, of course, impossible. Hence, there is some systematic error, and it is most likely in the primary quantum yield measurements. More recently, Orlando et al. [306] measured the photolysis quantum yields between 570 and 635 nm.

Johnston et al. [186] have recently re-analyzed the available laboratory data relevant to NO_3 photolysis, including quantum yield studies, chemiluminescence, LIF studies, and molecular-beam-scattering experiments. Their model reproduces the wavelength-dependent quantum yield data reasonably well. The new recommendation is based on the J-values calculated by Johnston et al. for overhead sun in the stratosphere:

$$J_1(\text{NO} + \text{O}_2) = 0.0201 \text{ s}^{-1}$$

$$J_2(\text{NO}_2 + \text{O}) = 0.156 \text{ s}^{-1}$$

Wavelength-specific quantum yields over the temperature range 190–298 K may be found in the tabulation by Johnston et al.

The spectroscopy of NO_3 has been reviewed by Wayne et al. [431]. The reader is referred to this work for a more detailed discussion of the cross section and quantum yield data and for estimates of the photodissociation rates as a function of zenith angle.

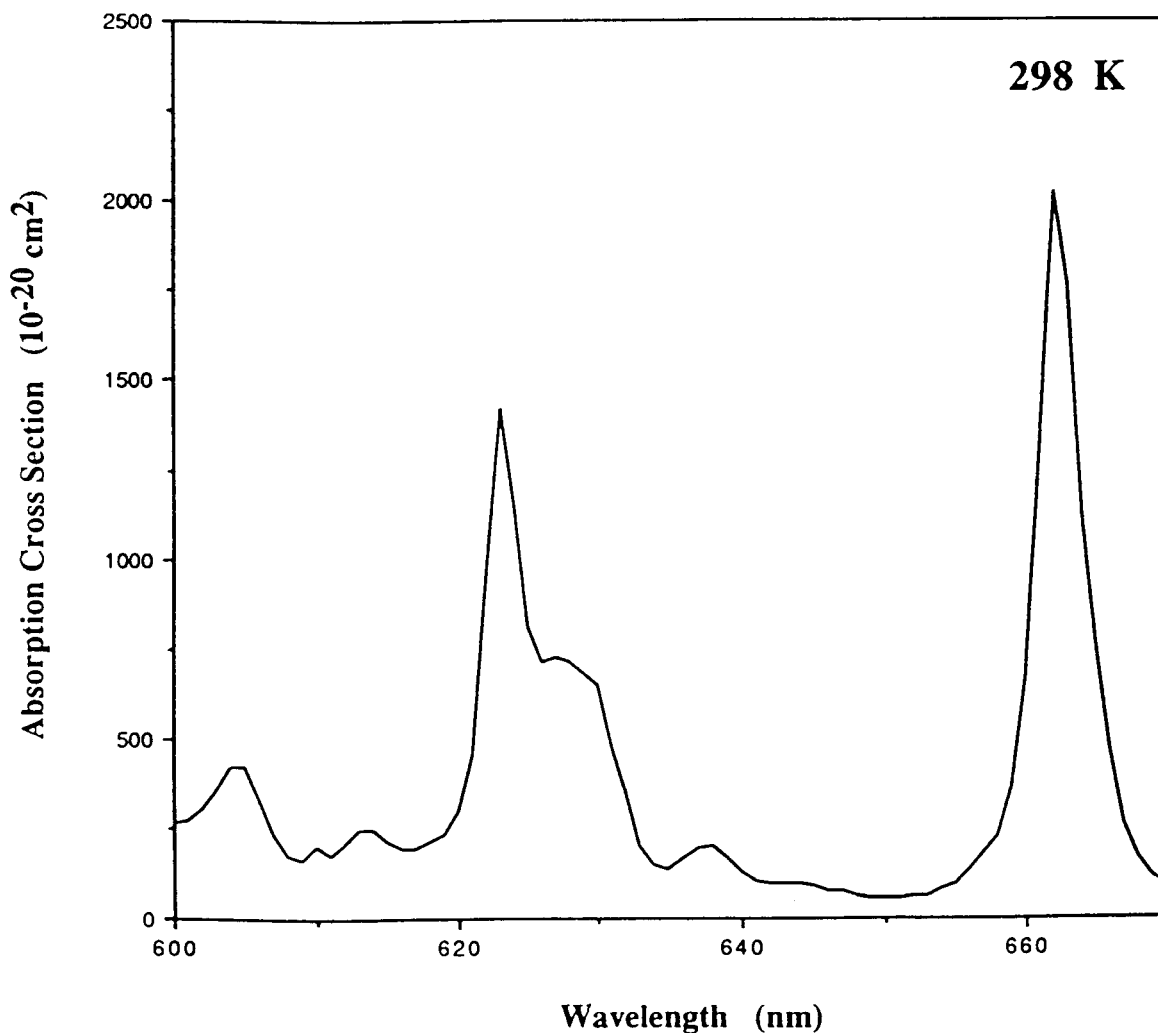


Figure 4-1. Absorption Spectrum of NO_3

Table 4-12. Absorption Cross Sections of NO₃ at 298 K

λ (nm)	$10^{20}\sigma$ (cm ²)	λ (nm)	$10^{20}\sigma$ (cm ²)	λ (nm)	$10^{20}\sigma$ (cm ²)
600	258	625	796	648	60
601	263	626	703	649	51
602	302	627	715	650	49
603	351	628	702	651	52
604	413	629	672	652	55
605	415	630	638	653	61
606	322	631	470	654	76
607	225	632	344	655	93
608	170	633	194	656	131
609	153	634	142	657	172
610	192	635	128	658	222
611	171	636	159	659	356
612	202	637	191	660	658
613	241	638	193	661	1308
614	242	639	162	662	2000
615	210	640	121	663	1742
616	190	641	99	664	1110
617	189	642	91	665	752
618	208	643	93	666	463
619	229	644	92	667	254
620	292	645	85	668	163
621	450	646	72	669	113
622	941	647	69	670	85
623	1407				
624	1139				

- C3. N₂O + hv → N₂ + O(¹D). The recommended values are taken from the work of Selwyn et al. [371], who measured the temperature dependence of the absorption cross sections in the atmospherically relevant wavelength region. They have fitted their data with the expression shown in Table 4-13; Table 4-14 presents the room temperature data. Hubrich and Stuhl [165] remeasured the N₂O cross sections at 298 K and 208 K and Merienne et al. [256] in the range from 220 K to 296 K. The results of these two sets of measurements are in very good agreement with those of Selwyn et al. The quantum yield for photodissociation is unity, and the products are N₂ and O(¹D) (Zelikoff and Aschenbrand [448], Paraskevopoulos and Cvetanovic [307], Preston and Barr [320], Simonaitis et al. [381]). The yield of N(⁴S) and NO(²Π) is less than 1% (Greenblatt and Ravishankara [147]).

Table 4-13. Mathematical Expression for Absorption Cross Sections of N₂O as a Function of Temperature*

$$\ln(\sigma(\lambda, T)) = \sum_{n=0}^4 A_n \lambda^n + (T - 300) \exp\left(\sum_{n=0}^3 B_n \lambda^n\right)$$

Where T: temperature K;

$$A_0 = 68.21023$$

$$A_1 = -4.071805$$

$$A_2 = 4.301146 \times 10^{-2}$$

$$A_3 = -1.777846 \times 10^{-4}$$

$$A_4 = 2.520672 \times 10^{-7}$$

λ : nm;

$$B_0 = 123.4014$$

$$B_1 = -2.116255$$

$$B_2 = 1.111572 \times 10^{-2}$$

$$B_3 = -1.881058 \times 10^{-5}$$

*Ranges of applicability: 173 nm < λ < 240 nm; 194 K < T < 320 K

Table 4-14. Absorption Cross Sections of N₂O at 298 K

λ (nm)	$10^{20}\sigma$ (cm ²)	λ (nm)	$10^{20}\sigma$ (cm ²)	λ (nm)	$10^{20}\sigma$ (cm ²)
173	11.3	196	6.82	219	0.115
175	12.6	198	5.35	221	0.0739
176	13.4	199	4.70	222	0.0588
177	14.0	200	4.09	223	0.0474
178	13.9	201	3.58	224	0.0375
179	14.4	202	3.09	225	0.0303
180	14.6	203	2.67	226	0.0239
181	14.6	204	2.30	227	0.0190
182	14.7	205	1.95	228	0.0151
183	14.6	206	1.65	229	0.0120
184	14.4	207	1.38	230	0.00955
185	14.3	208	1.16	231	0.00760
186	13.6	209	0.980	232	0.00605
187	13.1	210	0.755	233	0.00478
188	12.5	211	0.619	234	0.00360
189	11.7	212	0.518	235	0.00301
190	11.1	213	0.421	236	0.00240
191	10.4	214	0.342	237	0.00191
192	9.75	215	0.276	238	0.00152
193	8.95	216	0.223	239	0.00123
194	8.11	217	0.179	240	0.00101
195	7.57	218	0.142		

Several groups have investigated the isotopic fractionation of N₂O resulting from photolysis in the UV. Fractionation factors have been measured by several groups following photolysis at several wavelengths in the 193–213 nm range: Turatti et al. [404] employed high resolution FTIR spectroscopy; Rockmann et al. [340] used a modified isotope ratio mass spectrometric technique; and Rahn et al. [321] utilized conventional isotope ratio mass spectrometry. Zhang et al. [450] employed a low-resolution FTIR technique with N₂O photolysis at 213 nm, and Rockmann et al. [341] utilized a broadband photolysis source centered around 200 nm and simulating stratospheric actinic fluxes. The results are in reasonably good agreement, and indicate that the fractionation factors increase with photolysis wavelength from 193 to 213 nm. Furthermore, the fractionation factors show a clear dependence on the position of the ¹⁵N atom, in agreement with the theoretical model of Yung and Miller [447]; however, the theoretical calculations underestimate the laboratory results by about a factor of two. Analysis of the isotopic composition of stratospheric air samples yields results that are in qualitative agreement with the laboratory results, confirming that photolysis is the predominant sink for N₂O [148,341]. On the other hand, the fractionation factors measured in the atmospheric samples are smaller than those reported from the laboratory studies, indicating the influence of atmospheric diffusion and mixing [341].

- C4. N₂O₅ + hv → Products. The absorption cross sections of dinitrogen pentoxide, N₂O₅ have been measured at room temperature by Jones and Wulf [192] between 285 and 380 nm, by Johnston and Graham [188] between 210 and 290 nm, by Graham [143] between 205 and 380 nm, and for temperatures in the 223 to 300 K range by Yao et al. [436], between 200 and 380 nm. The agreement is good, particularly considering the difficulties in handling N₂O₅. The recommended cross section values, listed in Table 4-15, are taken from Yao et al. [436]. For wavelengths shorter than 280 nm there is little or no temperature dependence, and between 285 and 380 nm the temperature effect is best computed with the expression listed at the bottom of Table 4-15. Recent measurements of the cross sections and their temperature dependence by Harwood et al. [153] yield values in excellent agreement with this recommendation except at the longest wavelengths (380 nm) and lowest temperatures (233 K), where the new values are about 30% lower. However, the contribution to solar photodissociation from these longer wavelengths is negligible, and the differences between the predicted photolysis rates from the two sets of data are smaller than 3% (Harwood et al. [153]).

There are several studies on the primary photolysis products of N₂O₅: Swanson et al. [391] have measured the quantum yield for NO₃ production at 249 and at 350 nm, obtaining a value close to unity, which is consistent with the observations of Burrows et al. [59] for photolysis at 254 nm. Barker et al. [21] report a quantum yield

for O(³P) production at 290 nm of less than 0.1, and near unity for NO₃. For O-atom production Margitan (private communication, 1985) measured a quantum yield value of 0.35 at 266 nm, and Ravishankara et al. [331] report values of 0.72, 0.38, 0.21 and 0.15 at 248, 266, 287, and 289 nm, respectively, with a quantum yield near unity for NO₃ production at all these wavelengths. It appears, then, that NO₃ is produced with unit quantum yield while the O-atom, and hence the NO yield, increases at shorter wavelengths, with a consequent decrease in the NO₂ yield. The study of Oh et al. [299] indicates that, besides NO₃, the primary photolysis products are a wavelength-dependent mixture of NO₂, NO₂* and NO + O, where NO₂* represents one or more excited electronic states, most likely the ²B₁ state.

Table 4-15. Absorption Cross Sections of N₂O₅

λ (nm)	10 ²⁰ σ (cm ²)	λ (nm)	10 ²⁰ σ (cm ²)
205	820	250	40
210	560	255	32
215	370	260	26
220	220	265	20
225	144	270	16.1
230	99	275	13.0
235	77	280	11.7
240	62		

Note: For 285 nm < λ < 380 nm; 300 K > T > 225 K: 10²⁰σ = exp(2.735 + ((4728.5 – 17.127 λ)/T)) where σ is in cm²/molecule; λ in nm; and T in K.

- C5. HONO + hν → OH + NO. The ultraviolet spectrum of HONO between 300 and 400 nm has been studied by Stockwell and Calvert [389] by examination of its equilibrium mixtures with NO, NO₂, H₂O, N₂O₃ and N₂O₄; the possible interferences by these compounds were taken into account. More recently, Vasudev [421] measured relative cross sections by monitoring the OH photodissociation product with laser-induced fluorescence; and Bongartz et al. [38] determined absolute cross section values at 0.1 nm resolution in a system containing a highly diluted mixture of NO, NO₂, H₂O, and HONO, by measuring total NO_x (NO and NO₂). There are some discrepancies between these two recent sets of results in terms of relative peak heights; however, both yield essentially the same photodissociation rate provided Vasudev's relative data are normalized to match the cross section value reported by Bongartz et al. at 354 nm. At this wavelength the value reported earlier by Stockwell and Calvert is about 20% smaller. The recommended values, listed in Table 4-16, are taken from Bongartz et al.

Table 4-16. Absorption Cross Sections of HONO

λ (nm)	$10^{20}\sigma$ (cm ²)	λ (nm)	$10^{20}\sigma$ (cm ²)	λ (nm)	$10^{20}\sigma$ (cm ²)
310	1.3	339	18.8	368	52.0
311	1.9	340	10.0	369	38.8
312	2.8	341	17.0	370	17.8
313	2.2	342	38.6	371	11.3
314	3.6	343	14.9	372	10.0
315	3.0	344	9.7	373	7.7
316	1.4	345	10.9	374	6.2
317	3.1	346	12.3	375	5.3
318	5.6	347	10.4	376	5.3
319	3.6	348	9.1	377	5.0
320	4.9	349	7.9	387	5.8
321	7.8	350	11.2	379	8.0
322	4.9	351	21.2	380	9.6
323	5.1	352	15.5	381	11.3
324	7.1	353	19.1	382	15.9
325	5.0	354	58.1	383	21.0
326	2.9	355	36.4	384	24.1
327	6.6	356	14.1	385	20.3
328	11.7	357	11.7	386	13.4
329	6.1	358	12.0	387	9.0
330	11.1	359	10.4	388	5.6
331	17.9	360	9.0	389	3.4
332	8.7	361	8.3	390	2.7
333	7.6	362	8.0	391	2.0
334	9.6	363	9.6	392	1.5
335	9.6	364	14.6	393	1.1
336	7.2	365	16.8	394	0.6
337	5.3	366	18.3	395	1.0
338	10.0	367	30.2	396	0.4

- C6. $\text{HNO}_3 + h\nu \rightarrow \text{products}$. The recommended absorption cross sections and their temperature dependency, listed in Table 4-17, are taken from the work of Burkholder et al. [56]. The temperature effect is very important for estimates of atmospheric photodissociation; the results of Burkholder et al. agree well with those of Rattigan et al. [322,323], except at 238 K, where these latter authors report significantly smaller values.

The new cross section values agree reasonably well at room temperature with the data of Molina and Molina [267], which provided the basis for the earlier recommendation. These data are also in good agreement throughout the 190–330 nm range with the values reported by Biauume [32]. They are also in very good agreement with the data of Johnston and Graham [187], except towards both ends of the wavelength range. Okabe [301] has measured the cross sections in the 110–190 nm range and his results are 20–30% lower than those of Biauume and of Johnston and Graham around 185–190 nm.

Johnston et al. [185] measured a quantum yield value of ~ 1 for the $\text{OH} + \text{NO}_2$ channel in the 200–315 nm range, using end product analysis. The quantum yield for O-atom production at 266 nm has been measured to be 0.03, and that for H-atom production less than 0.002, by Margitan and Watson [234], who looked directly for these products using atomic resonance fluorescence. Jolly et al. [191] measured a quantum yield for OH production of 0.89 ± 0.08 at 222 nm. Turnipseed et al. [407] have measured a quantum yield near unity for OH production at 248 and 222 nm. However, at 193 nm they report this quantum yield to be only ~ 0.33 , and the quantum yield for production of O-atoms to be about 0.8. Thus, it appears that HONO is a major photolysis product at 193 nm. These results are qualitatively in agreement with those reported by Schiffman et al. [364], namely a quantum yield for OH production of 0.47 at 193 nm, and of 0.75 at 248 nm.

Table 4-17. Absorption Cross Sections and Temperature Coefficients of HNO₃ Vapor

λ (nm)	$10^{20}\sigma$ (cm ²)	$10^3 B$ (K ⁻¹)	λ (nm)	$10^{20}\sigma$ (cm ²)	$10^3 B$ (K ⁻¹)	λ (nm)	$10^{20}\sigma$ (cm ²)	$10^3 B$ (K ⁻¹)
192	1225	0	246	2.06	1.61	300	0.263	3.10
194	1095	0	248	2.00	1.44	302	0.208	3.24
196	940	1.70	250	1.97	1.34	304	0.167	3.52
198	770	1.65	252	1.96	1.23	306	0.133	3.77
200	588	1.66	254	1.95	1.18	308	0.105	3.91
202	447	1.69	256	1.95	1.14	310	0.0814	4.23
204	328	1.74	258	1.93	1.12	312	0.0628	4.70
206	231	1.77	260	1.91	1.14	314	0.0468	5.15
208	156	1.85	262	1.87	1.14	316	0.0362	5.25
210	104	1.97	264	1.83	1.18	318	0.0271	5.74
212	67.5	2.08	266	1.77	1.22	320	0.0197	6.45
214	43.9	2.17	268	1.70	1.25	322	0.0154	6.70
216	29.2	2.17	270	1.62	1.45	324	0.0108	7.16
218	20.0	2.21	272	1.53	1.49	326	0.00820	7.55
220	14.9	2.15	274	1.44	1.56	328	0.00613	8.16
222	11.8	2.06	276	1.33	1.64	330	0.00431	9.75
224	9.61	1.96	278	1.23	1.69	332	0.00319	9.93
226	8.02	1.84	280	1.12	1.78	334	0.00243	9.60
228	6.82	1.78	282	1.01	1.87	336	0.00196	10.5
230	5.75	1.80	284	0.909	1.94	338	0.00142	10.8
232	4.87	1.86	286	0.807	2.04	340	0.00103	11.8
234	4.14	1.90	288	0.709	2.15	342	0.00086	11.8
236	3.36	1.97	290	0.615	2.27	344	0.00069	9.30
238	2.93	1.97	292	0.532	2.38	346	0.00050	12.1
240	2.58	1.97	294	0.453	2.52	348	0.00042	11.9
242	2.34	1.88	296	0.381	2.70	350	0.00042	9.30

$$\sigma(\lambda, T) = \sigma(\lambda, 298) \exp(B(\lambda)(T - 298)); T \text{ in K}$$

- C7. HO₂NO₂ + hv → Products. There are five studies of the UV spectrum of HO₂NO₂ vapor: Cox and Patrick [91], Morel et al. [282], Graham et al. [145], Molina and Molina [267], and Singer et al. [382]. The latter three studies are the only ones covering the gas phase spectrum in the critical wavelength range for atmospheric photodissociation ($\lambda \geq 290$ nm). The recommended values, listed in Table 4-18, are an average of the work of Molina and Molina [267] and of Singer et al. [382], which are the more direct studies. The cross sections appear to be temperature independent between 298 and 253 K (Singer et al. [382]). MacLeod et al. [226] report that photolysis at 248 nm yields one third OH and NO₃ and two thirds HO₂ + NO₂.

Table 4-18. Absorption Cross Sections of HO₂NO₂ Vapor

λ (nm)	$10^{20}\sigma$ (cm ²)	λ (nm)	$10^{20}\sigma$ (cm ²)
190	1010	260	28.5
195	816	265	23.0
200	563	270	18.1
205	367	275	13.4
210	239	280	9.3
215	161	285	6.2
220	118	290	3.9
225	93.5	295	2.4
230	79.2	300	1.4
235	68.2	305	0.9
240	58.1	310	0.5
245	48.9	315	0.3
250	41.2	320	0.2
255	35.0	325	0.1

D1. $\text{CH}_2\text{O} + h\nu \rightarrow \text{H} + \text{HCO} (\Phi_1)$

$\text{CH}_2\text{O} + h\nu \rightarrow \text{H}_2 + \text{CO} (\Phi_2)$. The earlier recommendation for the formaldehyde absorption cross sections was based on the work carried out by Bass et al. [25] with a resolution of 0.05 nm at 296 K and 223 K, and by Moortgat et al. [277,279] with a resolution of 0.5 nm in the 210–360 K temperature range. More recently, Cantrell et al. [68] measured the cross sections in the 300–360 nm range between 223 K and 293 K, and Rogers [345] measured the cross sections in the 235–365 nm range at 296 K, both groups using Fourier transform spectrometry at a resolution of up to 0.011 nm (1 cm^{-1}). The agreement between these two reports is very good. The recommended values are those given by Cantrell et al. as a function of temperature; the reader is referred to the original article to obtain the high-resolution data. Table 4-19 lists the low-resolution cross sections taken from that work, that are suitable for atmospheric photodissociation calculations.

The quantum yields have been reported with good agreement by Horowitz and Calvert [162], Clark et al. [79], Tang et al. [400], Moortgat and Warneck [281], and Moortgat et al. [277,279]. The recommended values listed in Table 4-19 are based on the results of these investigators, as evaluated by S. Madronich (private communication, 1991). The quantum yield for the production of H_2 and CO is pressure- and temperature-dependent for wavelengths longer than about 330 nm (Moortgat et al. [279]). Table 4-19 gives the values at atmospheric pressure and room temperature; the reader is referred to the Moortgat et al. publication for information on values at lower pressures and temperatures.

Table 4-19. Absorption Cross Sections and Quantum Yields for Photolysis of CH_2O

λ (nm)	$10^{20} \sigma(\text{cm}^2)$		T-Parameters*		Φ_1 (H + HCO)	(H ₂ + CO)
	223 K	293 K	A	B		
301.25	1.38	1.36	1.37	-0.21	0.749	0.251
303.75	4.67	4.33	4.43	-4.73	0.753	0.247
306.25	3.32	3.25	3.27	-1.06	0.753	0.247
308.75	2.27	2.22	2.24	-0.724	0.748	0.252
311.25	0.758	0.931	0.882	2.48	0.739	0.261
313.75	3.65	3.40	3.47	-3.64	0.724	0.276
316.25	4.05	3.89	3.94	-2.30	0.684	0.316
318.75	1.66	1.70	1.69	0.659	0.623	0.368
321.25	1.24	1.13	1.16	-1.52	0.559	0.423
323.75	0.465	0.473	0.471	0.118	0.492	0.480
326.25	5.06	4.44	4.61	-8.86	0.420	0.550
328.75	2.44	2.29	2.34	-2.15	0.343	0.634
331.25	1.39	1.28	1.31	-1.53	0.259	0.697
333.75	0.093	0.123	0.114	0.432	0.168	0.739
336.25	0.127	0.131	0.130	0.050	0.093	0.728
338.75	3.98	3.36	3.54	-8.96	0.033	0.667
341.25	0.805	0.936	0.898	1.86	0.003	0.602
343.75	1.44	1.26	1.31	-2.64	0.001	0.535
346.25	0.004	0.071	0.052	0.957	0	0.469
348.75	0.009	0.040	0.031	0.438	0	0.405
351.25	0.169	0.235	0.216	0.948	0	0.337
353.75	1.83	1.55	1.63	-4.05	0	0.265
356.25	0.035	0.125	0.099	1.27	0	0.197

Note: The values are averaged for 2.5 nm intervals centered on the indicated wavelength.

* Cross section for $-50^\circ\text{C} < T < 20^\circ\text{C}$ calculated as $\sigma(T) = A + B \times 10^{-3} T$; T in $^\circ\text{C}$, and σ in 10^{-20} cm^2 .

D2. $\text{CH}_3\text{O}_2 + h\nu \rightarrow \text{Products}$. The absorption cross sections of the methylperoxy radical, CH_3O_2 , in the 195–310-nm region have been measured at room temperature by Parkes et al. [309], Hochenadel et al. [160], Parkes [308], Anastasi et al. [12], Kan et al. [197], Cox and Tyndall [93,94] at 250 nm only; Adachi et al. [5], Sander and Watson [360] at 250 nm only; Pilling and Smith [316] at 254 nm only, Kurylo et al. [206], McAdam et al. [250], Jenkin et al. [181], Wallington et al. [425], Moortgat et al. [280], Dagaut and Kurylo [99], Simon et al. [377], Jenkin and Cox [180], Lightfoot and Jemi-Alade [218] who measured the cross sections up to 777 K., Maricq and Wallington [240], Wallington et al. [427], Roehl et al. [342], and Fahr et al.

[114]. The absorption cross sections have been evaluated in earlier reviews by Lightfoot et al. [217] and Wallington et al. [426], who noted significant discrepancies in the both the shapes of the spectra and the absolute magnitude of the cross section values. The ultraviolet absorption spectra have recently been reevaluated by Tyndall et al. [408], who fitted the absorption spectra to a semilogarithmic Gaussian distribution function suggested by Lightfoot et al. [217] and Maric et al. [237] using:

$$\sigma = \sigma_{\max} \exp \left[-a \left(\ln \left(\frac{\lambda_{\max}}{\lambda} \right) \right)^2 \right]$$

Screening of the data suggested that most spectra published before 1987 did not constrain the shape of the spectrum very well as indicated by the large relative uncertainty of the width parameter a . The shape was determined by averaging the individual fitting parameters from McAdam et al., Moortgat et al. [280], Simon et al. [377], Lightfoot and Jemi-Alade [218], Jenkin and Cox [180] and Maricq and Wallington [240], which were judged to be most reliable by Tyndall et al. [408]. Absolute cross sections were based on relative measurements of absorption cross sections of CH_3O_2 and $\text{C}_2\text{H}_5\text{O}_2$ at 240 nm taken under identical conditions (Wallington et al. [426], Maricq and Wallington [240], Fenter et al. [120] and Roehl et al. [342]), combined with independent calibrations by Dagaut and Kurylo [99], Simon et al. [377] and Lightfoot and Jemi-Alade [218]. The fitting parameters are: $\sigma_{\max} = 4.26 \times 10^{-18} \text{ cm}^2 \text{ molecule}^{-1}$; $a = 44.4$; $\lambda_{\max} = 237.3 \text{ nm}$. Table 4-20 lists the recommended cross sections, which are taken from the review by Tyndall et al.

Photolysis of CH_3O_2 in the stratosphere and troposphere is slow and can be neglected, but the UV absorption cross sections are important in laboratory studies of reaction kinetics.

Table 4-20. Absorption Cross Sections of CH_3O_2 , $\text{C}_2\text{H}_5\text{O}_2$, and $\text{CH}_3\text{C}(\text{O})\text{O}_2$

λ (nm)	$10^{20} \sigma$ (cm^2)		
	CH_3O_2	$\text{C}_2\text{H}_5\text{O}_2$	$\text{CH}_3\text{C}(\text{O})\text{O}_2$
195.0			389
200.0			564
205.0	165		665
210.0	219	195	656
215.0	276	257	564
220.0	330	319	451
225.0	376	374	366
230.0	408	418	326
235.0	424	444	319
240.0	424	452	326
245.0	407	440	330
250.0	378	412	322
255.0	339	372	300
260.0	294	324	268
265.0	248	273	229
270.0	203	222	187
275.0	162	176	147
280.0	126	136	111
285.0	96.1	102	81.2
290.0	71.5	74.6	57.3
295.0	52.0	53.3	
300.0		37.3	

- D3. $\text{C}_2\text{H}_5\text{O}_2 + h\nu \rightarrow \text{Products}$. The absorption cross sections of the ethylperoxy radical, $\text{C}_2\text{H}_5\text{O}_2$, in the 200–310-nm region have been measured at room temperature by Adachi et al. [4], Anastasi et al. [13], Cattell et al. [70], Wallington et al. [426], Bauer et al. [27], Maricq and Wallington [240], Fenter et al. [120], Munk et al. [284]. The absorption cross sections have been evaluated in earlier reviews by Lightfoot et al. [217] and Wallington et al. [426], who noted significant discrepancies in the both the shapes of the spectra and the absolute magnitude of the cross section values. The ultraviolet absorption spectra have recently been reevaluated by Tyndall et al.

[408], who fitted the absorption spectra to a semilogarithmic Gaussian distribution function suggested by Lightfoot et al. and Maric et al. [237] using:

$$\sigma = \sigma_{\max} \exp \left[-a \left[\ln \left(\frac{\lambda_{\max}}{\lambda} \right) \right]^2 \right]$$

The shape was determined by averaging the individual fitting parameters from Wallington et al., Bauer et al., Maricq and Wallington and Fenter et al., which were judged to be most reliable by Tyndall et al. Absolute cross sections were based on relative measurements of absorption cross sections of CH₃O₂ and C₂H₅O₂ at 240 nm taken under identical conditions (Wallington et al. [426], Maricq and Wallington [240], Fenter et al. [120] and Roehl et al. [342]), combined with independent calibrations. The fitting parameters are $\sigma_{\max} = 4.52 \times 10^{-18}$ cm² molecule⁻¹; a = 49.0; $\lambda_{\max} = 239.4$ nm. Table 4-20 lists the recommended cross sections, which are taken from the review by Tyndall et al.

Photolysis of C₂H₅O₂ in the stratosphere and troposphere is slow and can be neglected, but the UV absorption cross sections are important in laboratory studies of reaction kinetics.

- D4. CH₃OOH + hv → Products. Vaghjiani and Ravishankara [414] measured the cross sections of CH₃OOH by monitoring the CH₃OOH concentration via trapping and titration. These results are recommended and are listed in Table 4-21. The earlier results of Molina and Arguello [274] are consistently 40% higher than the values shown in Table 4-21; this difference is believed to be due to difficulty in trapping CH₃OOH and measuring its concentration. CH₃OOH dissociates upon light absorption to give CH₃O with unit quantum yield (Vaghjiani and Ravishankara, [415]); these authors also observed some production of H and O atoms at shorter wavelengths (i.e., 193 nm). Thelen et al. [401] report unit quantum yield for OH production at 248 and 193 nm, in agreement with the results of Vaghjiani and Ravishankara.

Table 4-21. Absorption Cross Sections of CH₃OOH

λ (nm)	$10^{20} \sigma$ (cm ²)	λ (nm)	$10^{20} \sigma$ (cm ²)
220	15.4	300	0.41
230	9.62	310	0.24
240	6.05	320	0.14
250	3.98	330	0.079
260	2.56	340	0.047
270	1.70	350	0.027
280	1.09	360	0.016

- D5. HCN + hv → Products. Herzberg and Innes [159] have studied the spectroscopy of hydrogen cyanide, HCN, that starts absorbing weakly at $\lambda < 190$ nm.

The solar photodissociation rate for this molecule is rather small, even in the upper stratosphere; estimates of this rate would require additional studies of the absorption cross sections and quantum yields in the 200-nm region.

- D6. CH₃CN + hv → Products. McElcheran et al. [251] have reported the spectrum of acetonitrile or methyl cyanide, CH₃CN; the first absorption band appears at $\lambda < 220$ nm. More recently, Suto and Lee [390] and Zetzsch [449] have measured the cross sections around 200 nm; solar photodissociation is unimportant compared to reaction with OH radicals.
- D7. CH₃C(O)O₂ + hv → Products. The UV absorption spectrum of the acetylperoxy radical, CH₃C(O)O₂, exhibits two absorption maxima in the 185–285 nm region: a strong band near 207 nm, and a feature at 245 nm that is weaker by a factor of 2. The absorption cross sections have been measured at room temperature by Addison et al. [6], Basco and Parmer [24], Moortgat et al. [280], Maricq and Szente [239], and Roehl et al. [342]. The absorption cross sections have been evaluated in earlier reviews by Lightfoot et al. [217] and Wallington et al. [426], who noted significant discrepancies in the both the shapes of the spectra and the absolute magnitude of the cross section values. The ultraviolet absorption spectra have recently been reevaluated by Tyndall et al. [408], who fitted the absorption spectra to the sum of two Gaussian-shaped absorption bands:

$$\sigma = \sigma_{\max 1} \exp \left[-a_1 \left[\ln \left(\frac{\lambda_{\max 1}}{\lambda} \right) \right]^2 \right] + \sigma_{\max 2} \exp \left[-a_2 \left[\ln \left(\frac{\lambda_{\max 2}}{\lambda} \right) \right]^2 \right]$$

The shape was determined by averaging the individual fitting parameters from Maricq and Szente and Roehl et al., which were judged to be the most reliable to date; the data by Maricq and Szente were adjusted for their overcorrection for the contribution of CH_3O_2 . Absolute cross sections were based on relative measurements of absorption cross sections of $\text{C}_2\text{H}_5\text{O}_2$ at 240 nm taken under identical conditions. The fitting parameters are $\sigma_{\max 1} = 6.29 \times 10^{-18} \text{ cm}^2 \text{ molecule}^{-1}$; $\lambda_{\max 1} = 206.0 \text{ nm}$; $a_1 = 168.0$; $\sigma_{\max 2} = 3.26 \times 10^{-18} \text{ cm}^2 \text{ molecule}^{-1}$; $\lambda_{\max 2} = 246.1 \text{ nm}$; $a_2 = 64.2$. Table 4-20 lists the recommended cross sections, which are taken from the review by Tyndall et al.

Photolysis of $\text{CH}_3\text{C}(\text{O})\text{O}_2$ in the stratosphere and troposphere is slow and can be neglected, but the UV absorption cross sections are important in laboratory studies of reaction kinetics.

- D8. $\text{CH}_3\text{C}(\text{O})\text{O}_2\text{NO}_2 + h\nu \rightarrow \text{Products}$. Absorption spectra of $\text{CH}_3\text{C}(\text{O})\text{O}_2\text{NO}_2$ (PAN) have been measured by Senum et al. [372] over the range 200–300 nm, Libuda and Zabel [216] over the range 220–325 nm, and Talukdar et al. [395] over the spectral range 195–345 nm and temperature range 250–298 K. The three studies are in excellent agreement over their range of overlap, with the values of Senum et al. being slightly smaller (15–20%) beyond 250 nm. Libuda and Zabel carried out simultaneous infrared absorption studies that showed that the measured cross sections need to be corrected for impurities that are transparent in the ultraviolet but contribute to the sample pressure in the absorption cell. These corrections are on the order of 20%. The recommended cross sections (Table 4-22) are based on the measurements of Talukdar et al. because of the good agreement with Libuda and Zabel and the wider spectral coverage and temperature range of this study. The uncertainties in the reported cross sections are probably quite large (on the order of a factor of 2), decreasing to about 30% at shorter wavelengths. The only PAN quantum yield studies are those of Mazely et al. [248,249]. In these studies, PAN was photolyzed at 248 nm, with NO_2 and NO_3 products being observed by laser-induced fluorescence at 298 K. Quantum yields of 0.83 ± 0.09 were obtained for the $\text{CH}_3\text{C}(\text{O})\text{O}_2 + \text{NO}_2$ channel and 0.3 ± 0.1 for the $\text{CH}_3\text{C}(\text{O})\text{O} + \text{NO}_3$ channel.

Table 4-22. Absorption Cross Sections of PAN

λ (nm)	$10^{20} \sigma(298\text{K})$ (cm^2)	$10^3 B$ (K^{-1})	$\lambda(\text{nm})$	$10^{20} \sigma(298\text{K})$ (cm^2)	$10^3 B$ (K^{-1})
196	430	2.02	274	2.4	5.55
198	400	1.73	276	2.1	5.76
200	360	1.36	278	1.7	5.98
202	320	1.07	280	1.5	6.20
204	290	0.86	282	1.2	6.43
206	260	0.75	284	1.0	6.67
208	230	0.71	286	0.81	6.90
210	200	0.75	288	0.65	7.15
212	170	0.84	290	0.54	7.39
214	140	0.97	292	0.45	7.63
216	120	1.12	294	0.37	7.86
218	100	1.29	296	0.30	8.08
220	90	1.47	298	0.24	8.27
222	78	1.64	300	0.19	8.44
224	68	1.81	302	0.15	8.61
226	59	1.98	304	0.12	8.76
228	52	2.14	306	0.10	8.87
230	46	2.30	308	0.082	9.01
232	40	2.46	310	0.067	9.13
234	35	2.63	312	0.054	9.3
236	31	2.80	314	0.046	9.46
238	28	2.96	316	0.036	9.57
240	24	3.11	318	0.030	9.75
242	21	3.25	320	0.025	10.0
244	19	3.39	322	0.020	10.2
246	17	3.52	324	0.017	10.4
248	15	3.64	326	0.014	10.6
250	13	3.76	328	0.012	10.7
252	11	3.87	330	0.011	10.9
254	10	3.98	332	0.0086	11.2
256	8.9	4.10	334	0.0068	11.5
258	7.8	4.23	336	0.0061	11.7
260	6.8	4.38	338	0.0053	11.9
262	6.0	4.53	340	0.0050	12.2
264	5.2	4.68	342	0.0036	12.4
266	4.5	4.82	344	0.0024	12.5
268	3.9	4.97	346	0.0023	
270	3.4	5.14	348	0.0025	
272	2.9	5.34	350	0.0016	

Cross sections in the temperature range 250–298 K are calculated using the equation,

$$\ln(\sigma(T)/\sigma(298\text{K})) = B(T-298).$$

- E1. $\text{HF} + h\nu \rightarrow \text{H} + \text{F}$. The ultraviolet absorption spectrum of HF has been studied by Safary et al. [354]. The onset of absorption occurs at $\lambda < 170$ nm, so that photodissociation of HF should be unimportant in the stratosphere.
- E2. $\text{FNO} + h\nu \rightarrow \text{F} + \text{NO}$. The absorption cross sections have been measured by Burley et al. [58], who report their results in graphical form as well as in tabular form in 1-nm intervals, between 180 and 350 nm. The spectrum shows vibronic structure at wavelengths longer than 250 nm. The cross section values are listed in Table 4-23 in 2-nm intervals. The quantum yield for decomposition is expected to be unity (Brandon et al., [39]; Reid et al., [336]).

Table 4-23. Absorption Cross Sections of FNO

λ (nm)	$10^{20}\sigma$ (cm ²)	λ (nm)	$10^{20}\sigma$ (cm ²)	λ (nm)	$10^{20}\sigma$ (cm ²)
180	52.4	236	3.09	292	11.9
182	51.7	238	2.76	294	7.11
184	50.7	240	2.25	296	9.15
186	49.4	242	2.08	298	22.0
188	47.5	244	1.74	300	15.6
190	45.1	246	1.65	302	25.4
192	42.7	248	1.41	304	8.85
194	40.0	250	1.54	306	11.8
196	37.3	252	1.25	308	32.2
198	33.8	254	1.23	310	15.5
200	30.5	256	1.36	312	31.6
202	27.7	258	1.58	314	12.3
204	24.8	260	1.30	316	11.0
206	22.2	262	1.64	318	25.5
208	19.9	264	2.03	320	15.2
210	17.6	266	1.96	323	40.2
212	15.8	268	2.10	324	17.8
214	13.9	270	2.81	326	12.1
216	12.3	272	4.47	328	9.39
218	10.7	274	3.97	330	12.9
220	9.35	276	4.24	332	13.0
222	8.32	278	3.41	334	19.3
224	7.22	280	8.26	336	13.1
226	6.30	282	7.58	338	8.96
228	5.44	284	7.26	340	5.65
230	4.68	286	5.17	342	3.81
232	4.10	288	10.4	344	2.68
234	3.52	290	17.0	346	1.96
				348	1.48
				350	1.18

- E3. $\text{CF}_4 + h\nu \rightarrow$ products. See Note E4.
- E4. $\text{C}_2\text{F}_6 + h\nu \rightarrow$ products. CF_4 and C_2F_6 do not absorb in the ultraviolet at wavelengths longer than 105 and 120 nm, respectively (Sauvageau et al. [362,363]; Inn, [178]); therefore, they are not expected to photodissociate until they reach the mesosphere.
- E5. $\text{CF}_2\text{O} + h\nu \rightarrow$ Products. The recommended absorption cross sections for CF_2O , CCl_2O and CClFO are listed in Table 4-24, as averages over the 500 cm^{-1} intervals commonly employed for atmospheric modeling (the wavelength given in the table is the center of the interval). The values for CCl_2O are based on the work of Gillotay et al. [139], who measured the cross sections between 170 and 320 nm at temperatures ranging from 210 to 295 K; the temperature effect is significant only at wavelengths longer than 250 nm. These cross section values are in good agreement with those recommended earlier, which were based on the data of Chou et al. [76]. For CClFO the recommended values are based on this latter work between 184 and 199 nm, and they are taken from the work of Nölle et al. [296] at the longer wavelengths. These workers measured the cross sections at temperatures ranging from 223 to 298 K; the temperature effect is not important for atmospheric photodissociation calculations, as is the case with CCl_2O . For CF_2O the cross section values are taken from Molina and Molina [268] between 184 and 199 nm, and from Nölle et al. [297] at the longer wavelengths. These authors measured the cross sections at 296 K between 200 and 230 nm.

The photodissociation quantum yield for CCl_2O is unity (Calvert and Pitts [65]); the spectrum is a continuum. Similarly, the quantum yield for CClFO is taken as unity; the spectrum shows little structure. In contrast, the CF_2O spectrum is highly structured. Nevertheless, its photodissociation quantum yield is also taken as unity, as

reported by Nölle et al. [297]. The self-reaction of the CFO photodissociation product regenerates CF₂O, and hence the apparent quantum yield is less than unity.

Table 4-24. Absorption Cross Sections of CCl₂O, CCIFO, and CF₂O at 298 K

λ (nm)	$10^{20} \sigma(\text{cm}^2)$		
	CCl ₂ O	CCIFO	CF ₂ O
184.4	234	–	–
186.0	186	15.6	5.5
187.8	146	14.0	4.8
189.6	116	13.4	4.2
191.4	90.3	12.9	3.7
193.2	71.5	12.7	3.1
195.1	52.4	12.5	2.6
197.0	39.3	12.4	2.1
199.0	31.2	12.3	1.6
201.0	25.2	12.5	1.3
203.0	20.9	12.0	0.95
205.1	17.9	11.5	0.74
207.3	15.8	10.8	0.52
209.4	14.3	9.9	0.40
211.6	13.3	9.0	0.28
213.9	12.6	7.9	0.20
216.2	12.3	6.8	0.12
218.6	12.2	5.8	0.08
221.0	12.2	4.8	0.049
223.5	12.4	3.8	0.035
225.7	12.7	2.9	0.024
228.6	13.1	2.2	0.018

- E6. CF₃OH + hv → Products: An upper limit of 10⁻²¹ cm² has been determined experimentally by Molina and Molina [271] for the absorption cross sections of CF₃OH in the 190–300-nm wavelength range. This upper limit is in agreement with estimates based on similarities between CF₃OH and CH₃OH, as well as with quantum chemistry calculations, as reported by Schneider et al. [368].
- F1. Cl₂ + hv → Cl + Cl. The recommended absorption cross sections are taken from the work of Maric et al. [235]; they can be calculated at various temperatures with the expression given at the bottom of Table 4-25. For convenience, some room temperature values are also listed in the table. Ganske et al. [128] have also measured the cross sections at room temperature, and the agreement with the recommended values is excellent. These two sets of data also agree well with the earlier recommendation, which was based on the work of Seery and Britton [370], which is in turn in good agreement with the results reported by Gibson and Bayliss [131], Fergusson et al. [121], and Burkholder and Bair [51]. The estimated atmospheric photodissociation rate is only weakly affected by the temperature dependency of the cross sections.

Table 4-25. Absorption Cross Sections of Cl₂

λ (nm)	10 ²⁰ σ, 298K (cm ²)	λ (nm)	10 ²⁰ σ, 298K (cm ²)
260	0.20	370	8.4
270	0.82	380	5.0
280	2.6	390	2.9
290	6.2	400	1.8
300	11.9	410	1.3
310	18.5	420	0.96
320	23.7	430	0.73
330	25.5	440	0.54
340	23.5	450	0.38
350	18.8	460	0.26
360	13.2	470	0.16

$$\sigma = 10^{-20} \alpha^{0.5} \left\{ 27.3 \exp \left(-99.0 \alpha \left(\ln \left(\frac{329.5}{\lambda} \right) \right)^2 \right) + 0.932 \exp \left(-91.5 \alpha \left(\ln \left(\frac{406.5}{\lambda} \right) \right)^2 \right) \right\}$$

where $\alpha = \tanh(402.7/T)$; λ in nm, and T in K; 300 K > T > 195 K.

- F2. $\text{ClO} + h\nu \rightarrow \text{Cl} + \text{O}$. The absorption cross sections of chlorine monoxide, ClO, have been reviewed by Watson [430]. There are more recent measurements yielding results in reasonable agreement with the earlier ones, (1) Mandelman and Nicholls [232] in the 250–310 nm region; (2) Wine et al. [433] around 283 nm; (3) Rigaud et al. [337], (4) Jourdain et al. [194], (5) Sander and Friedl [357], (6) Trolier et al. [402] in the 270–310-nm region, and (7) Simon et al. [378] between 240 and 310 nm. The peak cross section at the top of the continuum is 5.2×10^{-18} , based on the average of studies (4)–(7) and Johnston et al. [189]. Figure 4-2 shows a spectrum of ClO. It should be noted that the cross sections on the structured part are extremely dependent on instrument resolution, and the figure is only a guide to the line positions and approximate shapes. The cross sections of the continuum are independent of temperature (Trolier et al. [402]), while the structured part is extremely temperature dependent. The bands sharpen and grow with a decrease in temperature.

The calculations of Coxon et al. [95] and Langhoff et al. [210] indicate that photodecomposition of ClO accounts for at most 2 to 3% of the total destruction rate of ClO in the stratosphere, which occurs predominantly by reaction with oxygen atoms and nitric oxide.

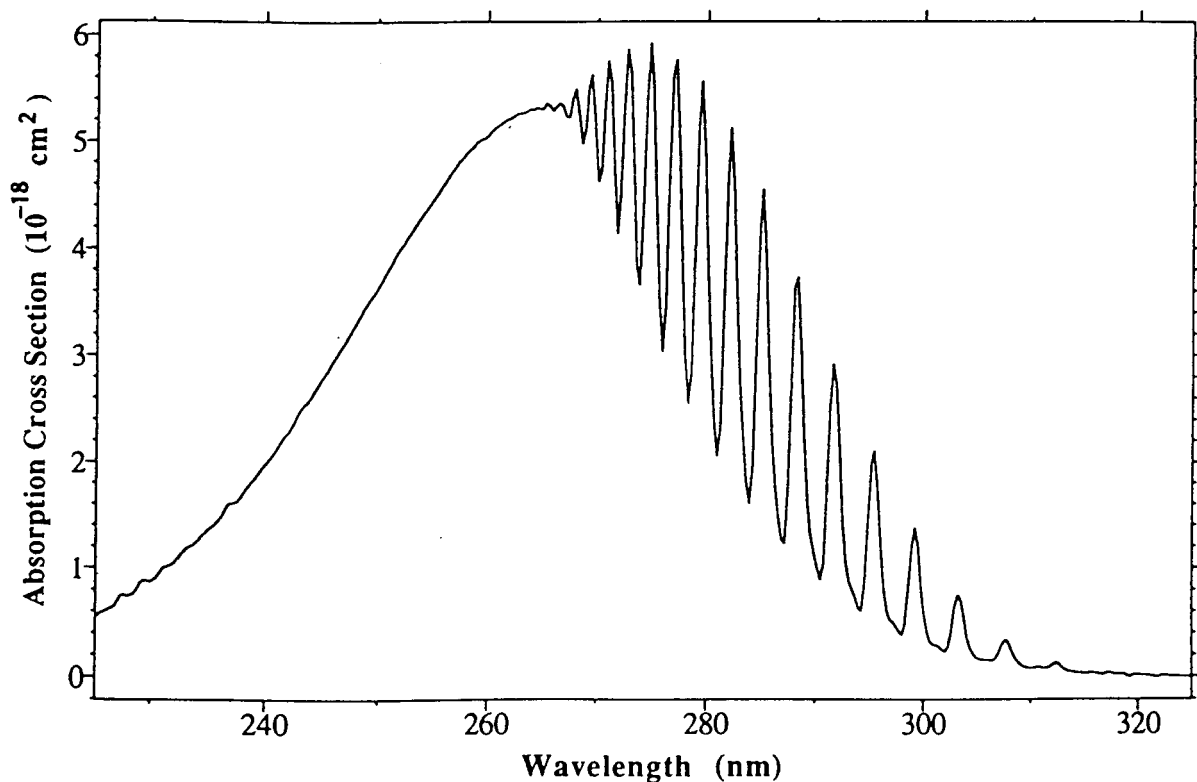


Figure 4-2. Absorption Spectrum of ClO

- F3. $\text{ClOO} + h\nu \rightarrow \text{ClO} + \text{O}$. Johnston et al. [189] measured the absorption cross sections of the ClOO radical using a molecular modulation technique that required interpretation of a complex kinetic scheme. More recently, Mauldin et al. [247] reported cross section measurements in the range from 220 to 280 nm, and Baer et al. [17] from 240 to 300 nm. These two studies are in very good agreement, yielding cross section values that are more than twice as large as the older Johnston et al. values. The recommended cross sections are listed in Table 4-26, and are taken from the work of Mauldin et al.

Table 4-26. Absorption Cross Sections of ClOO

λ (nm)	$10^{20} \sigma$ (cm ²)	λ (nm)	$10^{20} \sigma$ (cm ²)
220	611	252	2630
222	670	254	2370
224	747	256	2120
226	951	258	1890
228	1100	260	1610
230	1400	262	1370
232	1650	264	1120
234	1960	266	905
236	2240	268	725
238	2520	270	596
240	2730	272	435
242	2910	274	344
244	2960	276	282
246	2980	278	210
248	2950	280	200
250	2800		

F4. $\text{OCIO} + h\nu \rightarrow \text{O} + \text{ClO}$. The spectrum of OCIO is characterized by a series of well-developed progressions of bands extending from ~280 to 480 nm. The spectroscopy of this molecule has been studied extensively, and the quantum yield for photodissociation appears to be unity throughout the above wavelength range. See for example, the review by Watson [430]. Birks et al. [35] have estimated a half-life against atmospheric photodissociation of OCIO of a few seconds.

The recommended absorption cross section values are those reported by Wahner et al. [424], who measured the spectra with a resolution of 0.25 nm at 204, 296, and 378 K, in the wavelength range 240 to 480 nm. Table 4-27 lists the cross section values at the peak of the bands (a(0) to a(26)). Figure 4-3, from Wahner et al., shows the OCIO spectrum at 204 K and at room temperature. Hubinger and Nee [163] have extended the measurements of OCIO cross sections over the spectral range 125–470 nm. Frost et al. [126] have studied the spectrum at very high spectral resolution (0.1 cm^{-1}) and at low temperature (200 K) in molecular beam expansion. In both of these studies, cross sections were measured relative to values obtained by Wahner et al.

The photochemistry of OCIO is extremely complex, with several electronic excited states involved in the photodissociation dynamics. Several channels have been observed at wavelengths important in the stratosphere, including $\text{O} + \text{ClO}$, $\text{Cl} + \text{O}_2$ and isomerization to ClOO. Colussi [83] measured the quantum yield for chlorine atom production to be less than 0.01, and for oxygen atom production to be unity (within experimental error), both at 308 nm. Vaida et al. [417] and Ruhl et al. [352] reported chlorine atom production at 362 nm; and Bishenden et al. [36,37] measured the quantum yield for this process to be 0.15 ± 0.10 around that same wavelength. In contrast, Lawrence et al. [211] report a quantum yield for Cl-atom production in the 359–368-nm region of less than 5×10^{-4} . This conclusion is supported by photofragment studies of Davis and Lee [105], who report Cl yields <0.2% below 370 nm, rising to a maximum of 4% near 404 nm. The recommendation is to use a quantum yield value of unity for the production of O-atoms. While accurate absorption cross section values are valuable for atmospheric measurements of OCIO levels, the identity of the photodissociation products is only of minor importance in the context of atmospheric processes.

Table 4-27. Absorption Cross Sections of OCIO at the Band Peaks

$\lambda(\text{nm})$	$10^{20} \sigma(\text{cm}^2)$		
	204 K	296 K	378 K
475.53	–	13	–
461.15	17	17	16
446.41	94	69	57
432.81	220	166	134
420.58	393	304	250
408.83	578	479	378
397.76	821	670	547
387.37	1046	844	698
377.44	1212	992	808
368.30	1365	1136	920
359.73	1454	1219	984
351.30	1531	1275	989
343.44	1507	1230	938
336.08	1441	1139	864
329.22	1243	974	746
322.78	1009	791	628
317.21	771	618	516
311.53	542	435	390
305.99	393	312	291
300.87	256	219	216
296.42	190	160	167
291.77	138	114	130
287.80	105	86	105
283.51	089	72	90
279.64	073	60	79
275.74	059	46	–
272.93	053	33	–

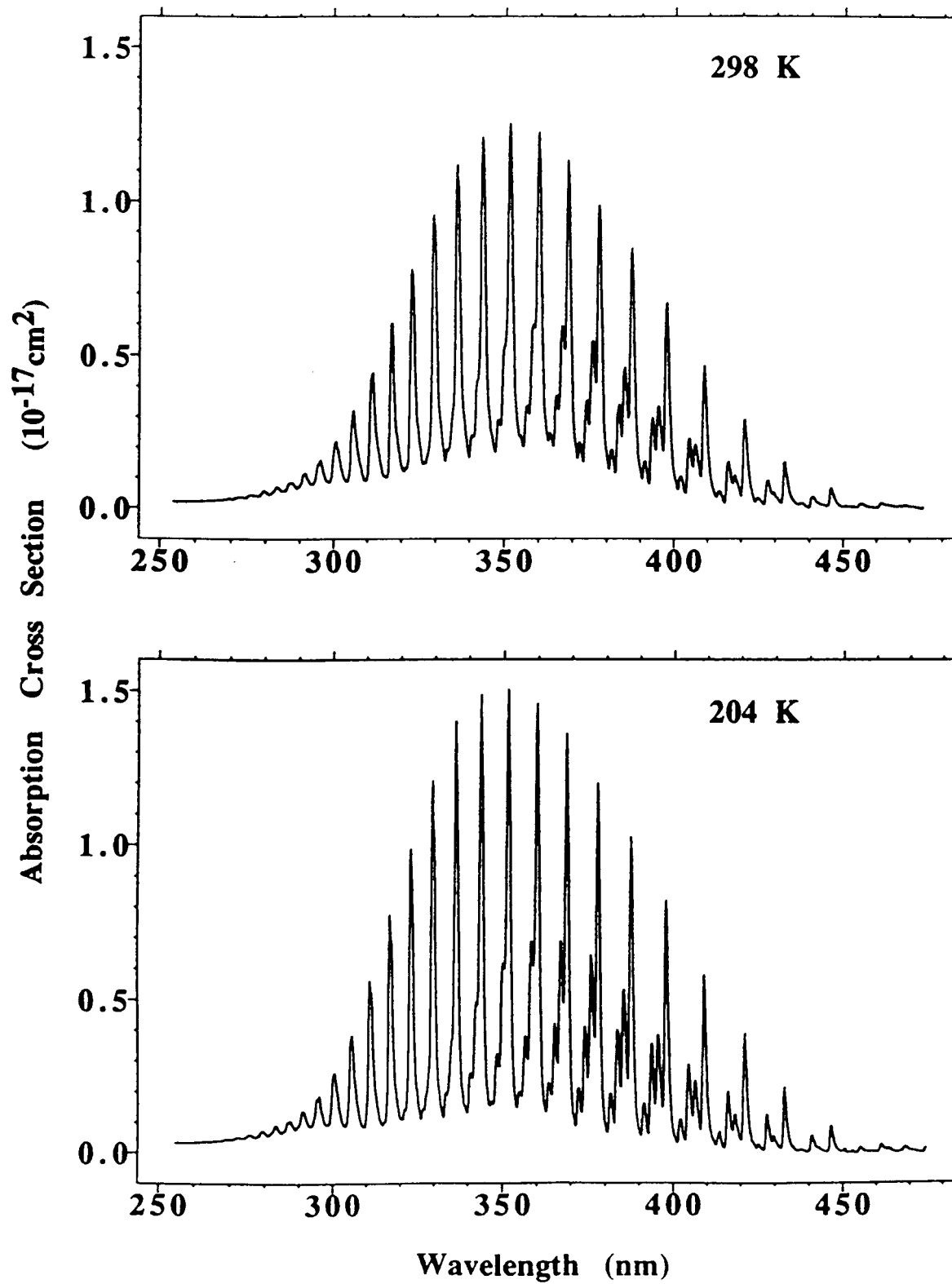


Figure 4-3. Absorption Spectrum of OCIO

- F5. $\text{ClO}_3 + h\nu \rightarrow \text{Products}$. The previous recommendation for absorption cross sections was based on the work of Goodeve and Richardson [141]. Lopez and Sicre [224] have shown that the spectrum reported by Goodeve and Richardson is most likely that of Cl_2O_6 . Thermochemical estimates by Colussi et al. [84] further corroborate this assignment. No recommendation is given at present for the ClO_3 cross sections.

Grothe and Willner (1994; 1995) have reported UV and IR spectra of ClO_3 trapped in a neon matrix. By monitoring the amount of ClO formed as a photolysis product, they estimated UV absorption cross sections of the order of $2 \times 10^{-18} \text{ cm}^2$ around 400–450 nm.

- F6. $\text{Cl}_2\text{O} + h\nu \rightarrow \text{Products}$. The preferred absorption cross sections, listed in Table 4-28, are those reported by Knauth et al. [202] at 298 K. They are in very good agreement with the cross sections measured by Lin [220] and by Molina and Molina [265]; the discrepancy is largest at the longest wavelengths. Nee [288] has recently reported cross section measurements in the 150–200 nm wavelength region.

Sander and Friedl [357] have measured the quantum yield for production of O-atoms to be 0.25 ± 0.05 , using a broadband photolysis source extending from 180 nm to beyond 400 nm. The main photolysis products are Cl and ClO . Using a molecular beam technique, Nelson et al. [289] found $\text{Cl} + \text{ClO}$ to be the primary photodissociation channel at 193, 248, and 308 nm. More recently, Nickolaisen et al. [292] reported that broadband photolysis at wavelengths beyond 300 nm results in pressure-dependent ClO quantum yields. Furthermore, these authors detected a transient absorption spectrum, that they assigned to a metastable triplet state of Cl_2O ; the implication is that the photodecomposition quantum yield is less than unity at atmospherically relevant wavelengths, in spite of the continuous nature of the absorption spectrum. Additional experimental work is needed to corroborate this interpretation.

Table 4-28. Absorption Cross Sections of Cl_2O

λ (nm)	$10^{20} \sigma$ (cm^2)	λ (nm)	$10^{20} \sigma$ (cm^2)
200	71.0	330	8.40
210	23.8	340	3.58
220	8.6	350	1.54
230	28.1	360	0.73
240	103	370	0.40
250	191	380	0.36
260	195	390	0.51
270	151	400	0.79
280	126	420	1.26
290	103	440	1.11
300	71.0	460	0.63
310	40.3	480	0.32
320	19.5	500	0.22

- F7. $\text{ClOOCl} + h\nu \rightarrow \text{Cl} + \text{ClOO}$. Recommended absorption cross sections in the wavelength range 190–450 nm for ClOOCl are listed in Table 4-29. The values for the wavelength range 200–360 nm are the average of experimental results reported by Cox and Hayman [90], DeMore and Tschuikow-Roux [107], Permien et al. [313], and Burkholder et al. [53]. For the 190–200-nm range the data are from DeMore and Tschuikow-Roux [107], these being the only data available in that range. Data at wavelengths greater than 360 nm were obtained from a linear extrapolation of the logarithm of the cross sections, using the expression $\log(10^{20} \sigma \text{ (cm}^2\text{)}) = -0.01915 \times \lambda(\text{nm}) + 7.589$. For $\lambda > 360$ nm the extrapolated data are considered to be more reliable than the experimental measurements because of the very small dimer cross sections in this region.

While the results of Cox and Hayman, DeMore and Tschuikow-Roux, Permien et al., and Burkholder et al. are in good agreement at wavelengths below 250 nm, there are significant discrepancies at longer wavelengths, which may be attributed to uncertainties in the spectral subtraction of impurities such as Cl_2O , Cl_2 , and Cl_2O_2 . Huder and DeMore [167] measured ClOOCl cross sections over the 190–310-nm range using a method that minimized the corrections required for impurities such as Cl_2O . The cross sections from this study are significantly smaller (up to a factor of 2) than the current recommendation, particularly when extrapolated beyond 400 nm. Additional measurements are needed, particularly at the longer wavelengths, to check the results of Huder and DeMore.

These studies also indicate that only one stable species is produced in the recombination reaction of ClO with itself, and that this species is dichlorine peroxide, ClOOCI, rather than ClOCIO. Using submillimeter wave spectroscopy, Birk et al. [34] have further established the structure of the recombination product to be ClOOCI. These observations are in agreement with the results of quantum mechanical calculations (McGrath et al. [254,255]; Jensen and Odershede [184]; Stanton et al. [387]).

Table 4-29. Absorption Cross Sections of ClOOCI at 200–250 K

λ (nm)	$10^{20}\sigma(\text{cm}^2)$						
190	565.0	256	505.4	322	23.4	388	1.4
192	526.0	258	463.1	324	21.4	390	1.3
194	489.0	260	422.0	326	19.2	392	1.2
196	450.0	262	381.4	328	17.8	394	1.1
198	413.0	264	344.6	330	16.7	396	1.0
200	383.5	266	311.6	332	15.6	398	0.92
202	352.9	268	283.3	334	14.4	400	0.85
204	325.3	270	258.4	336	13.3	402	0.78
206	298.6	272	237.3	338	13.1	404	0.71
208	274.6	274	218.3	340	12.1	406	0.65
210	251.3	276	201.6	342	11.5	408	0.60
212	231.7	278	186.4	344	10.9	410	0.54
214	217.0	280	172.5	346	10.1	412	0.50
216	207.6	282	159.6	348	9.0	414	0.46
218	206.1	284	147.3	350	8.2	416	0.42
220	212.1	286	136.1	352	7.9	418	0.38
222	227.1	288	125.2	354	6.8	420	0.35
224	249.4	290	114.6	356	6.1	422	0.32
226	280.2	292	104.6	358	5.8	424	0.29
228	319.5	294	95.4	360	5.5	426	0.27
230	365.0	296	87.1	362	4.5	428	0.25
232	415.4	298	79.0	364	4.1	430	0.23
234	467.5	300	72.2	366	3.8	432	0.21
236	517.5	302	65.8	368	3.5	434	0.19
238	563.0	304	59.9	370	3.2	436	0.17
240	600.3	306	54.1	372	2.9	438	0.16
242	625.7	308	48.6	374	2.7	440	0.15
244	639.4	310	43.3	376	2.4	442	0.13
246	642.6	312	38.5	378	2.2	444	0.12
248	631.5	314	34.6	380	2.1	446	0.11
250	609.3	316	30.7	382	1.9	448	0.10
252	580.1	318	28.0	384	1.7	450	0.09
254	544.5	320	25.6	386	1.6		

- F8. $\text{Cl}_2\text{O}_3 + h\nu \rightarrow \text{Products}$. The absorption cross sections of Cl_2O_3 have been measured by Hayman and Cox [155], Burkholder et al. [52], and Harwood et al. [154]. The results from these studies are significantly different in the spectral regions below 240 nm and in the long-wavelength tail beyond 300 nm. Table 4-30 lists the recommended values. These are derived by averaging the spectra of Burkholder et al. and Harwood et al., which are obtained by the most direct methods. Additional work is needed, particularly in the spectral region beyond 300 nm.

Table 4-30. Absorption Cross Sections of Cl₂O₃

λ (nm)	$10^{20} \sigma$ (cm ²)	λ (nm)	$10^{20} \sigma$ (cm ²)
220	1200	275	1470
225	1130	280	1240
230	1060	285	990
235	1010	290	760
240	1020	295	560
245	1120	300	400
250	1270	305	290
255	1450	310	210
260	1610	315	160
265	1680	320	140
270	1630		

- F9. Cl₂O₄ + hv → Products. The absorption cross sections of Cl₂O₄ have been measured by Lopez and Sicre [223]; their results are given in Table 4-31.

Table 4-31. Absorption Cross Sections of Cl₂O₄

λ (nm)	$10^{20} \sigma$ (cm ²)	λ (nm)	$10^{20} \sigma$ (cm ²)
200	161	255	42
205	97	260	31
210	72	265	22
215	64	270	14
220	71	275	8.8
225	75	280	5.5
230	95	285	4.0
235	95	290	2.7
240	87	295	2.2
245	72	300	1.7
250	56	305	1.2
		310	0.7

- F10. Cl₂O₆ + hv → Products. The absorption cross sections for Cl₂O₆ are listed in Table 4-32 and are taken from the work of Lopez and Sicre [224]. These authors show that the spectrum originally attributed to ClO₃ by Goodeve and Richardson [141] was most likely that of Cl₂O₆. The cross section values measured by Lopez and Sicre are several times larger than those reported by Goodeve and Richardson, but the shape of the spectrum is similar.

Table 4-32. Absorption Cross Sections of Cl₂O₆

λ (nm)	$10^{20} \sigma$ (cm ²)	λ (nm)	$10^{20} \sigma$ (cm ²)
200	1230	300	980
210	1290	310	715
220	1230	320	450
230	1080	330	285
240	1010	340	180
250	1010	350	112
260	1290	360	59
270	1440	370	28
280	1440	380	12
290	1290		

- F11. $\text{HCl} + h\nu \rightarrow \text{H} + \text{Cl}$. The absorption cross sections of HCl, listed in Table 4-33, are taken from the work of Inn [177].

Table 4-33. Absorption Cross Sections of HCl Vapor

$\lambda(\text{nm})$	$10^{20} \sigma (\text{cm}^2)$	$\lambda (\text{nm})$	$10^{20} \sigma (\text{cm}^2)$
145	281	190	14.5
150	345	195	6.18
155	382	200	2.56
160	332	205	0.983
165	248	210	0.395
170	163	215	0.137
175	109	220	0.048
180	58.8		

- F12. $\text{HOCl} + h\nu \rightarrow \text{OH} + \text{Cl}$. The absorption cross sections of HOCl vapor have been measured by several groups. Molina and Molina [265] and Knauth et al. [202] produced this species using equilibrium mixtures with Cl_2O and H_2O ; their results provided the basis for the earlier recommendation. More recently, Mishalanie et al. [261] and Permien et al. [313] used a dynamic source to generate the HOCl vapor. The cross section values reported by Molina and Molina [265], Mishalanie et al. [261], and Permien et al. [313] are in reasonable agreement between 250 and 330 nm. In this wavelength range, the values reported by Knauth et al. [202] are significantly smaller, e.g., a factor of 4 at 280 nm. Beyond 340 nm, the cross sections of Mishalanie et al. are much smaller than those obtained by the other three groups. At 365 nm, the discrepancy is about an order of magnitude.

Burkholder [50] has remeasured the absorption spectrum of HOCl over the wavelength range 200 to 380 nm, following photolysis of equilibrium mixtures of $\text{Cl}_2\text{O-H}_2\text{O-HOCl}$. The obtained spectrum displays two absorption maxima at 242 and 304 nm, and is in excellent agreement with the work of Knauth et al. [202], but in poor agreement with the measurements of Mishalanie et al. [261] and Permien et al. [313]. The discrepancies can be attributed mostly to difficulties in correcting the measured absorptions for the presence of Cl_2 and Cl_2O . In the study by Burkholder, several control experiments were carried out in order to check the internal consistency of the data. Moreover, Barnes et al. [23] examined the near-UV spectrum of HOCl by monitoring the OH fragments resulting from photodissociation, and revealed a third weak band centered at 387 nm extending down to 480 nm. The recommended cross sections up to 420 nm, calculated from an analytical expression provided by Barnes et al. [23] and based on the values of Burkholder [50] and Barnes et al. [23], are listed in Table 4-34. The work by Jungkamp et al. [196] yields cross section values in excellent agreement with this recommendation for wavelengths shorter than 350 nm.

Molina et al. [275] observed production of OH radicals in the laser photolysis of HOCl around 310 nm, and Butler and Phillips [62] found no evidence for O-atom production at 308 nm, placing an upper limit of ~ 0.02 for the primary quantum yield for the $\text{HCl} + \text{O}$ channel. Vogt and Schindler [422] used broadband photolysis in the 290–390 nm wavelength range, determining a quantum yield for OH production of >0.95 .

Table 4-34. Absorption Cross Sections of HOCl

λ (nm)	$10^{20} \sigma$ (cm ²)	λ (nm)	$10^{20} \sigma$ (cm ²)	λ (nm)	$10^{20} \sigma$ (cm ²)
200	7.18	274	5.26	348	1.55
202	6.39	276	4.94	350	1.43
204	5.81	278	4.74	352	1.33
206	5.46	280	4.64	354	1.24
208	5.37	282	4.62	356	1.17
210	5.54	284	4.68	358	1.11
212	5.98	286	4.79	360	1.06
214	6.68	288	4.95	362	1.02
216	7.63	290	5.13	364	0.985
218	8.81	292	5.33	366	0.951
220	10.2	294	5.52	368	0.919
222	11.6	296	5.71	370	0.888
224	13.2	298	5.86	372	0.855
226	14.7	300	5.99	374	0.822
228	16.2	302	6.08	376	0.786
230	17.5	304	6.12	378	0.748
232	18.7	306	6.12	380	0.708
234	19.6	308	6.07	382	0.667
236	20.2	310	5.97	384	0.624
238	20.5	312	5.84	386	0.580
240	20.6	314	5.66	388	0.535
242	20.3	316	5.45	390	0.491
244	19.8	318	5.21	392	0.447
246	19.0	320	4.95	394	0.405
248	18.1	322	4.67	396	0.364
250	17.0	324	4.38	398	0.325
252	15.8	326	4.09	400	0.288
254	14.6	328	3.79	402	0.254
256	13.3	330	3.50	404	0.222
258	12.1	332	3.21	406	0.194
260	10.9	334	2.94	406	0.168
262	9.73	336	2.68	410	0.144
264	8.68	338	2.44	412	0.124
266	7.75	340	2.22	414	0.105
268	6.94	342	2.02	416	0.089
270	6.25	344	1.84	418	0.075
272	5.69	346	1.69	420	0.063

F13. $\text{ClNO} + h\nu \rightarrow \text{Cl} + \text{NO}$. Nitrosyl chloride has a continuous absorption extending beyond 650 nm. There is good agreement between the work of Martin and Gareis [243] for the 240-to-420-nm wavelength region, of Ballash and Armstrong [20] for the 185 to 540 nm region, of Illies and Takacs [175] for the 190-to-400-nm region, and of Tyndall et al. [409] for the 190-to-350-nm region except around 230 nm, where the values of Ballash and Armstrong are larger by almost a factor of two. Roehl et al. [344] measured the absorption cross sections between 350 and 650 nm at several temperatures between 223 and 343 K. Their room temperature results agree to within 15% with those of Martin and Gareis [243], Ballash and Armstrong [20], and Tyndall et al. [409]. Table 4-35 lists the recommended cross sections: these are taken from the work of Tyndall et al. [409] between 190 and 350 nm (unchanged from the previous recommendation), and from Roehl et al. [344] beyond 350 nm.

The quantum yield for the primary photolytic process has been reviewed by Calvert and Pitts [65]. It is unity over the entire visible and near-ultraviolet bands.

Table 4-35. Absorption Cross Sections of ClNO

λ (nm)	$10^{20} \sigma$ (cm ²)	λ (nm)	$10^{20} \sigma$ (cm ²)	λ (nm)	$10^{20} \sigma$ (cm ²)	λ (nm)	$10^{20} \sigma$ (cm ²)
190	4320	246	45.2	302	10.3	370	11.0
192	5340	248	37.7	304	10.5	375	9.95
194	6150	250	31.7	306	10.8	380	8.86
196	6480	252	27.4	308	11.1	385	7.82
198	6310	254	23.7	310	11.5	390	6.86
200	5860	256	21.3	312	11.9	395	5.97
202	5250	258	19.0	314	12.2	400	5.13
204	4540	260	17.5	316	12.5	405	4.40
206	3840	262	16.5	318	13.0	410	3.83
208	3210	264	15.3	320	13.4	415	3.38
210	2630	266	14.4	322	13.6	420	2.89
212	2180	268	13.6	324	14.0	425	2.45
214	1760	270	12.9	326	14.3	430	2.21
216	1400	272	12.3	328	14.6	435	2.20
218	1110	274	11.8	330	14.7	440	2.20
220	896	276	11.3	332	14.9	445	2.07
222	707	278	10.7	334	15.1	450	1.87
224	552	280	10.6	336	15.3	455	1.79
226	436	282	10.2	338	15.3	460	1.95
228	339	284	9.99	340	15.2	465	2.25
230	266	286	9.84	342	15.3	470	2.50
232	212	288	9.71	344	15.1	475	2.61
234	164	290	9.64	346	15.1	480	2.53
236	120	292	9.63	348	14.9	485	2.33
238	101	294	9.69	350	14.2	490	2.07
240	82.5	296	9.71	355	13.6	495	1.78
242	67.2	298	9.89	360	12.9	500	1.50
244	55.2	300	10.0	365	12.0		

F14 ClNO₂ + hν → Products. The absorption cross sections of nitryl chloride, ClNO₂, have been measured between 230 and 330 nm by Martin and Gareis [243], between 185 and 400 nm by Illies and Takacs [175], and between 270 and 370 nm by Nelson and Johnston [291], and by Ganske et al. [128] between 200 and 370 nm. A major source of discrepancies in the data results from the presence of impurities. Table 4-36 lists the recommended values, which are taken from Ganske et al. Nelson and Johnston [291] report a value of one (within experimental error) for the quantum yield for production of chlorine atoms; they also report a negligible quantum yield for the production of oxygen atoms.

Table 4-36. Absorption Cross Sections of ClNO₂

λ (nm)	$10^{20} \sigma$ (cm ²)	λ (nm)	$10^{20} \sigma$ (cm ²)
190	2690	290	17.3
200	468	300	14.9
210	320	310	12.1
220	339	320	8.87
230	226	330	5.84
240	133	340	3.54
250	90.6	350	2.04
260	61.3	360	1.15
270	35.3	370	0.69
280	22.0		

- F15. $\text{ClONO} + h\nu \rightarrow \text{Products}$. Measurements in the near-ultraviolet of the cross sections of chlorine nitrite (ClONO) have been made by Molina and Molina [264]. Their results are listed in Table 4-37. The characteristics of the spectrum and the instability of ClONO strongly suggest that the quantum yield for decomposition is unity. The Cl–O bond strength is only about 20 kilocalories, so that chlorine atoms are likely photolysis products.

Table 4-37. Absorption Cross Sections of ClONO at 231 K

λ (nm)	$10^{20} \sigma$ (cm ²)	λ (nm)	$10^{20} \sigma$ (cm ²)
235	215.0	320	80.3
240	176.0	325	75.4
245	137.0	330	58.7
250	106.0	335	57.7
255	65.0	340	43.7
260	64.6	345	35.7
265	69.3	350	26.9
270	90.3	355	22.9
275	110.0	360	16.1
280	132.0	365	11.3
285	144.0	370	9.0
290	144.0	375	6.9
295	142.0	380	4.1
300	129.0	385	3.3
305	114.0	390	2.2
310	105.0	395	1.5
315	98.1	400	0.6

- F16. $\text{ClONO}_2 + h\nu \rightarrow \text{Products}$. The recommended cross sections are taken from the work of Burkholder et al. [55]; the values are listed in Table 4-38, together with the parameters needed to compute their temperature dependency. These values are in very good agreement with those reported by Molina and Molina [266], which provided the basis for the previous recommendation, and which supersedes the earlier work of Rowland, Spencer, and Molina [349].

The identity of the primary photolytic fragments has been investigated by several groups. Smith et al. [384] report $\text{O} + \text{ClONO}$ as the most likely products, using end product analysis and steady-state photolysis. The results of Chang et al. [71], who employed the very low-pressure photolysis (VLPPH) technique, indicate that the products are $\text{Cl} + \text{NO}_3$. Adler-Golden and Wiesenfeld [7], using a flash photolysis atomic absorption technique, find O-atoms to be the predominant photolysis product and report a quantum yield for Cl-atom production of less than 4%. Marinelli and Johnston [241] report a quantum yield for NO_3 production at 249 nm between 0.45 and 0.85, with a most likely value of 0.55; they monitored NO_3 by tunable dye-laser absorption at 662 nm. Margitan [233] used atomic resonance fluorescence detection of O- and Cl-atoms and found the quantum yield at 266 and at 355 nm to be 0.9 ± 0.1 for Cl-atom production and ~ 0.1 for O-atom production, with no discernible difference at the two wavelengths. These results were confirmed by Knauth and Schindler [203], who used end-product analysis to infer the quantum yields. Burrows et al. [61] report also Cl and NO_3 as the photolysis products at 254 nm, with a quantum yield of unity within experimental error. In contrast, Nikolaisen et al. [293] report relative branching ratios of 0.44 for production of ClO and NO_2 and 0.56 for production of Cl and NO_3 at wavelengths beyond 300 nm. Minton et al. [260], Nelson et al. [290], and Moore et al. [276] measured comparable yields for these two channels at 193, 248, and 308 nm, using a molecular beam technique.

The recommended quantum yield values for production of $\text{Cl} + \text{NO}_3$ (ϕ_1) and $\text{ClO} + \text{NO}_2$ (ϕ_2) are given at the bottom of Table 4-38 and are based on the work of Nelson et al. [290], Moore et al. [276], Nikolaisen et al. [293], and Ravishankara [326]. For wavelengths shorter than 308 nm the value of ϕ_1 is 0.6, and for ϕ_2 it is 0.4. For longer wavelengths ϕ_1 increases linearly to 0.9 at 350 nm, with the corresponding decrease in ϕ_2 to 0.1. There is no evidence for production of $\text{O} + \text{ClONO}$ in the more recent work; the production of O-atoms reported in some of the earlier studies might have resulted from decomposition of excited NO_3 .

Recent work by Nikolaisen et al. [293] indicates that the photodissociation quantum yield is less than unity at wavelengths longer than about 330 nm, because of the formation of a long-lived intermediate that might be

quenched under atmospheric conditions (a situation analogous to that of Cl₂O). Additional work is needed to address these issues, which have potentially important atmospheric consequences.

Table 4-38. Absorption Cross Sections of ClONO₂

λ (nm)	$10^{20}\sigma(\lambda,296)$ (cm ²)	A1	A2	λ (nm)	$10^{20}\sigma(\lambda,296)$ (cm ²)	A1	A2
196	310	9.90 (-5)	-8.38 (-6)	316	1.07	5.07 (-3)	1.56 (-5)
198	294	6.72 (-5)	-8.03 (-6)	318	0.947	5.24 (-3)	1.69 (-5)
200	282	-5.34 (-6)	-7.64 (-6)	320	0.831	5.40 (-3)	1.84 (-5)
202	277	-1.19 (-4)	-7.45 (-6)	322	0.731	5.55 (-3)	2.00 (-5)
204	280	-2.60 (-4)	-7.50 (-6)	324	0.647	5.68 (-3)	2.18 (-5)
206	288	-4.12 (-4)	-7.73 (-6)	326	0.578	5.80 (-3)	2.36 (-5)
208	300	-5.62 (-4)	-8.05 (-6)	328	0.518	5.88 (-3)	2.54 (-5)
210	314	-6.96 (-4)	-8.41 (-6)	330	0.466	5.92 (-3)	2.70 (-5)
212	329	-8.04 (-4)	-8.75 (-6)	332	0.420	5.92 (-3)	2.84 (-5)
214	339	-8.74 (-4)	-9.04 (-6)	334	0.382	5.88 (-3)	2.96 (-5)
216	345	-9.03 (-4)	-9.24 (-6)	336	0.351	5.80 (-3)	3.05 (-5)
218	341	-8.86 (-4)	-9.35 (-6)	338	0.326	5.68 (-3)	3.10 (-5)
220	332	-8.28 (-4)	-9.38 (-6)	340	0.302	5.51 (-3)	3.11 (-5)
222	314	-7.31 (-4)	-9.34 (-6)	342	0.282	5.32 (-3)	3.08 (-5)
224	291	-6.04 (-4)	-9.24 (-6)	344	0.264	5.07 (-3)	2.96 (-5)
226	264	-4.53 (-4)	-9.06 (-6)	346	0.252	4.76 (-3)	2.74 (-5)
228	235	-2.88 (-4)	-8.77 (-6)	348	0.243	4.39 (-3)	2.42 (-5)
230	208	-1.13 (-4)	-8.33 (-6)	350	0.229	4.02 (-3)	2.07 (-5)
232	182	6.18 (-5)	-7.74 (-6)	352	0.218	3.68 (-3)	1.76 (-5)
234	158	2.27 (-4)	-7.10 (-6)	354	0.212	3.40 (-3)	1.50 (-5)
236	138	3.72 (-4)	-6.52 (-6)	356	0.205	3.15 (-3)	1.27 (-5)
238	120	4.91 (-4)	-6.14 (-6)	358	0.203	2.92 (-3)	1.06 (-5)
240	105	5.86 (-4)	-5.98 (-6)	360	0.200	2.70 (-3)	8.59 (-6)
242	91.9	6.64 (-4)	-6.04 (-6)	362	0.190	2.47 (-3)	6.38 (-6)
244	81.2	7.33 (-4)	-6.27 (-6)	364	0.184	2.22 (-3)	3.66 (-6)
246	71.6	8.03 (-4)	-6.51 (-6)	366	0.175	1.93 (-3)	2.42 (-7)
248	62.4	8.85 (-4)	-6.59 (-6)	368	0.166	1.62 (-3)	-3.62 (-6)
250	56.0	9.84 (-4)	-6.40 (-6)	370	0.159	1.33 (-3)	-7.40 (-6)
252	50.2	1.10 (-3)	-5.93 (-6)	372	0.151	1.07 (-3)	-1.07 (-5)
254	45.3	1.22 (-3)	-5.33 (-6)	374	0.144	8.60 (-4)	-1.33 (-5)
256	41.0	1.33 (-3)	-4.73 (-6)	376	0.138	6.73 (-4)	-1.54 (-5)
258	37.2	1.44 (-3)	-4.22 (-6)	378	0.129	5.01 (-4)	-1.74 (-5)
260	33.8	1.53 (-3)	-3.79 (-6)	380	0.121	3.53 (-4)	-1.91 (-5)
262	30.6	1.62 (-3)	-3.37 (-6)	382	0.115	2.54 (-4)	-2.05 (-5)
264	27.8	1.70 (-3)	-2.94 (-6)	384	0.108	2.25 (-4)	-2.11 (-5)
266	25.2	1.78 (-3)	-2.48 (-6)	386	0.103	2.62 (-4)	-2.11 (-5)
268	22.7	1.86 (-3)	-2.00 (-6)	388	0.0970	3.33 (-4)	-2.08 (-5)
270	20.5	1.94 (-3)	-1.50 (-6)	390	0.0909	4.10 (-4)	-2.05 (-5)
272	18.5	2.02 (-3)	-1.01 (-6)	392	0.0849	5.04 (-4)	-2.02 (-5)
274	16.6	2.11 (-3)	-4.84 (-7)	394	0.0780	6.62 (-4)	-1.94 (-5)
276	14.9	2.02 (-3)	9.02 (-8)	396	0.0740	8.95 (-4)	-1.79 (-5)
278	13.3	2.29 (-3)	6.72 (-7)	398	0.0710	1.14 (-3)	-1.61 (-5)
280	11.9	2.38 (-3)	1.21 (-6)	400	0.0638	1.38 (-3)	-1.42 (-5)
282	10.5	2.47 (-3)	1.72 (-6)	402	0.0599	1.63 (-3)	-1.20 (-5)
284	9.35	2.56 (-3)	2.21 (-6)	404	0.0568	1.96 (-3)	-8.97 (-6)
286	8.26	2.66 (-3)	2.68 (-6)	406	0.0513	2.36 (-3)	-5.15 (-6)
288	7.24	2.75 (-3)	3.09 (-6)	408	0.0481	2.84 (-3)	-6.64 (-7)
290	6.41	2.84 (-3)	3.41 (-6)	410	0.0444	3.38 (-3)	4.47 (-6)
292	5.50	2.95 (-3)	3.74 (-6)	412	0.0413	3.96 (-3)	1.00 (-5)

λ (nm)	$10^{20}\sigma(\lambda,296)$ (cm ²)	A1	A2	λ (nm)	$10^{20}\sigma(\lambda,296)$ (cm ²)	A1	A2
294	4.67	3.08 (-3)	4.27 (-6)	414	0.0373	4.56 (-3)	1.60 (-5)
296	4.09	3.25 (-3)	5.13 (-6)	416	0.0356	5.22 (-3)	2.28 (-5)
298	3.57	3.45 (-3)	6.23 (-6)	418	0.0317	5.96 (-3)	3.07 (-5)
300	3.13	3.64 (-3)	7.36 (-6)	420	0.0316	6.70 (-3)	3.87 (-5)
302	2.74	3.83 (-3)	8.38 (-6)	422	0.0275	7.30 (-3)	4.58 (-5)
304	2.39	4.01 (-3)	9.30 (-6)	424	0.0242	7.82 (-3)	5.22 (-5)
306	2.09	4.18 (-3)	1.02 (-5)	426	0.0222	8.41 (-3)	5.95 (-5)
308	1.83	4.36 (-3)	1.11 (-5)	428	0.0207	9.11 (-3)	6.79 (-5)
310	1.60	4.53 (-3)	1.20 (-5)	430	0.0189	9.72 (-3)	7.52 (-5)
312	1.40	4.71 (-3)	1.30 (-5)	432	0.0188	9.96 (-3)	7.81 (-5)
314	1.22	4.89 (-3)	1.42 (-5)				

$$\sigma(\lambda, T) = \sigma(\lambda, 296) (1 + A_1 (T - 296) + A_2 (T - 296)^2); T \text{ in K}$$

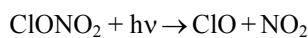
Quantum yields:



$$\phi_1 = 0.6 \quad (\lambda < 308 \text{ nm})$$

$$\phi_1 = 7.143 \times 10^{-3} \lambda \text{ (nm)} - 1.60 \quad (308 \text{ nm} < \lambda < 364 \text{ nm})$$

$$\phi_1 = 1.0 \quad (\lambda > 364 \text{ nm})$$



$$\phi_2 = 1 - \phi_1$$

F17. $\text{CCl}_4 + h\nu \rightarrow \text{Products}$. The absorption cross sections of CCl_4 have been measured at room temperature and 110–200 nm by Russell et al. [353]; at 204–250 nm by Gordus and Bernstein [142]; at 186–226 nm by Rowland and Molina [347]; at 170–230 nm by Roxlo and Mandl [350]; and at 160–275 nm by Hubrich and Stuhl [165]; at 297–477 K and 250 nm by Currie et al. [98], at 279 and 296 K and 190–252 nm by Vanlaethem-Meurée et al. [418]; at 225–295 K and 174–250 nm by Simon et al. [379]; and at 220–300 K and 186–240 nm by Prahlaad and Kumar [319]. The room temperature data agree within 10% between 190 and 235 nm and within 20% and 40% at 240 and 250 nm (except the value at 250 nm reported by Currie et al [98], which is lower than the half of the other values). The absorption curve based on the data (reported at 0.5-nm intervals) of Prahlaad and Kumar [319] shows wiggles over the whole range 186–240 nm obviously due to experimental uncertainties. In the range 180–186 nm, the values reported by Hubrich and Stuhl [165] are higher by up to 25% than those reported by Simon et al. [379], and the value at 186 nm reported by Prahlaad and Kumar [319] is lower by 18% than the value of Simon et al. [379]. In the maximum near 176 nm, the absorption cross section is $1.01 \times 10^{-17} \text{ cm}^2$, as reported by Hubrich and Stuhl [165] and Simon et al. [379], whereas the plotted spectrum reported by Roxlo and Mandl [350] shows a lower value of $\sim 7 \times 10^{-18} \text{ cm}^2$. For a wavelength of 313 nm, an absorption cross section of $\leq 3.7 \times 10^{-26} \text{ cm}^2$ was derived by Rebbert and Ausloos [332] from the $\text{C}_2\text{H}_5\text{Cl}$ yield in the photolysis of $\text{CCl}_4\text{-C}_2\text{H}_6$ mixtures. The preferred absorption cross sections at room temperature, listed in Table 4-39, are the mean of the values reported by Hubrich and Stuhl [165] and Simon et al. [379] at 174–192 nm, the values of Simon et al. [379] at 194–250 nm, and the data of Hubrich and Stuhl [165] at 255–275 nm.

The temperature dependence of the absorption cross sections becomes significant at wavelengths above 205 nm, where the cross sections decrease with decreasing temperature between 300 and 210 K as observed in good agreement by Simon et al. [379] and Prahlaad and Kumar [319]. Simon et al. [379] parameterized the cross sections and the temperature dependence by the polynomial expansion

$$\log_{10} \sigma(\lambda, T) = \sum A_n \lambda^n + (T - 273) \times \sum B_n \lambda^n$$

and reported smoothed values for $T = 210, 230, 250, 270,$ and 295 K , every 2 nm, and at wavelengths corresponding to the wavenumber intervals generally used in stratospheric photodissociation calculations. The parameters A_n and B_n for the ranges $T = 210\text{--}300 \text{ K}$ and $\lambda = 194\text{--}250 \text{ nm}$ are as follows:

$$\begin{aligned}
 A_0 &= -37.104 & B_0 &= 1.0739 \\
 A_1 &= -5.8218 \times 10^{-1} & B_1 &= -1.6275 \times 10^{-2} \\
 A_2 &= 9.9974 \times 10^{-3} & B_2 &= 8.8141 \times 10^{-5} \\
 A_3 &= -4.6765 \times 10^{-5} & B_3 &= -1.9811 \times 10^{-7} \\
 A_4 &= 6.8501 \times 10^{-8} & B_4 &= 1.5022 \times 10^{-10}
 \end{aligned}$$

Quantum yields ≥ 0.9 and ~ 0.75 for the photodissociative processes $\text{CCl}_4 + h\nu \rightarrow \text{CCl}_3 + \text{Cl}$ at 213.9 nm and $\text{CCl}_4 + h\nu \rightarrow \text{CCl}_2 + 2\text{Cl}$ at 163.3 nm, respectively, were derived from the gas-phase photolysis of CCl_4 in the presence of HCl, HBr, and C_2H_6 by Rebert and Ausloos [332]. A quantum yield for $\text{Cl}^*(^2\text{P}_{1/2})$ atom formation in the broad band photolysis of CCl_4 , $\Phi(\text{Cl}^*) = 0.78 \pm 0.27$, was reported by Clark and Husain [80].

Table 4-39. Absorption Cross Sections of CCl_4 at 295–298 K

λ (nm)	$10^{20} \sigma$ (cm^2)	λ (nm)	$10^{20} \sigma$ (cm^2)	λ (nm)	$10^{20} \sigma$ (cm^2)
174	956	204	61.0	234	2.20
176	1010	206	57.0	236	1.60
178	982.5	208	52.5	238	1.16
180	806	210	46.9	240	0.830
182	647	212	41.0	242	0.590
184	478.5	214	34.5	244	0.413
186	338.5	216	27.8	246	0.290
188	227	218	22.1	248	0.210
190	145.5	220	17.5	250	0.148
192	99.6	222	13.6	255	0.0661
194	76.7	224	10.2	260	0.0253
196	69.5	226	7.60	265	0.0126
198	68.0	228	5.65	270	0.00610
200	66.0	230	4.28	275	0.00239
202	63.8	232	3.04		

Notes:

174–192 nm: mean of Hubrich and Stuhl [165] and Simon et al. [379]

194–250 nm: Simon et al. [379]

255–275 nm: Hubrich and Stuhl [165].

- F18. $\text{CH}_3\text{OCl} + h\nu \rightarrow \text{Products}$. The absorption cross sections of CH_3OCl have been determined by Crowley et al. [96] and by Jungkamp et al. [196]. The preferred cross sections, listed in Table 4-40, are the mean of the values reported by these two groups. The agreement between the two sets of measurements is excellent at wavelengths longer than 250 nm; at the maximum near 230 nm the results of Jungkamp et al. are about 15% smaller.

Table 4-40. Absorption Cross Sections of CH₃OCl

λ (nm)	$10^{20} \sigma$ (cm ²)	λ (nm)	$10^{20} \sigma$ (cm ²)	λ (nm)	$10^{20} \sigma$ (cm ²)
230	14.9	290	1.32	350	0.662
232	15.4	292	1.34	352	0.611
234	15.7	294	1.35	354	0.574
236	15.9	296	1.37	356	0.529
238	15.8	298	1.40	358	0.482
240	15.5	300	1.43	360	0.445
242	14.9	302	1.45	362	0.411
244	14.2	304	1.47	364	0.389
246	13.2	306	1.48	366	0.356
248	12.2	308	1.49	368	0.331
250	11.1	310	1.49	370	0.298
252	9.96	312	1.48	372	0.273
254	8.86	314	1.47	374	0.246
256	7.77	316	1.46	376	0.225
258	6.80	318	1.43	378	0.209
260	5.87	320	1.41	380	0.202
262	5.05	322	1.37	382	0.186
264	4.31	324	1.33	384	0.17
266	3.69	326	1.30	386	0.16
268	3.16	328	1.24	388	0.15
270	2.71	330	1.20	390	0.13
272	2.35	332	1.14	392	0.14
274	2.06	334	1.09	394	0.13
276	1.83	336	1.04		
278	1.64	338	0.980		
280	1.53	340	0.918		
282	1.42	342	0.875		
284	1.37	344	0.822		
286	1.33	346	0.760		
288	1.32	348	0.709		

F19. CHCl₃ + hν → Products. The absorption cross sections of CHCl₃ have been measured at room temperature and in the far UV region at 113–182 nm by Lucazeau et al. [225]; at the Lyman-α line at 121.6 nm by Brownsword et al. [46]; and at 110–200 nm by Russell et al. [353]; at room temperature and 222.7 nm by Gordus and Bernstein [142]; at 160–255 nm by Hubrich and Stuhl [165]; at 279 and 296 K and 190–230 nm by Vanlaethem-Meurée et al. [418]; and at 225–295 K and 174–240 nm by Simon et al. [379]. The room temperature data of Vanlaethem-Meurée et al. [418] and Simon et al. [379] are identical at 190–210 nm and increasingly deviate up to ~15% at 212–240 nm. The data of Hubrich and Stuhl [165] and Simon et al. [379] agree within 10 % between 180 and 234 nm; however the values of Hubrich and Stuhl [165] become increasingly larger by up to ~25% than those of Simon et al. [379] in the long-wavelength tail. In the region of the absorption maximum at ~176 nm, there is the largest spread: a cross sections of $\sim 5 \times 10^{-18}$ cm² has been measured by Simon et al. [379] in contrast to values of 3.7×10^{-18} cm² reported by Hubrich and Stuhl [165] and $< 2 \times 10^{-18}$ cm² given in a plot by Lucazeau et al. [225]. We therefore recommend absorption cross sections only for the region above 180 nm. The values, listed in Table 4-41, are the mean of the values reported by Hubrich and Stuhl [165] and Simon et al. [379] for the range 180–240 nm. For the range 242–256 nm, these have been extrapolated ($\log \sigma = -1.2277 - 0.0844 \lambda$) (in italics).

The temperature dependence of the absorption cross sections becomes significant at wavelengths above 194 nm, where the cross sections decrease with decreasing temperature between 295 and 210 K. Simon et al. [379] parameterized the cross sections and the temperature dependence by the polynomial expansion $\log_{10} \sigma(\lambda, T) = \sum A_n \lambda^n + (T - 273) \times \sum B_n \lambda^n$ and reported smoothed values for T = 210, 230, 250, 270, and 295 K, every 2 nm, and at wavelengths corresponding to the wavenumber intervals generally used in

stratospheric photodissociation calculations. The parameters A_n and B_n for the ranges $T = 210\text{--}300$ K and $\lambda = 190\text{--}240$ nm are as follows:

$$\begin{array}{ll} A_0 = 269.80 & B_0 = 3.7973 \\ A_1 = -6.0908 & B_1 = -7.0913 \times 10^{-2} \\ A_2 = 4.7830 \times 10^{-2} & B_2 = 4.9397 \times 10^{-4} \\ A_3 = -1.6427 \times 10^{-4} & B_3 = -1.5226 \times 10^{-6} \\ A_4 = 2.0682 \times 10^{-7} & B_4 = 1.7555 \times 10^{-9} \end{array}$$

Quantum yields for H atom formation have been measured in the far UV by Brownsword et al. [46], [47]: $\Phi(\text{H}) = 0.23 \pm 0.03$ and 0.13 at 121.6 and 157.6 nm, respectively, whereas H atoms could not be detected in the photolysis at 193.3 nm.

Table 4-41. Absorption Cross Sections of CHCl_3 at 295–298 K

λ (nm)	$10^{20} \sigma$ (cm^2)	λ (nm)	$10^{20} \sigma$ (cm^2)	λ (nm)	$10^{20} \sigma$ (cm^2)
180	372	206	20.7	232	0.158
182	317	208	15.1	234	0.107
184	248	210	10.7	236	0.0730
186	186	212	7.48	238	0.0503
188	144	214	5.24	240	0.0347
190	113	216	3.60	242	0.0223
192	89.9	218	2.48	244	0.0151
194	76.1	220	1.69	246	0.01023
196	64.2	222	1.13	248	0.00694
198	53.0	224	0.750	250	0.00470
200	42.6	226	0.503	252	0.00319
202	34.4	228	0.342	254	0.00216
204	27.2	230	0.234	256	0.00147

Note: 180–240 nm: mean of Hubrich and Stuhl [165] and Simon et al. [379]

242–256 nm: extrapolation of mean of Hubrich and Stuhl [165] and Simon et al. [379] data.

- F20. $\text{CH}_2\text{Cl}_2 + h\nu \rightarrow \text{Products}$. The absorption cross sections of CH_2Cl_2 have been measured at room temperature and 110–200 nm by Russell et al. [353]; at the Lyman- α line at 121.6 nm by Brownsword et al. [46]; at 213 nm by Gordus and Bernstein [142], at 160–255 nm by Hubrich and Stuhl [165]; at 279 and 296 K and 176–216 nm by Vanlaethem-Meurée et al. [418]; and at 225–295 K and 176–220 nm by Simon et al. [379]. The room temperature data of Vanlaethem-Meurée et al. [418] and Simon et al. [379] are nearly identical. The data of Hubrich and Stuhl [165] agree with those of Simon et al. [379] within 12% at 176–206 nm and become increasingly larger at 185–220 nm by up to 50%. The preferred absorption cross sections, listed in Table 4-42, are the mean of the values reported by Hubrich and Stuhl [165] and Simon et al. [379] at 176–220 nm. For wavelengths above 220 nm, the average of their data at 200–210 nm has been extrapolated ($\log \sigma = -2.1337 - 0.08439 \lambda$) (in italics) at wavelengths up to 256 nm. The measured values of Hubrich and Stuhl [165] are smaller by up to 7% below 230 nm and become larger by up to 50% between 235 and 255 nm than the extrapolated values.

The temperature dependence of the absorption cross sections becomes significant at wavelengths above 190 nm, where the cross sections decrease with decreasing temperature between 295 and 210 K. Simon et al. [379] parameterized the cross sections and the temperature dependence by the polynomial expansion $\log_{10} \sigma(\lambda, T) = \sum A_n \lambda^n + (T - 273) \times \sum B_n \lambda^n$ and reported smoothed values for $T = 210, 230, 250, 270,$ and 295 K, every 2 nm, and at wavelengths corresponding to the wavenumber intervals generally used in stratospheric photodissociation calculations. The parameters A_n and B_n for the ranges $T = 210\text{--}300$ K and $\lambda = 176\text{--}220$ nm are as follows:

$$\begin{array}{ll} A_0 = -1431.8 & B_0 = -3.1171 \\ A_1 = 27.395 & B_1 = 6.7874 \times 10^{-2} \\ A_2 = -1.9807 \times 10^{-1} & B_2 = -5.5000 \times 10^{-4} \\ A_3 = 6.3468 \times 10^{-4} & B_3 = 1.9649 \times 10^{-6} \\ A_4 = -7.6298 \times 10^{-7} & B_4 = -2.6101 \times 10^{-9} \end{array}$$

Quantum yields for H atom formation have been measured in the far UV by Brownsword et al. [46], [47]: $\Phi(\text{H}) = 0.28 \pm 0.03$, 0.23, and 0.002 ± 0.001 at 121.6, 157.6, and 193.3 nm, respectively.

Table 4-42. Absorption Cross Sections of CH₂Cl₂ at 295–298 K

λ (nm)	$10^{20} \sigma$ (cm ²)	λ (nm)	$10^{20} \sigma$ (cm ²)	λ (nm)	$10^{20} \sigma$ (cm ²)
176	186	204	4.41	232	0.0194
178	182	206	3.07	234	0.0132
180	173	208	2.13	236	0.00892
182	156	210	1.45	238	0.00605
184	135	212	0.978	240	0.00410
186	110	214	0.651	242	0.00278
188	84.2	216	0.435	244	0.00188
190	61.0	218	0.291	246	0.00128
192	43.9	220	0.190	248	0.000866
194	30.5	222	0.135	250	0.000587
196	20.6	224	0.0918	252	0.000398
198	14.1	226	0.0623	254	0.000270
200	9.48	228	0.0422	256	0.000183
202	6.40	230	0.0286		

Note: 176–220 nm: mean of Hubrich and Stuhl [165] and Simon et al. [379]

222–256 nm: extrapolation of mean of Hubrich and Stuhl [165] and Simon et al. [379] data.

- F21. CH₃Cl + hv → Products. The absorption cross sections of CH₃Cl have been measured at room temperature and 110–200 nm by Russell et al. [353]; at the Lyman- α line at 121.6 nm by Brownsword et al. [46]; at 171.2 nm by Felps et al. [119]; and at 174–220 nm by Robbins [338]; at 208 and 298 K and 158–235 nm by Hubrich et al. [166]; at 255, 279, and 296 K and 186–216 nm by Vanlaethem-Meurée et al. [418]; and at 225–295 K and 174–216 nm by Simon et al. [379]. The room temperature data generally agree within 10% in the wavelength range 174–216 nm, those of Vanlaethem-Meurée et al. [418] and Simon et al. [379] are nearly identical. The value at 171 nm of Felps et al. [47] is smaller by ~15% than that of Hubrich et al. [166]. The preferred absorption cross sections, listed in

Table 4-43, are the mean of the values reported by Robbins [338], Hubrich et al. [166], and Simon et al. [379] at 174–184 nm, the mean of the values reported by Robbins [338], Hubrich et al. [166], Vanlaethem-Meurée et al. [418], and Simon et al. [379] at 186–216 nm, and the mean of the values reported by Robbins [338] and Hubrich et al. [166] at 218–220 nm. The values for the wavelength range 222–236 nm have been taken from an interpolation (at 2-nm intervals) of the 200–235-nm data of Hubrich et al. [166] ($\log \sigma = -0.24164 - 0.09743 \lambda$).

The temperature dependence of the absorption cross sections becomes significant at wavelengths above 194 nm, where the cross sections decrease with decreasing temperature between 295 and 210 K. There is very good agreement between the low-temperature values at 250–255 K of Vanlaethem-Meurée et al. [418] and Simon et al. [379]. The latter authors parameterized the cross sections and the temperature dependence by the polynomial expansion $\log_{10} \sigma(\lambda, T) = \sum A_n \lambda^n + (T - 273) \times \sum B_n \lambda^n$ and reported smoothed values for $T = 210, 230, 250, 270,$ and 295 K, every 2 nm, and at wavelengths corresponding to the wavenumber intervals generally used in stratospheric photodissociation calculations. The parameters A_n and B_n for the ranges $T = 210$ – 300 K and $\lambda = 174$ – 216 nm are as follows:

$$\begin{array}{ll} A_0 = -299.80 & B_0 = -7.1727 \\ A_1 = 5.1047 & B_1 = 1.4837 \times 10^{-1} \\ A_2 = -3.3630 \times 10^{-2} & B_2 = -1.1463 \times 10^{-3} \\ A_3 = 95805 \times 10^{-5} & B_3 = 3.9188 \times 10^{-6} \\ A_4 = -1.0135 \times 10^{-7} & B_4 = -4.9994 \times 10^{-9} \end{array}$$

Quantum yields for H atom formation have been measured in the far UV by Brownsword et al. [46], [47]: $\Phi(\text{H}) = 0.53 \pm 0.05, 0.29, 0.012 \pm 0.006$ at 121.6, 157.6, and 193.3 nm, respectively.

Table 4-43. Absorption Cross Sections of CH₃Cl at 295–298 K

λ (nm)	$10^{20} \sigma$ (cm ²)	λ (nm)	$10^{20} \sigma$ (cm ²)	λ (nm)	$10^{20} \sigma$ (cm ²)
174	110	196	3.96	218	0.0345
176	93.9	198	2.68	220	0.0220
178	78.2	200	1.77	222	0.0135
180	63.6	202	1.13	224	0.00859
182	46.5	204	0.731	226	0.00549
184	35.0	206	0.482	228	0.00350
186	25.8	208	0.313	230	0.00224
188	18.4	210	0.200	232	0.00143
190	12.8	212	0.127	234	0.000911
192	8.84	214	0.0860	236	0.000582
194	5.83	216	0.0534		

Note:

174–184 nm: mean of Robbins [338], Hubrich et al. [166], and Simon et al. [379]

186–216 nm: mean of Robbins [338], Hubrich et al. [166], Vanlaethem-Meurée et al. [418] and Simon et al. [379]

218–220 nm: mean of Robbins [338] and Hubrich et al. [166]

222–236 nm: extrapolation of Hubrich et al. [166] data.

- F22. CH₃CCl₃ + hv → Products. The absorption cross sections of CH₃CCl₃ have been measured at room temperature and 147 nm by Salomon et al. [355], and at 160–255 nm by Hubrich and Stuhl [165], who corrected (<10.7%) the absorption cross sections in the range 170–190 nm for the concentration and absorption cross sections of a 1,4-dioxane stabilizer present during the experiments. Measurements at 220–295 K and 182–240 nm were carried out by Vanlaethem-Meurée et al. [420] and at 223–333 K and 160–240 nm by Nayak et al. [287]. The latter authors also measured the absorption cross sections in the liquid phase at 235–260 nm and used a wavelength-shift procedure to convert the liquid-phase data into gas-phase data. The agreement of the room temperature data is within 20% at 165–205 nm (at 160 nm, the value reported by Nayak et al. [287] is larger by 50% than that reported by Hubrich and Stuhl [165]). Between 210 and 240 nm, the data of Vanlaethem-Meurée et al. [420] and Nayak et al. [287] are within 15%, whereas those of Hubrich and Stuhl [165] are larger by 100–150%. The preferred absorption cross sections, listed in Table 4-44, are the mean of the values reported by Hubrich and Stuhl [165] and Nayak et al. [287] at 170–180 nm, the mean of the values reported by Vanlaethem-Meurée et al. [420], Hubrich and Stuhl [165], and Nayak et al. [287] at 185–205 nm, and the mean of the values reported by Vanlaethem-Meurée et al. [420] and Nayak et al. [287] at 210–240 nm. For wavelengths above 240 nm, the average of their data at 220–240 nm has been extrapolated ($\log \sigma = -1.59792 - 0.08066 \lambda$) at wavelengths up to 255 nm. The measured values of Hubrich and Stuhl [165] are larger by up to ~140% at 250 nm and smaller by ~80% at 255 nm than the recommended values.

The temperature dependence of the absorption cross sections becomes significant at wavelengths above 210 nm, where the cross sections decrease with decreasing temperature, as observed in good agreement at 333–223 K by Nayak et al. [287] and at 295–210 K by Vanlaethem-Meurée et al. [420]. The latter authors parameterized the cross sections and the temperature dependence by the polynomial expansion $\log_{10} \sigma(\lambda, T) = \sum A_n \lambda^n + (T - 273) \times \sum B_n \lambda^n$ and reported smoothed values for T = 210, 230, 250, 270, and 295 K, every 2 nm, and at wavelengths corresponding to the wavenumber intervals generally used in stratospheric photodissociation calculations. The parameters A_n and B_n for the ranges T = 210–300 K and $\lambda = 182$ –240 nm reported by Gillotay and Simon [138] are as follows:

$$\begin{array}{ll}
 A_0 = 341.085191 & B_0 = -1.660090 \\
 A_1 = -7.273362 & B_1 = 3.079969 \times 10^{-2} \\
 A_2 = 5.498387 \times 10^{-2} & B_2 = -2.106719 \times 10^{-4} \\
 A_3 = -1.827552 \times 10^{-4} & B_3 = 6.264984 \times 10^{-7} \\
 A_4 = 2.238640 \times 10^{-7} & B_4 = -6.781342 \times 10^{-10}
 \end{array}$$

Table 4-44. Absorption Cross Sections of CH₃CCl₃ at 295–298 K

λ (nm)	$10^{20} \sigma$ (cm ²)	λ (nm)	$10^{20} \sigma$ (cm ²)	λ (nm)	$10^{20} \sigma$ (cm ²)
170	406	200	92.1	230	0.717
175	424	205	52.0	235	0.276
180	404	210	25.5	240	0.111
185	301	215	10.9	245	0.0437
190	212	220	4.47	250	0.0173
195	147	225	1.82	255	0.00682

Note: 170–180 nm: mean of Hubrich and Stuhl [165] and Nayak et al. [287]

185–205 nm: mean of Vanlaethem-Meurée et al. [420], Hubrich and Stuhl [165] and Nayak et al. [287]

210–240 nm: mean of Vanlaethem-Meurée et al. [420] and Nayak et al. [287]

245–255 nm: extrapolation of mean of Vanlaethem-Meurée et al. [420] and Nayak et al. [287] data.

- F23. CH₃H₂Cl + hv → Products. The absorption cross sections of CH₃CH₂Cl have been measured at room temperature and 147 nm by Ichimura et al. [173] and at 160–240 nm by Hubrich and Stuhl [165]. The data of Hubrich and Stuhl [165] are listed in Table 4-45.

Table 4-45. Absorption Cross Sections of CH₃CH₂Cl at 298 K

λ (nm)	$10^{20} \sigma$ (cm ²)	λ (nm)	$10^{20} \sigma$ (cm ²)	λ (nm)	$10^{20} \sigma$ (cm ²)
160	189.0	190	6.85	220	0.0127
165	110.0	195	2.56	225	0.00463
170	70.5	200	1.17	230	0.00117
175	44.4	205	0.375	235	0.000395
180	30.4	210	0.147	240	0.000156
185	13.6	215	0.0433		

Note: 160–240 nm, Hubrich and Stuhl [165].

- F24. CH₃CHClCH₃ + hv → Products. In a compilation of ultraviolet absorption cross sections of halocarbons by Gillotay and Simon [355] results are reported for (erroneously) CH₃CH₂ClCH₃, which presumably should be CH₃CHClCH₃. The data are listed in Table 4-46.

Table 4-46. Absorption Cross Sections of CH₃CHClCH₃ at 295 K

λ (nm)	$10^{20} \sigma$ (cm ²)	λ (nm)	$10^{20} \sigma$ (cm ²)	λ (nm)	$10^{20} \sigma$ (cm ²)
170	31.7	192	4.67	214	0.0965
172	27.0	194	3.49	216	0.0652
174	24.3	196	2.58	218	0.0444
176	22.1	198	1.88	220	0.0308
178	20.3	200	1.34	222	0.0212
180	18.0	202	0.954	224	0.0144
182	15.0	204	0.671	226	0.0107
184	12.2	206	0.463	228	0.00752
186	9.99	208	0.311	230	0.00580
188	7.93	210	0.214		
190	6.06	212	0.144		

Note: 170–230 nm, Gillotay and Simon [138].

F25. CH₂ClCH₂Cl + hv → Products.

F26. CH₂ClCH₂CH₂Cl + hv → Products.

F27. CH₂Cl(CH₂)₂CH₂Cl + hv → Products.

Absorption cross sections for these three dichloroalkanes at room temperature and 118–200 nm have been reported by Russell et al. [353].

F28. CCl₂O + hv → Products. See note for CF₂O + hv (Note E5).

F29. CClFO + hv → Products. See note for CF₂O + hv (Note E5).

F30. CFCl₃ (CFC-11) + hv → Products. The absorption cross sections of CFCl₃ have been measured at room temperature and 225 nm by Gordus and Bernstein [142], at 186–226 nm by Rowland and Molina [347], at 174–226 nm by Robbins and Stolarski [339], at 186–209 nm by Greene and Wayne [146]; at 213–296 K and 185–226 nm by Chou et al. [78]; at 208 and 298 K and 158–260 nm by Hubrich et al. [166] and Hubrich and Stuhl [165]; at 255, 279, and 296 K and 190–220 nm by Vanlaethem-Meurée et al. [419]; at 225–295 K and 174–230 nm by Simon et al. [379]; and at 220, 240, and 296 K and 200–238 nm by Mérienne et al. [256]. The room temperature data are in good agreement, generally within 10–15%. Absorption cross sections at 148–225 nm have also been derived from electron energy-loss measurements by Huebner et al. [171], which are up to 30% higher than the values obtained by optical measurements. The preferred absorption cross sections, listed in Table 4-47, are the values of Simon et al. [379] at 174–198 nm, the mean of the values reported by Simon et al. [379] and Mérienne et al. [256] at 200–230 nm, and the data of Hubrich and Stuhl [165] at 235–260 nm.

Measurements in the far UV at 60–145 nm have been reported by Gilbert et al. [132], and at 120–200 nm by Doucet et al. [110].

The temperature dependence becomes significant at wavelengths above 185 nm, where the cross sections decrease with decreasing temperature between 296 and 210 K (Hubrich et al. [166] observed such a behavior only above 200 nm). Simon et al. [379] parameterized the temperature dependence of the cross sections by the polynomial expansion $\log_{10} \sigma(\lambda, T) = \sum A_n \lambda^n + (T - 273) \times \sum B_n \lambda^n$ and reported smoothed values for T = 210, 230, 250, 270, and 295 K, every 2 nm, and at wavelengths corresponding to the wavenumber intervals generally used in stratospheric photodissociation calculations. The parameters A_n and B_n for the ranges T = 210–300 K and $\lambda = 174$ –230 nm are as follows:

$$\begin{array}{ll}
 A_0 = -84.611 & B_0 = -5.7912 \\
 A_1 = 7.9551 \times 10^{-1} & B_1 = 1.1689 \times 10^{-1} \\
 A_2 = -2.0550 \times 10^{-3} & B_2 = -8.8069 \times 10^{-4} \\
 A_3 = -4.4812 \times 10^{-6} & B_3 = 2.9335 \times 10^{-6} \\
 A_4 = 1.5838 \times 10^{-8} & B_4 = -3.6421 \times 10^{-9}
 \end{array}$$

A similar polynomial expansion, $\log_{10} \sigma(\lambda, T) = \sum a_n (\lambda - 200)^n + (T - 296) \times \sum b_n (\lambda - 200)^n$, for the ranges T = 220–296 K and $\lambda = 200$ –238 nm was used by Mérienne et al. [256] with the following parameters a_n and b_n:

$$\begin{aligned}
 a_0 &= -41.925548 & b_0 &= 3.58977 \times 10^{-4} \\
 a_1 &= -1.142857 \times 10^{-1} & b_1 &= 3.02973 \times 10^{-4} \\
 a_2 &= -3.12034 \times 10^{-3} & b_2 &= -1.13 \times 10^{-8} \\
 a_3 &= 3.6699 \times 10^{-5} & &
 \end{aligned}$$

A quantum yield for $\text{Cl}^*(^2\text{P}_{1/2})$ atom formation in the broad band photolysis of CFCl_3 , $\Phi(\text{Cl}^*) = 0.79 \pm 0.27$, was reported by Clark and Husain [80].

Table 4-47. Absorption Cross Sections of CFCl_3 at 295–298 K

λ (nm)	$10^{20} \sigma$ (cm ²)	λ (nm)	$10^{20} \sigma$ (cm ²)	λ (nm)	$10^{20} \sigma$ (cm ²)
174	313.0	198	78.0	222	1.72
176	324.0	200	63.2	224	1.17
178	323.5	202	49.1	226	0.790
180	314.0	204	37.3	228	0.532
182	296.0	206	28.1	230	0.354
184	272.0	208	20.4	235	0.132
186	243.0	210	15.1	240	0.0470
188	213.0	212	10.7	245	0.0174
190	179.0	214	7.54	250	0.0066
192	154.0	216	5.25	255	0.0029
194	124.3	218	3.65	260	0.0015
196	99.1	220	2.51		

Note: 174–198 nm: Simon et al. [379]

200–230 nm: mean of Simon et al. [379] and Mérienne et al. [256]

235–260 nm: Hubrich and Stuhl [165].

- F31. CF_2Cl_2 (CFC-12) + $h\nu \rightarrow$ Products. The absorption cross sections of CF_2Cl_2 have been measured at room temperature and 210 nm by Gordus and Bernstein [142], at 186–216 nm by Rowland and Molina [347], at 174–216 nm by Robbins and Stolarski [339], at 186–206 nm by Greene and Wayne [146]; at 234–442 K and 213.9 nm by Rebbert and Ausloos [333]; at 212, 252, and 296 K and 184–221 nm by Chou et al. [78]; at 208 and 298 K and 159–240 nm by Hubrich et al. [166]; at 255, 279, and 296 K and 190–216 nm by Vanlaethem-Meurée et al. [419]; at 225–295 K and 174–230 nm by Simon et al. [379]; and at 220, 240, and 296 K and 200–231 nm by Mérienne et al. [256]. The room temperature data are in good agreement, generally within 10–15%, except the data of Green and Wayne [146] above 195 nm and the data of Rowland and Molina [347] around 210 nm. Absorption cross sections at 148–218 nm have also been derived from electron energy-loss measurements by Huebner et al. [171], which agree within 10% with the data obtained by optical measurements around the absorption maximum and become higher than the optical data by up to 100% above 196 nm. The preferred absorption cross sections, listed in Table 4-51, are the values of Hubrich et al. [166] at 170–172 nm, the mean of the values reported by Hubrich et al. [166] and Simon et al. [379] at 174–178 nm, the values of Simon et al. [379] at 180–198 nm, the mean of the values reported by Simon et al. [379] and Mérienne et al. [256] at 200–226 nm, and the data of Mérienne et al. [256] at 228–230 nm. For the range 232–240 nm, the absorption curve above 210 nm of Mérienne et al. [256] has been extrapolated ($\log \sigma = 2.1448 - 0.1061 \lambda$). The measured values of Hubrich et al. [166] are lower by up to ~40% at 240 nm than the extrapolated values.

High-resolution absorption cross section measurements have been carried out by Secombe et al. [369] between 50 and 150 nm, and by Limao-Vieira et al. [219] between 113 and 225 nm using a synchrotron radiation light source. The results of Limao-Vieira et al. for the absorption band at 170–204 nm are in very good agreement with the recommendation in Table 4-48 (at wavelengths above 204 nm, noise effects become significant). The new cross section measurements for the far UV region from both recent studies significantly improve upon the earlier data of Gilbert et al. [132] for the wavelength range 60–135 nm and of Doucet et al. [110] for the wavelength range 120–200 nm.

The temperature dependence becomes significant at wavelengths above 186 nm, where the cross sections decrease with decreasing temperature between 296 and 210 K. Simon et al. [379] parameterized the temperature dependence of the cross sections by the polynomial expansion $\log_{10} \sigma(\lambda, T) = \sum A_n \lambda^n + (T - 273) \times \sum B_n \lambda^n$ and reported smoothed values for $T = 210, 230, 250, 270,$ and 295 K, every 2 nm, and at wavelengths

corresponding to the wavenumber intervals generally used in stratospheric photodissociation calculations. The parameters A_n and B_n for the ranges $T = 210\text{--}300$ K and $\lambda = 174\text{--}226$ nm are as follows:

$$\begin{array}{ll} A_0 = -711.02 & B_0 = 6.1648 \\ A_1 = 12.490 & B_1 = -1.2093 \times 10^{-1} \\ A_2 = -8.2865 \times 10^{-2} & B_2 = 8.8587 \times 10^{-4} \\ A_3 = 2.4091 \times 10^{-4} & B_3 = -2.8743 \times 10^{-6} \\ A_4 = -2.6113 \times 10^{-7} & B_4 = 3.4904 \times 10^{-9} \end{array}$$

A similar polynomial expansion, $\log_{10} \sigma(\lambda, T) = \sum a_n (\lambda - 200)^n + (T - 296) \times \sum b_n (\lambda - 200)^n$, for the ranges $T = 220\text{--}296$ K and $\lambda = 200\text{--}231$ nm was used by Mérienne et al. [256] with the following parameters a_n and b_n :

$$\begin{array}{ll} a_0 = -43.8954569 & b_0 = 4.8438 \times 10^{-3} \\ a_1 = -2.403597 \times 10^{-1} & b_1 = 4.96145 \times 10^{-4} \\ a_2 = -4.2619 \times 10^{-4} & b_2 = -5.6953 \times 10^{-6} \\ a_3 = 9.8743 \times 10^{-6} & \end{array}$$

A quantum yield for $\text{Cl}^*(^2P_{1/2})$ atom formation in the broad band photolysis of CF_2Cl_2 , $\Phi(\text{Cl}^*) = 0.75 \pm 0.26$, was reported by Clark and Husain [80].

Table 4-48. Absorption Cross Sections of CF_2Cl_2 at 295–298 K

λ (nm)	$10^{20} \sigma$ (cm ²)	λ (nm)	$10^{20} \sigma$ (cm ²)	λ (nm)	$10^{20} \sigma$ (cm ²)
170	124.0	194	31.5	218	0.103
172	151.0	196	21.1	220	0.0624
174	168.0	198	13.9	222	0.0381
176	185.5	200	8.71	224	0.0233
178	189.5	202	5.42	226	0.0140
180	179.0	204	3.37	228	0.0090
182	160.0	206	2.06	230	0.0057
184	134.0	208	1.26	232	0.0034
186	107.0	210	0.762	234	0.0021
188	82.8	212	0.458	236	0.0013
190	63.2	214	0.274	238	0.0008
192	45.50	216	0.163	240	0.0005

Note: 170–172 nm, Hubrich et al. [166],

174–178 nm, the mean of Hubrich et al. [166] and Simon et al. [379],

180–198 nm, Simon et al. [379],

200–230 nm, mean of Simon et al. [379] and Mérienne et al. [256],

232–240 nm, extrapolation of Mérienne et al. [256] data.

- F32. CF_3Cl (CFC-13) + $h\nu \rightarrow$ Products. The absorption cross sections of CF_3Cl have been measured at room temperature and 184–203 nm by Chou et al. [77]; at 255, 279, and 296 K and 172–200 nm by Vanlaethem-Meurée et al. [419]; at 208 and 298 K and 160–220 nm by Hubrich and Stuhl [165]; and at 225–295 K and 172–200 nm by Simon et al. [379]. The values of Vanlaethem-Meurée et al. [419] and Simon et al. [379] are identical, the room temperature values of Hubrich and Stuhl [165] deviate from the latter by up to about $\pm 25\%$, and the data of Chou et al. [77] are always larger by about 15–30% in the region 185–200 nm. The recommended absorption cross sections for CF_3Cl , presented in Table 4-49, are taken from Simon et al. [379] for the range 172–200 nm. The values at 202–220 nm are obtained by extrapolation of the absorption curve above 200 nm ($\log \sigma = -5.048 - 0.0834 \lambda$) of Simon et al. [379].

Measurements in the far UV at 65–130 nm have been reported by Gilbert et al. [132] and at 120–160 nm by Doucet et al. [110]. Measurements at the Lyman- α line at 121.6 nm have been carried out by Ravishankara et al. [328].

Temperature effects, if any, could not be detected by Vanlaethem-Meurée et al. [419] and Simon et al. [379], whereas Hubrich and Stuhl [165] report a decrease of the absorption cross sections between 298 and 208 K by

4% at 160 nm to 74% at 205 nm. Simon et al. [379] parameterized the cross sections and the temperature dependence of the absorption cross sections by the polynomial expansion

$$\log_{10} \sigma(\lambda, T) = \sum A_n \lambda^n + (T - 273) \times \sum B_n \lambda^n \text{ (with all } B_n = 0),$$

and reported smoothed values for T = 295 K, every 2 nm, and at wavelengths corresponding to the wavenumber intervals generally used in stratospheric photodissociation calculations. The parameters A_n for the ranges T = 210–300 K and λ = 172–200 nm are:

$$A_0 = -1.55.88, A_1 = 2.0993, A_2 = -1.0486 \times 10^{-2}, A_3 = 1.6718 \times 10^{-5}.$$

A quantum yield for Cl*(²P_{1/2}) atom formation in the broad band photolysis of CF₃Cl, Φ(Cl*) = 0.86 ± 0.29, was reported by Clark and Husain [80].

Table 4-49. Absorption Cross Sections of CF₃Cl at 295 K

λ (nm)	10 ²⁰ σ (cm ²)	λ (nm)	10 ²⁰ σ (cm ²)	λ (nm)	10 ²⁰ σ (cm ²)
172	1.100	190	0.128	206	0.00595
174	0.970	192	0.0900	208	0.00406
176	0.825	194	0.0610	210	0.00276
178	0.681	196	0.0410	212	0.00188
180	0.542	198	0.0280	214	0.00128
182	0.425	200	0.0190	216	0.000872
184	0.326	200	0.0189	218	0.000594
186	0.244	202	0.0128	220	0.000405
188	0.175	204	0.00874		

Note: 172–200 nm, Simon et al. [379],

202–220 nm, extrapolation of Simon et al. [379] data.

- F33. CF₂ClCFCl₂ (CFC-113) + hν → Products. The absorption cross sections of CF₂ClCFCl₂ have been measured at 298 K and 184–224 nm by Chou et al. [77]; at 208 and 298 K and 160–250 nm by Hubrich and Stuhl [165]; and at 225–295 K and 184–230 nm by Simon et al. [380]. The room temperature values agree within about 10% except in the region around 190 nm where the values of Hubrich and Stuhl [165] are smaller by up to 20% than the other values. The preferred absorption cross sections, listed in Table 4-50, are the values of Hubrich and Stuhl [165] at 175–180 nm, a value at 184 nm interpolated between those of Hubrich and Stuhl [165] at 180 nm and Simon et al. [380] at 186 nm, and the values of Simon et al. [380] at 186–230 nm. For the range 232–250 nm, the absorption curve of Simon et al. [380] above 230 nm has been extrapolated (log σ = -0.9860 - 0.0894 λ). The measured values of Hubrich and Stuhl [165] are larger than the extrapolated values by ~20–80% at 232–250 nm.

Measurements in the far UV at 110–200 nm have been carried out by Doucet et al. [111].

The temperature dependence becomes significant at wavelengths above 194 nm and below 170 nm, where the cross sections decrease with decreasing temperature. This was observed by Simon et al. [380] at 295–225 K and by Hubrich and Stuhl [165] at 298 and 208 K. Simon et al. [380] parameterized the temperature dependence of the cross sections by the polynomial expansion $\log_{10} \sigma(\lambda, T) = \sum A_n \lambda^n + (T - 273) \times \sum B_n \lambda^n$ and reported smoothed values for T = 210, 230, 250, 270, and 295 K, every 2 nm, and at wavelengths corresponding to the wavenumber intervals generally used in stratospheric photodissociation calculations. The parameters A_n and B_n for the ranges T = 210–300 K and λ = 182–230 nm are as follows:

$$\begin{array}{ll} A_0 = -1087.9 & B_0 = 12.493 \\ A_1 = 20.004 & B_1 = -2.3937 \times 10^{-1} \\ A_2 = -1.3920 \times 10^{-1} & B_2 = 1.7142 \times 10^{-3} \\ A_3 = 4.2828 \times 10^{-4} & B_3 = -5.4393 \times 10^{-6} \\ A_4 = -4.9384 \times 10^{-7} & B_4 = 6.4548 \times 10^{-8}. \end{array}$$

Table 4-50. Absorption Cross Sections of CF₂CICFCl₂ at 295–298 K

λ (nm)	$10^{20} \sigma$ (cm ²)	λ (nm)	$10^{20} \sigma$ (cm ²)	λ (nm)	$10^{20} \sigma$ (cm ²)
175	192	204	5.80	228	0.0410
180	155	206	4.00	230	0.0270
184	123	208	2.65	232	0.0188
186	104	210	1.80	234	0.0124
188	83.5	212	1.15	236	0.00824
190	64.5	214	0.760	238	0.00546
192	48.8	216	0.505	240	0.00361
194	36.0	218	0.318	242	0.00239
196	26.0	220	0.220	244	0.00159
198	18.3	222	0.145	246	0.00105
200	12.5	224	0.0950	248	0.000696
202	8.60	226	0.0630	250	0.000461

Note: 175–180 nm: Hubrich and Stuhl [165]

184 nm: interpolation: Hubrich and Stuhl (180 nm) and Simon et al. (186 nm)

186–230 nm: Simon et al. [380]

232–250 nm: extrapolation of Simon et al. [380] data.

- F34. CF₂CICF₂Cl (CFC-114) + hν → Products. The absorption cross sections of CF₂CICF₂Cl have been measured at room temperature and 184–219 nm by Chou et al. [77]; at 208 and 298 K and 160–235 nm by Hubrich and Stuhl [165]; and at 225–295 K and 182–220 nm by Simon et al. [380]. The room temperature values of Simon et al. [380] and Chou et al. [77] agree within 5% except for a hump around 195 nm in the absorption curve reported by Chou et al. [77]. The values of Hubrich and Stuhl [165] are always larger than those of Simon et al. [380], around 190 nm by up to ~40% and between 200 and 220 nm up to ~50% with increasing wavelength. The recommended absorption cross sections, listed in Table 4-51, are the values of Simon et al. [380] at 172–220 nm. For the range 222–235 nm, the absorption curve above 200 nm of Simon et al. [380] has been extrapolated ($\log \sigma = -1.8233 - 0.00913 \lambda$). The measured values of Hubrich et al. [165] are larger by ~40% in that range than the extrapolated values

Measurements at the Lyman- α line at 121.6 nm have been carried out by Ravishankara et al. [328]; and at 110–190 nm by Doucet et al. [111].

The temperature dependence has been observed at wavelengths above 190 nm, where Simon et al. [380] report decreasing cross sections with decreasing temperature 295–210 K. Hubrich and Stuhl [165] report for the range 160–210 nm and between 298 and 208 K a small decrease of the cross sections (generally <10%, except two data points). Simon et al. [380] parameterized the temperature dependence of the cross sections by the polynomial expansion $\log_{10} \sigma(\lambda, T) = \sum A_n \lambda^n + (T - 273) \times \sum B_n \lambda^n$ and reported smoothed values for T = 210, 230, 250, 270, and 295 K, every 2 nm, and at wavelengths corresponding to the wavenumber intervals generally used in stratospheric photodissociation calculations. The parameters A_n and B_n for the ranges T = 210–300 K,

$\lambda = 172$ – 220 nm are as follows:

$$\begin{array}{ll}
 A_0 = -160.50 & B_0 = -1.5296 \\
 A_1 = 2.4807 & B_1 = 3.5248 \times 10^{-2} \\
 A_2 = -1.5202 \times 10^{-2} & B_2 = -2.9951 \times 10^{-4} \\
 A_3 = 3.8412 \times 10^{-5} & B_3 = 1.1129 \times 10^{-6} \\
 A_4 = -3.4373 \times 10^{-8} & B_4 = -1.5259 \times 10^{-9}
 \end{array}$$

Table 4-51. Absorption Cross Sections of CF₂CICF₂Cl at 295 K

λ (nm)	$10^{20} \sigma$ (cm ²)	λ (nm)	$10^{20} \sigma$ (cm ²)	λ (nm)	$10^{20} \sigma$ (cm ²)
172	69.0	194	2.56	216	0.0290
174	55.0	196	1.75	218	0.0190
176	43.0	198	1.20	220	0.0122
178	34.0	200	0.800	222	0.00809
180	26.2	202	0.540	224	0.00531
182	19.8	204	0.370	226	0.00349
184	15.0	206	0.245	228	0.00229
186	11.0	208	0.160	230	0.00151
188	7.80	210	0.104	232	0.00099
190	5.35	212	0.0680	234	0.00065
192	3.70	214	0.0440	235	0.00053

Note: 172–220 nm: Simon et al. [380]
222–235 nm: extrapolation of Simon et al. [380] data.

- F35. CF₃CF₂Cl (CFC-115) + hv → Products. The absorption cross sections of CF₃CF₂Cl have been measured at room temperature and 184–207 nm by Chou et al. [77]; at 208 and 298 K and 160–230 nm by Hubrich and Stuhl [165]; and at 225–295 K and 172–204 nm by Simon et al. [380]. The room temperature data of Simon et al. [380] and Hubrich and Stuhl [165] agree within ~20%, where Hubrich and Stuhl [165] report the larger values over the range 172–204 nm. The data of Chou et al. [77] are larger by up to more than 50% than those of Simon et al. [380]. The preferred absorption cross sections, listed in Table 4-52, are the mean of the values reported by Hubrich and Stuhl [165] and Simon et al. [380] at 172–204 nm. The mean of the values measured by Hubrich and Stuhl [165] and those obtained by extrapolating the absorption curve of Simon et al. [380] ($\log \sigma = -6.2191 - 0.0756 \lambda$) were taken for the range 205–230 nm (the extrapolated values become larger by up to nearly 50% with increasing wavelength than the measured values of Hubrich and Stuhl [165]).

Measurements at the Lyman- α line at 121.6 nm have been carried out by Ravishankara et al. [328]; and at 120–175 nm by Doucet et al. [111].

Temperature effects, if any, could not be detected for this highly fluorinated species. Simon et al. [380] parameterized the absorption cross sections by the polynomial expansion $\log_{10} \sigma(\lambda, T) = \sum A_n \lambda^n + (T - 273) \times \sum B_n \lambda^n$ (with all $B_n = 0$), and reported smoothed values for T = 295 K, every 2 nm, and at wavelengths corresponding to the wavenumber intervals generally used in stratospheric photodissociation calculations. The parameters A_n for the ranges T = 210–300 K and $\lambda = 172$ –204 nm are

$$A_0 = 5.8281, A_1 = 2.900 \times 10^{-1}, A_2 = 1.325 \times 10^{-3}, A_3 = -2.6851 \times 10^{-6}.$$

Table 4-52. Absorption Cross Sections of CF₃CF₂Cl at 295–298 K

λ (nm)	$10^{20} \sigma$ (cm ²)	λ (nm)	$10^{20} \sigma$ (cm ²)	λ (nm)	$10^{20} \sigma$ (cm ²)
172	5.50	188	0.403	204	0.0218
174	4.13	190	0.287	205	0.0187
176	3.08	192	0.203	210	0.00700
178	2.25	194	0.143	215	0.00273
180	1.58	196	0.0985	220	0.00107
182	1.13	198	0.0685	225	0.00046
184	0.790	200	0.0474	230	0.00018
186	0.563	202	0.0325		

Note: 172–204 nm: mean of Hubrich and Stuhl [165] and Simon et al. [380]
205–230 nm: mean of Hubrich and Stuhl [165] and extrapolated Simon et al. [380] data.

- F36. CHFCl₂ (HCFC-21) + hv → Products. The absorption cross sections of CHFCl₂ have been measured at room temperature and 208 nm by Gordus and Bernstein [142]; at 174–222 nm by Robbins and Stolarski [339]; at 184–205 nm by Green and Wayne [146]; and at 213.9 nm by Rebbert et al. [335]; at 208 and 298 K and 158–235 nm by Hubrich et al. [166]; and at 225–295 K and 174–222 nm by Simon et al. [379]. The results of

these groups (except those of Green and Wayne [146] which deviate strongly) are in good agreement, generally within 15%, although the data of Hubrich et al. [166] show humps around 205 and 220 nm, where the agreement is only ~40%. The preferred absorption cross sections, listed in Table 4-53, are the values of Simon et al. [379] at 174–222 nm. For the range 224–236 nm, the absorption curve above 200 nm of Simon et al. [283] has been extrapolated ($\log \sigma = 0.9806 - 0.1014 \lambda$). The measured values of Hubrich et al. [166] deviate from the extrapolated values by up to ~–20% and +50%.

Measurements in the far UV at 60–120 nm have been reported by Gilbert et al. [132], measurements at 120–200 nm by Doucet et al. [110], and a measurement at 147 nm by Rebbert et al. [335].

The temperature dependence becomes significant at wavelengths above 190 nm, where the cross sections decrease with decreasing temperature between 296 and 210 K. Simon et al. [379] parameterized the temperature dependence of the cross sections by the polynomial expansion $\log_{10} \sigma(\lambda, T) = \sum A_n \lambda^n + (T - 273) \times \sum B_n \lambda^n$ and reported smoothed values for $T = 210, 230, 250, 270,$ and 295 K, every 2 nm, and at wavelengths corresponding to the wavenumber intervals generally used in stratospheric photodissociation calculations. The parameters A_n and B_n for the ranges $T = 210$ – 300 K and $\lambda = 174$ – 222 nm are as follows:

$$\begin{array}{ll} A_0 = -514.56 & B_0 = -3.0577 \\ A_1 = 8.7940 & B_1 = 6.6539 \times 10^{-2} \\ A_2 = -5.6840 \times 10^{-2} & B_2 = -5.3964 \times 10^{-4} \\ A_3 = 1.5894 \times 10^{-4} & B_3 = 1.9322 \times 10^{-6} \\ A_4 = 1.6345 \times 10^{-7} & \end{array}$$

Table 4-53. Absorption Cross Sections of CHFCl₂ at 295–298 K

λ (nm)	$10^{20} \sigma$ (cm ²)	λ (nm)	$10^{20} \sigma$ (cm ²)	λ (nm)	$10^{20} \sigma$ (cm ²)
174	166.0	198	8.10	222	0.0319
176	164.5	200	5.24	224	0.0195
178	155.0	202	3.35	225	0.0154
180	138.0	204	2.12	226	0.0122
182	116.0	206	1.34	228	0.00766
184	92.4	208	0.836	230	0.00480
186	71.5	210	0.522	232	0.00301
188	53.2	212	0.325	234	0.00189
190	38.4	214	0.203	235	0.00150
192	26.9	216	0.127	236	0.00119
194	18.4	218	0.0797		
196	12.3	220	0.0503		

Note: 174–222 nm: Simon et al. [379]

224–236 nm: extrapolation of Simon et al. [379] data.

- F37. CHF₂Cl (HCFC-22) + hv → Products. The absorption cross sections of CHF₂Cl have been measured at room temperature and 174–202 nm by Robbins and Stolarski [339] and at 181–194 nm by Green and Wayne [146]; at 208 K and 298 K and 158–220 nm by Hubrich et al. [166], and at 225–295 K and 174–204 nm by Simon et al. [379]. The results of Robbins and Stolarski [339], Hubrich et al. [166], and Simon et al. [379] are in good agreement generally within 15–20%, however those of Green and Wayne [146] deviate strongly. The preferred absorption cross sections, listed in Table 4-54, are the values of Hubrich et al. [166] at 170–172 nm and the values of Simon et al. [379] at 174–204 nm. For the range 206–220 nm, the absorption curve above 190 nm of Simon et al. [379] has been extrapolated ($\log \sigma = -4.1001 - 0.0870 \lambda$). The measured values of Hubrich et al. [166] deviate from the extrapolated values by up to 20%.

Measurements in the far UV at 60–160 nm have been reported by Gilbert et al. [132], and measurements at 120–200 nm by Doucet et al. [110].

A weak temperature dependence has been observed above 190 nm, where the cross sections decrease with decreasing temperature between 296 and 210 K. Simon et al. [379] parameterized the cross sections and the temperature dependence by the polynomial expansion $\log_{10} \sigma(\lambda, T) = \sum A_n \lambda^n + (T - 273) \times \sum B_n \lambda^n$ and reported

smoothed values for T = 210, 230, 250, 270, and 295 K, every 2 nm, and at wavelengths corresponding to the wavenumber intervals generally used in stratospheric photodissociation calculations. The parameters A_n and B_n for the ranges T = 210–300 K and $\lambda = 174$ –204 nm are as follows:

$$\begin{aligned} A_0 &= -106.029 & B_0 &= -1.3399 \times 10^{-1} \\ A_1 &= 1.5038 & B_1 &= 2.7405 \times 10^{-3} \\ A_2 &= -8.2476 \times 10^{-3} & B_2 &= -1.8028 \times 10^{-5} \\ A_3 &= 1.4206 \times 10^{-5} & B_3 &= 3.8504 \times 10^{-8} \end{aligned}$$

Table 4-54. Absorption Cross Sections of CHF₂Cl at 295–298 K

λ (nm)	$10^{20} \sigma$ (cm ²)	λ (nm)	$10^{20} \sigma$ (cm ²)	λ (nm)	$10^{20} \sigma$ (cm ²)
170	12.9	188	0.372	206	0.00842
172	9.79	190	0.245	208	0.00636
174	5.72	192	0.156	210	0.00426
176	4.04	194	0.103	212	0.00285
178	2.76	196	0.072	214	0.00191
180	1.91	198	0.048	216	0.00128
182	1.28	200	0.032	218	0.00086
184	0.842	202	0.0220	220	0.00057
186	0.576	204	0.0142		

Note: 170–172 nm: Hubrich et al. [166]

174–204 nm: Simon et al. [379]

206–220 nm: extrapolation of Simon et al. [379] data.

- F38. CH₂FCl (HCFC-31) + hv → Products. The absorption cross sections of CH₂FCl have been measured at 208 and 298 K and 160–230 nm by Hubrich and Stuhl [165]. The room temperature data at 160–230 nm are listed in Table 4-55.

Measurements in the far UV at 60–120 nm have been reported by Gilbert et al. [132], and measurements at 120–200 nm by Doucet et al. [110].

Table 4-55. Absorption Cross Sections of CH₂FCl at 298 K

λ (nm)	$10^{20} \sigma$ (cm ²)	λ (nm)	$10^{20} \sigma$ (cm ²)	λ (nm)	$10^{20} \sigma$ (cm ²)
160	47.9	185	4.20	210	0.0188
165	55.9	190	1.95	215	0.00560
170	43.0	195	0.544	220	0.00215
175	23.3	200	0.209	225	0.00049
180	12.5	205	0.069	230	0.00026

Note: 160–230 nm: Hubrich and Stuhl [165].

- F39. CF₃CHCl₂ (HCFC-123) + hv → Products. The absorption cross sections of CF₃CHCl₂ have been measured at room temperature and 185–204 nm by Green and Wayne [146]; at 225–295 K and 170–250 nm by Gillotay and Simon [136]; at 203–295 K and 190–230 nm by Orlando et al. [305]; and at 223–333 K and 160–230 nm by Nayak et al. [286]. The agreement between the results of the latter three groups is within 25% in the region below 220 nm. The results of Green and Wayne [146] are very different below 200 nm. The preferred absorption cross sections at 295 K, listed in Table 4-56, are the mean of the values reported by Gillotay and Simon [136] and Nayak et al. [286] at 170–188 nm and the mean of the values reported by Gillotay and Simon [136], Orlando et al. [305], and Nayak et al. [286] at 190–230 nm. For the range 232–250 nm, the absorption curve above 210 nm of Orlando et al. [305] has been extrapolated ($\log \sigma = -3.1097 - 0.0794 \lambda$).

The studies of the temperature dependence show a decrease of the absorption cross sections with decreasing temperature at wavelengths above 178–180 nm and below 170 nm. Between 170–180 nm, the reverse behavior was observed by Gillotay and Simon [136] and Nayak et al. [286]. An irregular temperature dependence was reported by Orlando et al. [305] for the range 210–230 nm, where the absorption curves show wiggles.

Various parameterized fits, i.e., polynomial expansions of the logarithm of the absorption cross section, have been proposed for the temperature dependence. Gillotay and Simon [136] parameterized the cross sections and the temperature dependence by the polynomial expansion $\log_{10} \sigma(\lambda, T) = \sum A_n \lambda^n + (T - 273) \times \sum B_n \lambda^n$ and reported smoothed values for $T = 210, 230, 250, 270,$ and 295 K, every 2 nm, and at wavelengths corresponding to the wavenumber intervals generally used in stratospheric photodissociation calculations. The parameters A_n and B_n for the ranges $T = 210\text{--}300$ K and $\lambda = 182\text{--}250$ nm are as follows:

$$\begin{aligned} A_0 &= -513.996354 & B_0 &= 1.757133 \\ A_1 &= 9.089141 & B_1 &= -3.499205 \times 10^{-2} \\ A_2 &= -6.136794 \times 10^{-2} & B_2 &= 2.593563 \times 10^{-4} \\ A_3 &= 1.814826 \times 10^{-4} & B_3 &= -8.489357 \times 10^{-7} \\ A_4 &= -1.999514 \times 10^{-7} & B_4 &= 1.037756 \times 10^{-9}. \end{aligned}$$

Nayak et al. [286] report sixth-order polynomial coefficients for the functions $\log_{10}(\sigma_T) = \sum C_n (\lambda - 170)^n$ at $T = 223, 233, 253, 273, 295, 313,$ and 333 K and for the range $160\text{--}230$ nm. The parameters C_n are as follows:

	223 K	273 K	295 K	333 K
C_0	-17.6732	-17.6773	-17.6792	-17.6722
C_1	1.70233×10^{-2}	1.3636×10^{-2}	1.19392×10^{-2}	9.07941×10^{-3}
C_2	-7.39366×10^{-4}	-4.98553×10^{-4}	-3.71661×10^{-4}	-1.29566×10^{-4}
C_3	-1.83761×10^{-4}	-1.70566×10^{-4}	-1.61218×10^{-4}	-1.56667×10^{-4}
C_4	7.80778×10^{-6}	6.73373×10^{-6}	6.03101×10^{-6}	5.56409×10^{-6}
C_5	-1.29836×10^{-7}	-1.02726×10^{-7}	-8.76762×10^{-8}	-7.77379×10^{-8}
C_6	8.05415×10^{-10}	5.66688×10^{-10}	4.61745×10^{-10}	3.93859×10^{-10}

A double expansion in terms of twelve parameters, $\ln \sigma(\lambda, T) = \sum (\sum a_{ij} (T - 245.4)^{i-1}) (\lambda - 206.214)^{j-1}$, $i = 1\text{--}4$, $j = 1\text{--}3$, $T = 203\text{--}295$ K, $\lambda = 190\text{--}230$ nm, was used by Orlando et al. [305]:

$$\begin{aligned} a_{11} &= -4.500 \times 10^{-1} & a_{12} &= 3.529 \times 10^{-3} & a_{13} &= -4.181 \times 10^{-8} \\ a_{21} &= -1.985 \times 10^{-1} & a_{22} &= 6.826 \times 10^{-5} & a_{23} &= 1.555 \times 10^{-6} \\ a_{31} &= -2.802 \times 10^{-4} & a_{32} &= -1.018 \times 10^{-5} & a_{33} &= 4.037 \times 10^{-8} \\ a_{41} &= 6.312 \times 10^{-5} & a_{42} &= -3.055 \times 10^{-7} & a_{43} &= -2.473 \times 10^{-9} \end{aligned}$$

Table 4-56. Absorption Cross Sections of CF_3CHCl_2 at 295 K

λ (nm)	$10^{20} \sigma$ (cm^2)	λ (nm)	$10^{20} \sigma$ (cm^2)	λ (nm)	$10^{20} \sigma$ (cm^2)
170	192	198	17.1	226	0.0880
172	207	200	11.9	228	0.0599
174	214	202	8.24	230	0.0451
176	213	204	5.70	232	0.0295
178	202	206	3.89	234	0.0205
180	184	208	2.67	236	0.0142
182	161	210	1.82	238	0.0098
184	135	212	1.23	240	0.0068
186	109	214	0.838	242	0.0047
188	85.5	216	0.573	244	0.0033
190	62.2	218	0.384	246	0.0023
192	46.4	220	0.266	248	0.0016
194	33.9	222	0.180	250	0.0011
196	24.2	224	0.124		

Note: 170–188 nm: mean of the values of Gillotay and Simon [136] and Nayak et al. [286]
 190–230 nm: mean of the values of Gillotay and Simon [136], Orlando et al. [305], and Nayak et al. [286]
 232–250 nm: extrapolation of Orlando et al. [305] data.

- F40. CF_3CHFCl (HCFC-124) + $h\nu \rightarrow$ Products. The absorption cross sections of CF_3CHFCl have been measured at 203–295 K and 190–230 nm by Orlando et al. [305]; and at 210–295 K and 170–230 nm by Gillotay and Simon [137]. The agreement is better than 10 % between 190 and 220 nm, whereas above 220 nm the values of Orlando et al. [305] become increasingly larger by up to 133% than those of Gillotay and Simon [137]. The preferred room temperature values, listed in Table 4-57, are the values of Gillotay and Simon [137] at 170–188 nm and 222–230 nm and the mean of the values reported by Gillotay and Simon [137] and Orlando et al. [305] at 190–220 nm.

The temperature dependence of the cross sections has been measured by both groups and a decrease of the absorption cross sections with decreasing temperature was observed at 170–230 nm by Gillotay and Simon [137] and at 190–215 nm by Orlando et al. [305]. An irregular temperature behavior was reported by Orlando et al. [305] for the range 215–230 nm, where the absorption curves show wiggles. Parameterized fits, i.e., polynomial expansions of the logarithm of the absorption cross section, have been derived. Gillotay and Simon [137] parameterized the cross sections and the temperature dependence by the polynomial expansion $\log_{10} \sigma(\lambda, T) = \sum A_n \lambda^n + (T - 273) \times \sum B_n \lambda^n$ and reported smoothed values for $T = 210, 230, 250, 270,$ and 295 K, every 2 nm, and at wavelengths corresponding to the wavenumber intervals generally used in stratospheric photodissociation calculations. The parameters A_n and B_n for the ranges $T = 210\text{--}300$ K and $\lambda = 170\text{--}230$ nm are as follows:

$$\begin{aligned} A_0 &= -101.230250 & B_0 &= -5.795712 \times 10^{-2} \\ A_1 &= 1.333519 & B_1 &= 1.053901 \times 10^{-3} \\ A_2 &= -6.888672 \times 10^{-3} & B_2 &= -6.530379 \times 10^{-6} \\ A_3 &= 1.114172 \times 10^{-5} & B_3 &= 1.382056 \times 10^{-8} \end{aligned}$$

A double expansion in terms of twelve parameters, $\ln \sigma(\lambda, T) = \sum (\sum a_{ij} (T-251.7)^{j-1}) (\lambda - 206.214)^{i-1}$, $i = 1\text{--}4, j = 1\text{--}3, T = 203\text{--}295$ K, $\lambda = 190\text{--}230$ nm, was used by Orlando et al. [305]:

$$\begin{aligned} a_{11} &= -4.967 \times 10^{-1} & a_{12} &= 6.562 \times 10^{-3} & a_{13} &= 1.735 \times 10^{-5} \\ a_{21} &= -2.025 \times 10^{-1} & a_{22} &= 2.788 \times 10^{-4} & a_{23} &= -3.974 \times 10^{-6} \\ a_{31} &= 6.839 \times 10^{-4} & a_{32} &= 5.523 \times 10^{-6} & a_{33} &= -3.092 \times 10^{-7} \\ a_{41} &= 1.275 \times 10^{-4} & a_{42} &= -2.959 \times 10^{-7} & a_{43} &= -1.182 \times 10^{-8} \end{aligned}$$

Table 4-57. Absorption Cross Sections of CF_3CHFCl at 295 K

λ (nm)	$10^{20} \sigma$ (cm ²)	λ (nm)	$10^{20} \sigma$ (cm ²)	λ (nm)	$10^{20} \sigma$ (cm ²)
170	13.6	192	0.548	214	0.00859
172	11.1	194	0.387	216	0.00610
174	8.85	196	0.267	218	0.00431
176	6.93	198	0.185	220	0.00312
178	5.33	200	0.128	222	0.00214
180	4.03	202	0.0868	224	0.00153
182	3.00	204	0.0594	226	0.00111
184	2.20	206	0.0401	228	0.00082
186	1.60	208	0.0269	230	0.00061
188	1.14	210	0.0186		
190	0.772	212	0.0126		

Note: 170–188 nm, Gillotay and Simon [137],
190–220 nm, mean of the values of Gillotay and Simon [137] and Orlando et al. [305],
222–230 nm, Gillotay and Simon [137].

- F41. $\text{CF}_3\text{CH}_2\text{Cl}$ (HCFC-133) + $h\nu \rightarrow$ Products. The absorption cross sections of $\text{CF}_3\text{CH}_2\text{Cl}$ have been measured at room temperature and 147 nm ($\sigma = 1.35 \times 10^{-17}$ cm²) by Ichimura et al. [174], and 186–203 nm by Green and Wayne [146], and at 208 and 298 K and 160–245 nm by Hubrich and Stuhl [165]. There is no good agreement between the results at wavelengths above 180 nm. Table 4-58 gives the recommended room temperature data of Hubrich and Stuhl [165].

Table 4-58. Absorption Cross Sections of CF₃CH₂Cl at 298 K

λ (nm)	$10^{20} \sigma$ (cm ²)	λ (nm)	$10^{20} \sigma$ (cm ²)	λ (nm)	$10^{20} \sigma$ (cm ²)
160	59.4	190	6.20	220	0.0887
165	64.6	195	2.95	225	0.0226
170	56.4	200	1.14	230	0.0147
175	37.3	205	0.598	235	0.00404
180	22.8	210	0.328	240	0.00181
185	11.6	215	0.169	245	0.00054

Note: 160–245 nm, Hubrich and Stuhl [165].

- F42. CH₃CFCl₂ (HCFC-141b) + hv → Products. The absorption cross sections of CH₃CFCl₂ have been measured at 210–295 K and 170–240 nm by Gillotay and Simon [136]; at 203–295 K and 190–230 nm by Orlando et al. [305] (data of Orlando et al. reported by Gillotay and Simon [138]); at 203–295 K and 190–230 nm by Talukdar et al. [393]; and at room temperature and 190–240 nm by Fahr et al. [113], who investigated the spectrum both for the gas and liquid phases and used a wavelength-shift procedure to convert the liquid-phase data into gas-phase data. The agreement between the values reported by Gillotay and Simon [136] and Fahr et al. [113] for the 190–240-nm region is very good (1–10% up to 236 nm); the results of Orlando et al. [305] are also in good agreement with these, but only in the region 190–210 nm. The agreement of the results of Talukdar et al. [393] is not as good, their absorption cross sections become smaller below 210 nm by up to ~20% and become larger above 210 nm by up to about 70% than the above mentioned data. The preferred absorption cross sections, listed in Table 4-59, are the values of Gillotay and Simon [136] at 170–188 nm and the mean of the values reported by Gillotay and Simon [136] and Fahr et al. [113] at 190–240 nm.

A decrease of the absorption cross sections with decreasing temperature at wavelengths above 188 nm and below 172 nm and the reverse behavior between 172 and 188 nm was observed by Gillotay and Simon [136]. They parameterized the cross sections and the temperature dependence of the absorption cross sections using the polynomial expansion $\log_{10} \sigma(\lambda, T) = \sum A_n \lambda^n + (T - 273) \times \sum B_n \lambda^n$. They derived the parameters

$$\begin{array}{ll}
 A_0 = -682.913042 & B_0 = 4.04747 \\
 A_1 = 12.122290 & B_1 = -8.05899 \times 10^{-2} \\
 A_2 = -8.187699 \times 10^{-2} & B_2 = 5.946552 \times 10^{-4} \\
 A_3 = 2.437244 \times 10^{-4} & B_3 = -1.945048 \times 10^{-6} \\
 A_4 = -2.719103 \times 10^{-7} & B_4 = 2.380143 \times 10^{-9}
 \end{array}$$

for the ranges 210–300 K and 172–240 nm and list smoothed values for T = 210, 230, 250, 270, and 295 K at 2-nm intervals and at wavelengths corresponding to the wavenumber intervals generally used in stratospheric photodissociation calculations. A similar temperature behavior was observed by Orlando et al. [305] only between 190 and 210 nm, and by Talukdar et al. [393] only above 197 nm.

Table 4-59. Absorption Cross Sections of CH₃CFCl₂ at 295–298 K

λ (nm)	$10^{20} \sigma$ (cm ²)	λ (nm)	$10^{20} \sigma$ (cm ²)	λ (nm)	$10^{20} \sigma$ (cm ²)
170	143.1	194	47.2	218	0.382
172	145.1	196	34.1	220	0.248
174	154.2	198	24.0	222	0.161
176	162.9	200	16.6	224	0.105
178	172.6	202	11.3	226	0.0680
180	172.3	204	7.56	228	0.0444
182	162.9	206	5.02	230	0.0290
184	146.4	208	3.30	232	0.0189
186	125.7	210	2.16	234	0.0123
188	103.6	212	1.40	236	0.00801
190	83.0	214	0.909	238	0.00518
192	63.6	216	0.589	240	0.00334

Note: 170–188 nm, Gillotay and Simon [136],
190–240 nm, mean of Gillotay and Simon [136] and Fahr et al. [113].

- F43. CH₃CF₂Cl (HCFC-142b) + hν → Products. The absorption cross sections of CH₃CF₂Cl have been measured at room temperature and 120–180 nm by Doucet et al. [111]; at 184–210 nm by Green and Wayne [146]; at 298 and 208 K and 160–230 nm by Hubrich and Stuhl [165]; at 210–295 K and 170–230 nm by Gillotay and Simon [136]; at 203–295 K and 190–230 nm by Orlando et al. [305]; and at 223–333 K and 160–210 nm by Nayak et al. [286]. At wavelengths below 200 nm, the values of Hubrich and Stuhl [165] and Nayak et al. [286] are within 15%, those of Gillotay and Simon [136] and Orlando et al. [305] are lower than the latter by up to 30%. At wavelengths between 200 and 215 nm, the values of Gillotay and Simon [136], Orlando et al. [305], and Nayak et al. [286] agree within 15%. Above 215 nm, the absorption curve reported by Orlando et al. [305] shows wiggles with deviations by up to 100% from the data of Gillotay and Simon [136]. Also the values reported for the range 205–230 nm by Hubrich and Stuhl [165] become increasingly large by up to 600% than those of Gillotay and Simon [136]. The results of Green and Wayne [146] are very different from all other data. The preferred room temperature absorption cross sections, listed in Table 4–60, are the mean of the values reported by Hubrich and Stuhl [165], Gillotay and Simon [136], and Nayak et al. [286] at 175–185 nm, the mean of the values reported by Gillotay and Simon [136], Orlando et al. [305], and Nayak et al. [286] at 190–210 nm, and the values reported by Gillotay and Simon [136] at 212–230 nm.

A decrease of the absorption cross sections with decreasing temperature was observed by Gillotay and Simon [136] and Nayak et al. [286] over the wavelength range 160–230 nm and by Orlando et al. [305] between 190 and 200 nm. An irregular temperature behavior was reported by Orlando et al. [305] for the range 215–230 nm, where the absorption curves for the various temperatures show several crossings. Various parameterized fits for the temperature dependence of the absorption cross sections have been offered. Gillotay and Simon [136] used the polynomial expansion $\log_{10} \sigma(\lambda, T) = \sum A_n \lambda^n + (T - 273) \times \sum B_n \lambda^n$ and reported smoothed values for T = 210, 230, 250, 270, and 295 K, every 2 nm, and at wavelengths corresponding to the wavenumber intervals generally used in stratospheric photodissociation calculations. Their parameters A_n and B_n for the ranges T = 210–300 K and $\lambda = 172$ –230 nm are as follows:

$$\begin{aligned}
 A_0 &= -328.092008 & B_0 &= 4.289533 \times 10^{-1} \\
 A_1 &= 6.342799 & B_1 &= -9.042817 \times 10^{-3} \\
 A_2 &= -4.810362 \times 10^{-2} & B_2 &= 7.018009 \times 10^{-5} \\
 A_3 &= 1.611991 \times 10^{-4} & B_3 &= -2.389065 \times 10^{-7} \\
 A_4 &= -2.042613 \times 10^{-7} & B_4 &= 3.039799 \times 10^{-10}
 \end{aligned}$$

Nayak et al. [286] report fourth-order polynomial coefficients C_n(T) for the functions $\log_{10}(\sigma_T) = \sum C_n (\lambda - 160)^n$ at T = 223, 233, 253, 273, 295, 313, and 333 K and for the range 160–210 nm. The parameters C_n are as follows

	223 K	273 K	295 K	333 K
C ₀	-18.2361	-18.2441	-18.2406	-18.1777
C ₁	-1.26669 × 10 ⁻²	-7.37889 × 10 ⁻³	-6.48269 × 10 ⁻³	-2.39647 × 10 ⁻²
C ₂	-2.32945 × 10 ⁻³	-2.66537 × 10 ⁻³	-2.80923 × 10 ⁻³	-7.23910 × 10 ⁻⁴
C ₃	2.81933 × 10 ⁻⁵	4.19193 × 10 ⁻⁵	5.01979 × 10 ⁻⁵	-1.08049 × 10 ⁻⁵
C ₄	-1.37963 × 10 ⁻⁷	-2.88472 × 10 ⁻⁷	-3.96860 × 10 ⁻⁷	1.37618 × 10 ⁻⁷

A double expansion in terms of twelve parameters, $\ln \sigma(\lambda, T) = \sum (\sum a_{ij} (T-245.4)^{j-1}) (\lambda - 206.214)^{i-1}$, $i = 1-4$, $j = 1-3$, $T = 203-295$ K, $\lambda = 190-230$ nm, was used by Orlando et al. [305]:

$$\begin{aligned}
 a_{11} &= -4.973 \times 10^{-1} & a_{12} &= 9.077 \times 10^{-3} & a_{13} &= -4.651 \times 10^{-5} \\
 a_{21} &= -2.175 \times 10^{-1} & a_{22} &= 4.712 \times 10^{-4} & a_{23} &= -1.005 \times 10^{-5} \\
 a_{31} &= 4.133 \times 10^{-4} & a_{32} &= -6.432 \times 10^{-5} & a_{33} &= 1.141 \times 10^{-6} \\
 a_{41} &= 7.145 \times 10^{-5} & a_{42} &= -5.396 \times 10^{-6} & a_{43} &= 1.187 \times 10^{-7}
 \end{aligned}$$

Quantum yields for Cl (²P_{3/2}) and Cl* (²P_{1/2}) atom formation in the photolysis of CH₃CF₂Cl at 193.3 nm have been measured by Brownsword et al. [49] and quantum yields for H atom formation in the photolysis at 121.6 and 193.3 nm by Brownsword et al. [48]: $\Phi(\text{Cl} + \text{Cl}^*) = 0.90 \pm 0.17$ with $\Phi(\text{Cl}) = 0.65 \pm 0.12$ and $\Phi(\text{Cl}^*) = 0.25 \pm 0.05$ at 193.3 nm, and $\Phi(\text{H}) = 0.53 \pm 0.12$ and 0.06 ± 0.02 at 121.6 and 193.3 nm, respectively.

Table 4-60. Absorption Cross Sections of CH₃CF₂Cl at 295–298 K

λ (nm)	$10^{20} \sigma$ (cm ²)	λ (nm)	$10^{20} \sigma$ (cm ²)	λ (nm)	$10^{20} \sigma$ (cm ²)
170	27.1	200	0.145	218	0.00243
175	14.0	202	0.0949	220	0.00145
180	6.38	204	0.0622	222	0.000845
185	2.73	206	0.0399	224	0.000484
190	1.02	208	0.0256	226	0.000271
192	0.706	210	0.0161	228	0.000148
194	0.482	212	0.0105	230	0.0000783
196	0.324	214	0.00652		
198	0.218	216	0.00401		

Note:

170–185 nm: mean of Gillotay and Simon [136], Hubrich and Stuhl [165], and Nayak et al. [286]

190–210 nm: mean of Gillotay and Simon [136], Orlando et al. [305], and Nayak et al. [286]

212–230 nm: Gillotay and Simon [136].

F44. CF₃CF₂CHCl₂ (HCFC-225ca) + hv → Products

F45. CF₂ClCF₂CHFCI (HCFC-225cb) + hv → Products. The absorption spectra of these compounds in the gaseous and liquid phases at 298 K have been measured by Braun et al. [40]. Table 4-61 lists the absorption cross sections for the gas phase taken from this work. The originally listed (0.5-nm intervals) absorption coefficients ε in (atm, 298 K)⁻¹ cm⁻¹ ($\sigma = 4.06 \times 10^{-20} \varepsilon$) for both phases have been fitted with third-order polynomial expansions $\log_{10} \varepsilon = \sum a_n (\lambda - 160)^n$ with

$$a_0 = 1.425, a_1 = 4.542 \times 10^{-2}, a_2 = -2.036 \times 10^{-3}, a_3 = 1.042 \times 10^{-5} \text{ for HCFC-225ca at 170–270 nm,}$$

$$a_0 = 1.677, a_1 = -2.175 \times 10^{-2}, a_2 = -1.484 \times 10^{-3}, a_3 = 1.147 \times 10^{-5} \text{ for HCFC-225cb at 165–250 nm.}$$

Table 4-61. Absorption Cross Sections of CF₃CF₂CHCl₂ and CF₂CICF₂CFCI at 298 K

λ (nm)	10 ²⁰ σ (cm ²)		λ (nm)	10 ²⁰ σ (cm ²)	
	CF ₃ CF ₂ CHCl ₂ (HCFC-225ca)	CF ₂ CICF ₂ CFCI (HCFC-225cb)		CF ₃ CF ₂ CHCl ₂ (HCFC-225ca)	CF ₂ CICF ₂ CFCI (HCFC-225cb)
160	268.7	187.9	202	11.58	0.479
162	236.8	173.3	204	8.185	0.369
164	207.6	154.8	206	5.802	0.291
166	189.0	135.1	208	4.084	0.254
168	181.4	113.2	210	2.903	0.250
170	182.7	91.35	212	2.042	
172	182.8	70.68	214	1.429	
174	189.0	54.73	216	1.05	
176	190.9	40.68	218	0.727	
178	187.9	30.04	220	0.463	
180	177.5	21.11	222	0.308	
182	161.1	14.90	224	0.209	
184	140.3	10.47	226	0.145	
186	118.3	7.308	228	0.0987	
188	96.51	5.075	230	0.0653	
190	74.30	3.492	232	0.0434	
192	57.08	2.412	234	0.0299	
194	42.83	1.661	236	0.0193	
196	31.75	1.165	238	0.0134	
198	23.22	0.873	239	0.0119	
200	16.24	0.633			

Note: HCFC-225ca, 160–239 nm, Braun et al. [40],

HCFC-225cb, 160–210 nm, Braun et al. [40].

- G1. BrO + hv → Br + O. The BrO radical has a banded spectrum in the 290–380 nm range. The strongest absorption feature is around 338 nm. The measured cross sections are both temperature- and resolution-dependent. As an example, the spectrum measured by Wahner et al. [423] is shown in Figure 4-4. The bands are due to a vibrational progression in the A ← X system, and the location of the bands, along with the assignments and cross sections measured using 0.4 nm resolution, are shown in Table 4-62. BrO is expected to dissociate upon light absorption. As a guide, the cross sections averaged over 5 nm wavelength intervals are taken from the work of Cox et al. [92], and are listed in Table 4-63. These authors estimate a BrO lifetime against atmospheric photodissociation of ~20 seconds at the earth's surface, for a solar zenith angle of 30°.

The earlier BrO cross section measurements were carried out mostly around 338 nm, and these have been reviewed by CODATA ([81,82]).

Table 4-62. Absorption Cross Sections at the Peak of Various Bands in the A ← X Spectrum of BrO

v', v''	λ (nm)	$10^{20} \sigma(\text{cm}^2)$	
		298 K	223 K
13,0	313.5	712	938
12,0	317.0	1010	1360
11,0	320.8	1180	1570
10,0	325.0	1130	1430
9,0	329.1	1130	1390
8,0	333.5	1210	1470
7,0	338.3	1550	1950
6,0	343.7	935	1110
5,0	348.8	703	896
4,0	354.7	722	1050
3,0	360.4	264	344
2,0	367.7	145	154
1,0	374.5	90	96

Spectral resolution is 0.4 nm, fwhm.

Table 4-63. Absorption Cross Sections of BrO

λ (nm)	$10^{20} \sigma(\text{cm}^2)$ average
300–305	200
305–310	259
310–315	454
315–320	391
320–325	600
325–330	753
330–335	628
335–340	589
340–345	515
345–350	399
350–355	228
355–360	172
360–365	161
365–370	92
370–375	51

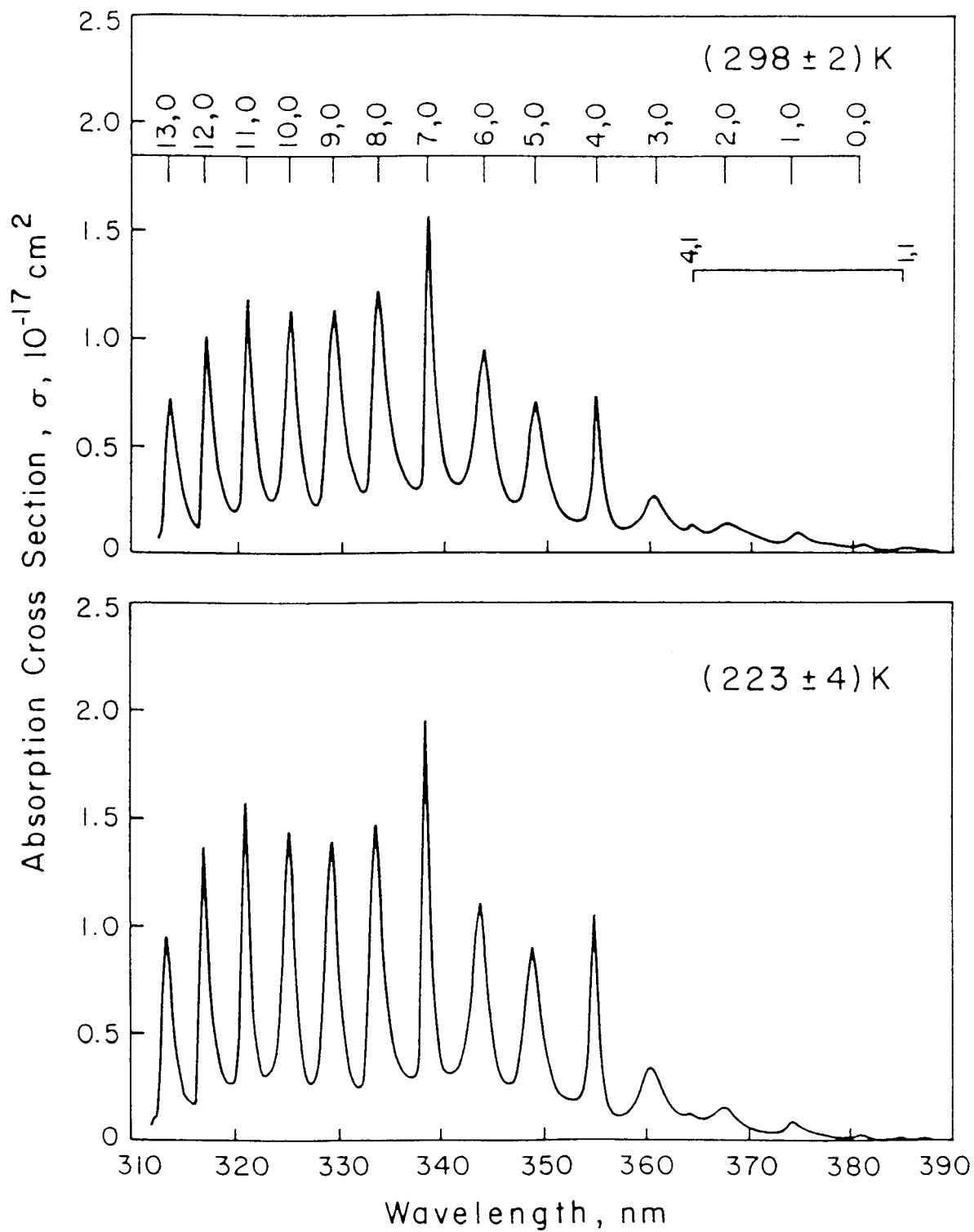


Figure 4-4. Absorption Spectrum of BrO

G2. HOBr + hv → Products. The absorption spectrum of HOBr has been measured by Orlando and Burkholder [304], Deters et al. [108], Benter et al. [31], Rattigan et al. [324], and Ingham et al. [176]. The spectra cluster has been measured in two groups. Orlando and Burkholder [304], Deters et al. [108], and Benter et al. [31] observe between 240 and 400 nm two absorption bands with maxima near 284 and 351 nm; the spectra agree reasonably well in their shape, but show a sharp decrease in cross section above 400 nm. In contrast, the cross sections reported by Rattigan et al. [324] and Ingham et al. [176] are roughly 50 % larger between 300 and 400 nm.

In addition, the spectrum obtained by Rattigan et al. shows a pronounced tail extending to 520 nm, whereas Ingham et al. observe unambiguously a third weaker absorption band ranging to 550 nm with a maximum at 457 nm. These last two studies confirm the observations of Barnes et al. [22], who showed that laser photolysis of HOBr between 440–600 nm gives rise to OH fragments. The presence of a weak band beyond 400 nm is attributable to the presence of a forbidden transition from the ground electronic to a triplet state predicted by the ab initio calculations of Francisco et al. [122]. The differences in the spectral shapes are probably attributable to impurities such as Br₂O and Br₂, and/or the use of different Br₂O cross sections. However, the presence of impurities alone cannot explain the large difference in cross sections at the peak of the absorption bands.

The recommended absorption cross sections are listed in , in the range from 250 to 550 nm; below 250 nm the data are uncertain and no recommendation is given. The cross section values in the table are based on the latest study by Ingham et al. [176]. These authors generated HOBr in situ by laser photolytic production of OH in the presence of Br₂, and determined the HOBr spectrum using a gated diode camera shortly after the pulse, circumventing the problem associated with the presence of the strong absorbing impurity Br₂O, which was encountered in previous studies. The calibration of the absorption cross sections was made relative to the established cross sections of Br₂.

The data presented in Table 4-64 are computed with the following expression taken from Ingham et al. [176], which is based on a combination of three Gaussian fits, one for each absorption band:

$$\sigma(\lambda) = 24.77 \exp \left\{ -109.80 \left[\ln \left(\frac{284.01}{\lambda} \right) \right]^2 \right\} + 12.22 \exp \left\{ -93.63 \left[\ln \left(\frac{350.57}{\lambda} \right) \right]^2 \right\} + 2.283 \exp \left\{ -242.40 \left[\ln \left(\frac{457.38}{\lambda} \right) \right]^2 \right\}$$

$\sigma(\lambda): 10^{-20} \text{ cm}^2 \text{ molecule}^{-1}; 250 < \lambda < 550 \text{ nm.}$

Benter et al. [31] measured quantum yields for HOBr photolysis at 261 and 363 nm (near the peaks of the second absorption bands). The observed quantum yield for Br formation at 363 nm was greater than 0.95, and a unity quantum yield into the product channel OH + Br is recommended. The other channel O + HBr was not observed. The laser photofragment study of Barnes et al. [22] claimed that OH was the major photolysis product at wavelengths beyond 400 nm. Lock et al. [222] found that at 490 and 510 nm OH and Br fragments are in their respective vibrational and spin-orbit ground states. The assumption of unit quantum yield of OH formation should be confirmed experimentally.

Table 4-64. Absorption Cross Sections of HOBr

λ (nm)	$10^{20} \sigma$ (cm ²)	λ (nm)	$10^{20} \sigma$ (cm ²)	λ (nm)	$10^{20} \sigma$ (cm ²)
250	4.15	355	12.1	460	2.28
255	6.19	360	11.5	465	2.14
260	10.5	365	10.5	470	1.91
265	14.6	370	9.32	475	1.62
270	18.7	375	7.99	480	1.30
275	22.1	380	6.65	485	0.993
280	24.3	385	5.38	490	0.723
285	25.0	390	4.22	495	0.502
290	24.0	395	3.23	500	0.333
295	21.9	400	2.43	505	0.212
300	19.1	405	1.80	510	0.129
305	16.2	410	1.36	515	0.076
310	13.6	415	1.08	520	0.042
315	11.8	420	0.967	525	0.023
320	10.8	425	0.998	530	0.012
325	10.5	430	1.15	535	0.0059
330	10.8	435	1.40	540	0.0029
335	11.3	440	1.68	545	0.0013
340	11.9	445	1.96	550	0.0006
345	12.3	450	2.18		
350	12.4	455	2.29		

- G3. $\text{BrONO}_2 + h\nu \rightarrow \text{Products}$. The bromine nitrate cross sections have been measured at room temperature by Spencer and Rowland [386] in the wavelength region 186–390 nm, and by Burkholder et al. [54] from 200–500 nm. The results from both studies are in excellent agreement over the range of spectral overlap. The recommended cross sections (Table 4-65) are taken from Burkholder et al.

The only study of photolysis products is that of Nickolaisen and Sander [292]. In that study, quantum yields for the $\text{Br} + \text{NO}_3$ and $\text{BrO} + \text{NO}_2$ channels were measured using broadband photolysis in quartz ($\lambda > 200$ nm) and pyrex ($\lambda > 300$ nm) reaction cells with the assumption that these were the only reaction pathways. The quantum yields were $\Phi_{\text{BrO}+\text{NO}_2} = 0.71$ and $\Phi_{\text{Br}+\text{NO}_3} = 0.29$.

Table 4-65. Absorption Cross Sections of BrONO₂ at 298 K

λ (nm)	$10^{20} \sigma$ (cm ²)	λ (nm)	$10^{20} \sigma$ (cm ²)	λ (nm)	$10^{20} \sigma$ (cm ²)
200	680	305	16.2	410	1.81
205	520	310	14.2	415	1.66
210	361	315	12.4	420	1.50
215	293	320	11.0	425	1.38
220	258	325	9.82	430	1.30
225	231	330	8.94	435	1.20
230	205	335	8.22	440	1.11
235	174	340	7.64	445	1.04
240	139	345	7.17	450	0.930
245	106	350	6.66	455	0.834
250	79.5	355	6.21	460	0.743
255	60.1	360	5.69	465	0.652
260	47.1	365	5.17	470	0.566
265	38.9	370	4.66	475	0.461
270	33.8	375	4.16	480	0.390
275	30.5	380	3.69	485	0.275
280	27.9	385	3.23	490	0.243
285	25.6	390	2.88	495	0.214
290	23.2	395	2.53	500	0.135
295	20.7	400	2.25		
300	18.4	405	1.99		

- G4. $\text{BrCl} + h\nu \rightarrow \text{Br} + \text{Cl}$. The recommended absorption cross sections are given by the expression listed at the bottom of Table 4-66, which is taken from the work of Maric et al. [236]. For convenience, some room temperature values are also listed in the table. Hubinger and Nee [164] have also measured the cross sections at room temperature. Their results are in excellent agreement with the recommended values.

Table 4-66. Absorption Cross Sections of BrCl at 298 K

λ (nm)	$10^{20} \sigma$ (cm ²)	λ (nm)	$10^{20} \sigma$ (cm ²)
200	2.4	390	34.7
210	4.0	400	28.2
220	5.4	410	21.9
230	6.0	420	16.9
240	5.1	430	14.2
250	3.7	440	12.4
260	2.5	450	11.1
270	1.5	460	9.6
280	1.2	470	8.0
290	0.63	480	6.8
300	0.61	490	5.0
310	1.2	500	3.8
320	2.8	510	3.1
330	7.4	520	2.3
340	14.2	530	1.5
350	22.9	540	0.96
360	33.3	550	0.76
370	38.7	560	0.31
380	38.5		

$$\sigma = 10^{-20} \alpha^{0.5} \left\{ 7.34 \exp \left[-68.6 \alpha \left(\ln \frac{227.6}{\lambda} \right)^2 \right] + 43.5 \exp \left[-123.6 \alpha \left(\ln \frac{372.5}{\lambda} \right)^2 \right] + 11.2 \exp \left[-84.8 \alpha \left(\ln \frac{442.4}{\lambda} \right)^2 \right] \right\}$$

where $\alpha = \tanh \left(\frac{318.8}{T} \right)$, λ in nm and T in K, $200 \text{ nm} < \lambda < 600 \text{ nm}$., $195 \text{ K} < T < 300 \text{ K}$.

- G5. $\text{CH}_3\text{Br} + h\nu \rightarrow \text{Products}$. The absorption cross sections of CH_3Br have been measured at room temperature and 205–270 nm by Davidson [104]; at 204–260 nm by Gordus and Bernstein [142]; at 174–270 nm by Robbins [338]; at 200–260 nm by Uthman et al. [413]; at 190–290 nm by Molina et al. [272]; at 201.6 nm by Felps et al. [119]; at 180–264 nm by Man et al. [230]; and at 210–295 K and 180–280 nm by Gillotay and Simon [133]. Above 180 nm and below 270 nm, the room temperature values of Gordus and Bernstein [142], Robbins [338], Uthman et al. [413], Molina et al. [272], Gillotay and Simon [133], and the values of Davidson [104] above 210 nm are in very good agreement, i.e., generally within 10% and around the absorption maximum at 200–202 nm within 2%. The value at 202 nm of Felps et al. [119] is lower by ~10% than the rest of the data. The data of Man et al. [230], given as a plot in their paper, are lower by 20–30% over the whole absorption band than the above mentioned agreeing data sets. The preferred absorption cross sections, listed in Table 4-67, are the values of Robbins [338] at 174–178 nm; the mean of the values reported by Gillotay and Simon [133] and Robbins [338] at 180–188 nm; the mean of the values reported by Gillotay and Simon [133], Uthman et al. [413], and Robbins [338] at 190–198 nm; the mean of the values reported by Gillotay and Simon [133], Molina et al. [272], Uthman et al. [413], and Robbins [338] at 200–260 nm; the mean of the values reported by Gillotay and Simon [133], Molina et al. [272], and Robbins [338] at 262–268 nm; the mean of the values reported by Gillotay and Simon [133] and Molina et al. [272] at 270–280 nm; and the data of Molina et al. [272] at 285–290 nm.

A slight temperature dependence was observed above 220 nm, where the absorption cross sections decrease with decreasing temperature 295–210 K. Gillotay and Simon [133] parameterized the cross sections and the temperature dependence by the polynomial expansion $\log_{10} \sigma(\lambda, T) = \sum A_n \lambda^n + (T - 273) \times \sum B_n \lambda^n$ and reported smoothed values for $T = 210, 230, 250, 270,$ and 295 K, every 2 nm, and at wavelengths corresponding to the wavenumber intervals generally used in stratospheric photodissociation calculations. The parameters A_n and B_n for the ranges $T = 210\text{--}300$ K and $\lambda = 200\text{--}280$ nm are as follows:

$$\begin{array}{ll} A_0 = 46.520 & B_0 = 9.3408 \times 10^{-1} \\ A_1 = -1.4580 & B_1 = -1.6887 \times 10^{-2} \\ A_2 = 1.1469 \times 10^{-2} & B_2 = 1.1487 \times 10^{-4} \\ A_3 = -3.7627 \times 10^{-5} & B_3 = -3.4881 \times 10^{-7} \\ A_4 = 4.3264 \times 10^{-8} & B_4 = 3.9945 \times 10^{-10} \end{array}$$

Quantum yields for Br and H atom formation in the photodissociation of CH_3Br were measured at 298 K by Talukdar et al. [399]. The quantum yields for Br atom formation were found to be close to unity, $\Phi(\text{Br}) = 1.05 \pm 0.11, 1.10 \pm 0.20,$ and 1.01 ± 0.16 at 193, 222, and 248 nm, respectively; the quantum yield for H atom formation in the photolysis at 193 nm was measured to be $\Phi(\text{H}) = 0.002 \pm 0.001$, whereas H atoms could not be detected in the photolysis at 222 and 248 nm. Broad band flash photolysis of CH_3Br produced $\text{Br}^*(^2\text{P}_{1/2})$ atoms with a quantum yield $\Phi(\text{Br}^*) = 0.15 \pm 0.12$ as reported by Ebenstein et al. [112].

Table 4-67. Absorption Cross Sections of CH₃Br at 295–296 K

λ (nm)	$10^{20}\sigma$ (cm ²)	λ (nm)	$10^{20}\sigma$ (cm ²)	λ (nm)	$10^{20}\sigma$ (cm ²)
174	533	212	59.9	250	0.921
176	1010	214	54.2	252	0.683
178	1280	216	47.9	254	0.484
180	44.6	218	42.3	256	0.340
182	19.8	220	36.6	258	0.240
184	21.0	222	31.1	260	0.162
186	27.8	224	26.6	262	0.115
188	35.2	226	22.2	264	0.0795
190	44.2	228	18.1	266	0.0551
192	53.8	230	14.7	268	0.0356
194	62.6	232	11.9	270	0.0246
196	69.7	234	9.41	272	0.0172
198	76.1	236	7.38	274	0.0114
200	79.0	238	5.73	276	0.00808
202	79.2	240	4.32	278	0.00553
204	78.0	242	3.27	280	0.00382
206	75.2	244	2.37	285	0.00110
208	70.4	246	1.81	290	0.00030
210	65.5	248	1.31		

Note: 174–178 nm, Robbins [338],

180–188 nm, mean of Gillotay and Simon [133] and Robbins [338],

190–198 nm, mean of Gillotay and Simon [133], Uthman et al. [413], and Robbins [338],

200–260 nm, mean of Gillotay and Simon [133], Molina et al. [272], Uthman et al. [413] and Robbins [338],

262–268 nm, mean of Gillotay and Simon [133], Molina et al. [272], and Robbins [338],

270–280 nm, mean of Gillotay and Simon [133] and Molina et al. [272],

285–290 nm, Molina et al. [272].

- G6. CH₂Br₂ + hv → Products. The absorption cross sections of CH₂Br₂ have been measured at room temperature and 200–300 nm by Molina et al. [272]; at 210–295 K and 174–290 nm by Gillotay et al. [138], [135]; and at 250–348 K and 215–300 nm by Mössinger et al. [283]. The results are in good agreement, at 200–255 nm within 10% and up to 275 nm within 30%. The preferred room temperature values, listed in Table 4-68, are the values of Gillotay et al. [138], [1325] at 174–198 nm; the mean of the values reported by Molina et al. [272] and Gillotay et al. [138], [135] for the wavelength range 200–215 nm; the mean of the values reported by the three groups for the wavelength range 220–290 nm; and the values of Mössinger et al. [283] at 295–300 nm.

Both studies of the temperature dependence show a decrease of the absorption cross sections with decreasing temperature at wavelength above ~235–239 nm, and the reverse behavior around the absorption maximum down to 207 nm. At lower wavelengths, Gillotay et al. [135,138] report between 210 and 295 K a slight increase of σ at 175–189 nm and a slight decrease around the weaker absorption maximum at 198–201 nm. The latter group parameterized the cross sections and the temperature dependence by the polynomial expansion $\log_{10} \sigma(\lambda, T) = \sum A_n \lambda^n + (T - 273) \times \sum B_n \lambda^n$ and report smoothed values for T = 210, 230, 250, 270, and 295 K, every 2 nm, and at wavelengths corresponding to the wavenumber intervals generally used in stratospheric photodissociation calculations. The parameters A_n and B_n for the ranges 210–290 nm and 210–300 K are as follows:

$$\begin{array}{ll}
 A_0 = -70.211776 & B_0 = 2.899280 \\
 A_1 = 1.940326 \times 10^{-1} & B_1 = -4.327724 \times 10^{-2} \\
 A_2 = 2.726152 \times 10^{-3} & B_2 = 2.391599 \times 10^{-4} \\
 A_3 = -1.695472 \times 10^{-5} & B_3 = -5.807506 \times 10^{-7} \\
 A_4 = 2.500066 \times 10^{-8} & B_4 = 5.244883 \times 10^{-10}
 \end{array}$$

Mössinger et al. [283] list the temperature coefficients B(λ) at 5-nm intervals for the ranges 215–300 nm and 250–348 K for the empirical relation $\ln \sigma(\lambda, T) = \ln \sigma(\lambda, 298\text{K}) + B(\lambda)(T-298)$. The formulae used by Gillotay et al. [135,138] and Mössinger et al. [283] produce cross sections which agree at 250 K within 5% in the range 215–265 nm and within 10% in the range 270–285 nm.

Table 4-68. Absorption Cross Sections of CH₂Br₂ at 295–298 K

λ (nm)	10^{20} σ (cm ²)	λ (nm)	10^{20} σ (cm ²)	10^3 B (K ⁻¹)	λ (nm)	10^{20} σ (cm ²)	10^3 B (K ⁻¹)
174	1170.9	198	226.0		255	14.10	3.91
176	662.4	200	225.6		260	6.607	5.16
178	377.2	205	215.3		265	3.037	6.33
180	241.0	210	234.5		270	1.347	7.75
182	178.4	215	263.2	-2.02	275	0.590	8.74
184	154.4	220	272.0	-1.79	280	0.255	11.6
186	153.5	225	247.4	-1.50	285	0.114	13.8
188	166.1	230	195.8	-0.96	290	0.0499	15.3
190	187.0	235	138.9	-0.04	295	0.0210	16.5
192	209.3	240	88.60	0.71	300	0.0090	21.9
194	222.5	245	51.90	1.80			
196	228.3	250	28.03	2.70			

Note: Absorption cross sections σ : 174–198 nm, Gillotay et al. [138], [135], 200–210 nm, mean of Molina et al. [272] and Gillotay et al. [138], [135], 215–290 nm, mean of Molina et al [272], Gillotay et al. [138], [135], and Mössinger et al. [283], 295–300 nm, Mössinger et al.[283].
Temperature coefficients B: 215–300 nm, Mössinger et al.[283].

- G7. CHBr₃ + hv → Products. The absorption cross sections of CHBr₃ have been measured at 240–295 K and 170–310 nm by Gillotay et al. [133] and at 256–296 K and 286–362 nm by Moortgat et al. [278]; the agreement in the overlap region is excellent. The recommended cross sections at room temperature, listed in Table 4-69, are the values of Gillotay et al. [133] for the range 170–284 nm; the mean of the values reported by Gillotay et al. [133] and Moortgat et al. [278] for the range 286–310 nm; and the values of Moortgat et al. [278] at 286–362 nm.

The studies of the temperature dependence show an increase of the absorption cross sections with decreasing temperature around the three absorption maxima at 178–189 nm, 194–208 nm, and 208–234 nm, and a decrease of the absorption cross sections below 179 nm, at 189–194 nm and above 235 nm. Gillotay et al. [133] parameterized the cross sections and the temperature dependence by the polynomial expansion

$$\log_{10}(\sigma(\lambda, T)) = \sum A_n \lambda^n + (T - 273) \times \sum B_n \lambda^n$$

and report smoothed values for T = 210, 230, 250, 270, and 295 K, every 2 nm, and at wavelengths corresponding to the wavenumber intervals generally used in stratospheric photodissociation calculations. The parameters A_n and B_n for the ranges 240–310 nm and 210–300 K are given by Gillotay and Simon [135]:

$$\begin{aligned} A_0 &= -110.2782 & B_0 &= -1.5312 \times 10^{-1} \\ A_1 &= 1.0281 & B_1 &= 1.6109 \times 10^{-3} \\ A_2 &= -3.6626 \times 10^{-3} & B_2 &= -5.8075 \times 10^{-6} \\ A_3 &= 4.1226 \times 10^{-6} & B_3 &= 7.2893 \times 10^{-9} \end{aligned}$$

For wavelengths longer than 290 nm, the atmospherically important range, Moortgat et al. [278] give the expression

$$\sigma(\lambda, T) = \exp \{ (0.06183 - 0.000241 \lambda) (273 - T) - (2.376 + 0.14757 \lambda) \} \quad (\lambda = 290\text{--}340 \text{ nm}, T = 210\text{--}300 \text{ K})$$

These two formulae produce continuous absorption curves for the range 240–340 nm also at low temperatures

At wavelengths longer than 290 nm, the cross sections are relatively small; the presence of impurities as well as optical artifacts arising, e.g., from adsorption of CHBr₃ on the cell windows, complicate the measurements. Hence, additional investigations of the spectrum would be useful.

Table 4-69. Absorption Cross Sections of CHBr₃ at 295–296 K

λ (nm)	$10^{20} \sigma$ (cm ²)	λ (nm)	$10^{20} \sigma$ (cm ²)	λ (nm)	$10^{20} \sigma$ (cm ²)
170	1603.8	236	323.9	302	0.534
172	1173.2	238	294.7	304	0.397
174	969.6	240	272.8	306	0.297
176	872.0	242	253.3	308	0.222
178	857.6	244	233.7	310	0.165
180	831.3	246	214.4	312	0.127
182	770.3	248	193.9	314	0.0952
184	683.3	250	174.1	316	0.0712
186	570.4	252	157.7	318	0.0529
188	470.8	254	136.1	320	0.0390
190	399.1	256	116.4	322	0.0289
192	360.2	258	98.6	324	0.0215
194	351.3	260	82.8	326	0.0162
196	366.1	262	68.9	328	0.0121
198	393.6	264	56.9	330	0.00916
200	416.4	266	46.7	332	0.00690
202	433.6	268	38.0	334	0.00525
204	440.6	270	30.8	336	0.00396
206	445.0	272	24.8	338	0.00307
208	451.4	274	19.8	340	0.00240
210	468.5	276	15.8	342	0.00176
212	493.4	278	12.5	344	0.00135
214	524.2	280	9.88	346	0.00102
216	553.5	282	7.77	348	0.00080
218	573.9	284	6.10	350	0.00064
220	582.6	286	4.79	352	0.00054
222	578.0	288	3.74	354	0.00046
224	557.8	290	2.89	356	0.00032
226	527.2	292	2.20	358	0.00024
228	486.8	294	1.69	360	0.00017
230	441.2	296	1.28	362	0.00013
232	397.4	298	0.956		
234	361.8	300	0.719		

Note: 170–284 nm, Gillotay et al. [133],
 286–310 nm, mean of Gillotay et al. [133] and Moortgat et al. [278],
 312–362 nm, Moortgat et al. [278].

- G8. CH₂BrCH₂Br + hv → Products. The absorption cross sections of CH₂BrCH₂Br have been measured at room temperature and 190–270 nm by Uthman et al. [413]. Their data are listed in Table 4-70.

Table 4-70. Absorption Cross Sections of CH₂BrCH₂Br at 295 K

λ (nm)	$10^{20} \sigma$ (cm ²)	λ (nm)	$10^{20} \sigma$ (cm ²)	λ (nm)	$10^{20} \sigma$ (cm ²)
190	230	218	170	246	9.3
192	250	220	150	248	7.1
194	270	222	130	250	5.9
196	290	224	110	252	4.4
198	300	226	89	254	4.0
200	310	228	75	256	2.8
202	310	230	62	258	2.1
204	300	232	50	260	1.9
206	290	234	41	262	1.7
208	280	236	32	264	1.4
210	260	238	26	266	1.1
212	230	240	20	268	0.9
214	210	242	16	270	0.7
216	190	244	11		

Note: 190–270 nm, Uthman et al. [413].

- G9. C₂H₅Br + hv → Products. The absorption cross sections of C₂H₅Br have been measured at 295 K and 200–260 nm by Zhang et al. [451]. This wavelength range shows part of an absorption band with a maximum of $\sim 6 \times 10^{-19}$ cm² at ~ 200 nm. Estimated values at 5-nm intervals, read from a logarithmic plot, are presented in Table 4-71.

Table 4-71. Absorption Cross Sections of C₂H₅Br at 295 K

λ (nm)	$10^{20} \sigma$ (cm ²)	λ (nm)	$10^{20} \sigma$ (cm ²)	λ (nm)	$10^{20} \sigma$ (cm ²)
200	60.5	225	23.7	250	1.12
205	59.5	230	14.9	255	0.53
210	53.5	235	8.30	260	0.23
215	44.5	240	4.30		
220	34.0	245	2.28		

Note: 200–260 nm, Zhang et al. [451], estimated values read from logarithmic plot.

- G10. CH₂ClBr (Halon-1011) + hv → Products. The absorption cross sections of CH₂ClBr have been measured at room temperature and 210–260 nm by Cadman and Simons [64], and at 187–290 nm by Orkin et al. [303]. The data of Cadman and Simons [64], which are given only on a plot in their paper, are smaller by $\leq 20\%$ than the data of Orkin et al. [303]. The recommended absorption cross sections, listed in Table 4-72, are the data of Orkin et al. [303].

Quantum yields for Br (²P_{3/2}) and Br* (²P_{1/2}) atom formation in the photolysis of CH₂ClBr at 193–242 nm and 248–268 nm have been measured by Zou et al. [452] and McGivern et al. [253], respectively. Reported values are as follows:

	193 nm	234 nm	248.5 nm	261.5 nm	266.7 nm:
$\Phi(\text{Br } (^2\text{P}_{3/2}))$	0.82 ± 0.10	0.80 ± 0.10	0.86 ± 0.10	0.84 ± 0.10	0.91 ± 0.10
$\Phi(\text{Br}^* (^2\text{P}_{1/2}))$	0.18 ± 0.10	0.20 ± 0.10	0.14 ± 0.10	0.16 ± 0.10	0.09 ± 0.10

Table 4-72. Absorption Cross Sections of CH₂ClBr at 295 K

λ (nm)	$10^{20} \sigma$ (cm ²)	λ (nm)	$10^{20} \sigma$ (cm ²)	λ (nm)	$10^{20} \sigma$ (cm ²)
187	151.1	222	57.4	258	1.45
188	126.4	224	50.5	260	1.09
190	104.6	226	44.1	262	0.807
192	100.5	228	38.2	264	0.596
194	104.7	230	32.8	266	0.440
196	111.8	232	28.0	268	0.322
198	119.4	234	23.6	270	0.235
200	124.7	236	19.7	272	0.170
202	127.1	238	16.3	274	0.123
204	126.3	240	13.4	276	0.089
206	122.5	242	10.8	278	0.064
208	116.3	244	8.73	280	0.046
210	108.4	246	6.94	282	0.033
212	99.6	248	5.46	284	0.024
214	90.5	250	4.24	286	0.0178
216	81.5	252	3.29	288	0.0129
218	72.9	254	2.52	290	0.0098
220	64.8	256	1.92		

Note: 187–290 nm, Orkin et al. [303].

- G11. CHClBr₂ (Halon-1012) + hv → Products. The absorption cross sections of CHClBr₂ have been measured at room temperature and 106–200 nm by Ibuki et al. [172]; and at 240, 261, and 296 K and 200–310 nm by Bilde et al. [33]. Two absorption bands are apparent above 200 nm, one maximizing near 210 nm and the other near 240 nm. Near the band maxima, the cross sections at 240 K are approximately higher by 10% than those at room temperature. A positive temperature dependence of the cross sections is evident in the long-wavelength tail of the spectrum, the room temperature cross section being about 15% higher at 270 nm than that obtained at 240 K. The recommended absorption cross sections, listed in Table 4-73, are the room temperature data of Bilde et al. [33] (originally listed at 1-nm intervals); values at 2-nm intervals are given for wavelengths above 212 nm, and values at 1-nm intervals are given or the region of the first absorption maximum (200–212 nm), where the absorption curve shows a somewhat irregular behavior.

Table 4-73. Absorption Cross Sections of CHClBr₂ at 296 K

λ (nm)	$10^{20} \sigma$ (cm ²)	λ (nm)	$10^{20} \sigma$ (cm ²)	λ (nm)	$10^{20} \sigma$ (cm ²)
200	274.6	230	141.4	272	9.415
201	282.8	232	136.4	274	7.552
202	293.9	234	131.4	276	5.950
203	306.7	236	126.8	278	4.687
204	314.2	238	122.2	280	3.691
205	320.6	240	116.0	282	2.884
206	324.9	242	109.2	284	2.261
207	323.7	244	101.2	286	1.734
208	322.9	246	92.70	288	1.331
209	324.6	248	83.52	290	1.016
210	317.8	250	74.04	292	0.7907
211	306.2	252	64.83	294	0.6116
212	297.4	254	55.95	296	0.4583
214	279.4	256	47.67	298	0.3489
216	261.7	258	39.92	300	0.2692
218	234.9	260	33.35	302	0.2076
220	215.1	262	27.50	304	0.1588
222	199.1	264	22.50	306	0.1208
224	184.5	266	18.28	308	0.0945
226	165.3	268	14.78	310	0.0742
228	151.7	270	11.82		

Note: 200–310 nm, Bilde et al. [33]

- G12. CHCl₂Br (Halon-1021) + hν → Products. The absorption cross sections of CHCl₂Br have been measured at room temperature and 106–200 nm by Ibuki et al. [172]; at room temperature and 201–270 nm by Cadman and Simons [64]; and at 253, 273 and 298 K and 200–320 nm by Bilde et al. [33]. The data of Cadman and Simons [64], which are given only in a plot in their paper, agree between 200 and 260 nm within ≤15% with the room temperature data of Bilde et al. [33], the absorption maximum, however, is shifted to lower wavelengths. The recommended absorption cross sections, listed in Table 4-74, are those reported by Bilde et al. [33].

A decrease of the absorption cross sections with decreasing temperature was observed between 298 and 253 K over the whole spectrum. The cross section in the absorption maximum, which has been observed at 220 nm by Bilde et al. [33], is approximately 6% lower at 253 K than at room temperature. An increasingly positive temperature dependence was observed at longer wavelengths, the room temperature cross section at 320 nm becoming about four times larger than those at 253 K.

Table 4-74. Absorption Cross Sections of CHCl₂Br at 298 K

λ (nm)	$10^{20} \sigma$ (cm ²)	λ (nm)	$10^{20} \sigma$ (cm ²)	λ (nm)	$10^{20} \sigma$ (cm ²)
200	115.0	230	58.1	276	1.63
202	93.8	232	54.6	278	1.32
204	81.1	234	50.0	280	1.07
206	73.6	236	45.8	282	0.865
208	69.0	238	41.6	284	0.694
209	69.8	240	37.3	286	0.573
210	68.8	242	33.0	288	0.454
211	67.4	244	29.3	290	0.384
212	68.4	246	25.8	292	0.317
213	70.0	248	22.2	294	0.265
214	70.1	250	19.2	296	0.217
215	70.2	252	16.5	298	0.176
216	71.1	254	13.6	300	0.146
217	71.0	256	11.5	302	0.118
218	70.7	258	9.75	304	0.0962
219	71.3	260	8.19	306	0.0761
220	71.6	262	6.82	308	0.0617
221	70.6	264	5.61	310	0.0496
222	69.3	266	4.68	312	0.0395
223	68.7	268	3.74	314	0.0317
224	68.2	270	3.01	316	0.0259
226	65.2	272	2.48	318	0.0210
228	62.2	274	2.02	320	0.0171

Note: 200–320 nm, Bilde et al. [33].

- G13. CCl₃Br (Halon-1031) + $h\nu \rightarrow$ Products. The absorption cross sections of CCl₃Br have been measured at room temperature and 170–230 nm by Roxlo and Mandl [350] and at 207–305 nm by Cadman and Simons [64]. Both groups report their results as plots only. Estimated absorption cross sections are listed in Table 4-75, which are the results of Roxlo and Mandl [350] at 170–200 nm; the mean of the results of both groups at 205–230 nm; and the results of Cadman and Simons [64] at 235–305 nm.

Quantum yields for Br*(²P_{1/2}) atom formation in the photolysis at 234 and 265 nm, $\Phi(\text{Br}^*) = 0.31 \pm 0.01$ and 0.68 ± 0.02 , respectively, were reported by Jung et al. [195].

Table 4-75. Absorption Cross Sections of CCl₃Br at 298 K

λ (nm)	$10^{20} \sigma$ (cm ²)	λ (nm)	$10^{20} \sigma$ (cm ²)	λ (nm)	$10^{20} \sigma$ (cm ²)
170	600	220	49	270	19
175	600	225	46	275	11
180	1050	230	52	280	7.2
185	1100	235	50	285	5.0
190	850	240	50	290	3.3
195	530	245	49	295	2.2
200	230	250	48	300	1.4
205	140	255	46	305	1.0
210	90	260	42		
215	66	265	34		

Note: 170–200 nm, Roxlo and Mandl [350],

205–230 nm, mean of Roxlo and Mandl [350] and Cadman and Simons [64],

235–305 nm, Cadman and Simons [64].

- G14. CHF₂Br (Halon-1201) + hv → Products. The absorption cross sections of CHF₂Br have been measured at room temperature and 207–255 nm by Davidson [104]; at 190–280 nm by Talukdar et al. [394]; and at 190–280 nm by Orkin and Kasimovskaya [302]. Gillotay et al. [138] carried out measurements at 210–295 K and in the wavelength range 166–267 nm and report only smoothed values for T = 210, 230, 250, 270, and 295 K and at wavelengths corresponding to the wavenumber intervals generally used in stratospheric photodissociation calculations. The results of Davidson [104], Orkin and Kasimovskaya [302], and Gillotay et al. [138] are in excellent agreement at wavelengths below 240 nm; the values of Gillotay et al. [138] become increasingly smaller by up to about 40% at 260 nm, and those of Davidson [104] become smaller by up to about 30% at 250 nm than the values of Orkin and Kasimovskaya [302]. The results of Talukdar et al. [394], who report a plot on a logarithmic scale for measured values at 190–280 nm and extrapolated values up to 360 nm, appear to be in agreement with the results of Orkin and Kasimovskaya [302]. The preferred values, listed in Table 4-76, are the values of Gillotay et al. [138] at the centers of the 500-cm⁻¹ intervals between 168 and 188 nm, and the values of Orkin and Kasimovskaya [302] at 190–280 nm.

With decreasing temperature 295–210 K, an increase of the absorption cross sections around the absorption maximum at 168–215 nm and a decrease at wavelengths above 215 nm was observed by Gillotay et al. [104] (the interpolation formula has not been reported for this molecule).

Table 4-76. Absorption Cross Sections of CHF₂Br at 298 K

λ (nm)	10 ²⁰ σ (cm ²)	λ (nm)	10 ²⁰ σ (cm ²)	λ (nm)	10 ²⁰ σ (cm ²)
168.10	3.97	206	23.2	246	0.299
170.95	8.21	208	21.2	248	0.220
173.15	12.5	210	19.0	250	0.161
174.65	15.6	212	16.8	252	0.117
176.20	18.8	214	14.6	254	0.0849
177.80	21.9	216	12.6	256	0.0615
179.40	24.5	218	10.6	258	0.0444
181.00	26.6	220	8.85	260	0.0319
182.65	28.3	222	7.25	262	0.0230
184.35	29.6	224	5.88	264	0.0166
186.05	30.6	226	4.71	266	0.0121
187.80	31.4	228	3.73	268	0.0087
190	32.5	230	2.91	270	0.0063
192	32.4	232	2.24	272	0.0046
194	31.8	234	1.71	274	0.0034
196	31.0	236	1.30	276	0.0024
198	29.9	238	0.982	278	0.0018
200	28.6	240	0.735	280	0.0012
202	27.0	242	0.547		
204	25.2	244	0.405		

Note: 168–188 nm, Gillotay et al. [138],
190–280 nm, Orkin and Kasimovskaya [302].

- G15. CF₂Br₂ (Halon-1202) + hv → Products. The absorption cross sections of CF₂Br₂ have been measured at room temperature and 215–290 nm by Davidson [104]; at 200–310 nm by Walton et al. [428]; at 190–340 nm by Molina et al. [272]; at 190–320 nm by Orkin and Kasimovskaya [302]; at 210–295 K and 170–304 nm by Gillotay and Simon [134]; and at 210–296 K and 190–320 nm by Burkholder et al. [57]. The room temperature data, except those of Walton [428], are in good agreement, i.e., better than 10%, over their common wavelength range from 190 to 300 nm. In the absorption maximum around 226 nm, the older data of Davidson [172] and Molina et al. [272] are the highest and lowest, respectively, and the more recent data agree within 5% (the absorption maximum reported by Walton [428] is larger by ~50%). At wavelengths above 300 nm, the values of Orkin and Kasimovskaya [302] and Burkholder et al. [57] agree within 15%, whereas those of Molina et al. [272] become increasingly larger by up to ~200% at 320 nm (and larger by up to ~660% than the extrapolated values at 340 nm, see below). The preferred absorption cross sections, listed in Table 4-77, are the values of Gillotay and Simon [134] at 170–188 nm; the mean of the values reported by Gillotay and Simon [134], Orkin and Kasimovskaya [302], and Burkholder et al. [57] for the wavelength range 190–304 nm; and the mean of the values reported by the latter two groups for the range 306–320 nm. For wavelengths 322–340 nm, the mean

of the values of Orkin and Kasimovskaya [302], and Burkholder et al.[57] for the range 306–320 nm have been extrapolated ($\log \sigma = 1.85109 - 0.07755 \lambda$).

Measurements in the far UV were reported by Doucet et al. [109] for the wavelength range 60–220 nm and by Seccombe et al. [369] for the wavelength range 55–175 nm.

Both studies of the temperature dependence show an increase of the absorption cross sections in the two absorption bands around 190 and 226 nm with decreasing temperature 296–210 K and the reverse effect at wavelengths above 240 nm and below 177 nm. Gillotay and Simon [134] observed a regular temperature behavior, i.e., an increase of the maximum absorption cross section at ~225 nm by $\sim 0.09 \times 10^{-18} \text{ cm}^2 \text{ molecule}^{-1}$ per 20-K temperature decrease. Burkholder et al.[57] observed a less pronounced temperature behavior below 250 K (the maximum absorption cross sections agree within 1%), so that their maximum cross section at 210 K is lower by 5% than that observed by Gillotay and Simon [134] (in contrast to the cross sections at room temperature which are nearly identical). Different parameterizations for the temperature dependence of the absorption cross section have been proposed. Gillotay and Simon [134] give the polynomial expansion $\log_{10} \sigma(\lambda, T) = \sum A_n \lambda^n + (T - 273) \times \sum B_n \lambda^n$ and report smoothed values for $T = 210, 230, 250, 270,$ and 295 K , every 2 nm, and at wavelengths corresponding to the wavenumber intervals generally used in stratospheric photodissociation calculations. The parameters A_n and B_n for the ranges 222–304 nm and 210–300 K are as follows:

$$\begin{array}{ll} A_0 = -206.2 & B_0 = 1.0460 \times 10^{-1} \\ A_1 = 2.3726 & B_1 = -1.4124 \times 10^{-3} \\ A_2 = -1.0527 \times 10^{-2} & B_2 = 6.9015 \times 10^{-6} \\ A_3 = 1.9239 \times 10^{-5} & B_3 = -1.5164 \times 10^{-8} \\ A_4 = -1.2242 \times 10^{-8} & B_4 = 1.3990 \times 10^{-11} \end{array}$$

Burkholder et al. [57] give the expansion

$$\log_{10} \sigma(\lambda, T) = (\sum A_i (\lambda - 268.7998)^i) (1 + (296 - T) \sum B_i (\lambda - 268.7998)^i)$$

and report the following parameters A_i and B_i for the ranges 235–260 nm and 210–296 K:

$$\begin{array}{ll} A_0 = -44.42756 & B_0 = 1.481886 \times 10^{-4} \\ A_1 = -1.464955 \times 10^{-1} & B_1 = 6.77182 \times 10^{-6} \\ A_2 = -5.692188 \times 10^{-4} & B_2 = 1.154347 \times 10^{-7} \\ A_3 = 1.155366 \times 10^{-5} & B_3 = -2.77145 \times 10^{-11} \\ A_4 = -1.399502 \times 10^{-7} & B_4 = -6.619515 \times 10^{-11} \end{array}$$

A parameterization for extrapolated absorption cross sections up to 400 nm,

$$\log_{10} \sigma(\lambda, T) = (\sum A_i (\lambda - 301.0104)^i) + (\lambda - 260) (\sum B_i (T - 251.2)^i)$$

has also been reported by Burkholder et al. [57].

The quantum yield for formation of CF_2O and Br_2 in the photolysis of CF_2Br_2 at 206, 248, and 302 nm, in the presence of O_2 has been measured to be unity by Molina and Molina [269], independent of pressure, in contrast to an earlier report by Walton [428] that the quantum yield at 265 nm decreases from unity when the system pressure is raised to 50 torr of CO_2 . Primary quantum yields for Br atom formation, $\Phi(\text{Br}) = 1.96 \pm 0.27, 1.63 \pm 0.19,$ and $1.01 \pm 0.15,$ in the photodissociation of CF_2Br_2 at 193, 222, and 248 nm, respectively, were measured at 298 K by Talukdar et al. [399]. A quantum yield for CF_2 formation, $\Phi(\text{CF}_2) = 1.15 \pm 0.30,$ in the 193-nm photolysis was reported by Talukdar et al. [397].

Table 4-77. Absorption Cross Sections of CF₂Br₂ at 295–296 K

λ (nm)	$10^{20} \sigma$ (cm ²)	λ (nm)	$10^{20} \sigma$ (cm ²)	λ (nm)	$10^{20} \sigma$ (cm ²)
170	124.5	228	253.4	286	0.336
172	78.1	230	244.7	288	0.245
174	55.3	232	230.2	290	0.178
176	49.5	234	211.9	292	0.128
178	60.3	236	191.6	294	0.0926
180	75.0	238	169.3	296	0.0672
182	86.6	240	147.3	298	0.0487
184	100.9	242	125.8	300	0.0352
186	111.8	244	106.0	302	0.0253
188	118.0	246	87.8	304	0.0183
190	115.9	248	72.0	306	0.0130
192	110.3	250	58.3	308	0.00919
194	101.6	252	46.5	310	0.00650
196	91.4	254	36.8	312	0.00456
198	82.1	256	28.9	314	0.00319
200	74.9	258	22.4	316	0.00222
202	71.7	260	17.3	318	0.00157
204	73.4	262	13.1	320	0.00105
206	80.7	264	9.90	322	0.000759
208	93.0	266	7.47	324	0.000531
210	110.0	268	5.59	326	0.000371
212	131.0	270	4.17	328	0.000260
214	154.9	272	3.08	330	0.000182
216	180.4	274	2.27	332	0.000127
218	204.7	276	1.66	334	0.000089
220	226.0	278	1.21	336	0.000062
222	244.2	280	0.888	338	0.000044
224	253.3	282	0.647	340	0.000030
226	256.8	284	0.470		

Note: 170–188 nm: Gillotay and Simon [134]

190–304 nm: mean of Gillotay and Simon [134], Orkin and Kasimovskaya [302], and Burkholder et al. [57]

306–320 nm: mean of Orkin and Kasimovskaya [302] and Burkholder et al. [57]

322–340 nm: extrapolation of mean of Orkin and Kasimovskaya [302], and Burkholder et al. [57] data.

- G16. CF₂ClBr (Halon-1211) + hv → Products. The absorption cross sections of CF₂ClBr have been measured at room temperature and 191–307 nm by Giolando et al. [140]; at 190–330 nm by Molina et al. [272]; at 190–304 nm by Orkin and Kasimovskaya [302]; at 210–295 K and 170–302 nm by Gillotay and Simon [134]; and at 210–296 K and 190–320 nm by Burkholder et al. [57]. The agreement between the room temperature data of Orkin and Kasimovskaya [302], Gillotay and Simon [134], and Burkholder et al. [57] is very good in the region of the absorption band, i.e., within 10% over the range 190–240 nm and within 3% in the maximum at 205–206 nm, with one exception: Gillotay and Simon [134] observed a structure near the absorption maximum, different from the other observations, which resulted in values higher by about 10% at 200–202 nm. Molina et al. [272] reported values for the range 190–240 nm which are lower by 10–20% than the above mentioned data. The few data points (at 10-nm intervals) of Giolando et al. [140] fit well to the absorption curves reported by Orkin and Kasimovskaya [302], Gillotay and Simon [134], and Burkholder et al. [57]. The deviations between the various data sets increase at longer wavelengths to ≤30% at 300 nm and up to 55% at 320 nm. The preferred absorption cross sections at 295–298 K, listed in Table 4-78, are the values of Gillotay and Simon [134] at 170–188 nm; the mean of the values reported by Molina et al. [272], Gillotay and Simon [134], Burkholder et al. [57] and Orkin and Kasimovskaya [302] at 190–302 nm; the mean of the values reported by Molina et al. [272], Burkholder et al. [57], and Orkin and Kasimovskaya [302] at 304 nm; and the mean of the values reported by Molina et al. [272] and Burkholder et al. [57] at 306–320 nm.

Measurements in the far UV at 60–220 nm were reported by Doucet et al. [109].

Both studies of the temperature dependence show an increase of the absorption cross sections in the absorption band around 204–206 nm with decreasing temperature 296–210 K and the reverse effect at wavelengths above 233 nm and below 180 nm. Gillotay and Simon [134] observed a regular temperature behavior, i.e., an increase of the maximum absorption cross section by $\sim 0.05 \times 10^{-18} \text{ cm}^2 \text{ molecule}^{-1}$ per 20 K temperature decrease. Burkholder et al. [57] observed a less pronounced temperature behavior (the maximum absorption cross sections agree within 2.5%), so that their maximum cross section at 210 K is lower by 15% than that observed by Gillotay and Simon [134] (in contrast to the cross sections at room temperature which are within 4%). Different parameterizations for the temperature dependence of the absorption cross section have been proposed. Gillotay and Simon [134] give the polynomial expansion

$$\log_{10} \sigma(\lambda, T) = \sum A_n \lambda^n + (T - 273) \times \sum B_n \lambda^n$$

and report smoothed values for $T = 210, 230, 250, 270,$ and 295 K , every 2 nm, and at wavelengths corresponding to the wavenumber intervals generally used in stratospheric photodissociation calculations. The parameters A_n and B_n for the ranges 200–302 nm and 210–300 K are as follows:

$$\begin{array}{ll} A_0 = -134.80 & B_0 = 3.3070 \times 10^{-1} \\ A_1 = 1.7084 & B_1 = -5.0957 \times 10^{-3} \\ A_2 = -9.1540 \times 10^{-3} & B_2 = 2.9361 \times 10^{-5} \\ A_3 = 2.1644 \times 10^{-5} & B_3 = -7.6198 \times 10^{-8} \\ A_4 = -1.9863 \times 10^{-8} & B_4 = 7.6825 \times 10^{-11} \end{array}$$

Burkholder et al. [57] give the expansion

$$\log_{10} \sigma(\lambda, T) = (\sum A_i (\lambda - 259.8989)^i) (1 + (296 - T) \sum B_i (\lambda - 259.8989)^i)$$

and report the following parameters A_i and B_i for the ranges 220–260 nm and 210–296 K:

$$\begin{array}{ll} A_0 = -45.4087 & B_0 = 1.528905 \times 10^{-4} \\ A_1 = -1.304811 \times 10^{-1} & B_1 = 6.024833 \times 10^{-6} \\ A_2 = -6.995443 \times 10^{-4} & B_2 = 1.030995 \times 10^{-7} \\ A_3 = 6.159709 \times 10^{-6} & B_3 = -6.387931 \times 10^{-11} \\ A_4 = -9.384074 \times 10^{-9} & B_4 = -3.718503 \times 10^{-11} \end{array}$$

A parameterization for extrapolated absorption cross sections up to 400 nm,

$$\log_{10} \sigma(\lambda, T) = (\sum A_i (\lambda - 292.2083)^i) + (\lambda - 260) (\sum B_i (T - 251.2)^i)$$

has also been reported by Burkholder et al. [57].

Quantum yields for Cl and Br atom formation in the photodissociation of CF_2ClBr at 193, 222, and 248 nm, $\Phi(\text{Cl}) = 1.03 \pm 0.14, 0.27 \pm 0.04,$ and 0.18 ± 0.03 , $\Phi(\text{Br}) = 1.04 \pm 0.13, 0.86 \pm 0.11,$ and 0.75 ± 0.13 , respectively, and a quantum yield for CF_2 formation in the 193-nm photolysis, $\Phi(\text{CF}_2) = 0.91 \pm 0.30$, were measured at 298 K by Talukdar et al. [397].

Table 4-78. Absorption Cross Sections of CF₂ClBr at 295–298 K

λ (nm)	$10^{20} \sigma$ (cm ²)	λ (nm)	$10^{20} \sigma$ (cm ²)	λ (nm)	$10^{20} \sigma$ (cm ²)
170	323.0	222	68.3	274	0.250
172	234.2	224	60.4	276	0.184
174	176.0	226	52.7	278	0.135
176	120.9	228	45.7	280	0.0991
178	84.7	230	39.2	282	0.0724
180	58.1	232	33.8	284	0.0527
182	41.9	234	28.8	286	0.0385
184	35.0	236	24.4	288	0.0282
186	34.1	238	20.4	290	0.0205
188	38.9	240	16.9	292	0.0148
190	46.1	242	13.9	294	0.0106
192	57.0	244	11.4	296	0.00764
194	69.1	246	9.28	298	0.00544
196	81.4	248	7.50	300	0.00391
198	93.5	250	5.99	302	0.00279
200	106.0	252	4.76	304	0.00207
202	113.3	254	3.76	306	0.00161
204	117.4	256	2.94	308	0.00113
206	118.7	258	2.29	310	0.000803
208	117.7	260	1.76	312	0.000569
210	114.2	262	1.36	314	0.000403
212	108.5	264	1.03	316	0.000288
214	101.5	266	0.784	318	0.000213
216	93.6	268	0.593	320	0.000159
218	85.3	270	0.447		
220	76.8	272	0.336		

Note: 170–188 nm: Gillotay and Simon [134]

190–302 nm: mean of Molina et al. [272], Gillotay and Simon [134], Burkholder et al. [57], and Orkin and Kasimovskaya [302]

304 nm: mean of Molina et al. [272], Burkholder et al. [57], and Orkin and Kasimovskaya [302]

306–320 nm: mean of Molina et al. [272] and Burkholder et al. [57].

- G17. CF₃Br (Halon-1301) + hv → Products. The absorption cross sections of CF₃Br have been measured at room temperature and 207–255 nm by Davidson [172]; at 170–230 nm by Roxlo and Mandl [350]; at 180–400 nm by Pence et al. [312]; at 190–300 nm by Molina et al. [272]; at 190–270 nm by Orkin and Kasimovskaya [302]; at 210–295 K and 168–280 nm by Gillotay and Simon [134]; and at 210–296 K and 190–285 nm by Burkholder et al. [57]. The agreement between the room temperature data is very good, i.e., 10% and better, in the region of the absorption band between 190 and 230 nm with the exception of the data of Davidson [253] below 210 nm and the whole data set of Roxlo and Mandl [350]. Pence et al. [312] report a plot of the absorbance (in arbitrary units) and give for 193 nm an absorption cross section smaller by one order of magnitude than the rest of the data for 193 nm. At wavelengths above 250 nm, Burkholder et al. [57] and Orkin and Kasimovskaya [302] measured higher values (up to ~35% at 270 nm) than those reported by Molina et al. [272] and Gillotay and Simon [134]. The preferred absorption cross sections at 295–298 K, listed in Table 4-79, are the values of Gillotay and Simon [134] at 168–188 nm, the mean of the values reported by Molina et al. [272], Gillotay and Simon [134], Burkholder et al. [57], and Orkin and Kasimovskaya [302] at 190–270 nm, the mean of the values reported by Molina et al. [272], Gillotay and Simon [134], and Burkholder et al. [57] at 272–280 nm, and the values of Molina et al. [272] at 295–300 nm.

Measurements in the far UV at 60–220 nm were reported by Doucet et al. [109].

Both studies of the temperature dependence show an increase of the absorption cross sections in the absorption band between 174 and 216 nm with decreasing temperature 296–210 K and the reverse effect at wavelengths above 218 nm and below 174 nm. Gillotay and Simon [134] observed a regular temperature behavior, i.e., an increase of the maximum absorption cross section by $\sim 0.06 \times 10^{-19} \text{ cm}^2 \text{ molecule}^{-1}$ per 20 K temperature decrease. Burkholder et al. [57] observed a less pronounced temperature behavior (the maximum absorption cross sections agree within 2%), so that their maximum cross section at 210 K is lower by ~25% than that

observed by Gillotay and Simon [134] (in contrast to the cross sections at room temperature which are within 6%). Different parameterizations for the temperature dependence of the absorption cross section have been proposed. Gillotay and Simon [134] give the polynomial expansion

$$\log_{10} \sigma(\lambda, T) = \sum A_n \lambda^n + (T - 273) \times \sum B_n \lambda^n$$

and report smoothed values for T = 210, 230, 250, 270, and 295 K, every 2 nm, and at wavelengths corresponding to the wavenumber intervals generally used in stratospheric photodissociation calculations. The parameters A_n and B_n for the ranges 178–280 nm and 210–300 K are as follows:

$A_0 = 62.563$	$B_0 = -9.1755 \times 10^{-1}$
$A_1 = -2.0068$	$B_1 = 1.8575 \times 10^{-2}$
$A_2 = 1.6592 \times 10^{-2}$	$B_2 = -1.3857 \times 10^{-4}$
$A_3 = -5.6465 \times 10^{-5}$	$B_3 = 4.5066 \times 10^{-7}$
$A_4 = 6.7459 \times 10^{-8}$	$B_4 = -5.3803 \times 10^{-10}$

Burkholder et al. [57] give the expansion

$$\log_{10} \sigma(\lambda, T) = (\sum A_i (\lambda - 242.2466)^i) (1 + (296 - T) \sum B_i (\lambda - 242.266)^i)$$

and report the following parameters A_i and B_i for the ranges 214–285 nm and 210–296 K:

$A_0 = -46.70542$	$B_0 = 1.694026 \times 10^{-4}$
$A_1 = -1.55047 \times 10^{-1}$	$B_1 = 8.723247 \times 10^{-6}$
$A_2 = -1.020187 \times 10^{-3}$	$B_2 = 5.953165 \times 10^{-9}$
$A_3 = 2.246169 \times 10^{-5}$	$B_3 = -3.872168 \times 10^{-9}$
$A_4 = -1.300982 \times 10^{-7}$	$B_4 = -1.803325 \times 10^{-11}$

Quantum yields for Br ($\text{Br}(^2P_{3/2}) + \text{Br}^*(^2P_{1/2})$) atom formation in the photodissociation of CF_3Br at 193 and 222 nm, $\Phi(\text{Br} + \text{Br}^*) = 1.12 \pm 0.16$ and 0.92 ± 0.15 , respectively, were measured at 298 K by Talukdar et al. [399]. A quantum yield for $\text{Br}^*(^2P_{1/2})$ atom formation at 193 nm, $\Phi(\text{Br}^*) = 0.56 \pm 0.05$, was reported by Pence et al. [312].

Table 4-79. Absorption Cross Sections of CF₃Br at 295–298 K

λ (nm)	$10^{20} \sigma$ (cm ²)	λ (nm)	$10^{20} \sigma$ (cm ²)	λ (nm)	$10^{20} \sigma$ (cm ²)
168	0.517	210	12.1	252	0.107
170	0.696	212	11.4	254	0.0743
172	0.928	214	10.6	256	0.0516
174	1.22	216	9.71	258	0.0357
176	1.60	218	8.65	260	0.0248
178	2.05	220	7.56	262	0.0171
180	2.61	222	6.50	264	0.0118
182	3.26	224	5.47	266	0.00827
184	4.02	226	4.52	268	0.00580
186	4.88	228	3.69	270	0.00399
188	5.82	230	2.91	272	0.00271
190	6.56	232	2.32	274	0.00188
192	7.58	234	1.80	276	0.00129
194	8.63	236	1.39	278	0.00092
196	9.61	238	1.04	280	0.00064
198	10.5	240	0.766	285	0.00022
200	11.3	242	0.563	290	0.00008
202	11.9	244	0.414	295	0.00003
204	12.4	246	0.296	300	0.00001
206	12.5	248	0.212		
208	12.4	250	0.149		

Note: 170–188 nm: Gillotay and Simon [134]

190–270 nm: mean of Molina et al. [272], Gillotay and Simon [134], Burkholder et al. [57] and Orkin and Kasimovskaya [302]

272–280 nm: mean of Molina et al. [272] and Burkholder et al. [57]

285–300 nm: Molina et al. [272].

- G18. CF₃CH₂Br (Halon-2301) + hv → Products. The absorption cross sections of CF₃CH₂Br have been measured at 295 K and 190–294 nm by Orkin and Kasimovskaya [302]. Their results are listed in Table 4-80.

Table 4-80. Absorption Cross Sections of CF₃CH₂Br at 295 K

λ (nm)	$10^{20} \sigma$ (cm ²)	λ (nm)	$10^{20} \sigma$ (cm ²)	λ (nm)	$10^{20} \sigma$ (cm ²)
190	45.4	226	16.6	262	0.190
192	49.5	228	14.1	264	0.137
194	52.5	230	11.9	266	0.0983
196	54.4	232	9.85	268	0.0705
198	55.1	234	8.10	270	0.0504
200	54.7	236	6.58	272	0.0361
202	53.3	238	5.28	274	0.0258
204	51.2	240	4.20	276	0.0184
206	48.6	242	3.31	278	0.0132
208	45.7	244	2.58	280	0.0096
210	42.5	246	2.01	282	0.0069
212	39.1	248	1.53	284	0.0048
214	35.7	250	1.16	286	0.0034
216	32.2	252	0.876	288	0.0025
218	28.8	254	0.653	290	0.0018
220	25.5	256	0.484	292	0.0013
222	22.3	258	0.357	294	0.0011
224	19.4	260	0.261		

Note: 190–294 nm, Orkin and Kasimovskaya [302].

- G19. CF_3CHClBr (Halon-2311) + $h\nu \rightarrow$ Products. The absorption cross sections of CF_3CHClBr have been measured at room temperature and 190–310 nm by Orkin and Kasimovskaya [302]; at 210–295 K and 170–290 nm by Gillotay et al. [138]; and at 223–298 K and 200–310 nm by Bilde et al. [33]. The room temperature values are in good agreement within 5–15% at wavelengths below 280 nm, where Gillotay et al. [138], [135] report the lowest, Orkin and Kasimovskaya [302] the highest values. At wavelengths above 280 nm, the data of Bilde et al. [33] become increasingly higher (up to 100% at 310 nm) than those of Orkin and Kasimovskaya [302]. The preferred absorption cross sections, listed in Table 4-81, are the values of Gillotay et al. [138] at 170–188 nm; the mean of the values reported by Gillotay et al. [138] and Orkin and Kasimovskaya [302] at 190–198 nm; the mean of the values reported by the three groups at 200–290 nm; and the mean of the values reported by Orkin and Kasimovskaya [302] and Bilde et al. [33] at 292–310 nm.

The study of the temperature dependence by Gillotay et al. [138] shows an increase of the absorption cross sections in the absorption band between 192 and 238 nm with decreasing temperature 295–210 K and the reverse effect at wavelengths above 238 nm and below 192 nm; the increase in the absorption maximum at ~ 202 nm is $\sim 0.024 \times 10^{-18} \text{ cm}^2 \text{ molecule}^{-1}$ per 20 K temperature decrease, i.e., an increase by $\sim 10\%$ between 295 and 210 K. Bilde et al. [33] observed a less pronounced temperature behavior in the absorption band (the maximum absorption cross sections agree within 3%) and a decrease of the absorption cross sections with decreasing temperature at wavelengths above 214 nm.

Gillotay and Simon [138] parameterized the cross sections and the temperature dependence of the absorption cross section by the polynomial expansion

$$\log_{10} \sigma(\lambda, T) = \sum A_n \lambda^n + (T - 273) \times \sum B_n \lambda^n$$

and report smoothed values for $T = 210, 230, 250, 270,$ and 295 K, every 2 nm, and at wavelengths corresponding to the wavenumber intervals generally used in stratospheric photodissociation calculations. The parameters A_n and B_n for the ranges 190–290 nm and 210–300 K are as follows:

$A_0 = -127.157358$	$B_0 = -7.959828 \times 10^{-2}$
$A_1 = 1.635435$	$B_1 = 1.978026 \times 10^{-3}$
$A_2 = -9.002683 \times 10^{-3}$	$B_2 = -1.627866 \times 10^{-5}$
$A_3 = 2.190678 \times 10^{-5}$	$B_3 = 5.480744 \times 10^{-8}$
$A_4 = 2.062651 \times 10^{-8}$	$B_4 = -6.480935 \times 10^{-11}$

Table 4-81. Absorption Cross Sections of CF₃CHClBr at 295–298 K

λ (nm)	$10^{20} \sigma$ (cm ²)	λ (nm)	$10^{20} \sigma$ (cm ²)	λ (nm)	$10^{20} \sigma$ (cm ²)
170	702.6	218	78.7	266	0.980
172	614.6	220	71.0	268	0.765
174	496.8	222	63.3	270	0.575
176	379.8	224	56.3	272	0.444
178	281.1	226	49.5	274	0.339
180	206.1	228	43.3	276	0.258
182	153.3	230	37.3	278	0.196
184	118.4	232	32.2	280	0.149
186	97.1	234	27.6	282	0.111
188	86.6	236	23.6	284	0.0818
190	93.4	238	20.0	286	0.0606
192	99.8	240	16.8	288	0.0448
194	107.1	242	14.0	290	0.0331
196	114.3	244	11.7	292	0.0263
198	119.7	246	9.51	294	0.0198
200	121.5	248	7.79	296	0.0147
202	123.0	250	6.38	298	0.0109
204	122.3	252	5.15	300	0.00808
206	119.7	254	4.13	302	0.00583
208	115.1	256	3.31	304	0.00450
210	109.0	258	2.63	306	0.00313
212	102.0	260	2.06	308	0.00235
214	94.6	262	1.61	310	0.00180
216	86.7	264	1.26		

Note: 170–188 nm, Gillotay et al. [138], [135],
 190–198 nm, mean of Gillotay et al. [138][135] and Orkin and Kasimovskaya [302],
 200–290 nm, mean of Gillotay et al. [138][135], Orkin and Kasimovskaya [302], and Bilde et al. [33],
 292–310 nm, mean of Orkin and Kasimovskaya [302] and Bilde et al. [33].

- G20. CF₃CHFBr (Halon-2401) + $h\nu$ → Products. The absorption cross sections of CF₃CHFBr have been measured at 295 K and 190–280 nm by Orkin and Kasimovskaya [302]. Their results are listed in Table 4-82.

Table 4-82. Absorption Cross Sections of CF₃CHFBr at 295 K

λ (nm)	$10^{20} \sigma$ (cm ²)	λ (nm)	$10^{20} \sigma$ (cm ²)	λ (nm)	$10^{20} \sigma$ (cm ²)
190	24.9	222	11.0	254	0.226
192	26.1	224	9.38	256	0.166
194	27.0	226	7.91	258	0.121
196	27.5	228	6.58	260	0.0873
198	27.7	230	5.42	262	0.0628
200	27.4	232	4.42	264	0.0450
202	26.9	234	3.53	266	0.0325
204	26.0	236	2.79	268	0.0235
206	24.8	238	2.19	270	0.0171
208	23.4	240	1.69	272	0.0124
210	21.9	242	1.30	274	0.0093
212	20.2	244	0.991	276	0.0069
214	18.3	246	0.736	278	0.0053
216	16.5	248	0.556	280	0.0040
218	14.6	250	0.416		
220	12.8	252	0.308		

Note: 190–280 nm, Orkin and Kasimovskaya [302].

G21. $\text{CF}_2\text{BrCF}_2\text{Br}$ (Halon-2402) + $h\nu \rightarrow$ Products. The absorption cross sections of $\text{CF}_2\text{BrCF}_2\text{Br}$ have been measured at room temperature and 195–320 nm by Molina et al. [272] and at 190–300 nm by Orkin and Kasimovskaya [302]; at 210–295 K and 170–280 nm by Gillotay et al. [138], and at 210–296 K and 190–320 nm by Burkholder et al. [57]. The room temperature data are in very good agreement, in the absorption band at 180–240 nm generally within 10%, in the absorption maximum at ~200 nm within 5%, and in the long-wavelength tail up to 310 nm within 15 %. The preferred absorption cross sections at 295–298 K, listed in Table 4-83, are the values of Gillotay et al. [138] at 170–186 nm; the mean of the values reported by Molina et al. [40], Gillotay et al. [138], Burkholder et al. [57], and Orkin and Kasimovskaya [302] at 196–280 nm; the mean of the values reported by Molina et al. [272], Burkholder et al. [57], and Orkin and Kasimovskaya [302] at 282–300 nm; and the mean of the values reported by Molina et al. [272] and Burkholder et al. [57] at 302–320 nm. In the region around 190 nm, there is some uncertainty, because there is no continuous transition between the absorption curve of Gillotay et al. [138] and that obtained by averaging the data of Gillotay et al. [138], Burkholder et al. [57], and Orkin and Kasimovskaya [302]. We therefore smoothed the absorption curve between 186 and 196 nm and give estimated values for 188, 190, 192, and 194 nm.

The results of the two temperature studies are rather controversial. A regular, but weak decrease of the absorption cross sections at 194–280 nm with decreasing temperature 295 to 210 K and the reverse effect below 194 nm was observed by Gillotay et al. [138]; the decrease in the absorption maximum at ~200 nm is $\sim 0.010 \times 10^{-18} \text{ cm}^2 \text{ molecule}^{-1}$ per 20-K temperature decrease, i.e., a decrease by ~4% between 295 and 210 K. Burkholder et al. [57] observed a strong increase over the whole absorption band (increase of the absorption maximum by 20%) with decreasing temperature 296–210 K, and the reverse effect above 230 nm. So, low-temperature data of these two groups are not comparable. Different parameterizations of the temperature dependence of the absorption cross section have been proposed. Gillotay and Simon [350] give the polynomial expansion

$$\log_{10} \sigma(\lambda, T) = \sum A_n \lambda^n + (T - 273) \times \sum B_n \lambda^n$$

and report smoothed values for $T = 210, 230, 250, 270,$ and 295 K , every 2 nm, and at wavelengths corresponding to the wavenumber intervals generally used in stratospheric photodissociation calculations. The parameters A_n and B_n for the ranges 190–290 nm and 210–300 K are as follows:

$A_0 = 34.026000$	$B_0 = 4.010664 \times 10^{-1}$
$A_1 = -1.152616$	$B_1 = -8.358968 \times 10^{-3}$
$A_2 = 8.959798 \times 10^{-3}$	$B_2 = 6.415741 \times 10^{-5}$
$A_3 = -2.9089 \times 10^{-5}$	$B_3 = -2.157554 \times 10^{-7}$
$A_4 = 3.307212 \times 10^{-8}$	$B_4 = 2.691871 \times 10^{-10}$

Burkholder et al. [57] give the expansion

$$\log_{10} \sigma(\lambda, T) = (\sum A_i (\lambda - 242.4015)^i) (1 + (296 - T) \sum B_i (\lambda - 242.4015)^i)$$

and report the following parameters A_i and B_i for the ranges 190–320 nm and 210–296 K:

$A_0 = -43.69218$	$B_0 = 3.301341 \times 10^{-5}$
$A_1 = -1.124704 \times 10^{-1}$	$B_1 = 4.695917 \times 10^{-6}$
$A_2 = -1.213301 \times 10^{-3}$	$B_2 = 6.128629 \times 10^{-8}$
$A_3 = 5.275007 \times 10^{-6}$	$B_3 = -5.443107 \times 10^{-10}$
$A_4 = 6.936195 \times 10^{-8}$	$B_4 = -1.035596 \times 10^{-11}$

Quantum yields for Br atom formation in the photodissociation of $\text{CF}_2\text{BrCF}_2\text{Br}$ at 193, 233, and 266 nm, $\Phi(\text{Br}) = 1.9 \pm 0.1, 1.9 \pm 0.1,$ and $1.4 \pm 0.1,$ respectively, were measured at room temperature by Zou et al. [453]. These values indicate bond breaking of both C–Br bonds in nearly all the $\text{CF}_2\text{BrCF}_2\text{Br}$ molecules at 193 and 233 nm and in an appreciable fraction of the parent molecules still at 266 nm.

Table 4-83. Absorption Cross Sections of CF₂BrCF₂Br at 296 K

λ (nm)	$10^{20} \sigma$ (cm ²)	λ (nm)	$10^{20} \sigma$ (cm ²)	λ (nm)	$10^{20} \sigma$ (cm ²)
170	50.9	222	59.6	274	0.112
172	56.4	224	52.6	276	0.0813
174	62.3	226	45.9	278	0.0592
176	68.5	228	39.7	280	0.0428
178	75.1	230	33.9	282	0.0300
180	81.8	232	28.8	284	0.0216
182	88.6	234	24.1	286	0.0152
184	95.3	236	19.9	288	0.0109
186	101.8	238	16.4	290	0.00784
188	107.0	240	13.2	292	0.00569
190	112.0	242	10.6	294	0.00410
192	116.5	244	8.45	296	0.00301
194	120.0	246	6.68	298	0.00219
196	122.3	248	5.25	300	0.00161
198	123.7	250	4.03	302	0.00124
200	124.3	252	3.12	304	0.00094
202	123.6	254	2.37	306	0.00071
204	120.3	256	1.78	308	0.00054
206	115.9	258	1.34	310	0.00042
208	110.4	260	0.973	312	0.00033
210	104.2	262	0.718	314	0.00026
212	97.4	264	0.529	316	0.00020
214	90.1	266	0.390	318	0.00016
216	82.4	268	0.287	320	0.00014
218	74.8	270	0.211		
220	67.0	272	0.154		

Note: 170–186 nm: Gillotay et al. [138]

188–194 nm: values estimated by smoothing the absorption curve

196–280 nm: mean of Molina et al. [272], Gillotay et al. [138], Burkholder et al. [57], and Orkin and Kasimovskaya [302]

282–300 nm: mean of Molina et al. [272], Burkholder et al. [57], and Orkin and Kasimovskaya [302]

302–320 nm: mean of Molina et al. [272] and Burkholder et al. [57].

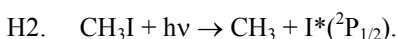
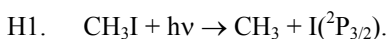
- G22. CF₃CF₂Br (Halon-2501) + hν → Products. Table 4-84 lists the absorption cross sections of CF₃CF₂Br measured at room temperature and reported at 5-nm intervals by Molina et al. [272]. The results of Zhang et al. [451], who report a plot on a logarithmic scale for measured values at 200–250 nm, are about 30% larger over that wavelength range than the results of Molina et al. [272]. Pence et al. [312] measured the absorption cross sections at 180–400 nm, report a plot of the absorbance (in arbitrary units) and give for 193 nm an absorption cross section smaller by ~40% than that reported by Molina et al. [272].

Broad band flash photolysis of CF₃CF₂Br produced Br*(²P_{1/2}) atoms with a quantum yield Φ(Br*) = 0.48 ± 0.02 as reported by Ebenstein et al. [112]. A quantum yield for Br*(²P_{1/2}) atom formation at 193 nm, Φ(Br*) = 0.16 ± 0.08, was reported by Pence et al. [312].

Table 4-84. Absorption Cross Sections of CF₃CF₂Br at 298 K

λ (nm)	$10^{20} \sigma$ (cm ²)	λ (nm)	$10^{20} \sigma$ (cm ²)	λ (nm)	$10^{20} \sigma$ (cm ²)
190	18.1	230	3.83	270	0.0112
195	18.4	235	2.22	275	0.00505
200	18.1	240	1.20	280	0.00218
205	16.9	245	0.620	285	0.00100
210	14.8	250	0.305	290	0.00045
215	12.0	255	0.135	295	0.00020
220	8.94	260	0.0590	300	0.00009
225	6.13	265	0.0260		

Note: 190–300 nm, Molina et al. [272].



The absorption cross sections of CH₃I have been measured at room temperature and 147 nm by Rebbert et al. [334], at 200–360 nm by Porret and Goodeve [317], at 200–310 nm by Baughcum and Leone [29], at 180–400 nm by Pence et al. [312]; at 257.7 nm by Felps et al. [119], at 205–335 nm by Jenkin et al. [182], at 205–360 nm by Man et al. [230], and at 192–225 nm by Kwok and Phillips [208], who also measured the CH₃I spectrum in cyclohexane solution. Measurements were also carried out at 223–333 K and 160–330 nm by Fahr et al. [116]; at 243–333 K and 235–365 nm by Rattigan et al. [325]; and at 210–298 K and 200–350 nm by Roehl et al. [343]. Fahr et al. [116] also measured the absorption cross sections at 330–400 nm for the liquid phase and used a wavelength-shift procedure to convert them into gas-phase values. The room temperature data for the absorption band at 210–305 nm are in reasonable to good agreement, whereby Rattigan et al. [325] report the lowest values and Fahr et al. [116] the highest values over the whole absorption band. The agreement generally is better than 15% except for the region around the absorption maximum where the spread is ~30%. Rattigan et al. [325] and Fahr et al. [116] report values of $1.07 \times 10^{-18} \text{ cm}^2$ and $1.4 \times 10^{-18} \text{ cm}^2$, respectively, for the maximum at ~260 nm, and the rest of the data ranges between $1.15 \times 10^{-18} \text{ cm}^2$ and $1.22 \times 10^{-18} \text{ cm}^2$. At wavelengths 305–330 nm, the agreement is still within 20%. At wavelengths below 210 nm, the few data points reported by Jenkin et al. [182] and Roehl et al. [343] and the absorption curve reported by Kwok and Phillips [209] obviously fit into the strong and highly structured band system observed by Fahr et al. [116] between 160 and 205 nm. The preferred room temperature absorption cross sections for the wavelength range above 210 nm, listed in Table 4-85, are the mean of the values reported by Jenkin et al. [182], Fahr et al. [116], and Roehl et al. [343] at 210–230 nm; the mean of the values reported by Jenkin et al. [182], Fahr et al. [116], Rattigan et al. [325], and Roehl et al. [343] at 235–330 nm; the mean of the values reported by Fahr et al. [116], Rattigan et al. [325], and Roehl et al. [343] at 335–350 nm; and the values of Rattigan et al. [325] at 355–365 nm. The data of Man et al. [230] are given only as a plot in their paper and have therefore not been included in the evaluation.

The three temperature studies are in qualitative agreement. An increase of the absorption cross sections in the absorption band at 210–270 nm with decreasing temperature 333–210 K has been observed. Very small temperature effects are reported by Rattigan et al. [325] for the temperature range 243–333 K, and by Fahr et al. [116] and Roehl et al. [343] for the range between room temperature and ~240–250 K and at 313–333 K. At wavelengths above 270 nm and below 210 nm, the absorption cross sections decrease with decreasing temperature. The low temperature absorption spectra observed by the three groups differ in the same manner as their room temperature spectra, i.e., Fahr et al. [116] report the highest and Rattigan et al. [325] the lowest values for the absorption band.

A simple analytical expression for the temperature dependence,

$$\sigma(\lambda, T) = \sigma(298 \text{ K}) (1 + a_1(T-298) + a_2(T-298)^2)$$

and the fitting parameters $a_1(\lambda)$ and $a_2(\lambda)$ for $\lambda = 200\text{--}350 \text{ nm}$ and $T = 210\text{--}298 \text{ K}$ give Roehl et al. [343].

Another simple parameterization, $\ln \sigma(\lambda, T) = \ln \sigma(\lambda, 298 \text{ K}) + B(T-298)$, and parameters $B(\lambda)$ for $\lambda = 235\text{--}355 \text{ nm}$ and $T = 243\text{--}333 \text{ K}$ report Rattigan et al. [325]. The parameters a_1 , a_2 , and B are listed also in Table 4-85.

Quantum yields for $\text{I}^*({}^2\text{P}_{1/2})$ atom formation in the photolysis of CH₃I at several wavelengths between 222 and 333.5 nm have been reported: $\Phi(\text{I}^*) = 0.63 \pm 0.02$, 0.79 ± 0.02 , 0.69 ± 0.02 , and 0.43 ± 0.02 at 222, 266, 280,

and ~305 nm by Uma and Das [410], [411], [412]; $\Phi(I^*) = 0.72 \pm 0.08$ at 248 nm by Gedanken [412], $\Phi(I^*) = 0.81 \pm 0.03$ and ~0.05 at 248 and 308 nm by Pence et al. [312], $\Phi(I^*) = 0.30$ at 304 nm by Kang et al. [198]; and $\Phi(I^*) = 0.47, 0.77,$ and 0.92 at 325.8, 329.4, and 333.5 nm by Ogorzalek Loo et al. [298]. The latter authors report also quantum yields for CD₃I:

$\Phi(I^*)$:	0.66	0.59	0.83	0.91	0.90	0.57	0.80	0.92	>0.95	0.61	0.84
λ , nm:	312.6	314.4	317.0	319.8	322.9	324.5	327.8	330.5	333.8	336.2	339.3

Brewer et al. [42] report $\Phi(I^*) = 0.75 \pm 0.02$ at 248 nm for CD₃I.

Quantum yields for I(²P_{3/2}) atom formation, $\Phi(I)$, can be derived from $\Phi(I) = 1 - \Phi(I^*)$.

Table 4-85. Absorption Cross Sections of CH₃I at 296–298 K and Temperature Coefficients

λ (nm)	$10^{20} \sigma$ (cm ²)	$10^3 a_1(K^{-1})$	$10^5 a_2(K^{-2})$	$10^3 B(K^{-1})$	λ (nm)	$10^{20} \sigma$ (cm ²)	$10^3 a_1(K^{-1})$	$10^5 a_2(K^{-2})$	$10^3 B(K^{-1})$
210	3.62	3.07	2.42		290	8.04	6.14	2.57	4.98
215	5.08	2.61	2.28		295	4.00	7.27	2.91	6.38
220	6.90	1.06	1.22		300	2.06	7.82	3.53	6.97
225	9.11	1.74	1.96		305	1.10	7.82	3.85	6.84
230	12.6	1.47	1.67		310	0.621	7.37	3.71	6.78
235	20.5	1.91	2.04	0.67	315	0.359	6.98	3.47	6.75
240	38.1	1.74	2.06	0.61	320	0.221	7.39	3.54	6.53
245	65.6	1.52	2.15	0.34	325	0.126	7.23	2.82	6.79
250	96.3	1.20	2.11	0.08	330	0.0684	8.93	3.74	7.82
255	117.7	0.890	1.95	-0.10	335	0.0388	10.88	4.88	9.34
260	119.7	0.882	1.93	-0.12	340	0.0212	11.30	4.46	10.95
265	102.9	1.21	2.00	0.10	345	0.0114	15.68	8.44	13.58
270	75.9	1.77	2.11	0.54	350	0.00609	15.94	8.22	16.83
275	49.6	2.52	2.12	1.33	355	0.00320			18.91
280	29.2	3.62	2.24	2.43	360	0.00190			17.28
285	15.6	4.84	2.38	3.74	365	0.00090			23.63

Note: Absorption cross sections σ : 210–230 nm: mean of Jenkin et al. [182], Fahr et al. [116], and Roehl et al. [343].

235–330 nm: mean of Jenkin et al. [182], Fahr et al. [116], Rattigan et al. [325], and Roehl et al. [343].

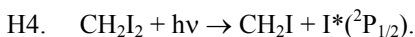
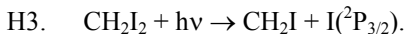
335–350 nm: mean of Fahr et al. [116], Rattigan et al. [325], and Roehl et al. [343].

355–365 nm: Rattigan et al. [325].

Temperature coefficients a_1 and a_2 : 210–298 K, Roehl et al. [343]:

$$(\sigma(\lambda, T) = \sigma(298 \text{ K}) [1 + a_1(T-298) + a_2(T-298)^2]),$$

Temperature coefficients B: 243–333 K, Rattigan et al. [325] ($\ln \sigma(\lambda, T) = \ln \sigma(\lambda, 298 \text{ K}) + B(T-298)$).



The absorption cross sections of CH₂I₂ have been measured at room temperature and 180–400 nm by Pence et al. [312], at 220–360 nm by Schmitt and Comes [365], at 200–360 nm by Baughcum and Leone [29], at 265–341 nm by Koffend and Leone [205]; and at 220–400 nm by Kwok and Phillips [207], who measured the spectrum also in methanol and cyclohexane. Measurements at 273 and 298 K and 205–380 nm have also been carried out by Roehl et al. [343]; and at 273, 298, and 348 K and 215–385 nm by Mössinger et al. [283]. There are absorption maxima at or below 215 nm, and around 250 and 290 nm. The room temperature data of the various teams (except those of Kwok and Phillips [207], which are presented only as a plot) are in very good agreement, i.e., generally within 5–10% between 230 and 380 nm, were the older data of Schmitt and Comes [365] and Koffend and Leone [205] for the prominent absorption band around 290 nm are higher than those of Roehl et al. [343] and Mössinger et al. [283]. The values of Kwok and Phillips [207] for the prominent absorption band around 290 nm are lower by 15–20% than the rest of the data. The preferred room temperature absorption cross sections, listed in Table 4-86, are the values of Roehl et al. [343] at 205–215 nm, the mean of

the values reported by Roehl et al. [343] and Mössinger et al. [283] at 220–380 nm, which are very close, and the value of Mössinger et al. [283] at 385 nm.

Both temperature studies show, that decreasing the temperature from 298 or 348 K to 273 K causes a slight increase of the absorption cross sections between 275 and 300 nm (~2% in the maximum at 290 nm between 298 and 273 K) and a slight decrease outside this wavelength region. A simple empirical relation for the temperature dependence between 273 and 348 K, $\ln \sigma(\lambda, T) = \ln \sigma(\lambda, 298\text{K}) + B(\lambda) \cdot (T-298)$, and temperature coefficients $B(\lambda)$ for $\lambda = 205\text{--}375$ nm at 5-nm intervals are given by Mössinger et al. [283]. The temperature coefficients B are also listed in Table 4-86 (an erroneous B value at 305 nm has been corrected by Dr. Mössinger via a personal communication).

Quantum yields for $\text{I}^*(^2\text{P}_{1/2})$ atom formation in the photolysis of CH_2I_2 at 193, 248, and 308 nm, $\Phi(\text{I}^*) = \sim 0.05$, 0.46 ± 0.04 , and 0.25 ± 0.02 , respectively, have been reported by Pence et al. [312]. Quantum yields for $\text{I}(^2\text{P}_{3/2})$ atom formation, $\Phi(\text{I})$, can be derived from $\Phi(\text{I}) = 1 - \Phi(\text{I}^*)$.

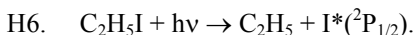
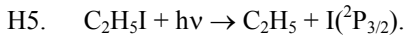
Table 4-86. Absorption Cross Sections of CH_2I_2 at 298 K

λ (nm)	$10^{20} \sigma$ (cm^2)	$10^3 B$ (K^{-1})	λ (nm)	$10^{20} \sigma$ (cm^2)	$10^3 B$ (K^{-1})
205	407.0		300	357.0	-0.37
210	404.0		305	338.5	-0.16
215	366.0	0.15	310	313.5	0.07
220	260.0	0.14	315	280.0	0.15
225	197.5	0.19	320	244.0	0.27
230	133.0	0.51	325	203.0	0.27
235	109.0	0.56	330	161.5	0.51
240	122.5	0.15	335	120.5	0.55
245	150.0	0.18	340	83.3	1.36
250	157.0	0.67	345	53.7	1.99
255	139.5	1.58	350	32.6	3.19
260	120.5	2.04	355	19.2	4.09
265	130.0	1.30	360	10.9	5.39
270	178.5	0.00	365	6.05	6.77
275	255.0	-0.71	370	3.45	8.25
280	328.5	-1.24	375	1.93	11.3
285	371.5	-1.21	380	1.17	
290	380.5	-0.94	385	0.769	
295	371.5	-0.58			

Note:

Absorption cross sections σ : 205–215 nm, Roehl et al. [343], 220–380 nm, mean of Roehl et al. [343] and Mössinger et al. [283], 385 nm, Mössinger et al. [283].

Temperature coefficients B : 273–348 K, Mössinger et al. [283] ($\ln \sigma(\lambda, T) = \ln \sigma(\lambda, 298 \text{ K}) + B(T-298)$).



The absorption cross sections of $\text{C}_2\text{H}_5\text{I}$ have been measured at room temperature and 147 nm ($\sigma = 1.48 \times 10^{-17} \text{ cm}^2$) by Rebbert et al. [334], at 205–360 nm by Porret and Goodeve [318]; at 223–298 K and 205–365 nm by Roehl et al. [343], at 243–333 K and 235–355 nm by Rattigan et al. [325], and at 323 K and 220–320 nm by Zhang et al. [451]. The room temperature data are in good agreement, the values of Roehl et al. [343] are higher by 5–15% at 235–325 nm and become increasingly higher up to 125% at 355 nm than the values of Rattigan et al. [325]. The latter authors found their data to agree within 10–15% with the plotted values of Porret and Goodeve [318]. The preferred absorption cross sections, listed in Table 4-87, are the mean of the values reported by Roehl et al. [343] and Rattigan et al. [325] in the common wavelength range 235–355 nm, and the data of Roehl et al. [343] at 215–230 nm.

The temperature studies of Roehl et al. [343] and Rattigan et al. [325] show, that decreasing the temperature in the range 333–223 K causes an increase of the absorption cross section in the absorption band at ~230–270 nm and a decrease at longer wavelengths. The differences between the low-temperature data of the two groups are

comparable with those between the room temperature data. The data for 323 K, reported by Zhang et al. [451] as a plot on a logarithmic scale, are larger by 10–40% around the absorption maximum and up to more than 200% in the long-wavelength tail than the data for 313 and 333 K reported by Rattigan et al. [325]. A simple analytical expression for the temperature dependence, $\sigma(\lambda, T) = \sigma(298 \text{ K}) [1 + a_1(T-298) + a_2(T-298)^2]$, and the fitting parameters $a_1(\lambda)$ and $a_2(\lambda)$ for $\lambda = 205\text{--}365 \text{ nm}$ and $T = 223\text{--}298 \text{ K}$ give Roehl et al. [343]. Another simple parameterization, $\ln \sigma(\lambda, T) = \ln \sigma(\lambda, 298 \text{ K}) + B(T-298)$, and parameters $B(\lambda)$ for $\lambda = 235\text{--}355 \text{ nm}$ and $T = 243\text{--}333 \text{ K}$ is reported by Rattigan et al. [325]. The parameters a_1 , a_2 , and B are listed also in Table 4-87.

Quantum yields for $I^*(^2P_{1/2})$ atom formation in the photolysis of C_2H_5I at a few wavelengths between 222 and 305 nm have been reported: $\Phi(I^*) = 0.57 \pm 0.02$, 0.72 (or 0.73) ± 0.02 , 0.60 ± 0.02 , and 0.39 ± 0.02 at 222, 266, 280, and $\sim 305 \text{ nm}$ by Uma and Das [410], [411], [412]; $\Phi(I^*) = 0.78 \pm 0.07$ at 248 nm by Gedanken [130]; $\Phi(I^*) = 0.68 \pm 0.02$ at 248 nm by Brewer et al. [42], $\Phi(I^*) = 0.22$ at 304 nm by Kang et al. [198]. Quantum yields for $I(^2P_{3/2})$ atom formation, $\Phi(I)$, can be derived from $\Phi(I) = 1 - \Phi(I^*)$.

At 147 nm, the overall process $C_2H_5I + h\nu \rightarrow C_2H_4 + H + I$ was observed with a quantum yield of 0.75 by Rebbert et al. [334].

Table 4-87. Absorption Cross Sections of C_2H_5I at 298 K and Temperature Coefficients

λ (nm)	$10^{20} \sigma$ (cm^2)	$10^3 a_1(K^{-1})$	$10^5 a_2(K^{-2})$	$10^3 B(K^{-1})$	λ (nm)	$10^{20} \sigma$ (cm^2)	$10^3 a_1(K^{-1})$	$10^5 a_2(K^{-2})$	$10^3 B(K^{-1})$
205	11.9	6.38	3.15		285	19.1	3.85	0.926	3.61
210	4.22	4.07	6.28		290	10.3	5.47	1.65	4.83
215	4.56	4.93	6.75		295	5.38	7.00	2.52	6.33
220	6.18	4.06	5.70		300	2.78	8.56	4.11	7.48
225	9.09	2.81	3.81		305	1.44	9.31	4.89	8.08
230	14.3	2.62	3.83		310	0.777	10.56	6.87	7.55
235	23.2	1.28	2.17	-0.27	315	0.416	10.83	6.81	7.92
240	41.7	0.876	1.96	-0.40	320	0.227	11.98	9.76	8.27
245	69.3	0.233	1.62	-0.62	325	0.127	12.98	11.3	8.81
250	99.3	-0.111	1.58	-0.79	330	0.0743	14.56	17.5	9.30
255	119.7	-1.03	0.606	-0.82	335	0.0403	18.81	24.6	10.20
260	121.8	-1.48	-0.0332	-0.75	340	0.0246	13.90	9.08	11.16
265	105.9	-1.09	1.2×10^{-6}	-0.44	345	0.0133	18.86	22.1	12.41
270	80.6	-0.538	-0.257	0.36	350	0.00840	20.19	20.1	11.28
275	54.4	0.770	0.0299	1.23	355	0.00488	-7.04	-40.5	12.20
280	33.5	2.01	0.110	2.36					

Note: Absorption cross sections σ : 205–230 nm, Roehl et al. [343], 235–355 nm, mean of Roehl et al. [343] and Rattigan et al. [325].
 Temperature coefficients a_1 and a_2 : 223–298 K, Roehl et al. [343]
 $(\sigma(\lambda, T) = \sigma(298 \text{ K}) [1 + a_1(T-298) + a_2(T-298)^2])$,
 Temperature coefficients B : 243–333 K, Rattigan et al. [325]
 $(\ln \sigma(\lambda, T) = \ln \sigma(\lambda, 298 \text{ K}) + B(T-298))$.

- H7. $\text{CH}_3\text{CHI}_2 + h\nu \rightarrow \text{Products}$. The absorption cross sections of CH_3CHI_2 have been measured at 298 K and 220–360 nm by Schmitt and Comes [365]. Their data are listed in Table 4-88.

Table 4-88. Absorption Cross Sections of CH_3CHI_2 at 298 K

λ (nm)	$10^{20} \sigma$ (cm^2)	λ (nm)	$10^{20} \sigma$ (cm^2)	λ (nm)	$10^{20} \sigma$ (cm^2)
220	304	270	183	320	222
225	240	275	243	325	201
230	181	280	304	330	175
235	144	285	352	335	138
240	138	290	374	340	107
245	151	295	366	345	75.7
250	157	300	339	350	49.3
255	143	305	305	355	31.7
260	133	310	273	360	19.1
265	145	315	247		

Note: 220–360 nm, Schmitt and Comes [365].

- H8. $\text{CH}_3\text{CH}_2\text{CH}_2\text{I} + h\nu \rightarrow \text{Products}$.

- H9. $\text{CH}_3\text{CHICH}_3 + h\nu \rightarrow \text{Products}$.

The absorption cross sections of 1- $\text{C}_3\text{H}_7\text{I}$ have been measured at 223–298 K and 205–335 nm, those of 2- $\text{C}_3\text{H}_7\text{I}$ at 223–298 K and 205–380 nm by Roehl et al. [343]. The absorption cross sections of 2- $\text{C}_3\text{H}_7\text{I}$ in the gas phase and in cyclohexane solution have also been measured at room temperature and 235–305 nm by Phillips et al. [315]. The gas-phase data reported by Phillips et al. [315] and given as a plot in their paper are larger by 30–70% over the whole absorption band than the data of Roehl et al. [343]. Room temperature values at 147 nm for 1- $\text{C}_3\text{H}_7\text{I}$ and 2- $\text{C}_3\text{H}_7\text{I}$ have been reported by Rebbert et al. [334]. The recommended room temperature values for 1- $\text{C}_3\text{H}_7\text{I}$ and 2- $\text{C}_3\text{H}_7\text{I}$, listed in Table 4-89, are taken from the paper of Roehl et al. [343].

Decreasing the temperature in the range 298–223 K causes an increase of the absorption cross sections around the absorption maximum, at 245–265 nm for 1- $\text{C}_3\text{H}_7\text{I}$ and at 240–270 nm for 2- $\text{C}_3\text{H}_7\text{I}$, and a decrease in the long-wavelength tail. Decrease of the absorption cross sections with decreasing temperature generally has been observed in the short-wavelength tail of the absorption band except for slight increases between 273 and 248 K in the case of 1- $\text{C}_3\text{H}_7\text{I}$ and between 248 and 223 K in the case of 2- $\text{C}_3\text{H}_7\text{I}$. At wavelengths below the minimum (~210 nm), the absorption cross sections decrease with decreasing temperature between 298 and 223 K. The temperature dependence has been parameterized by the analytical expression

$$\sigma(\lambda, T) = \sigma(298 \text{ K}) [1 + a_1(T-298) + a_2(T-298)^2]$$

and the fitting parameters $a_1(\lambda)$ and $a_2(\lambda)$ for $T = 223\text{--}298 \text{ K}$ and $\lambda = 205\text{--}335 \text{ nm}$ (1- $\text{C}_3\text{H}_7\text{I}$) and $\lambda = 205\text{--}380 \text{ nm}$ (2- $\text{C}_3\text{H}_7\text{I}$) are reported by Roehl et al. [343]. These are listed also in Table 4-89.

Quantum yields for $\text{I}^*(^2\text{P}_{1/2})$ atom formation in the photolysis of $\text{C}_3\text{H}_7\text{I}$ at a few wavelengths have been reported: $\Phi(\text{I}^*) = 0.54 \pm 0.02$, 0.66 ± 0.02 , 0.56 ± 0.02 , and 0.35 ± 0.02 at 222, 266, 280, and ~305 nm by Uma and Das [410], [412]; $\Phi(\text{I}^*) = 0.60 \pm 0.02$ at 248 nm by Brewer et al. [42], $\Phi(\text{I}^*) = 0.20$ at 304 nm by Kang et al. [198] for 1- $\text{C}_3\text{H}_7\text{I}$; $\Phi(\text{I}^*) = 0.40 \pm 0.02$, 0.44 ± 0.03 , and 0.19 ± 0.02 at 222, 266, and ~305 nm by Uma and Das [411], and $\Phi(\text{I}^*) = 0.26 \pm 0.02$ at 248 nm by Brewer et al. [42] for 2- $\text{C}_3\text{H}_7\text{I}$. Quantum yields for $\text{I}(^2\text{P}_{3/2})$ atom formation, $\Phi(\text{I})$, can be derived from $\Phi(\text{I}) = 1 - \Phi(\text{I}^*)$.

At 147 nm, Rebbert et al. [334] observed the main overall processes $1\text{-C}_3\text{H}_7\text{I} + h\nu \rightarrow \text{C}_3\text{H}_6 + \text{H} + \text{I}$ and

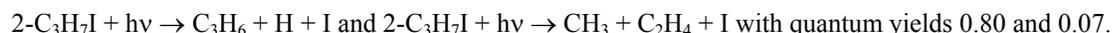


Table 4-89. Absorption Cross Sections of C₃H₇I at 298 K and Temperature Coefficients

λ (nm)	1-C ₃ H ₇ I			2-C ₃ H ₇ I		
	$10^{20} \sigma$ (cm ²)	$10^3 a_1$ (K ⁻¹)	$10^5 a_2$ (K ⁻²)	$10^{20} \sigma$ (cm ²)	$10^3 a_1$ (K ⁻¹)	$10^5 a_2$ (K ⁻²)
205	15.6	7.60	4.37	44.9	15.14	8.46
210	5.05	0.283	1.57	4.53	7.84	7.23
215	5.14	-1.49	-2.46	3.57	4.96	5.08
220	6.84	-1.59	-2.97	4.20	1.55	1.27
225	10.4	-0.891	-2.14	6.45	2.21	1.99
230	17.7	-0.375	-1.26	11.0	1.60	1.80
235	32.8	-0.311	-1.04	20.4	0.480	0.681
240	58.1	-0.611	-0.804	38.2	-0.333	0.121
245	91.9	-0.949	-0.609	66.7	-0.680	0.0947
250	124	-1.22	-0.611	102	-0.795	0.289
255	141	-1.55	-0.776	133	-0.966	0.570
260	136	-1.44	-0.867	148	-1.14	0.512
265	113	-1.02	-1.04	143	-0.589	0.824
270	82.2	-0.306	-1.16	120	-0.439	0.281
275	53.4	0.524	-1.50	90.2	0.792	0.873
280	32.0	1.68	-1.66	61.4	1.65	0.466
285	18.1	3.08	-1.44	38.6	2.88	0.534
290	9.96	5.56	0.812	22.6	4.13	0.559
295	5.42	6.76	2.05	12.8	5.71	1.04
300	2.96	7.16	2.90	6.94	7.20	1.93
305	1.63	6.90	3.20	3.73	8.19	2.33
310	0.945	7.10	4.01	2.04	8.75	2.81
315	0.532	5.59	2.78	1.09	8.49	2.25
320	0.301	3.68	0.0140	0.627	10.79	4.36
325	0.177	4.23	0.0238	0.348	9.54	2.76
330	0.110	11.40	12.3	0.202	10.99	5.94
335	0.0627	15.76	25.8	0.115	12.37	7.58
340				0.0688	13.69	12.2
345				0.0402	16.32	17.1
350				0.0253	18.50	24.7
355				0.0150	19.41	24.3
360				0.0105	18.61	13.9
365				0.00666	29.85	50.9
370				0.00479	37.24	76.8
375				0.00535	36.71	80.7
380				0.00530	22.00	40.0

Note: Absorption cross sections σ : 205–380 nm, Roehl et al. [343],
 Temperature coefficients a_1 and a_2 : 223–298 K, Roehl et al. [343]
 $(\sigma(\lambda, T) = \sigma(298 \text{ K}) [1 + a_1(T-298) + a_2(T-298)^2])$.

- H10. $\text{C}_4\text{H}_9\text{I} + h\nu \rightarrow \text{C}_4\text{H}_9 + \text{I}({}^2\text{P}_{3/2})$.
 H11. $\text{C}_4\text{H}_9\text{I} + h\nu \rightarrow \text{C}_4\text{H}_9 + \text{I}^*({}^2\text{P}_{1/2})$.
 H12. $(\text{CH}_3)_2\text{CHCH}_2\text{I} + h\nu \rightarrow (\text{CH}_3)_2\text{CCH}_2 + \text{I}({}^2\text{P}_{3/2})$.
 H13. $(\text{CH}_3)_2\text{CHCH}_2\text{I} + h\nu \rightarrow (\text{CH}_3)_2\text{CCH}_2 + \text{I}^*({}^2\text{P}_{1/2})$.
 H14. $(\text{CH}_3)_3\text{CI} + \rightarrow (\text{CH}_3)_3\text{C} + \text{I}({}^2\text{P}_{3/2})$.
 H15. $(\text{CH}_3)_3\text{CI} + \rightarrow (\text{CH}_3)_3\text{C} + \text{I}^*({}^2\text{P}_{1/2})$.

Absorption cross sections for *n*- and *iso*-C₄H₉I are not available. Absorption cross sections of *tert*-C₄H₉I have been measured at 323 K by Phillips et al. [315]. An absorption band between 230 and 310 nm exhibits a maximum of $\sim 2.1 \times 10^{-18}$ cm² at ~ 268 nm. Estimated values at 5-nm intervals, read from a logarithmic plot, are presented in Table 4-90.

Quantum yields for I*(²P_{1/2}) atom formation in the photolysis of *n*-C₄H₉I at several wavelengths between 222 and 305 nm have been reported: $\Phi(I^*) = 0.51 \pm 0.02$, 0.64 ± 0.03 , 0.50 ± 0.03 , and 0.30 ± 0.02 at 222, 266, 280, and ~ 305 nm by Uma and Das [410], [412]; $\Phi(I^*) = 0.53 \pm 0.03$ at 248 nm by Brewer et al. [42], $\Phi(I^*) = 0.14$ at 304 nm by Kang et al. [198].

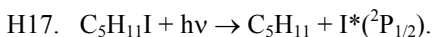
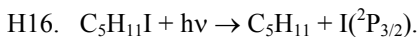
Quantum yields for I*(²P_{1/2}) atom formation in the photolysis of *iso*-C₄H₉I, $\Phi(I^*) = 0.71 \pm 0.01$, 0.56 ± 0.03 , and 0.35 ± 0.02 at 266, 280, and ~ 305 nm, have been reported by Uma and Das [412], $\Phi(I^*) = 0.20 \pm 0.02$ at 248 nm by Brewer et al. [42].

Quantum yields for I atom formation in the photolysis of *tert*-C₄H₉I, $\Phi(I(^2P_{3/2}) + I(^2P_{1/2})) = 0.93$ and 0.92 at 277 and 304 nm, have been reported by Kim et al. [201]. Quantum yields for I*(²P_{1/2}) atom formation, $\Phi(I(^2P_{1/2})) = 0.33 \pm 0.03$, 0.20 ± 0.03 , and 0.12 ± 0.03 , in the photolysis at 222, 266, and ~ 305 nm, have been reported by Uma and Das [411], $I(^2P_{1/2}) = 0.41 \pm 0.10$ and 0.03 ± 0.02 at 248 nm by Gedanken [412] and Brewer et al. [42], respectively.

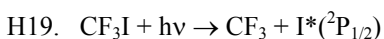
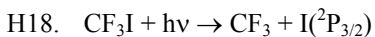
Table 4-90. Absorption Cross Sections of (CH₃)₃CI at 298 K

λ (nm)	$10^{20} \sigma$ (cm ²)	λ (nm)	$10^{20} \sigma$ (cm ²)	λ (nm)	$10^{20} \sigma$ (cm ²)
235	28.5	265	209	295	54.0
240	42.5	270	211	300	34.0
245	64.8	275	186	305	21.5
250	98.0	280	150	310	14.0
255	140	285	116		
260	180	290	83.0		

Note: 235–310 nm, Phillips et al. [315], estimated from logarithmic plot.



Absorption cross sections for *n*-C₅H₁₁I are not available. A quantum yield for I*(²P_{1/2}) atom formation in the photolysis of *n*-C₅H₁₁I at 222 nm, $\Phi(I^*) = 0.50 \pm 0.03$, has been measured by Uma and Das [410].



The absorption cross sections of CF₃I have been measured at room temperature and 170–230 nm by Roxlo and Mandl [350]; at room temperature and in shock waves at 625 and 1050 K and 220–360 nm by Brouwer and Troe [45]; at 200–298 K and 216–370 nm by Solomon et al. [385]; at 218–333 K and 160–350 nm by Fahr et al. [115]; and at 243–333 K and 235–390 nm by Rattigan et al. [325]. Measurements in the long-wavelength tail of the absorption band up to 455 nm and at temperatures up to ~ 4000 K were also carried out with hot molecules excited by IR laser pulses by Bagratashvili et al. [18] and Abel et al. [2][3].

There is good agreement between the room temperature values above 200 nm, i.e., better than 20% around the absorption maximum at 265–270 nm and better than 15% below 255 nm and at 280–350 nm. Fahr et al. [115] report the highest absorption maximum of 7×10^{-19} cm², compared to 6.4×10^{-19} , 6.2×10^{-19} , and 5.9×10^{-19} cm² reported by Solomon et al. [385], Brouwer and Troe [45], and Rattigan et al. [325], respectively. The long-wavelength data of Solomon et al. [385] become increasingly higher by up to $\sim 70\%$ than those of Rattigan et al. [325]. The preferred absorption cross sections, listed in Table 4-91, are the data of Fahr et al. [115] at 180–215 nm; the mean of the values reported by Brouwer and Troe [45], Solomon et al. [385], and Fahr et al. [115] at 220–230 nm; the mean of the values reported by Brouwer and Troe [45], Solomon et al. [385], Fahr et al. [115], and Rattigan et al. [325] at 235–310 nm; the mean of the values reported by Solomon et al. [385], Fahr et al. [115], and Rattigan et al. [325] at 315–350 nm; and the values of Rattigan et al. [325] at 355–385 nm.

Fahr et al. [115] observed in the short-wavelength region a band centered at about 171 nm with cross sections up to $3.6 \times 10^{-17} \text{ cm}^2$, which shows vibrational structure, and a band with a maximum approaching values of 10^{-16} cm^2 at or below 160 nm. The plotted spectrum at 170–230 nm reported by Roxlo and Mandl [350] is not in agreement with the results of Fahr et al. [115].

The temperature studies of Solomon et al. [385], Fahr et al. [115], and Rattigan et al. [325] agree in the observation, that the absorption cross sections increase in the region of the maximum (~240–280 nm) with decreasing temperature from 333 K or room temperature down to temperatures of 240–250 K; the ratios $\sigma(298 \text{ K})/\sigma(\sim 240 \text{ K})$ and $\sigma(333 \text{ K})/\sigma(\sim 240 \text{ K})$ around the maximum are ~0.9, the ratios $\sigma(333 \text{ K})/\sigma(298 \text{ K})$ are ~1. Solomon et al. [385] observed a further increase of the cross sections down to 200 K, whereas Fahr et al. [115] observed a slight decrease between 253 and 218 K. A decrease of the absorption cross sections above 280 nm and between 333 and 200 K was observed by the three groups; the ratios $\sigma(298 \text{ K})/\sigma(\sim 240 \text{ K})$ increase from ~1.0 to ~1.9 at 280–340 nm, the ratios $\sigma(333 \text{ K})/\sigma(298 \text{ K})$ are around 1.3. Thus, the temperature dependences reported by the three groups are compatible at least in the range 240–333 K.

Solomon et al. [385] and Rattigan et al. [325] fitted their spectra to the expression

$$\ln \sigma(\lambda, T) = \ln \sigma(\lambda, 298 \text{ K}) + B(T-298)$$

and report the temperature coefficients $B(\lambda)$ for $T = 200\text{--}298 \text{ K}$ and $\lambda = 216\text{--}344 \text{ nm}$ (at 2-nm intervals) and for $T = 243\text{--}333 \text{ K}$ and $\lambda = 235\text{--}390 \text{ nm}$ (at 5-nm intervals), respectively. The temperature coefficients B reported by Solomon et al. [385] are nearly constantly larger by $\sim 0.8 \times 10^{-3}$ than those of Rattigan et al. [325] at 235–300 nm and become smaller by up to 1.75×10^{-3} between 315 and 345 nm. The B values reported by Rattigan et al. [325] for the ranges 235–385 nm and 243–333 K are listed also in Table 4-91.

Fahr et al. [115] gave fits for the long-wavelength tail using the expressions $\sigma(\lambda) = \sigma_0(\lambda) \exp(-L/\lambda)$ for $\lambda > 320 \text{ nm}$ and $\sigma(T) = \sigma_0(T) \exp(-\theta/T)$ and reported values for the parameters $\sigma_0(\lambda)$ and L at $T = 218, 235, 253, 273, 295, \text{ and } 333 \text{ K}$ and for $\sigma_0(T)$ and θ at 300, 310, 320, 330, 340, and 350 nm.

In the short-wavelength region at 160–180 nm, a decrease of the absorption cross sections with decreasing temperature 333–218 K has been observed by Fahr et al. [115].

Since CF_3I serves as model system for studying the dynamics of $\text{I}^*(^2\text{P}_{1/2})$ atom production by UV photolysis, there is a great number of studies which measure $\text{I}^*(^2\text{P}_{1/2})/\text{I}(^2\text{P}_{3/2})$ branching ratios and $\text{I}^*(^2\text{P}_{1/2})$ quantum yields from CF_3I photolysis in the wavelength region of the absorption band. The following quantum yields were reported for the range between 248 and 308 nm:

$\Phi(\text{I}^*) = 0.89 \pm 0.01, 0.87 \pm 0.04, \text{ and } 0.88$ at 248 nm by Brewer et al. [42], Gedanken et al. [130], and Felder [117], respectively;

$\Phi(\text{I}^*) = 0.89 \pm 0.05, 0.79 \pm 0.03 \text{ and } 0.63 \pm 0.02$ at 266, 280, and ~305 nm by Kavita and Das [199];

$\Phi(\text{I}^*) = 0.87$ at 277 nm by Kim et al. [200]; $\Phi(\text{I}^*) = 0.69$ at 304 nm by Kang et al. [198];

$\Phi(\text{I}^*) = 0.21$ at 308 nm by Felder [118], and

$\Phi(\text{I}^*) =$	0.99 ± 0.01	0.91 ± 0.01	0.89 ± 0.01	0.84 ± 0.01	0.81 ± 0.01	0.69 ± 0.01
$\lambda \text{ (nm)} =$	275	279	283	290	293	295
$\Phi(\text{I}^*) =$	0.68 ± 0.01	0.63 ± 0.02	0.61 ± 0.02	0.47 ± 0.01	0.41 ± 0.0	0.37 ± 0.01
$\lambda \text{ (nm)} =$	296	297	298	300	302	303

by Furlan et al. [127].

Quantum yields for $\text{I}(^2\text{P}_{3/2})$ atom formation, $\Phi(\text{I})$, can be derived from $\Phi(\text{I}) = 1 - \Phi(\text{I}^*)$

Table 4-91. Absorption Cross Sections of CF₃I at 295–300 K

λ (nm)	$10^{20} \sigma$ (cm ²)	$10^3 B$ (K ⁻¹)	λ (nm)	$10^{20} \sigma$ (cm ²)	$10^3 B$ (K ⁻¹)
180	3.11		285	33.4	0.55
185	0.75		290	22.7	1.65
190	0.28		295	14.3	2.98
195	0.16		300	8.60	4.22
200	0.15		305	5.06	5.61
205	0.19		310	2.82	6.84
210	0.34		315	1.62	7.68
215	0.68		320	0.905	8.27
220	1.52		325	0.485	8.74
225	2.88		330	0.262	9.25
230	5.03		335	0.142	9.92
235	8.21	0.16	340	0.0750	10.27
240	13.6	-0.16	345	0.0407	11.71
245	21.8	-0.52	350	0.0210	12.85
250	32.4	-0.86	355	0.0115	13.26
255	45.2	-1.17	360	0.0064	14.65
260	56.9	-1.37	365	0.0036	14.63
265	63.4	-1.43	370	0.002	15.49
270	63.1	-1.30	375	0.0011	17.14
275	56.1	-0.94	380	0.0007	17.66
280	45.1	-0.62	385	0.0004	19.71

Note: Absorption cross sections σ : 180–215 nm: Fahr et al. [115]

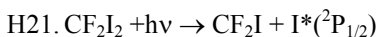
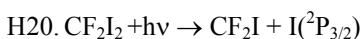
220–230 nm: mean of Brouwer and Troe [45], Solomon et al. [385], and Fahr et al. [115]

235–310 nm: mean of Brouwer and Troe [45], Solomon et al. [385], Fahr et al. [115], and Rattigan et al. [325]

315–350 nm: mean of Solomon et al. [385], Fahr et al. [115], and Rattigan et al. [325]

355–385 nm: Rattigan et al. [325].

Temperature coefficients B: 243–333 K, Rattigan et al. [325] ($\ln \sigma(\lambda, T) = \ln \sigma(\lambda, 298 \text{ K}) + B(T-298)$).

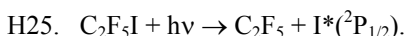
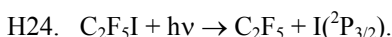


The photodissociation of CF₂I₂ has been studied at room temperature and wavelengths 248, 308, 337, and 351 nm by Wannemacher et al. [429] and Baum et al. [30]. These authors report also plots of the absorption spectrum at room temperature and between 190 and 420 nm, which suggest the presence of at least two overlapping transitions corresponding to the different dissociation processes. Numerical absorption data belonging to Wannemacher et al. and Baum et al. were obtained via personal communication by Pfister and Huber [314]. The absorption cross sections listed in Table 4-92 are normalized to a maximum value $\sigma = 2.929 \times 10^{-18} \text{ cm}^2 \cdot \text{molecule}^{-1}$ at 300 nm, which was derived from five different spectra and has an uncertainty of $\pm 16\%$.

Table 4-92. Absorption Cross Sections of CF₂I₂ at 294 K

λ (nm)	$10^{20} \sigma$ (cm ²)	λ (nm)	$10^{20} \sigma$ (cm ²)	λ (nm)	$10^{20} \sigma$ (cm ²)
190	3163	270	203.1	350	66.24
195	4616	275	215.7	355	57.76
200	4070	280	224.3	360	49.81
205	2285	285	236.4	365	41.51
210	837.0	290	259.5	370	33.92
215	238.1	295	281.9	375	26.85
220	75.78	300	292.9	380	18.90
225	36.39	305	288.5	385	13.60
230	29.50	310	266.7	390	9.892
235	35.51	315	235.6	395	6.713
240	47.34	320	198.6	400	4.240
245	66.07	325	163.9	405	3.356
250	89.21	330	135.5	410	1.943
255	118.0	335	111.6	415	1.413
260	150.1	340	91.33	420	0.7066
265	180.5	345	78.25		

Note: 190–420 nm, Wannenmacher et al. [429], Baum et al. [30], and Pfister and Huber [314].



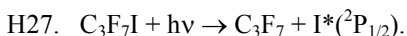
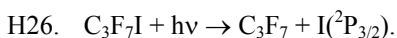
The absorption cross sections of C₂F₅I have been measured at 295 K and 268 nm ($\sigma = 6.39 \times 10^{-19}$ cm²) by Pence et al. [312] and at 323 K and 220–320 nm by Zhang et al. [451]. The absorption band extending over the 220–320-nm range has a maximum of $\sim 6.7 \times 10^{-19}$ cm² at ~ 269 nm. Estimated values at 5-nm intervals, read from a logarithmic plot, are presented in Table 4-93.

Quantum yields for I*(²P_{1/2}) atom formation in the photolysis of C₂F₅I at 266, 288, and ~ 305 nm, $\Phi(I^*) = 0.97 \pm 0.03$, 0.75 ± 0.03 , and 0.83 ± 0.05 , respectively, have been reported by Kavita and Das [199]. Quantum yields for I(²P_{3/2}) atom formation, $\Phi(I)$, can be derived from $\Phi(I) = 1 - \Phi(I^*)$.

Table 4-93. Absorption Cross Sections of C₂F₅I at 323 K

λ (nm)	$10^{20} \sigma$ (cm ²)	λ (nm)	$10^{20} \sigma$ (cm ²)	λ (nm)	$10^{20} \sigma$ (cm ²)
220	1.95	255	49.8	290	35.3
225	3.27	260	60.0	295	25.0
230	5.60	265	65.5	300	16.3
235	9.40	270	66.8	305	10.4
240	16.0	275	63.2	310	6.4
245	25.3	280	56.1	315	3.9
250	37.5	285	46.5	320	2.3

Note: 235–310 nm, Zhang et al. [451], estimated from logarithmic plot.



The absorption cross sections of 1-C₃F₇I have been measured at room temperature and 265–341 nm by Koffend and Leone [205] and at 180–400 nm by Pence et al. [312]. The latter authors report a plot of the absorbance (in arbitrary units), which shows an absorption band between ~ 220 and 340 nm with the maximum at ~ 268 nm, and absorption cross sections only for 248, 268, and 308 nm. The data for 268 and 308 nm are in good agreement with the corresponding data reported by Koffend and Leone [205]. The recommended absorption cross sections of 1-C₃F₇I, listed in Table 4-94, are the value for 248 nm reported by Pence et al. [312]; the mean of the values of Pence et al. [312] and Koffend and Leone [205] at 268 nm; and, for the range 270–340 nm,

values obtained by interpolation and extrapolation at 5-nm intervals of the data reported at odd wavelength by Koffend and Leone [205].

Quantum yields for $I^*(^2P_{1/2})$ atom formation in the photolysis of C_3F_7I at 266, 288, and ~ 305 nm,

$\Phi(I^*) = 0.83 \pm 0.02$, 0.89 ± 0.03 , and 0.90 ± 0.05 for 1- C_3F_7I and

$\Phi(I^*) = 0.83 \pm 0.01$, 0.80 ± 0.03 , and 0.89 ± 0.02 for 2- C_3F_7I ,

have been reported by Kavita and Das [199].

Quantum yields for $I(^2P_{3/2})$ atom formation, $\Phi(I)$, can be derived from $\Phi(I) = 1 - \Phi(I^*)$.

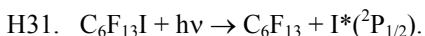
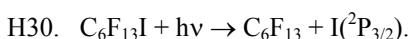
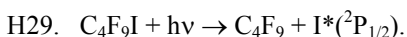
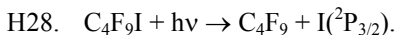
Table 4-94. Absorption Cross Sections of 1- C_3F_7I at 295–298 K

λ (nm)	$10^{20} \sigma$ (cm ²)	λ (nm)	$10^{20} \sigma$ (cm ²)	λ (nm)	$10^{20} \sigma$ (cm ²)
248	31.0	290	43.7	320	3.3
268	77.3	295	31.8	325	2.0
270	77.0	300	21.3	330	1.2
275	74.0	305	14.2	335	0.70
280	66.5	310	9.2	340	0.42
285	56.2	315	5.5		

Note: 248 nm, Pence et al. [312],

268 nm, mean of Pence et al. [312] and Koffend and Leone [205]

270–340 nm, 5-nm inter- and extrapolation of Koffend and Leone [205] data.



Absorption cross sections are not available for these perfluoroalkyl iodides.

Quantum yields for $I^*(^2P_{1/2})$ atom formation in the photolysis of both iodides at 266, 288, and ~ 305 nm,

$\Phi(I^*) = 0.75 \pm 0.03$, 0.80 ± 0.03 , and 0.87 ± 0.02 for *n*- C_4F_9I and

$\Phi(I^*) = 0.82 \pm 0.02$, 0.74 ± 0.03 , and 0.82 ± 0.01 for *n*- $C_6F_{13}I$,

have been reported by Kavita and Das [199].

Quantum yields for $I(^2P_{3/2})$ atom formation, $\Phi(I)$, can be derived from $\Phi(I) = 1 - \Phi(I^*)$.

- H32. $CH_2ICl + hv \rightarrow CH_2Cl + I$. The absorption cross sections of CH_2ICl have been measured at room temperature and 205–330 nm by Schmitt and Comes [366]; at 192–225 nm and 215–400 nm by Kwok and Phillips [208], [209], who also measured the CH_2ICl spectrum in cyclohexane solution. Measurements have also been carried out at 223–298 K and 205–355 nm by Roehl et al. [343] and at 243–333 K and 235–390 nm by Rattigan et al. [325]. The room temperature data of Roehl et al. [343] and Rattigan et al. [325] are in good agreement, where the values of Rattigan et al. [325] are lower by $\leq 10\%$ between 240 and 345 nm. The older data of Schmitt and Comes [366] and the data of Kwok and Phillips [209] are higher with absorption maxima near 270 nm of 1.94×10^{-18} and 1.5×10^{-18} cm², respectively, compared to 1.35×10^{-18} and 1.21×10^{-18} cm² reported by the other two groups. The data of Kwok and Phillips [208] at 205 and 210 nm are lower by more than 80 % than the data of Roehl et al. [343]. The preferred absorption cross sections, listed in Table 4-95, are the data of Roehl et al. [343] at 205–230 nm; the mean of the values reported by Roehl et al. [343] and Rattigan et al. [325] at 235–355 nm; and the data of Rattigan et al. [325] at 360–390 nm. The data of Schmitt and Comes [366] and Kwok and Phillips [208], [209] are given only as a plots in their papers and have therefore not been included in the evaluation.

Both temperature studies show an increase of the absorption cross sections around the absorption maximum (~ 250 – 285 nm) with decreasing temperature between 333 and 223 K and the reverse effect above 285 nm. The absorption maxima at ~ 250 K reported by the two groups agree within 15%. A simple analytical expression for

the temperature dependence, $\sigma(\lambda, T) = \sigma(298 \text{ K}) [1 + a_1(T-298) + a_2(T-298)^2]$, and the fitting parameters $a_1(\lambda)$ and $a_2(\lambda)$ for $\lambda = 205\text{--}355 \text{ nm}$ and $T = 223\text{--}298 \text{ K}$ give Roehl et al. [343]. Another simple parameterization, $\ln \sigma(\lambda, T) = \ln \sigma(\lambda, 298 \text{ K}) + B(T-298)$, and parameters $B(\lambda)$ for $\lambda = 235\text{--}390 \text{ nm}$ and $T = 243\text{--}333 \text{ K}$ report Rattigan et al. [325]. The temperature coefficients a_1 , a_2 , and B are given also in Table 4-95.

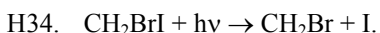
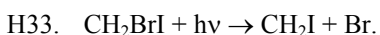
Table 4-95. Absorption Cross Sections of CH₂I at 298 K and Temperature Coefficients

λ (nm)	$10^{20} \sigma$ (cm ²)	$10^3 a_1$ (K ⁻¹)	$10^5 a_2$ (K ⁻²)	$10^3 B$ (K ⁻¹)	λ (nm)	$10^{20} \sigma$ (cm ²)	$10^3 a_1$ (K ⁻¹)	$10^5 a_2$ (K ⁻²)	$10^3 B$ (K ⁻¹)
205	132	-1.59	-3.83		300	25.9	2.38	-0.0473	2.56
210	42.1	8.47	3.76		305	16.7	3.13	0.394	3.08
215	11.1	6.12	4.30		310	10.9	3.13	0.303	3.50
220	7.50	0.232	0.129		315	7.16	2.74	-0.317	3.56
225	9.76	-0.0938	0.660		320	4.79	2.44	-0.533	3.46
230	14.9	-0.268	-1.4×10^{-1}		325	3.23	2.87	0.140	3.44
235	21.2	-0.512	-0.388	0.24	330	2.14	8.52	-4.21	3.72
240	32.1	-0.793	-0.664	0.12	335	1.40	2.02	-2.25	4.09
245	45.9	-0.929	-0.758	-0.02	340	0.906	5.20	4.54	4.87
250	63.3	-1.22	-1.13	-0.11	345	0.569	7.05	6.88	5.69
255	84.5	-1.25	-0.998	-0.28	350	0.350	9.12	11.7	6.88
260	106	-1.56	-1.14	-0.44	355	0.225	12.27	18.9	8.16
265	122	-1.05	-0.294	-0.55	360	0.133			9.01
270	128	-1.33	-0.593	-0.59	365	0.081			11.06
275	121	-1.07	-0.298	-0.47	370	0.048			11.47
280	104	-0.618	-0.309	-0.18	375	0.027			12.77
285	81.1	-0.326	-0.554	0.32	380	0.017			15.14
290	58.5	0.300	-0.711	0.99	385	0.008			19.12
295	39.9	1.55	-0.245	1.73	390	0.006			20.48

Note: Absorption cross sections σ : 205–230 nm, Roehl et al. [343], 235–355 nm, mean of Roehl et al. [343] and Rattigan et al. [325], 360–390 nm, Rattigan et al. [325].

Temperature coefficients a_1 and a_2 : 223–298 K, Roehl et al. [343] ($\sigma(\lambda, T) = \sigma(298 \text{ K}) [1 + a_1(T-298) + a_2(T-298)^2]$).

Temperature coefficients B : 243–333 K, Rattigan et al. [325] ($\ln \sigma(\lambda, T) = \ln \sigma(\lambda, 298 \text{ K}) + B(T-298)$).



The absorption cross sections of CH₂BrI have been measured at room temperature and 180–360 nm by Man et al. [230]; and at 273, 298, and 348 K and 215–390 nm by Mössinger et al. [283]. The spectrum exhibits two absorption bands with maxima near 210 and 267 nm which can be assigned to electronic transitions to repulsive states antibonding in C–Br and C–I, respectively. The results of the two studies are not in quantitative agreement: Mössinger et al. [283] report room temperature absorption cross sections of 5.7×10^{-18} and $2.3 \times 10^{-18} \text{ cm}^2$ at 215 and 270 nm, whereas a plot in the paper of Man et al. [230] gives the larger values of $\sim 1 \times 10^{-17}$ and $3.5 \times 10^{-18} \text{ cm}^2$, respectively. We recommend the data of Mössinger et al. [283], which are listed in Table 4-96.

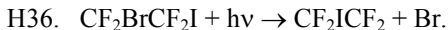
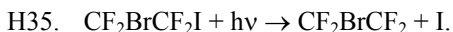
The absorption cross sections increase with decreasing temperature around the band maxima and decrease in their long-wavelength tails at 220–240 nm and above 290 nm. The temperature dependence was parameterized by Mössinger et al. [283] by the empirical relation $\ln \sigma(\lambda, T) = \ln \sigma(\lambda, 298 \text{ K}) + B(T-298)$. The temperature coefficients $B(\lambda)$ are listed also in Table 4-96 (an erroneous B value at 280 nm has been corrected by Dr. Mössinger via a personal communication).

Table 4-96. Absorption Cross Sections of CH₂BrI at 298 K and Temperature Coefficients

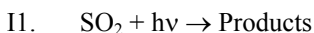
λ (nm)	$10^{20} \sigma$ (cm ²)	$10^3 B$ (K ⁻¹)	λ (nm)	$10^{20} \sigma$ (cm ²)	$10^3 B$ (K ⁻¹)	λ (nm)	$10^{20} \sigma$ (cm ²)	$10^3 B$ (K ⁻¹)
215	567	-2.16	275	214	-1.22	335	5.52	3.89
220	423	-0.12	280	184	-0.94	340	3.50	4.79
225	269	1.34	285	150	-0.53	345	2.24	5.74
230	155	2.06	290	110	0.10	350	1.41	6.73
235	97.9	2.05	295	82.5	0.63	355	0.817	9.47
240	80.9	1.01	300	60.6	1.03	360	0.498	11.5
245	93.7	0.00	305	42.9	1.13	365	0.303	11.6
250	125	-0.58	310	31.4	1.41	370	0.165	14.3
255	170	-1.16	315	23.1	1.52	375	0.098	17.4
260	207	-1.29	320	16.8	1.71	380	0.070	
265	228	-1.45	325	11.5	2.36	385	0.039	
270	229	-1.73	330	8.02	2.99	390	0.025	

Note: Absorption cross sections σ : 205–380 nm, Mössinger et al. [283].

Temperature coefficients B: 273–348 K, Mössinger et al. [283] ($\ln \sigma(\lambda, T) = \ln \sigma(\lambda, 298 \text{ K}) + B(T-298)$).

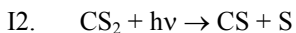


The absorption spectrum of CF₂BrCF₂I has been measured at room temperature and 190–350 nm by Pence et al. [312]. The spectrum, reported as a plot (with arbitrary absorbance units), exhibits an absorption band with the maximum near 268 nm corresponding to the C–I bond and part of an absorption band with the maximum at or below 193 nm corresponding to the C–Br bond. A cross section $\sigma = 2.36 \times 10^{-18} \text{ cm}^2$ and a quantum yield for Br*(²P_{1/2}) atom formation, $\Phi(\text{Br}^*) = 0.07 \pm 0.05$, at 193 nm have been reported.



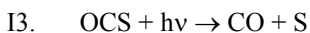
The UV absorption spectrum of SO₂ is highly structured, with a very weak absorption in the 340–390 nm region, a weak absorption in the 260–340 nm region, and a strong absorption extending from 180 to 235 nm; the threshold wavelength for photodissociation is ~220 nm. The atmospheric photochemistry of SO₂ has been reviewed by Heicklen et al. [157] and by Calvert and Stockwell [66]. Direct photo-oxidation at wavelengths longer than ~300 nm by way of the electronically excited states of SO₂ appears to be relatively unimportant.

The absorption cross sections have been measured by McGee and Burris [252] at 295 and 210 K, between 300 and 324 nm, which is the wavelength region commonly used for atmospheric monitoring of SO₂. Manatt and Lane [231] have recently compiled and evaluated the earlier cross section measurements between 106 and 403 nm.



The CS₂ absorption spectrum is rather complex. Its photochemistry has been reviewed by Okabe [300]. There are two distinct regions in the near UV spectrum: a strong absorption extending from 185 to 230 nm, and a weaker one in the 290–380 nm range. The threshold wavelength for photodissociation is ~280 nm. Absorption cross section measurements have been reported recently by Xu and Joens [435] between 187 and 230 nm.

The photo-oxidation of CS₂ in the atmosphere has been discussed by Wine et al. [432], who report that electronically excited CS₂ may react with O₂ to yield eventually OCS.



The absorption cross sections of OCS have been measured by Breckenridge and Taube [41], who presented their 298 K results in graphical form, between 200 and 260 nm; by Rudolph and Inn [351] between 200 and ~300 nm (see also Turco et al. [406]), at 297 and 195 K; by Leroy et al. [213] at 294 K, between 210 and 260 nm, using photographic plates; and by Molina et al. [263] between 195 and 260 nm, in the 195 K to 403 K temperature range. The results are in good agreement in the regions of overlap, except for $\lambda > 280 \text{ nm}$, where the cross section values reported by Rudolph and Inn [351] are significantly larger than those reported by Molina et al. [263]. The latter authors concluded that solar photodissociation of OCS in the troposphere occurs only to a negligible extent.

The recommended cross sections, given in Table 4-97, are taken from Molina et al. [263]. (The original publication also lists a table with cross section values averaged over 1 nm intervals, between 185 and 300 nm.)

Rudolph and Inn [351] reported a quantum yield for photodissociation of 0.72, based on measurements of the quantum yield for CO production in the 220–254 nm range. Additional measurements would be useful.

Table 4-97. Absorption Cross Sections of OCS

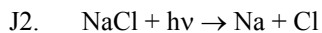
λ (nm)	$10^{20}\sigma(\text{cm}^2)$		λ (nm)	$10^{20}\sigma(\text{cm}^2)$	
	295 K	225 K		295 K	225 K
186.1	18.9	13.0	228.6	26.8	23.7
187.8	8.33	5.63	231.2	22.1	18.8
189.6	3.75	2.50	233.9	17.1	14.0
191.4	2.21	1.61	236.7	12.5	9.72
193.2	1.79	1.53	239.5	8.54	6.24
195.1	1.94	1.84	242.5	5.61	3.89
197.0	2.48	2.44	245.4	3.51	2.29
199.0	3.30	3.30	248.5	2.11	1.29
201.0	4.48	4.50	251.6	1.21	0.679
203.1	6.12	6.17	254.6	0.674	0.353
205.1	8.19	8.27	258.1	0.361	0.178
207.3	10.8	10.9	261.4	0.193	0.0900
209.4	14.1	14.2	264.9	0.0941	0.0419
211.6	17.6	17.6	268.5	0.0486	0.0199
213.9	21.8	21.8	272.1	0.0248	0.0101
216.2	25.5	25.3	275.9	0.0119	0.0048
218.6	28.2	27.7	279.7	0.0584	0.0021
221.5	30.5	29.4	283.7	0.0264	0.0009
223.5	31.9	29.5	287.8	0.0012	0.0005
226.0	30.2	27.4	292.0	0.0005	0.0002
			296.3	0.0002	–

I4. $\text{SF}_6 + h\nu \rightarrow \text{Products}$

The species SF_6 does not absorb at wavelengths longer than 130 nm; it is expected to have an atmospheric residence time of thousands of years (Ravishankara et al. [329]; Ko et al. [204]).

J1. $\text{NaOH} + h\nu \rightarrow \text{Na} + \text{OH}$

The spectrum of NaOH vapor is poorly characterized. Rowland and Makide [346] inferred the absorption cross section values and the average solar photodissociation rate from the flame measurements of Daidoji [100]. Additional measurements are required.



There are several studies of the UV absorption spectra of NaCl vapor. For a review of the earlier work, which was carried out at high temperatures, see Rowland and Rogers [348]. The recommended cross sections, listed in Table 4-98, are taken from the work of Silver et al. [376], who measured spectra of gas phase NaCl at room temperature in the range from ~190 to 360 nm by directly monitoring the product Na atoms.

Table 4-98. Absorption Cross Sections of NaCl Vapor at 300 K

λ (nm)	$10^{20}\sigma(\text{cm}^2)$
189.7	612
193.4	556
203.1	148
205.3	90.6
205.9	89.6
210.3	73.6
216.3	151
218.7	46.3
225.2	146
230.4	512
231.2	947
234.0	1300
237.6	638
241.4	674
248.4	129
251.6	251
254.8	424
260.2	433
268.3	174
277.0	40
291.8	0.8

4.3 References

1. *The Stratosphere 1981: Theory and Measurements*; National Aeronautics and Space Administration, 1982.
2. Abel, B., B. Herzog, H. Hippler and J. Troe, 1989, *J. Chem. Phys.*, **91**, 890-899, 900-905.
3. Abel, B., H. Hippler and J. Troe, 1992, *J. Chem. Phys.*, **96**, 8863-8871.
4. Adachi, H., N. Basco and D. G. L. James, 1979, *Int. J. Chem. Kinet.*, **11**, 1211-1229.
5. Adachi, H., N. Basco and D. G. L. James, 1980, *Int. J. Chem. Kinet.*, **12**, 949.
6. Addison, M. C., J. P. Burrows, R. A. Cox and R. Patrick, 1980, *Chem. Phys. Lett.*, **73**, 283.
7. Adler-Golden, S. M. and J. R. Wiesenfeld, 1981, *Chem. Phys. Lett.*, **82**, 281.
8. Allen, M. and J. E. Frederick, 1982, *J. Atmos. Sci.*, **39**, 2066-2075.
9. Amoruso, A., M. Cacciani, A. DiSarra and G. Fiocco, 1990, *J. Geophys. Res.*, **95**, 20565.
10. Amoruso, A., L. Crescentini, G. Fiocco and M. Volpe, 1993, *J. Geophys. Res.*, **98**, 16857-16863.
11. Amoruso, A., L. Crescentini, M. Silvia Cola and G. Fiocco, 1996, *J. Quant. Spectrosc. Radiat. Transfer*, **56**, 145-152.
12. Anastasi, C., I. W. M. Smith and D. A. Parkes, 1978, *J. Chem. Soc. Faraday Trans. 1*, **74**, 1693-1701.
13. Anastasi, C., D. J. Waddington and A. Woolley, 1983, *J. Chem. Soc. Faraday Trans.*, **79**, 505-516.
14. Anderson, G. P. and L. A. Hall, 1983, *J. Geophys. Res.*, **88**, 6801-6806.
15. Anderson, G. P. and L. A. Hall, 1986, *J. Geophys. Res.*, **91**, 14509-14514.
16. Armerding, W., F. J. Comes and B. Schulke, 1995, *J. Phys. Chem.*, **99**, 3137-3143.
17. Baer, S., H. Hippler, R. Rahn, M. Siefke, N. Seitzinger and J. Troe, 1991, *J. Chem. Phys.*, **95**, 6463-6470.
18. Bagratashvili, V. N., S. I. Ionov, G. V. Mishakov and V. A. Semchishen, 1985, *Chem. Phys. Lett.*, **115**, 144-148.
19. Ball, S. M., G. Hancock, S. E. Martin and J. C. Pinot de Moira, 1997, *Chem. Phys. Lett.*, **264**, 531-538.
20. Ballash, N. M. and D. A. Armstrong, 1974, *Spectrochim Acta*, **30A**, 941-944.
21. Barker, J. R., L. Brouwer, R. Patrick, M. J. Rossi, P. L. Trevor and D. M. Golden, 1985, *Int. J. Chem. Kinet.*, **17**, 991-1006.
22. Barnes, R. J., M. Lock, J. Coleman and A. Sinha, 1996, *J. Phys. Chem.*, **100**, 453-457.
23. Barnes, R. J., A. Sinha and H. A. Michelsen, 1998, *J. Phys. Chem. A*, **102**, 8855-8859.
24. Basco, N. and S. S. Parmar, 1985, *Int. J. Chem. Kinet.*, **17**, 891.
25. Bass, A. M., L. C. Glasgow, C. Miller, J. P. Jesson and S. L. Filken, 1980, *Planet. Space Sci.*, **28**, 675.
26. Bass, A. M., A. E. Ledford and A. H. Laufer, 1976, *J. Res. NBS*, **80A**, 143-166.
27. Bauer, D., J. N. Crowley and G. K. Moortgat, 1992, *J. Photochem. and Photobiol.*, **A65**, 3530-3538.
28. Bauer, D., D. O. L. and A. J. Hynes, 2000, *Phys. Chem. Chem. Phys.*, **2**, 1421-1424.
29. Baughum, S. L. and S. R. Leone, 1980, *J. Chem. Phys.*, **72**, 6531-6545.
30. Baum, G. P., P. Felder and R. J. Huber, 1993, *J. Chem. Phys.*, **98**, 1999-2010.
31. Benter, T., C. Feldmann, U. Kirchner, M. Schmidt, S. Schmidt and R. N. Schindler, 1995, *Ber. Bunsenges. Phys. Chem.*, **99**, 1144-1147.
32. Biaume, F., 1973, *J. Photochem.*, **2**, 139.
33. Bilde, M., T. J. Wallington, G. Ferronato, J. J. Orlando, G. S. Tyndall, E. Estupinan and S. Haberkorn, 1998, *J. Phys. Chem. A*, **102**, 1976-1986.
34. Birk, M., R. R. Friedl, E. A. Cohen, H. M. Pickett and S. P. Sander, 1989, *J. Chem. Phys.*, **91**, 6588-6597.
35. Birks, J. W., B. Shoemaker, T. J. Leck, R. A. Borders and L. J. Hart, 1977, *J. Chem. Phys.*, **66**, 4591-4599.
36. Bishenden, E., J. Haddock and D. J. Donaldson, 1991, *J. Phys. Chem.*, **95**, 2113.
37. Bishenden, E., J. Haddock and D. J. Donaldson, 1992, *J. Phys. Chem.*, **96**, 6513.
38. Bongartz, A., J. Kames, F. Welter and U. Schurath, 1991, *J. Phys. Chem.*, **95**, 1076-1082.
39. Brandon, J. T., S. A. Reid, D. C. Robie and H. Reisler, 1992, *J. Chem. Phys.*, **97**, 5246.
40. Braun, M., A. Fahr, R. Klein, M. J. Kurylo and R. E. Huie, 1991, *J. Geophys. Res.*, **96**, 13009.
41. Breckenridge, W. and H. H. Taube, 1970, *J. Chem. Phys.*, **52**, 1713-1715.
42. Brewer, P., P. Das, G. Ondrey and R. Bersohn, 1983, *J. Chem. Phys.*, **79**, 720-723.
43. Brion, J., A. Chakir, D. Daumont, J. Malicet and C. Parisse, 1993, *Chem. Phys. Lett.*, **213**, 610-612.
44. Brock, J. C. and R. T. Watson, 1980, *Chem. Phys.*, **46**, 477-484.
45. Brouwer, L. and J. Troe, 1981, *Chem. Phys. Lett.*, **82**, 1-4.
46. Brownsword, R. A., M. Hillenkamp, T. Laurent, R. K. Vatsa, H.-R. Volpp and J. Wolfrum, 1997, *J. Chem. Phys.*, **106**, 1359-1366.
47. Brownsword, R. A., M. Hillenkamp, T. Laurent, R. K. Vatsa, H.-R. Volpp and J. Wolfrum, 1997, *J. Phys. Chem. A*, **101**, 5222-5227.

48. Brownsword, R. A., M. Hillenkamp, T. Laurent, J. Wolfrum, H.-R. Volpp, R. K. Vatsa and H.-S. Yoo, 1997, *J. Chem. Phys.*, **107**, 779-785.
49. Brownsword, R. A., P. Schmiechen, H.-R. Volpp, H. P. Upadhyaya, Y. J. Jung and K.-H. Jung, 1999, *J. Chem. Phys.*, **110**, 11823-11829.
50. Burkholder, J. B., 1993, *J. Geophys. Res.*, **98**, 2963-2974.
51. Burkholder, J. B. and E. J. Bair, 1983, *J. Phys. Chem.*, **87**, 1859-1863.
52. Burkholder, J. B., R. L. Mauldin, R. J. Yokelson, S. Solomon and A. R. Ravishankara, 1993, *J. Phys. Chem.*, **97**, 7597-7605.
53. Burkholder, J. B., J. J. Orlando and C. J. Howard, 1990, *J. Phys. Chem.*, **94**, 687-695.
54. Burkholder, J. B., A. R. Ravishankara and S. Solomon, 1995, *J. Geophys. Res.*, **100**, 16793-16800.
55. Burkholder, J. B., R. K. Talukdar and A. R. Ravishankara, 1994, *Geophys. Res. Lett.*, **21**, 585-588.
56. Burkholder, J. B., R. K. Talukdar, A. R. Ravishankara and S. Solomon, 1993, *J. Geophys. Res.*, **98**, 22937-22948.
57. Burkholder, J. B., R. R. Wilson, T. Gierczak, R. Talukdar, S. A. McKeen, J. J. Orlando, G. L. Vaghjiani and A. R. Ravishankara, 1991, *J. Geophys. Res.*, **96**, 5025-5043.
58. Burley, J. D., C. E. Miller and H. S. Johnston, 1993, *J. Molec. Spec.*, **158**, 377-391.
59. Burrows, J. P., G. S. Tyndall and G. K. Moortgat, 16th Informal Conf. on Photochemistry, 1984, Boston.
60. Burrows, J. P., G. S. Tyndall and G. K. Moortgat, 1985, *J. Phys. Chem.*, **89**, 4848-4856.
61. Burrows, J. P., G. S. Tyndall and G. K. Moortgat, 1988, *J. Phys. Chem.*, **92**, 4340-4348.
62. Butler, P. J. D. and L. F. Phillips, 1983, *J. Phys. Chem.*, **87**, 183-184.
63. Cacciani, M., A. D. Sarra, G. Fiocco and A. Amoroso, 1989, *J. Geophys. Res.*, **94**, 8485-8490.
64. Cadman, P. and J. P. Simons, 1966, *Trans. Faraday Soc.*, **62**, 631-641.
65. Calvert, J. G. and J. N. Pitts; John Wiley & Sons, Inc., pp. 230-231: New York, 1966.
66. Calvert, J. G. and W. R. Stockwell. In *Acid Precipitation: SO₂, NO, NO₂ Oxidation Mechanisms: Atmospheric Considerations*; Ann Arbor Sci. Publishers: Ann Arbor, Michigan, 1983.
67. Canosa-Mas, C. E., M. Fowles, P. J. Houghton and R. P. Wayne, 1987, *J. Chem. Soc. Faraday Trans. 2*, **83**, 1465.
68. Cantrell, C. A., J. A. Davidson, A. H. McDaniel, R. E. Shetter and J. G. Calvert, 1990, *J. Phys. Chem.*, **94**, 3902-3908.
69. Cantrell, C. A., J. A. Davidson, R. E. Shetter, B. A. Anderson and J. G. Calvert, 1987, *J. Phys. Chem.*, **91**, 5858-5863.
70. Cattell, F. C., J. Cavanagh, R. A. Cox and M. E. Jenkin, 1986, *J. Chem. Soc. Faraday Trans. 2*, **82**, 1999-2018.
71. Chang, J. S., J. R. Barker, J. E. Davenport and D. M. Golden, 1979, *Chem. Phys. Lett.*, **60**, 385-390.
72. Cheung, A. S. C., K. Yoshino, J. R. Esmond, S. S. L. Chiu, D. E. Freeman and W. H. Parkinson, 1990, *J. Chem. Phys.*, **92**, 842-849.
73. Cheung, A. S. C., K. Yoshino, W. H. Parkinson and D. E. Freeman, 1984, *Geophys. Res. Lett.*, **11**, 580-582.
74. Cheung, A. S. C., K. Yoshino, W. H. Parkinson, S. L. Guberman and D. E. Freeman, 1986, *Planet. Space Sci.*, **34**, 1007-1021.
75. Chiu, S. S. L., A. S. C. Cheung, K. Yoshino, J. R. Esmond, D. E. Freeman and W. H. Parkinson, 1990, *J. Chem. Phys.*, **93**, 5539-5543.
76. Chou, C. C., G. Crescentini, H. Vera-Ruiz, W. S. Smith and F. S. Rowland. "Stratospheric Photochemistry of CF₂O, CClFO, and CCl₂O"; 173rd American Chemical Society Meeting, 1977, New Orleans, LA.
77. Chou, C. C., R. J. Milstein, W. S. Smith, H. Vera-Ruiz, M. J. Molina and F. S. Rowland, 1978, *J. Phys. Chem.*, **82**, 1.
78. Chou, C. C., W. S. Smith, H. V. Ruiz, K. Moe, G. Crescentini, M. J. Molina and F. S. Rowland, 1977, *J. Phys. Chem.*, **81**, 286-290.
79. Clark, J. H., C. B. Moore and N. S. Nogar, 1978, *J. Chem. Phys.*, **68**, 1264-1271.
80. Clark, R. H. and D. Husain, 1984, *J. Photochem.*, **24**, 103-115.
81. CODATA, 1980, *J. Phys. Chem. Ref. Data*, **9**, 295-471.
82. CODATA, 1982, *J. Phys. Chem. Ref. Data*, **11**, 327-496.
83. Colussi, A. J., 1990, *J. Phys. Chem.*, **94**, 8922-8926.
84. Colussi, A. J., S. P. Sander and R. R. Friedl, 1992, *J. Phys. Chem.*, **96**, 4442-4445.
85. Coquart, B., A. Jenouvrier and M. F. Merienne, 1995, *J. Atm. Chem.*, **21**, 251-261.
86. Coquart, B., M. F. Merienne and A. Jenouvrier, 1990, *Planet. Space Sci.*, **38**, 287.
87. Corcoran, T. C., E. J. Beiting and M. O. Mitchell, 1992, *J. Molecular Spectroscopy*, **154**, 119-128.
88. Cox, R. A., R. A. Barton, E. Ljungstrum and D. W. Stocker, 1984, *Chem. Phys. Lett.*, **108**, 228-232.
89. Cox, R. A. and J. P. Burrows, 1979, *J. Phys. Chem.*, **83**, 2560-2568.
90. Cox, R. A. and G. D. Hayman, 1988, *Nature*, **332**, 796-800.
91. Cox, R. A. and R. Patrick, 1979, *Int. J. Chem. Kinet.*, **11**, 635.

92. Cox, R. A., D. W. Sheppard and M. P. Stevens, 1982, *J. Photochem.*, **19**, 189-207.
93. Cox, R. A. and G. Tyndall, 1979, *Chem. Phys. Lett.*, **65**, 357.
94. Cox, R. A. and G. S. Tyndall, 1980, *J. Chem. Soc. Faraday Trans. 2*, **76**, 153.
95. Coxon, J. A., W. E. Jones and D. A. Ramsey. 12th International Symposium on Free Radicals, 1976, Laguna Beach, California.
96. Crowley, J. N., R. Helleis, R. Muller, G. K. Moortgat, P. J. Crutzen and J. J. Orlando, 1994, *J. Geophys. Res.*, **99**, 20683-20688.
97. Crowley, J. N., F. G. Simon, J. P. Burrows, G. K. Moortgat, M. E. Jenkin and R. A. Cox, 1991, *J. Photochem. and Photobiol. A: Chem.*, **60**, 1-10.
98. Currie, J., J. H. Sidebottom and J. Tedder, 1974, *Int. J. Chem. Kinet.*, **6**, 481-492.
99. Dagaut, P. and M. J. Kurylo, 1990, *J. Photochem. and Photobiol. A: Chem.*, **51**, 133.
100. Daidoji, H., 1979, *Bunseki Kagaku*, **28**, 77
101. Daumont, D., J. Brion, J. Charbonnier and J. Malicet, 1992, *J. Atmos. Chem.*, **15**, 145-155.
102. Davenport, J. E. "Determination of NO₂ Photolysis Parameters for Stratospheric Modeling," FAA-EQ-78-14, Federal Aviation Administration, Washington, DC. 1978.
103. Davidson, J. A., C. A. Cantrell, A. H. McDaniel, R. E. Shetter, S. Madronich and J. G. Calvert, 1988, *J. Geophys. Res.*, **93**, 7105-7112.
104. Davidson, N., 1951, *J. Am. Chem. Soc.*, **73**, 467-468.
105. Davis, H. F. and Y. T. Lee, 1992, *J. Phys. Chem.*, **96**, 5681-5684.
106. DeMore, W. B. and O. Raper, 1964, *J. Phys. Chem.*, **68**, 412-414.
107. DeMore, W. B. and E. Tschuikow-Roux, 1990, *J. Phys. Chem.*, **94**, 5856-5860.
108. Deters, B., J. P. Burrows, S. Himmelmann and C. Blindauer, 1996, *Ann. Geophysicae*, **14**, 468-475.
109. Doucet, J., J. R. Gilbert, P. Sauvageau and C. Sandorfy, 1975, *J. Chem. Phys.*, **62**, 366-369.
110. Doucet, J., P. Sauvageau and C. Sandorfy, 1973, *J. Chem. Phys.*, **58**, 3708-3716.
111. Doucet, J., P. Sauvageau and C. Sandorfy, 1975, *J. Chem. Phys.*, **62**, 355-359.
112. Ebenstein, W. L., J. R. Wiesenfeld and G. L. Wolk, 1978, *Chem. Phys. Lett.*, **53**, 185-189.
113. Fahr, A., W. Braun and M. J. Kurylo, 1993, *J. Geophys. Res.*, **98**, 20467-20472.
114. Fahr, A., A. H. Laufer, M. Kraus and R. Osman, 1997, *J. Phys. Chem A*, **101**, 4879-4886.
115. Fahr, A., A. K. Nayak and R. E. Huie, 1995, *Chem. Phys.*, **199**, 275-284.
116. Fahr, A., A. K. Nayak and M. J. Kurylo, 1995, *Chem. Phys.*, **197**, 195-203.
117. Felder, P., 1991, *Chem. Phys.*, **155**, 435-445.
118. Felder, P., 1992, *Chem. Phys. Lett.*, **197**, 425-432.
119. Felps, W. S., K. Rupnik and S. P. McGlynn, 1991, *J. Phys. Chem.*, **95**, 639-656.
120. Fenter, F. F., V. Catoire, R. Lesclaux and P. D. Lightfoot, 1993, *J. Phys. Chem.*, **97**, 3530-3538.
121. Fergusson, W. C., L. Slotin and W. G. Style, 1936, *Trans. Far. Soc.*, **32**, 956.
122. Francisco, J. S., M. R. Hand and I. H. Williams, 1996, *J. Phys. Chem.*, **100**, 9250-9253.
123. Frederick, J. E. and R. D. Hudson, 1979, *J. Atmos. Sci.*, **36**, 737-745.
124. Frederick, J. E. and J. E. Mentall, 1982, *Geophys. Res. Lett.*, **9**, 461-464.
125. Frost, G. J., L. M. Goss and V. Vaida, 1996, *J. Geophys. Res.*, **101**, 3869-3877.
126. Frost, G. J., L. M. Goss and V. Vaida, 1996, *J. Geophys. Res.*, **101**, 3879-3884.
127. Furlan, A., T. Gejo and R. J. Huber, 1996, *J. Phys. Chem.*, **100**, 7956-7961.
128. Ganske, J. A., H. N. Berko and B. J. Finlayson-Pitts, 1992, *J. Geophys. Res.*, **97**, 7651-7656.
129. Gardner, E. P., P. D. Sperry and J. G. Calvert, 1987, *J. Geophys. Res.*, **92**, 6642-6652.
130. Gedanken, A., 1987, *Chem. Phys. Lett.*, **137**, 462-466.
131. Gibson, G. E. and N. S. Bayliss, 1933, *Phys. Rev.*, **44**, 188.
132. Gilbert, R., P. Sauvageau and C. Sandorfy, 1974, *J. Chem. Phys.*, **60**, 4820-4824.
133. Gillotay, D., A. Jenouvrier, B. Coquart, M. F. Merienne and P. C. Simon, 1989, *Planet. Space Sci.*, **37**, 1127-1140.
134. Gillotay, D. and P. C. Simon, 1989, *J. Atmos. Chem.*, **8**, 41-62.
135. Gillotay, D. and P. C. Simon, 1990, *Aeronomica Acta A*, **356**, 1-173.
136. Gillotay, D. and P. C. Simon, 1991, *J. Atmos. Chem.*, **12**, 269-285.
137. Gillotay, D. and P. C. Simon, 1991, *J. Atmos. Chem.*, **13**, 289-299.
138. Gillotay, D., P. C. Simon and L. Dierickx, 1988, *Aeronomica Acta*, **A335**, 1-25.
139. Gillotay, D., P. C. Simon and L. Dierickx, 1993, *Aeronomica Acta*, **A368**, 1-15.
140. Giolando, D. M., G. B. Fazekas, W. D. Taylor and G. A. Takacs, 1980, *J. Photochem.*, **14**, 335.

141. Goodeve, C. F. and F. D. Richardson, 1937, *Trans. Faraday. Soc.*, **33**, 453-457.
142. Gordus, A. A. and R. B. Bernstein, 1954, *J. Chem. Phys.*, **22**, 790-795.
143. Graham, R. A. Photochemistry of NO₃ and the Kinetics of the N₂O₅-O₃ System. Ph. D. Thesis, University of California, Berkeley, CA, 1975.
144. Graham, R. A. and H. S. Johnston, 1978, *J. Phys. Chem.*, **82**, 254-268.
145. Graham, R. A., A. M. Winer and J. N. Pitts, Jr., 1978, *Geophys. Res. Lett.*, **5**, 909.
146. Green, R. G. and R. P. Wayne, 1976/77, *J. Photochem.*, **6**, 375-377.
147. Greenblatt, G. D. and A. R. Ravishankara, 1990, *J. Geophys. Res.*, **95**, 3539-3547.
148. Griffith, D. W. T., G. C. Toon, B. Sen, J.-F. Blavier and R. A. Toth, 2000, *Geophys. Res. Lett.*, **27**, 2485-2488.
149. Hancock, G. and A. Hofzumahaus "Experimental Study of the Altitude Dependence of the Tropospheric Ozone Photolysis Frequency, J(O(1D)) Between 0 and 12 km Height (ATOP)," ENV4-CT95-0158, EU R and D Programme Environment and Climate 1997.
150. Harder, J. W., J. W. Brault, P. V. Johnston and G. H. Mount, 1996, *J. Geophys. Res.*, submitted.
151. Harker, A. B., W. Ho and J. J. Ratto, 1977, *Chem. Phys. Lett.*, **50**, 394-397.
152. Harwood, M. H. and R. L. Jones, 1994, *J. Geophys. Res.*, **99**, 22995-22964.
153. Harwood, M. H., R. L. Jones, R. A. Cox, E. Lutman and O. V. Rattigan, 1993, *J. Photochem. Photobiol. A: Chem.*, **73**, 167-175.
154. Harwood, M. H., D. M. Rowley, R. A. Freshwater, R. A. Cox and R. L. Jones, 1995, *J. Chem. Soc. Faraday Trans*, **91**, 3027-3032.
155. Hayman, G. D. and R. A. Cox, 1989, *Chem. Phys. Lett.*, **155**, 1-7.
156. Hearn, A. G., 1961, *Proc. Phys. Soc. London*, **78**, 932-940.
157. Heicklen, J., N. Kelly and K. Partymiller, 1980, *Rev. Chem. Intermediates*, **3**, 315-404.
158. Herman, J. R. and J. E. Mentall, 1982, *J. Geophys. Res.*, **87**, 8967-8975.
159. Herzberg, G. and K. K. Innes, 1957, *Canad. J. Phys.*, **35**, 842.
160. Hochanadel, C. J., J. A. Ghormley, J. W. Boyle and P. J. Ogren, 1977, *J. Phys. Chem.*, **81**, 3.
161. Hochanadel, C. J., J. A. Ghormley and P. J. Ogren, 1972, *J. Chem. Phys.*, **56**, 4426-4432.
162. Horowitz, A. and J. G. Calvert, 1978, *Int. J. Chem. Kinet.*, **10**, 805.
163. Hubinger, S. and J. B. Nee, 1994, *Chem. Phys.*, **181**, 247-257.
164. Hubinger, S. and J. B. Nee, 1995, *J. Photochem. and Photobiol. A: Chem.*, **85**, 1-7.
165. Hubrich, C. and F. Stuhl, 1980, *J. Photochem.*, **12**, 93-107.
166. Hubrich, C., C. Zetzsch and F. Stuhl, 1977, *Ber. Bunsenges. Phys. Chem.*, **81**, 437-442.
167. Huder, K. J. and W. B. DeMore, 1995, *J. Phys. Chem.*, **99**, 3905-3908.
168. Hudson, R. D., 1971, *Reviews of Geophysics and Space Physics*, **9**, 305-399.
169. Hudson, R. D., 1974, *Canad. J. Chem.*, **52**, 1465-1478.
170. Hudson, R. D. and L. J. Kieffer. Absorption Cross Sections of Stratospheric Molecules. In *The Natural Stratosphere of 1974*; CIAP, 1975; Vol. Monograph 1; pp (5-156)-(5-194).
171. Huebner, R. H., J. Bushnell, D. L., R. J. Celotta, S. R. Mielczarek and C. E. Kuyatt, 1975, *Nature*, **257**, 376-378.
172. Ibuki, T., 1992, *J. Chem. Phys.*, **96**, 8793-8798.
173. Ichimura, T., A. W. Kirk, G. Kramer and E. Tschuikow-Roux, 1976/1977, *J. Photochem.*, **6**, 77-90.
174. Ichimura, T., A. W. Kirk and E. Tschuikow-Roux, 1977, *J. Phys. Chem.*, **81**, 1153-1156.
175. Illies, A. J. and G. A. Takacs, 1976, *J. Photochem.*, **6**, 35-42.
176. Ingham, T., D. Bauer, J. Landgraf and J. N. Crowley, 1998, *J. Phys. Chem. A*, **102**, 3293-3298.
177. Inn, E. C. Y., 1975, *J. Atmos. Sci.*, **32**, 2375.
178. Inn, E. C. Y., 1980, *J. Geophys. Res.*, **85**, 7493.
179. Inn, E. C. Y. and Y. Tanaka, 1953, *J. Opt. Soc. Am.*, **43**, 870-873.
180. Jenkin, M. E. and R. A. Cox, 1991, *J. Phys. Chem.*, **95**, 3229.
181. Jenkin, M. E., R. A. Cox, G. Hayman and L. J. Whyte, 1988, *J. Chem. Soc. Faraday Trans. 2*, **84**, 913.
182. Jenkin, M. E., T. P. Murrells, S. J. Shalliker and G. D. Hayman, 1993, *J. Chem. Soc. Faraday Trans.*, **89**, 433-446.
183. Jenouvrier, A., B. Coquart and M. F. Merienne, 1986, *J. Quant. Spectros. Radiat. Transfer* **36**, 349-354.
184. Jensen, F. and J. Oddershede, 1990, *J. Phys. Chem.*, **94**, 2235.
185. Johnston, H. S., S. Chang and G. Whitten, 1974, *J. Phys. Chem.*, **78**, 1-7.
186. Johnston, H. S., H. F. Davis and Y. T. Lee, 1996, *J. Phys. Chem.*, **100**, 4713-4723.
187. Johnston, H. S. and R. Graham, 1973, *J. Phys. Chem.*, **77**, 62.
188. Johnston, H. S. and R. Graham, 1974, *Canad. J. Chem.*, **52**, 1415-1423.

189. Johnston, H. S., E. D. Morris, Jr. and J. Van den Bogaerde, 1969, *J. Am. Chem. Soc.*, **91**, 7712-7727.
190. Johnston, H. S., M. Paige and F. Yao, 1984, *J. Geophys. Res.*, **89**, 661.
191. Jolly, G. S., D. L. Singleton, D. J. McKenney and G. Paraskevopoulos, 1986, *J. Chem. Phys.*, **84**, 6662-6667.
192. Jones, E. L. and O. R. Wulf, 1937, *J. Chem. Phys.*, **5**, 873.
193. Jones, I. T. N. and K. Bayes, 1973, *J. Chem. Phys.*, **59**, 4836-4844.
194. Jourdain, J. L., G. Le Bras, G. Poulet, J. Combourieu, P. Rigaud and B. LeRoy, 1978, *Chem. Phys. Lett.*, **57**, 109.
195. Jung, Y.-J., M. S. Park, Y. S. Kim, K.-H. Jung and H.-R. Volpp, 1999, *J. Chem. Phys.*, **111**, 4005-4012.
196. Jungkamp, T. P. W., U. Kirchner, M. Schmidt and R. N. Schindler, 1995, *J. Photochem. Photobiol. A: Chemistry*, **99**, 1-6.
197. Kan, C. S., R. D. McQuigg, M. R. Whitbeck and J. G. Calvert, 1979, *Int. J. Chem. Kinet.*, **11**, 921.
198. Kang, W. K., K. W. Jung, D.-C. Kim and K.-H. Jung, 1996, *J. Chem. Phys.*, **104**, 5815-5820.
199. Kavita, K. and P. K. Das, 2000, *J. Chem. Phys.*, **112**, 8426-8431.
200. Kim, Y. S., W. K. Kang and K.-H. Jung, 1996, *J. Chem. Phys.*, **105**, 551-557.
201. Kim, Y. S., W. K. Kang, D.-C. Kim and K.-H. Jung, 1997, *J. Phys. Chem. A*, **101**, 7576-7581.
202. Knauth, H. D., H. Alberti and H. Clausen, 1979, *J. Phys. Chem.*, **83**, 1604-1612.
203. Knauth, H. D. and R. N. Schindler, 1983, *Z. Naturforsch.*, **38a**, 893.
204. Ko, M. K. W., D. S. Nien, W. C. Wang, G. Shia, A. Goldman, F. J. Murcray, D. G. Murcray and C. P. Rinsland, 1993, *J. Geophys. Res.*, **98**, 10499-10507.
205. Koffend, J. B. and S. R. Leone, 1981, *Chem. Phys. Lett.*, **81**, 136-141.
206. Kurylo, M. J., T. J. Wallington and P. A. Ouellette, 1987, *J. Photochem.*, **39**, 201-215.
207. Kwok, W. M. and D. L. Phillips, 1996, *J. Chem. Phys.*, **104**, 2529-2540.
208. Kwok, W. M. and D. L. Phillips, 1997, *Chem. Phys. Lett.*, **270**, 506-516.
209. Kwok, W. M. and D. L. Phillips, 1997, *Mol. Phys.*, **90**, 315-326.
210. Langhoff, S. R., L. Jaffe and J. O. Arnold, 1977, *J. Quant. Spectrosc. Radiat. Transfer*, **18**, 227.
211. Lawrence, W. G., K. C. Clemmshaw and V. A. Apkarian, 1990, *J. Geophys. Res.*, **95**, 18591.
212. Lee, L. C., 1982, *J. Chem. Phys.*, **76**, 4909-4915.
213. Leroy, B., G. Le Bras and P. Rigaud, 1981, *Ann. Geophys.*, **37**, 297-302.
214. Lewis, B. R., L. Berzins and J. H. Carver, 1986, *J. Quant. Spectrosc. Radiat. Transfer*, **36**, 209-232.
215. Lewis, B. R., L. Berzins, J. H. Carver and S. T. Gibson, 1986, *J. Quant. Spectrosc. Radiat. Transfer*, **36**, 187-207.
216. Libuda, H. G. and F. Zabel, 1995, *Ber. Bunsenges. Phys. Chem.*, **99**, 1205-1213.
217. Lightfoot, P. D., R. A. Cox, J. N. Crowley, M. Destriau, G. D. Hayman, M. E. Jenkin, G. K. Moortgat and F. Zabel, 1992, *Atmos. Environ.*, **26A**, 1805-1961.
218. Lightfoot, P. D. and A. A. Jemi-Alade, 1991, *J. Photochem. and Photobiol. A: Chem.*, **59**, 1-10.
219. Limao-Vieira, P., S. Eden, P. A. Kendall, N. J. Mason and S. V. Hoffmann, 2002, *Chem. Phys. Lett.*, **364**, 535-541.
220. Lin, C. L., 1976, *J. Chem. Eng. Data*, **21**, 411.
221. Lin, C. L., N. K. Rohatgi and W. B. DeMore, 1978, *Geophys. Res. Lett.*, **5**, 113-115.
222. Lock, M., R. J. Barnes and A. Sinha, 1996, *J. Phys. Chem.*, **100**, 7972-7980.
223. Lopez, M. I. and J. E. Sicre, 1988, *J. Phys. Chem.*, **92**, 563-564.
224. Lopez, M. I. and J. E. Sicre, 1990, *J. Phys. Chem.*, **94**, 3860-3863.
225. Lucazeau, G. and C. Sandorfy, 1970, *J. Mol. Spectrosc.*, **35**, 214-231.
226. MacLeod, H., G. P. Smith and D. M. Golden, 1988, *J. Geophys. Res.*, **93**, 3813-3823.
227. Magnotta, F. and H. S. Johnston, 1980, *Geophys. Res. Lett.*, **7**, 769-772.
228. Majer, J. R. and J. P. Simons. Photochemical Processes in Halogenated Compounds. In *Advances in Photochemistry*; Interscience, 1964; Vol. 2; pp 137-181.
229. Malicet, J., D. Daumont, J. Charbonnier, C. Parisse, A. Chakir and J. Brion, 1995, *J. Atm. Chem*, **21**, 263-273.
230. Man, S.-Q., W. M. Kwok, D. L. Phillips and A. E. Johnson, 1996, *J. Chem. Phys.*, **105**, 5842-5857.
231. Manatt, S. L. and A. L. Lane, 1993, *J. Quant. Spectrosc. Radiat. Transfer*, **50**, 267-276.
232. Mandelman, M. and R. W. Nicholls, 1977, *J. Quant. Spectrosc. Radiat. Trans.*, **17**, 483.
233. Margitan, J. J., 1983, *J. Phys. Chem.*, **87**, 674-679.
234. Margitan, J. J. and R. T. Watson, 1982, *J. Phys. Chem.*, **86**, 3819-3824.
235. Maric, D., J. P. Burrows, R. Meller and G. K. Moortgat, 1993, *J. Photochem. Photobiol. A Chem.*, **70**, 205-214.
236. Maric, D., J. P. Burrows and G. K. Moortgat, 1994, *J. Photochem. Photobiol. A: Chem.*, **83**, 179-192.
237. Maric, D., J. N. Crowley and J. P. Burrows, 1997, *J. Phys. Chem.*, **101**, 2561-2567.
238. Maricq, M. M. and J. J. Szente, 1994, *J. Phys. Chem.*, **98**, 2078-2082.
239. Maricq, M. M. and J. J. Szente, 1996, *J. Phys. Chem.*, **100**, 4507-4513.

240. Maricq, M. M. and T. J. Wallington, 1992, *J. Phys. Chem.*, **96**, 982-986.
241. Marinelli, W. J. and H. S. Johnston, 1982, *Chem. Phys. Lett.*, **93**, 127-132.
242. Marinelli, W. J., D. M. Swanson and H. S. Johnston, 1982, *J. Chem. Phys.*, **76**, 2864-2870.
243. Martin, H. and R. Gareis, 1956, *Z. Elektrochemie*, **60**, 959-964.
244. Matsumi, Y., F. J. Comes, G. Hancock, A. Hofzumahaus, A. J. Hynes, M. Kawasaki and A. R. Ravishankara, 2002, *J. Geophys. Res.*, **in press**.
245. Mauersberger, K., J. Barnes, D. Hanson and J. Morton, 1986, *Geophys. Res. Lett.*, **13**, 671-673.
246. Mauersberger, K., D. Hanson, J. Barnes and J. Morton, 1987, *J. Geophys. Res.*, **92**, 8480-8482.
247. Mauldin, R. L., III, J. B. Burkholder and A. R. Ravishankara, 1992, *J. Phys. Chem.*, **96**, 2582-2588.
248. Mazely, T. L., R. R. Friedl and S. P. Sander, 1995, *J. Phys. Chem.*, **99**, 8162-8169.
249. Mazely, T. L., R. R. Friedl and S. P. Sander, 1997, *J. Phys. Chem.*, **101**, 7090-7097.
250. McAdam, K., B. Veyret and R. Lesclaux, 1987, *Chem. Phys. Lett.*, **133**, 39-44.
251. McElcheran, D. E., M. H. J. Wijnen and E. W. R. Steacie, 1958, *Can. J. Chem.*, **36**, 321.
252. McGee, T. J. and J. Burris, 1987, *J. Quant. Spectrosc. Radiat. Trans.*, **37**, 165-182.
253. McGivern, W. S., R. Li, P. Zou and S. W. North, 1999, *J. Chem. Phys.*, **111**, 5771-5779.
254. McGrath, M. P., K. C. Clemmshaw, F. S. Rowland and W. J. Hehre, 1988, *Geophys. Res. Lett.*, **15**, 883-886.
255. McGrath, M. P., K. C. Clemmshaw, F. S. Rowland and W. J. Hehre, 1990, *J. Phys. Chem.*, **94**, 6126-6132.
256. Merienne, M. F., B. Coquart and A. Jenouvrier, 1990, *Planet. Space Sci.*, **38**, 617-625.
257. Merienne, M. F., A. Jenouvrier and B. Coquart, 1995, *J. Atm. Chem.*, **20**, 281-297.
258. Minschwaner, K., G. P. Anderson, L. A. Hall and K. Yoshino, 1992, *J. Geophys. Res.*, **97**, 10103-10108.
259. Minschwaner, K. and D. E. Siskind, 1993, *J. Geophys. Res.*, **98**, 20401-20412.
260. Minton, T. K., C. M. Nelson, T. A. Moore and M. Okumura, 1992, *Science*, **258**, 1342-1345.
261. Mishalanie, E. A., J. C. Rutkowski, R. S. Hutte and J. W. Birks, 1986, *J. Phys. Chem.*, **90**, 5578-5584.
262. Mitchell, D. N., R. P. Wayne, P. J. Allen, R. P. Harrison and R. J. Twin, 1980, *J. Chem. Soc. Faraday Trans. 2*, **76**, 785.
263. Molina, L. T., J. J. Lamb and M. J. Molina, 1981, *Geophys. Res. Lett.*, **8**, 1008
264. Molina, L. T. and M. J. Molina, 1977, *Geophys. Res. Lett.*, **4**, 83-86.
265. Molina, L. T. and M. J. Molina, 1978, *J. Phys. Chem.*, **82**, 2410-2414.
266. Molina, L. T. and M. J. Molina, 1979, *J. Photochem.*, **11**, 139-144.
267. Molina, L. T. and M. J. Molina, 1981, *J. Photochem.*, **15**, 97.
268. Molina, L. T. and M. J. Molina. "Chemistry of Fluorine in the Stratosphere"; 182nd American Chemical Society National Meeting, 1982, New York.
269. Molina, L. T. and M. J. Molina, 1983, *J. Phys. Chem.*, **87**, 1306.
270. Molina, L. T. and M. J. Molina, 1986, *J. Geophys. Res.*, **91**, 14,501-14,508.
271. Molina, L. T. and M. J. Molina, 1996, *Geophys. Res. Lett.*, **23**, 563-565.
272. Molina, L. T., M. J. Molina and F. S. Rowland, 1982, *J. Phys. Chem.*, **86**, 2672-2676.
273. Molina, L. T., S. D. Schinke and M. J. Molina, 1977, *Geophys. Res. Lett.*, **4**, 580-582.
274. Molina, M. J. and G. Arguello, 1979, *Geophys. Res. Lett.*, **6**, 953-955.
275. Molina, M. J., T. Ishiwata and L. T. Molina, 1980, *J. Phys. Chem.*, **84**, 821-826.
276. Moore, T. A., M. Okumura, M. Tagawa and T. K. Minton, 1995, *Faraday Discuss.*, **100**, 295-307.
277. Moortgat, G. K., W. Klippel, K. H. Mobius, W. Seiler and P. Warneck FAA-EE-80-47, Federal Aviation Administration, Washington, DC 1980.
278. Moortgat, G. K., R. Meller and W. Schneider. Temperature dependence (256-296K) of the absorption cross-sections of bromoform in the wavelength range 285-360 nm. In *The Tropospheric Chemistry of Ozone in the Polar Regions*; Niki, H., Becker, K. H., Eds.; Springer-Verlag: Berlin, 1993; pp 359-369.
279. Moortgat, G. K., W. Seiler and P. Warneck, 1983, *J. Chem. Phys.*, **78**, 1185-1190.
280. Moortgat, G. K., B. Veyret and R. Lesclaux, 1989, *J. Phys. Chem.*, **93**, 2362-2368.
281. Moortgat, G. K. and P. Warneck, 1979, *J. Chem. Phys.*, **70**, 3639-3651.
282. Morel, O., R. Simonaitis and J. Heicklen, 1980, *Chem. Phys. Lett.*, **73**, 38.
283. Mossinger, J. C., D. E. Shallcross and R. A. Cox, 1998, *J. Chem. Soc. Faraday Trans.*, **94**, 1391-1396.
284. Munk, J., P. Pagsberg, E. Ratajczak and A. Sillesen, 1986, *J. Phys. Chem.*, **90**, 2752-2757.
285. Murtagh, D. P., 1988, *Planet. Space Sci.*, **36**, 819-828.
286. Nayak, A. K., T. J. Buckley, M. J. Kurylo and A. Fahr, 1996, *J. Geophys. Res.*, **101**, 9055-9062.
287. Nayak, A. K., M. J. Kurylo and A. Fahr, 1995, *J. Geophys. Res.*, **100**, 11185-11189.
288. Nee, J. B., 1991, *J. Quant. Spectrosc. Radiat. Transfer*, **46**, 55.

289. Nelson, C. M., T. A. Moore and M. Okumura, 1994, *J. Chem. Phys.*, **100**, 8055-8064.
290. Nelson, C. M., T. A. Moore, M. Okumura and T. K. Minton, 1996, *Chem. Phys.*, **2248**, 287-307.
291. Nelson, H. H. and H. S. Johnston, 1981, *J. Phys. Chem.*, **85**, 3891.
292. Nickolaisen, S. L. and S. P. Sander, 1996, Manuscript in preparation.
293. Nickolaisen, S. L., S. P. Sander and R. R. Friedl, 1996, *J. Phys. Chem.*, **100**, 10165.
294. Nicolet, M. and R. Kennes, 1989, *Planet. Space Sci.*, **37**, 459-491.
295. Nicovich, J. M. and P. H. Wine, 1988, *J. Geophys. Res.*, **93**, 2417.
296. Nolle, A., H. Heydtmann, R. Meller and G. K. Moortgat, 1993, *Geophys. Res. Lett.*, **20**, 707-710.
297. NÖlle, A., H. Heydtmann, R. Meller, W. Schneider and G. K. Moortgat, 1992, *Geophys. Res. Lett.*, **19**, 281-284.
298. Ogorzalek Loo, R., H.-P. Haerri, G. E. Hall and P. L. Houston, 1989, *J. Chem. Phys.*, **90**, 4222-4236.
299. Oh, D., W. Sisk, A. Young and H. Johnston, 1986, *J. Chem. Phys.*, **85**, 7146-7158.
300. Okabe, H. In *Photochemistry of Small Molecules*; John Wiley and Sons Inc.: New York, 1978; pp 217.
301. Okabe, H., 1980, *J. Chem. Phys.*, **72**, 6642.
302. Orkin, V. L. and E. E. Kasimovskaya, 1995, *J. Atm. Chem*, **21**, 1-11.
303. Orkin, V. L., V. G. Khamaganov, A. G. Guschin, R. E. Huie and M. J. Kurylo, 1997, *J. Phys. Chem. A*, **101**, 174-178.
304. Orlando, J. J. and J. B. Burkholder, 1995, *J. Phys. Chem.*, **99**, 1143-1150.
305. Orlando, J. J., J. B. Burkholder, S. A. McKeen and A. R. Ravishankara, 1991, *J. Geophys. Res.*, **96**, 5013-5023.
306. Orlando, J. J., G. S. Tyndall, G. K. Moortgat and J. G. Calvert, 1993, *J. Phys. Chem.*, **97**, 10996-11000.
307. Paraskevopoulos, G. and R. J. Cvetanovic, 1969, *J. Am. Chem. Soc.*, **91**, 7572.
308. Parkes, D. A., 1977, *Int. J. Chem. Kinet.*, **9**, 451.
309. Parkes, D. A., D. M. Paul, C. P. Quinn and R. C. Robson, 1973, *Chem. Phys. Lett.*, **23**, 425-429.
310. Parrish, D. D., P. C. Murphy, D. L. Albritton and F. C. Fehsenfeld, 1983, *Atmos. Environ.*, **17**, 1365.
311. Paukert, T. T. and H. S. Johnston, 1972, *J. Chem. Phys.*, **56**, 2824-2838.
312. Pence, W., S. Baughum and S. Leone, 1981, *J. Phys. Chem.*, **85**, 3844-3851.
313. Permien, T., R. Vogt and R. N. Schindler. Mechanisms of Gas Phase-Liquid Phase Chemical Transformations. In *Air Pollution Report #17*; Cox, R. A., Ed.; Environmental Research Program of the CEC.: Brussels, 1988.
314. Pfister, R. and R. J. Huber, 2002, personal communication.
315. Phillips, D. L., A. B. Myers and J. J. Valentini, 1992, *J. Phys. Chem.*, **96**, 2039-2044.
316. Pilling, M. J. and M. J. C. Smith, 1985, *J. Phys. Chem.*, **89**, 4713-4720.
317. Porret, D. and C. F. Goodeve, 1937, *Trans. Faraday Soc.*, **33**, 690-693.
318. Porret, D. and C. F. Goodeve, 1938, *Proc. Roy. Soc. London A*, **165**, 31-42.
319. Prahlad, V. and V. Kumar, 1995, *J. Quant. Spectrosc. Radiat. Transfer*, **54**, 945-955.
320. Preston, K. F. and R. F. Barr, 1971, *J. Chem. Phys.*, **54**, 3347-3348.
321. Rahn, T., H. Zhang, M. Wahlen and G. A. Blake, 1998, *Geophys. Res. Lett.*, **25**, 4489-4492.
322. Rattigan, O., E. Lutman, R. L. Jones and R. A. Cox, 1992, *J. Photochem. Photobiol. A: Chem.*, **66**, 313-326.
323. Rattigan, O., E. Lutman, R. L. Jones, R. A. Cox, K. Clemitshaw and J. Williams, 1992, *J. Photochem. Photobiol. A: Chem.*, **69**, 125-126.
324. Rattigan, O. V., D. J. Lary, R. L. Jones and R. A. Cox, 1996, *J. Geophys. Res.*, **101**, 23021-23033.
325. Rattigan, O. V., D. E. Shallcross and R. A. Cox, 1997, *J. Chem. Soc. Soc. Faraday Trans.*, **93**, 2839-2846.
326. Ravishankara, A. R., 1995, *Faraday Discuss*, **100**, 335.
327. Ravishankara, A. R. and R. L. Mauldin, 1986, *J. Geophys. Res.*, **91**, 8709-8712.
328. Ravishankara, A. R., S. Solomon, A. A. Turnipseed and R. F. Warren, 1993, *Science*, **259**, 194-199.
329. Ravishankara, A. R., S. Solomon, A. A. Turnipseed and R. F. Warren, 1993, *Science*, **259**, 194-199.
330. Ravishankara, A. R. and P. H. Wine, 1983, *Chem. Phys. Lett.*, **101**, 73.
331. Ravishankara, A. R., P. H. Wine, C. A. Smith, P. E. Barbone and A. Torabi, 1986, *J. Geophys. Res.*, **91**, 5355-5360.
332. Rebbert, R. E. and P. Ausloos, 1976/1977, *J. Photochem.*, **6**, 265-276.
333. Rebbert, R. E. and P. J. Ausloos, 1975, *J. Photochem.*, **4**, 419-434.
334. Rebbert, R. E., S. G. Lias and P. Ausloos, 1973, *Int. J. Chem. Kinet.*, **5**, 893-908.
335. Rebbert, R. E., S. G. Lias and P. Ausloos, 1978, *J. Photochem.*, **8**, 17-27.
336. Reid, S. A., J. T. Brandon and H. Reisler, 1993, *J. Phys. Chem.*, **97**, 540.
337. Rigaud, P., B. Leroy, G. Le Bras, G. Poulet, J. L. Jourdain and J. Combourieu, 1977, *Chem. Phys. Lett.*, **46**, 161.
338. Robbins, D. E., 1976, *Geophys. Res. Lett.*, **3**, 213-216. See also Erratum, *GRL*, 1976, Vol. 3, p. 757.
339. Robbins, D. E. and R. S. Stolarski, 1976, *Geophys. Res. Lett.*, **3**, 603-606.

340. Rockmann, T. J., C. A. M. Brenninkmeijer, M. Wollenhaupt, J. N. Crowley and P. J. Crutzen, 2000, *Geophys. Res. Lett.*, **27**, 1399-1402.
341. Rockmann, T. J., J. Kaiser, C. A. M. Brenninkmeijer, J. N. Crowley, R. Borchers, W. A. Brand and P. J. Crutzen, 2001, *J. Geophys. Res.*, **106**, 10,403-10,410.
342. Roehl, C. M., D. Bauer and G. K. Moortgat, 1996, *J. Phys. Chem.*, **100**, 4038-4047.
343. Roehl, C. M., J. B. Burkholder, G. K. Moortgat, A. R. Ravishankara and P. J. Crutzen, 1997, *J. Geophys. Res.*, **102**, 12819-12829.
344. Roehl, C. M., J. J. Orlando and J. G. Calvert, 1992, *J. Photochem. Photobiol. A: Chem.*, **69**, 1-5.
345. Rogers, J. D., 1990, *J. Phys. Chem.*, **94**, 4011-4015.
346. Rowland, F. S. and Y. Makide, 1982, *Geophys. Res. Lett.*, **9**, 473.
347. Rowland, F. S. and M. J. Molina, 1975, *Rev. Geophys. Space Phys.*, **13**, 1-35.
348. Rowland, F. S. and P. J. Rogers, 1982, *Proc. Natl. Acad. Sci. USA*, **79**, 2737.
349. Rowland, F. S., J. E. Spencer and M. J. Molina, 1976, *J. Phys. Chem.*, **80**, 2711-2713.
350. Roxlo, C. and A. Mandl, 1980, *J. Appl. Phys.*, **51**, 2969-2972.
351. Rudolph, R. N. and E. C. Y. Inn, 1981, *J. Geophys. Res.*, **86**, 9891.
352. Ruhl, E., A. Jefferson and V. Vaida, 1990, *J. Phys. Chem.*, **94**, 2990.
353. Russell, B. R., L. O. Edwards and J. W. Raymond, 1973, *J. Am. Chem. Soc.*, **95**, 2129-2133.
354. Safary, E., J. Romand and B. Vodar, 1951, *J. Chem. Phys.*, **19**, 379.
355. Salomon, D., A. W. Kirk and E. Tschuikow-Roux, 1977, *J. Photochem.*, **7**, 345-353.
356. Sander, S. P., 1986, *J. Phys. Chem.*, **90**, 4135-4142.
357. Sander, S. P. and R. R. Friedl, 1989, *J. Phys. Chem.*, **93**, 4764-4771.
358. Sander, S. P., R. R. Friedl, W. B. DeMore, D. M. Golden, M. J. Kurylo, R. F. Hampson, R. E. Huie, G. K. Moortgat, A. R. Ravishankara, C. E. Kolb and M. J. Molina "Chemical Kinetics and Photochemical Data for Use in Stratospheric Modeling, Evaluation Number 13," JPL Publication 00-3, Jet Propulsion Laboratory, California Institute of Technology, Pasadena, CA, 2000.
359. Sander, S. P., M. Peterson, R. T. Watson and R. Patrick, 1982, *J. Phys. Chem.*, **86**, 1236-1240.
360. Sander, S. P. and R. T. Watson, 1981, *J. Phys. Chem.*, **85**, 2960.
361. Sandorfy, C., 1976, *Atmos. Environ.*, **10**, 343-351.
362. Sauvageau, P., J. Doucet, R. Gilbert and C. Sandorfy, 1974, *J. Chem. Phys.*, **61**, 391.
363. Sauvageau, P., R. Gilbert, P. P. Berlow and C. Sandorfy, 1973, *J. Chem. Phys.*, **59**, 762.
364. Schiffman, A., D. D. Nelson, Jr. and D. J. Nesbitt, 1993, *J. Chem. Phys.*, **98**, 6935-6946.
365. Schmitt, G. and F. J. Comes, 1980, *J. Photochem.*, **14**, 107-123.
366. Schmitt, G. and F. J. Comes, 1987, *J. Photochem. Photobiol. A*, **41**, 13-30.
367. Schneider, W., G. K. Moortgat, J. P. Burrows and G. Tyndall, 1987, *J. Photochem. Photobiol.*, **40**, 195-217.
368. Schneider, W. F., T. J. Wallington, K. Minschwaner and E. A. Stahlberg, 1995, *Environ. Sci. Technol.*, **29**, 247.
369. Seecombe, D. P., R. Y. L. Chim, R. P. Tucket, H. W. Jochims and H. Baumgaertel, 2001, *J. Chem. Phys.*, **114**, 4058-4073.
370. Seery, D. J. and D. Britton, 1964, *J. Phys. Chem.*, **68**, 2263.
371. Selwyn, G., J. Podolske and H. S. Johnston, 1977, *Geophys. Res. Lett.*, **4**, 427-430.
372. Senum, G. I., Y.-N. Lee and J. S. Gaffney, 1984, *J. Phys. Chem.*, **88**, 1269-1270.
373. Shardanand and A. D. P. Rao, 1977, *J. Quant. Spectrosc. Radiat. Transfer*, **17**, 433-439.
374. Shetter, R. E., J. A. Davidson, C. A. Cantrell, N. J. Burzynski and J. G. Calvert, 1988, *J. Geophys. Res.*, **93**, 7113-7118.
375. Silvente, E., R. C. Richter, M. Zheng, E. S. Saltzman and A. J. Hynes, 1997, *Chem. Phys. Lett.*, **264**, 309-315.
376. Silver, J. A., D. R. Worsnop, A. Freedman and C. E. Kolb, 1986, *J. Chem. Phys.*, **84**, 4378-4384.
377. Simon, F.-G., W. Schneider and G. K. Moortgat, 1990, *Int. J. Chem. Kinet.*, **22**, 791-813.
378. Simon, F. G., W. Schneider, G. K. Moortgat and J. P. Burrows, 1990, *J. Photochem. Photobiol.*, **A55**, 1-23.
379. Simon, P. C., D. Gillotay, N. Vanlaethem-Meuree and J. Wisenberg, 1988, *J. Atmos. Chem.*, **7**, 107-135.
380. Simon, P. C., D. Gillotay, N. Vanlaethem-Meuree and J. Wisenberg, 1988, *Annales Geophysicae*, **6**, 239-248.
381. Simonaitis, R., R. I. Greenberg and J. Heicklen, 1972, *Int. J. Chem. Kinet.*, **4**, 497.
382. Singer, R. J., J. N. Crowley, J. P. Burrows, W. Schneider and G. K. Moortgat, 1989, *J. Photochem. Photobiol.*, **48**, 17-32.
383. Smith, G. D., L. T. Molina and M. J. Molina, 2000, *J. Phys. Chem. A*, **104**, 8916-8921.
384. Smith, W. S., C. C. Chou and F. S. Rowland, 1977, *Geophys. Res. Lett.*, **4**, 517-519.
385. Solomon, S., J. B. Burkholder, A. R. Ravishankara and R. R. Garcia, 1994, *J. Geophys. Res.*, **99**, 20929-20935.
386. Spencer, J. E. and F. S. Rowland, 1978, *J. Phys. Chem.*, **82**, 7-10.
387. Stanton, J. F., C. M. L. Rittby, R. J. Bartlett and D. W. Toohey, 1991, *J. Phys. Chem.*, **95**, 2107-2110.

388. Stief, L. J., W. A. Payne and R. B. Klemm, 1975, *J. Chem. Phys.*, **62**, 4000-4008.
389. Stockwell, W. R. and J. G. Calvert, 1978, *J. Photochem.*, **8**, 193-203.
390. Suto, M. and L. C. Lee, 1985, *J. Geophys. Res.*, **90**, 13037-13040.
391. Swanson, D., B. Kan and H. S. Johnston, 1984, *J. Phys. Chem.*, **88**, 3115.
392. Takahashi, K., Y. Matsumi and M. Kawasaki, 1996, *J. Phys. Chem.*, **100**, 4084-4089.
393. Talukdar, R., A. Mellouki, T. Gierczak, J. B. Burkholder, S. A. McKeen and A. R. Ravishankara, 1991, *J. Phys. Chem.*, **95**, 5815-5821.
394. Talukdar, R., A. Mellouki, T. Gierczak, J. B. Burkholder, S. A. McKeen and A. R. Ravishankara, 1991, *Science*, **252**, 693-695.
395. Talukdar, R. K., J. B. Burkholder, A.-M. Schmoltner, J. M. Roberts, R. Wilson and A. R. Ravishankara, 1995, *J. Geophys. Res.*, **100**, 14163-14173.
396. Talukdar, R. K., M. K. Gilles, F. Battin-Leclerc, A. R. Ravishankara, J.-M. Fracheboud, J. J. Orlando and G. S. Tyndall, 1997, *Geophys. Res. Lett.*, **24**, 1091-1094.
397. Talukdar, R. K., M. Hunter, R. F. Warren, J. B. Burkholder and A. R. Ravishankara, 1996, *Chem. Phys. Lett.*, **262**, 669-674.
398. Talukdar, R. K., C. A. Longfellow, M. K. Gilles and A. R. Ravishankara, 1998, *Geophys. Res. Lett.*, **25**, 143-146.
399. Talukdar, R. K., G. L. Vaghjiani and A. R. Ravishankara, 1992, *J. Chem. Phys.*, **96**, 8194-8201.
400. Tang, K. Y., P. W. Fairchild and E. K. C. Lee, 1979, *J. Phys. Chem.*, **83**, 569.
401. Thelen, M.-A., P. Felder and J. R. Huber, 1993, *Chem. Phys. Lett.*, **213**, 275-281.
402. Trolier, M., R. L. Mauldin, III and A. R. Ravishankara, 1990, *J. Phys. Chem.*, **94**, 4896-4907.
403. Trolier, M. and J. R. Wiesenfeld, 1988, *J. Geophys. Res.*, **93**, 7119-7124.
404. Turatti, F., D. W. T. Griffith, S. R. Wilson, M. B. Esler, T. Rahn, H. Zhang and G. A. Blake, 2000, *Geophys. Res. Lett.*, **27**, 2489-2492.
405. Turco, R. P., 1975, *Geophys. Surveys*, **2**, 153-192.
406. Turco, R. P., R. J. Cicerone, E. C. Y. Inn and L. A. Capone, 1981, *J. Geophys. Res.*, **86**, 5373.
407. Turnipseed, A. A., G. L. Vaghjiani, J. E. Thompson and A. R. Ravishankara, 1992, *J. Chem. Phys.*, **96**, 5887.
408. Tyndall, G. S., R. A. Cox, C. Granier, R. Lesclaux, G. K. Moortgat, M. J. Pilling, A. R. Ravishankara and T. J. Wallington, 2001, *J. Geophys. Res.*, **106**, 12157-12182.
409. Tyndall, G. S., K. M. Stedman, W. Schneider, J. P. Burrows and G. K. Moortgat, 1987, *J. Photochem.*, **36**, 133-139.
410. Uma, S. and P. K. Das, 1994, *Can. J. Chem.*, **72**, 865-869.
411. Uma, S. and P. K. Das, 1995, *Chem. Phys. Lett.*, **241**, 335-338.
412. Uma, S. and P. K. Das, 1996, *J. Chem. Phys.*, **104**, 4470-4474.
413. Uthman, A. P., P. J. Demlein, T. D. Allston, M. C. Withiam, M. J. McClements and G. A. Takacs, 1978, *J. Phys. Chem.*, **82**, 2252-2257.
414. Vaghjiani, G. L. and A. R. Ravishankara, 1989, *J. Geophys. Res.*, **94**, 3487-3492.
415. Vaghjiani, G. L. and A. R. Ravishankara, 1990, *J. Chem. Phys.*, **92**, 996.
416. Vaghjiani, G. L., A. A. Turnipseed, R. F. Warren and A. R. Ravishankara, 1992, *J. Chem. Phys.*, **96**, 5878.
417. Vaida, V., S. Solomon, E. C. Richards, E. Ruhl and A. Jefferson, 1989, *Nature*, **342**, 405.
418. Vanlaethem-Meuree, N., J. Wisenberg and P. C. Simon, 1978, *Bull. Acad. Roy. Belgique Cl. Sci.*, **64**, 31.
419. Vanlaethem-Meuree, N., J. Wisenberg and P. C. Simon, 1978, *Bull. Acad. Roy. Belgique Cl. Sci.*, **64**, 42.
420. Vanlaethem-Meuree, N., J. Wisenberg and P. C. Simon, 1979, *Geophys. Res. Lett.*, **6**, 451-454.
421. Vasudev, R., 1990, *Geophys. Res. Lett.*, **17**, 2153-2155.
422. Vogt, R. and R. N. Schindler, 1992, *J. Photochem. Photobiol. A: Chem.*, **66**, 133-140.
423. Wahner, A., A. R. Ravishankara, S. P. Sander and R. R. Friedl, 1988, *Chem. Phys. Lett.*, **152**, 507.
424. Wahner, A., G. S. Tyndall and A. R. Ravishankara, 1987, *J. Phys. Chem.*, **91**, 2734-2738.
425. Wallington, T. J., P. Dagaut and M. J. Kurylo, 1988, *J. Photochem. Photobiol. A: Chemistry*, **42**, 173-185.
426. Wallington, T. J., P. Dagaut and M. J. Kurylo, 1992, *Chem. Rev.*, **92**, 667-710.
427. Wallington, T. J., M. M. Mariq, T. Ellerman and O. J. Nielsen, 1992, *J. Phys. Chem.*, **96**, 982-986.
428. Walton, J. C., 1972, *J. Chem. Soc. Farad. Trans.*, **68**, 1559.
429. Wannenmacher, E. A. J., P. Felder and R. J. Huber, 1991, *J. Chem. Phys.*, **95**, 986-997.
430. Watson, R. T., 1977, *J. Phys. Chem. Ref. Data*, **6**, 871-917.
431. Wayne, R. P., I. Barnes, J. P. Burrows, C. E. Canosa-Mas, J. Hjorth, G. Le Bras, G. K. Moortgat, D. Perner, G. Poulet, G. Restelli and H. Sidebottom, 1991, *Atmos. Environ.*, **25A**, 1-203.
432. Wine, P. H., W. L. Chameides and A. R. Ravishankara, 1981, *Geophys. Res. Lett.*, **8**, 543-546.

433. Wine, P. H., A. R. Ravishankara, D. L. Philen, D. D. Davis and R. T. Watson, 1977, *Chem. Phys. Lett.*, **50**, 101.
434. WMO *Atmospheric Ozone: 1985*; National Aeronautics and Space Administration: Geneva, 1986.
435. Xu, H. and J. A. Joens, 1993, *Geophys. Res. Lett.*, **20**, 1035-1037.
436. Yao, F., I. Wilson and H. Johnston, 1982, *J. Phys. Chem.*, **86**, 3611.
437. Yokelson, R. J., J. B. Burkholder, R. W. Fox, R. K. Talukdar and A. R. Ravishankara, 1994, *J. Phys. Chem.*, **98**, 13144-13150.
438. Yoshino, K., A. S. C. Cheung, J. R. Esmond, W. H. Parkinson, D. E. Freeman, S. L. Guberman, A. Jenouvrier, B. Coquart and M. F. Merienne, 1988, *Planet. Space Sci.*, **36**, 1469-1475.
439. Yoshino, K., J. R. Esmond, A. S. C. Cheung, D. E. Freeman and W. H. Parkinson, 1990, *J. Geophys. Res.*, **95**, 11743.
440. Yoshino, K., J. R. Esmond, A. S.-C. Cheung, D. E. Freeman and W. H. Parkinson, 1992, *Planet. Space Sci.*, **40**, 185-192.
441. Yoshino, K., J. R. Esmond, D. E. Freeman and W. H. Parkinson, 1993, *J. Geophys. Res.*, **98**, 5205-5211.
442. Yoshino, K., D. E. Freeman, J. R. Esmond, R. S. Friedman and W. H. Parkinson, 1988, *Planet. Space Sci.*, **36**, 1201-1210.
443. Yoshino, K., D. E. Freeman, J. R. Esmond, R. S. Friedman and W. H. Parkinson, 1989, *Planet. Space Sci.*, **37**, 419-426.
444. Yoshino, K., D. E. Freeman, J. R. Esmond and W. H. Parkinson, 1987, *Planet. Space Sci.*, **35**, 1067-1075.
445. Yoshino, K., D. E. Freeman and W. H. Parkinson, 1984, *J. Phys. Chem. Ref. Data*, **13**, 207-227.
446. Yoshino, K., D. F. Freeman, J. R. Esmond and W. H. Parkinson, 1983, *Planet. Space Sci.*, **31**, 339-353
447. Yung, Y. L. and C. E. Miller, 1997, *Science*, **278**, 1778-1780.
448. Zelikoff, M. and L. M. Aschenbrand, 1954, *J. Chem. Phys.*, **22** 1685-1687.
449. Zetzsch, C. In *Proceedings of the International Ozone Symposium 1988*; Bojkov, R., Fabian, P., Eds.; Deepak: Hampton, VA, 1989.
450. Zhang, H., P. O. Wennberg, V. H. Wu and G. A. Blake, 2000, *Geophys. Res. Lett.*, **27**, 2481-2484.
451. Zhang, L., W. Fuss and K. L. Kompa, 1990, *Chem. Phys.*, **144**, 289-297.
452. Zou, P., W. S. McGivern and S. W. North, 2000, *Phys. Chem. Chem. Phys.*, **2**, 3785-3790.
453. Zou, P., W. S. McGivern, O. Sokhabi, A. G. Suits and S. W. North, 2000, *J. Chem. Phys.*, **113**, 7149-7157.